Investigation of *Runx1* and Cathepsin-L as Potential Therapeutic Targets for Myocardial Infarction and Cardiac Ischaemia-Reperfusion Injury

Weihong He

MD

Submitted in fulfilment of the requirements for the Degree of Doctor of Philosophy to the Institute of Cardiovascular and Medical Sciences, College of Medical, Veterinary and Life Sciences, University of Glasgow, U.K.

Research conducted at the British Heart Foundation Glasgow Cardiovascular Research Centre, Institute of Cardiovascular and Medical Sciences, University of Glasgow, U.K.

September 2016

Abstract

Myocardial infarction (MI) is a leading cause of death worldwide. The fundamental treatment for MI is reperfusion of the ischaemic myocardium by primary percutaneous intervention (PPCI). Advances in PPCI techniques in recent years has led to an increased survival rate in patients undergoing MI. A larger proportion of patients surviving post- MI following PPCI face a later risk of developing heart failure due to the substantial left ventricular (LV) injury caused by MI. Post MI heart failure has become a frequent complication of MI and is associated with an extremely high mortality. To develop novel therapies for MI, two phases of the disease can be targeted. One is the period following PPCI in which ischaemia-reperfusion (IR) injury contributes to cardiac damage. At this stage, reducing IR injury can reduce cardiac damage and thereby improve cardiac function and survival. The other is the period of developing heart failure post MI, where adverse cardiac remodelling contributes to worsening cardiac function and progression of heart failure. Therefore, therapies targeting the remodelling process following MI may prevent deterioration of cardiac function and protect against heart failure.

Development of novel therapy for MI and IR injury requires experimental models which model the human disease. The clinical relevance of the animal model is associated with successful translation of novel therapies. Mouse models have become commonly used in translational research due to their cost efficiency and the ease of developing genetically-modified mice. However, inducing MI and IR injury in mice is a complex technique due to their small size and thus application of mouse models of MI and IR injury has been limited. The work in this thesis, has focussed on the MI and IR injury models in mice. MI and IR injury were successfully induced by performing left anterior descending coronary artery ligation in open-chest microsurgery and cardiac function following MI and IR injury was characterized using echocardiography and intra-left ventricular pressure-volume (PV) loops. Using these models and phenotyping techniques, two potential therapeutic targets were evaluated, one is cathepsin-L inhibition by a pharmacological inhibitor CAA0225, while the other was *Runx1* deficiency which was assessed in a cardiomyocyte-specific *Runx1*-deficient mouse.

Cathespin-L is a cysteine protease typically localized in lysosomes. In patients with

coronary heart diseases (CHD), cathepsin-L has been found at increased levels in the serum and plasma, and the elevation of cathepsin-L is correlated with disease severity. In this study, using a cathepsin-L inhibitor CAA0225, we tested the effects of cathepsin-L inhibition during IR injury in both Langendorff perfused *ex vivo* isolated rat hearts and an *in vivo* mouse model. In the Langendorff isolated heart model of IR injury, applying CAA0225 significantly improved systolic and diastolic cardiac function during IR injury and this improvement was paralleled by reduced infarct size. An inhibitor (CA074Me) of a separate member of the cathepsin family (cathepsin-B) was also tested in the Langendorff perfused hearts and although it improved the speed at which systolic function recovered post I/R injury, no other changes where noted in cardiac function. The beneficial effect of CAA0225 was further tested in *in vivo* mouse models of MI and IR injury. Intravenous injection of CAA0225 during the ischaemic period significantly improved cardiac systolic function following MI and IR injury at both 2 and 4 weeks, respectively. *In vivo* administration of CAA0225 reduced infarct size, as measured by a double-dye staining technique and may relate to normalization of adverse calcium handling in cardiomyocytes by CAA0225 during IR injury.

The *Runx1* gene is known to be related to lineage differentiation and function within the hematopoietic system. RUNX1 has been reported to be activated in border zone cardiomyocytes in humans and mice post MI. This finding indicated that the *Runx1* gene may play a role in cardiac remodelling post MI. To investigate the role of *Runx1*, MI and IR injury was induced in a tamoxifen-inducible cardiomyocyte-specific *Runx1*-deficient mouse model. *Runx1* deficiency significantly preserved cardiac function 8 weeks post MI and post IR injury injury and prevented LV dilation post MI. The underlying mechanism may relate to improved cardiomyocyte calcium handling.

In conclusion, the work in this thesis has assessed two separate targets, cathepsin-L and *Runx1* for their therapeutic potential in MI and IR injury. This work has significantly enhanced our knowledge on these novel targets and will inform the development of translational strategies for treatment of patients with MI.

Table of Contents

List of Figures

List of Tables

Acknowledgements

I would like to thank my supervisors Dr. Chris Loughrey and Dr. Stuart Nicklin for their guidance, support and encouragement throughout my PhD study. They are always positive and inspiring. It has been a fantastic experience working with them. To Chris especially I would like to extend my gratitude for his help and support in establishing my techniques for the investigation of myocardial infarction and ischaemia-reperfusion injury. The therapeutic targets studied in this thesis may become my life time interest and I will work with Chris to further explore their functions and mechanisms in my future career. Thanks to the knowledge and techniques I have learnt from Chris and Stuart during my PhD, which has established my academic research skills and forms the fundamental background for my future work on improving human health.

I would like to thank colleagues at the British Heart Foundation Glasgow Cardiovascular Research Centre (Dr. Charlotte McCarroll, Ms. Caroline Fattah, Ms. Katrin Nather, Ms. Ashley Cochrane, Ms. Carolyn Clarke, Ms. Lisa McArthur, Mr. Peter Bowman, Ms. Christine Stirton, Ms. Catherine Hawksby, Mr. Michael Dunne, Mr. Gregor Aitchison) for their help during my PhD study.

I would like to thank Professor Xuehong Wan, the Dean of West China Hospital, who supported me to study aboard after I finished my MD at West China Hospital a few years ago. Thanks to the Chinese government for providing funding for my PhD and thanks to the University of Glasgow, which provided me the opportunity to study in Glasgow. Thanks to the China Scholarship Council and the Education Section of the Chinese Embassy for their support during my stay in the UK. I wish my stay here may build long-term overseas collaboration in the future.

I would like to thank Professor Pin-Lan Li, my postdoc supervisor at Virginia Commonwealth University, who supported me to continue the work on my PhD thesis after I started my postdoc project in the USA.

Finally, I wish to thank my family for their support throughout my PhD study.

Declaration

The experimental work described in this thesis was carried out by myself except where acknowledged in the text and has not been presented as part of any other degree.
Some results during the period of research have been presented in abstract form and are detailed below:

*Joint First Author

W He*, CS McCarroll*, K Nather, EBA Elliott, SA Nicklin, CM Loughrey. The cathepsin-L inhibitor CAA0225 protects against myocardial ischaemia-reperfusion injury. Heart 2015;101:A1
(This abstract was selected for oral presentation at BSCR autumn meeting 2015, Glasgow)

CS McCarroll*, W He*, KK Foote, K Nather, C Fattah, EBA Elliott, A Cochrane, P Bowman, M Bell, T Kubin, T Braun, SA Nicklin, ER Cameron, CM Loughrey. *Runx1* deficiency protects against adverse cardiac remodelling following myocardial infarction. Heart 2015;101:A3

W He*, CS McCarroll*, EBA Elliott, CM Loughrey. The cathepsin-L inhibitor CAA0225 improves cardiac function during ischaemia-reperfusion. Biophysical Journal 2014; 106(2):729a

Prizes I have won during my PhD:

Best poster presentation at Glasgow heart theme meeting 2014

Best poster presentation at Glasgow heart theme meeting 2015

Abbreviations

Abbreviation	Full expression
$[Ca^{2+}]i$	Intracellular calcium ion concentration
$[Ca^{2+}]o$	Extracellular calcium ion concentration
αMHC	human α-myosin heavy chain
ßARK	beta adrenergic receptor kinase
P_{max}	peak left ventricular pressure
P_{min}	minimum left ventricular pressure
P_{dev}	left ventricular developed pressure
dP/dt_{max}	maximal rate of left ventricular pressure rise
dP/dt_{min}	maximal rate of left ventricular pressure fall
AAR	area at risk
ACE	angiotensin-converting enzyme
ACEi	angiotensin-converting enzyme inhibitors
AON	areas of non-viable
APC	anaphase-promoting complex
ATP	adenosine triphosphates
AV	atrioventricular
CABG	coronary artery bypass graft
CaMKII	calcium/calmodulin-dependent protein kinase II
CBF	core binding factor
CDK	cyclin-dependent kinase
cGMP	cyclic guanosine monophosphate
CHD	coronary heart disease
CICR	calcium-induced calcium release
CKMB	MB fraction of creatine kinase
CLIK	cathepsin L inhibitor Katunuma
cTn	cardiac troponin
DPX	dibutyl phthalate xylene
EC	excitation-contraction
ECG	electrocardiography
Echo	echocardiography

ECM	extracellular matrix
EDV	end diastolic volume
EF	ejection fraction
ERK	extracellular signal-regulated kinase
ESV	end systolic volume
ET-1	growth factors including endothelin-1
FS	fraction shortening
FAS	TNF receptor superfamily member 6
H&E	Haematoxylin and Eosin
HFpEF	heart failure with a preserved ejection fraction
HFrEF	heart failure with a reduced ejection fraction
HIPK	homeodomain-interacting protein kinase
HSC	hematopoietic stem cell
I_{Ca}	Calcium influx
IR	ischaemia-reperfusion
I.V.	intra-venous
IVS	interventricular septal thicknesses
LAD coronary artery	left anterior descending coronary artery
LBBB	left bundle branch block
LV	left ventricle/ventricular
LVID	left ventricular internal dimensions
LVIDd	left ventricular internal diameter at diastole
LVIDs	left ventricular internal diameter at systole
LVPWd	left ventricular posterior wall thickness at diastole
LVPWs	left ventricular posterior wall thickness at systole
MHC	myosin heavy chain
MI	myocardial infarction
MPTP	mitochondrial permeability transition pore
MRI	magnetic resonance imaging
NADPH	nicotinamide adenine dinucleotide phosphate
NCX	Na^+/Ca^{2+} exchanger
NO	nitric oxide
NSTEMI	non-ST elevation MI
PCI	percutaneous coronary intervention

PPCI	primary percutaneous coronary intervention
PLB	phospholamban
PV	pressure-volume
PW	posterior wall thicknesses
RAS	renin-angiotensin system
RAAS	renin-angiotensin-aldosterone system
RCA	right common carotid artery
ROS	reactive oxygen species
RyRs	ryanodine receptors
SA	sinoatrial
SERCA	Sarco-endoplasmic reticulum Ca^{2+}-ATPase
SPECT	single photon emission computed tomography
SR	sarcoplasmic reticulum
STEMI	ST elevation MI
STWS	Scott's Tap Water Substitute
TGF	transforming growth factor
TNF α	tumor necrosis factor alpha
Tnnt	troponin T
TTC	triphenyltetrazolium chloride

CHAPTER 1.
General introduction

1.1 Introduction

1.1.1 Heart

The mammalian heart is a muscular pump which is divided into the right and left sides and consists of four chambers (right and left ventricles and right and left atria). The primary function of the heart is to pump blood through blood vessels enabling delivery of oxygen and nutrients to organs and tissues of the body and removal of waste products. The cardiovascular system also plays a role in hormone distribution and temperature regulation. The heart wall comprises mainly of muscle fibres that are made of cardiomyocytes. Other major cell types also present including fibroblasts and endothelial cells. Fibroblasts secrete extracellular matrix polymers, which are associated with the degree of wall stiffness and elastic recoil (Souders et al., 2009). Endothelial cells line the inner surface of cardiac chambers with connective tissues and smooth muscle cells to form the non-thrombogenic endocardium (Harris and Black, 2010). The outside of the heart is lined by epicardium, comprising a flattened sheet of mesothelial cells over connective tissue. The outer surface of the heart is surrounded by the fibrous pericardium, under which the pericardial fluid lubricates the surfaces between epicardium and pericardium. Coronary arteries deliver oxygenated blood to the myocardium, which are composed of multiple vessels including three arteries that of importance in this thesis: the left anterior descending, circumflex branches and the right main coronary artery. These arteries distribute blood flow to different areas of myocardium. Small arteries and arterioles branch into numerous capillaries that lie next to cardiomyocytes. The coronary circulation has a high capillary-to-cardiomyocyte ratio and short diffusion distances, which ensures adequate oxygen supplies to cardiomyocytes and removal of metabolic waste products. The anatomic distribution of coronary vessels is heterogeneous among people; therefore, in clinical practice, the vascular involvement in ischaemic heart diseases needs to be verified by coronary imaging techniques such as coronary angiogram (Scanlon et al., 1999).

Cardiac contraction originates at the level of cardiomyocyte. The cardiomyocyte is packed with long and contractile myofibrils, of which sarcomere is the fundamental contractile unit. Sarcomere comprises two isoforms of filament, myosin and actin, and the Z lines lie between the sets of filamentous proteins.

The actin filament contains the tropomyosin-troponin complex that initiates cardiac contraction. At each Z line, the transverse tubular system (T-tubules) runs from the surface membrane into the interior of the cell, carrying Na^+ and Ca^{2+} channels and transmitting electrical excitation into the interior of the cells and thus activating myofibrils. The sarcoplasmic reticulum (SR) located inside the cytoplasm of cardiomyocytes, stores Ca^{2+} ions and plays a major role in coupling the electrical activity of the heart with its mechanical function in excitation-contraction (EC) coupling.

1.1.2 EC coupling

EC coupling is a sequence of events from electrical excitation of the cardiomyocyte to mechanical contraction of the heart. The extracellular and intracellular Ca^{2+} icons are fundamental in this process (Ringer, 1882a, Ringer, 1882b, Ringer, 1883b, Ringer, 1883a). There are four main stages of EC coupling:

The first stage is Ca^{2+} influx initiated by alteration of cell membrane potential during the action potential. The action potential originates from the pacemaker cells located at the sinoatrial (SA) node of the right atrium and then transmits rapidly to the atrioventricular (AV) node located in the lower atrial septum. The electrical impulse then runs through the fast-conduction muscle fibres known as the Bundle of His to the Purkinje fibres, and finally stimulates the ventricular myocytes. The signal transmits rapidly from one cardiomyocyte to the next though the gap junctions and the action potential travels along the surface membrane of the sarcolemma along T-tubules. This process triggers the opening of the voltage-gated L-type Ca^{2+} channels located at the T-tubules, which allows Ca^{2+} ions to enter the cardiomyocyte (Bers and Perez-Reyes, 1999).

The second stage is the calcium-induced calcium release (CICR). When Ca^{2+} ions enter the cardiomyocyte, a release of Ca^{2+} from sarcoplasmic reticulum is triggered *via* Ca^{2+} release channels known as ryanodine receptors (RyRs). The RyRs are located adjacent to the voltage-gated L-type Ca^{2+} channels and activated by an increase of local free Ca^{2+} concentration (Eisner et al., 1998).

The third stage is the Ca^{2+} mediated cross-linking and contraction, whereby the rise of the intracellular free Ca^{2+} concentration allows Ca^{2+} ions to bind to the myofilament protein troponin C. The troponin C is bound to tropomyosin as part of the tropomyosin-troponin complex. During the resting phase of cardiac contraction, the tropomyosin-troponin complex is bound to the thin actin filament of the sarcomere and obscures the myosin-binding sites on actin. When binding with Ca^{2+}, troponin C shifts the tropomyosin-troponin complex deeper into the actin groove and exposes the myosin-binding sites. This is followed by the binding of myosin to actin to form a cross-bridge. The head of myosin then pulls actin to the centre of sarcomere *via* ATP hydrolysis, which causes the contraction of cardiomyocytes and then of the whole heart (i.e. systole) (**Figure 1-1**) (Layland et al., 2005).

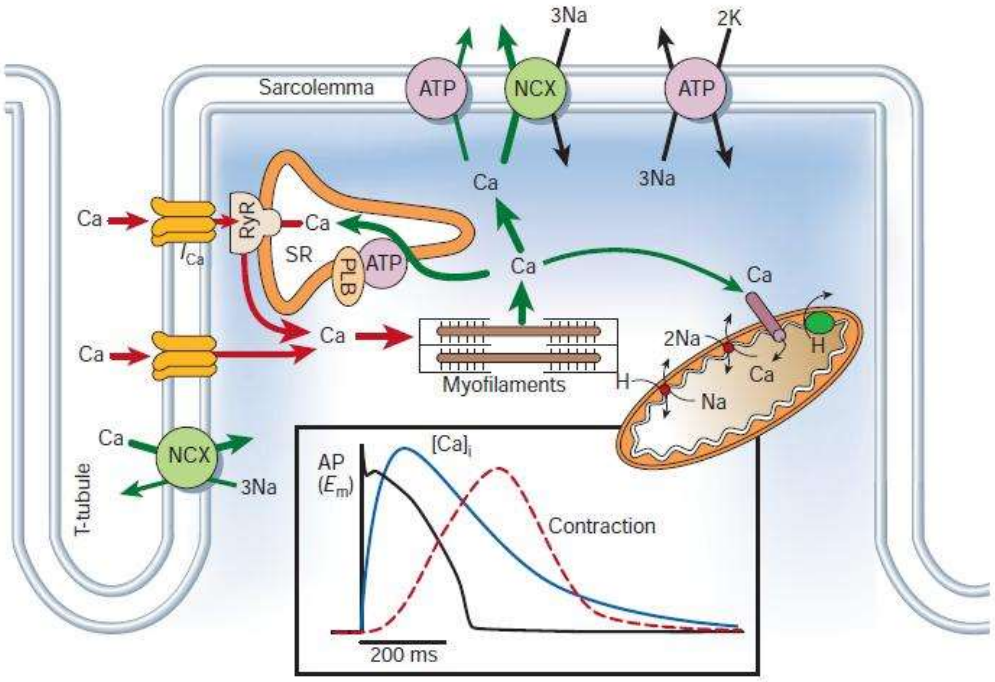

Figure 1-1. Calcium transport in excitation-contraction (EC) coupling within ventricular cardiomyocyte. During the action potential, calcium enters the myocyte through calcium influx (I_{Ca}) and NCX, and triggering calcium-induced calcium release (CICR) through RyR on the SR. Next the Ca^{2+} release activates the myofilaments and leads to contraction. At diastole, calcium is pumped into the SR by SR calcium ATPase (SERCA) and is extruded from the myocytes by NCX, leading to relaxation. Dephosphorylated phospholamban can inhibit SERCA. CaMKII phosphorylates calcium-handling proteins like phospholamban. ATP (ATPase); NCX (Na^+/Ca^{2+} exchanger); PLB (phospholamban); SR (sarcoplasmic reticulum); RyR (ryanodine receptor). Taken from review article Cardiac excitation–contraction coupling by Donald M. Bers (Bers, 2002)

The fourth stage is Ca^{2+} extrusion. Relaxation of cardiomyocytes allows the heart to be filled with blood during diastole, which requires the restoration of the intracellular free Ca^{2+} ions to resting levels. This dissociates Ca^{2+} from troponin,

which allows the tropomyosin-troponin complex to restructure and therefore obscure the actin binding sites and then prevent myosin binding. The SR Ca^{2+}-ATPase (SERCA) pumps, located on the surface membrane of the SR, transports the majority of the raised Ca^{2+} back into the SR. The remaining intracellular Ca^{2+} ions are removed by the sarcolemma sodium-calcium exchanger, which pumps a Ca^{2+} ion out of the cell in exchange for three Na^{+} ions into the cell. The sodium-calcium exchange is driven by both transmembrane voltage and sodium-calcium concentration gradients (Blaustein and Lederer, 1999). SERCA is regulated by phospholamban, an inhibitory protein, which inhibits SERCA in its basal unphosphorylated state by decreasing the affinity of SERCA to Ca^{2+} (James et al., 1989, Voss et al., 1994), and enhances the activity of SERCA in its phosphorylated state by increasing its affinity to Ca^{2+} (James et al., 1989) and pumps the raised Ca^{2+} back into the interior of SR. Abnormal intracellular calcium handling is a major cause of cardiac dysfunction under pathological conditions such as heart failure (Morgan et al., 1990).

1.2 Coronary artery diseases

Coronary artery disease, also known as ischaemic heart disease, is the most common type of cardiovascular disease and is the leading cause of adult death and disability in the world (Mendis et al., 2015). Coronary artery disease accounts for 12.8% of all deaths and more than seven million people die from coronary artery disease every year (Task Force on the management of et al., 2012). Coronary artery disease includes angina and myocardial infarction (MI, commonly known as a heart attack).

1.2.1 Myocardial Infarction (MI)

MI is defined pathologically as myocardial cell death due to prolonged ischaemia (Thygesen et al., 2012). MI is a worldwide leading health problem and it is under intensive research in both clinical trials and pre-clinical studies. In the clinical setting, acute MI is characterised by a number of different perspectives related to clinical history, electrocardiography (ECG), pathology and biochemical examinations (Van de Werf et al., 2008). The initial pathological progress of MI is myocardial ischaemia, of which typical symptoms include combinations of chest,

upper extremities, epigastric or mandibular discomfort or an ischaemic equivalent such as dyspnoea and fatigue. The discomfort associated with acute MI normally lasts more than 20 min (Thygesen et al., 2012). MI may occur with atypical symptoms including palpitations and cardiac arrest, or without symptoms in the elderly and critically ill patients. The electrocardiogram (ECG) characteristics of ischaemia include ST elevation in two contiguous leads in an ST elevation MI (STEMI), or without ST elevation called non-ST elevation MI (NSTEMI) (Thygesen et al., 2012). STEMI is a major ECG manifestation of ischaemic heart diseases and is usually caused by abrupt thrombotic occlusion of an epicardial coronary artery with a ruptured atherosclerotic plaque, while non-STEMI (NSTEMI) usually occurs by the partial occlusion of a major coronary artery or complete occlusion of a minor coronary artery. The great majority of STEMI will show a typical rise of sensitive and specific biomarkers of myocardial necrosis, such as increased blood levels of cardiac troponin (cTn) and the MB fraction of creatine kinase (CKMB) (Nienhuis et al., 2008). Cardiac troponin I and T are expressed almost exclusively in the heart as components of the contractile apparatus of myocardium (Jaffe, 2006). The elevations of cTn (I or T), in the blood reflect necrosis of myocardial cells with high myocardial tissue specificity and high clinical sensitivity (Jaffe, 2006). Non-invasive imaging techniques are used for diagnosis of MI and characterization of cardiac function post MI. Commonly used imaging techniques for MI include echocardiography, radionuclide ventriculography, single photon emission computed tomography (SPECT), and magnetic resonance imaging (MRI) (Schuijf et al., 2005, Kellman and Arai, 2012). Echocardiography is commonly used in the assessment of cardiac structure and function for parameters such as myocardial thickness and motion (Flachskampf et al., 2011).

The pathophysiological characteristics of MI involves a large number of processes, including myocardial contractile dysfunction, cell death and healing by fibrosis after hypoperfusion and ischaemia. The consequences of ischaemia vary depending on the ischaemic extent and duration. The deprivation of oxygen and nutrients during ischaemia disrupts normal oxidative phosphorylation and leads to a reduction in high-energy adenosine triphosphates (ATP) which are necessary for normal function. The oxygen deprivation and depletion can lead to irreversible cell death. The necrosis begins following 15-30 min of severe ischaemia without

collateral flow and progresses in a time-dependent manner from the subendocardium to the subepicardium, which is known as the wave front phenomenon (Van de Werf et al., 2008, Reimer et al., 1977, Reimer and Jennings, 1979). Necrosis of the cardiomyocytes in the area at risk takes at least 2–4 h to develop, which is dependent on the distribution of collateral circulation to the ischaemic area, persistent or intermittent coronary occlusion and the individual sensitivity of the cardiomyocytes to ischaemia (Thygesen et al., 2007).

MI has traditionally been known as a manifestation of necrotic cardiomyocyte death. However, recently different forms of cell death have been identified to contribute to infarct size, such as apoptosis and autophagy (Whelan et al., 2010). During hypoperfusion and ischaemia, the production of ATP is rapidly reduced in the myocardium, leading to a cascade of events which eventually lead to three main forms of cell death:

Necrosis is morphologically characterised by membrane destruction, swollen and ruptured mitochondria, myofibrillar contraction bands, microvascular destruction, inflammation and haemorrhage (Reimer et al., 1977, Reimer and Jennings, 1979, Kloner et al., 1983). During ischaemia, the depletion of ATP results in accumulation of AMP, which activates glycolytic enzymes and anaerobic metabolism (Cave et al., 2000, Das et al., 1987). Lack of available ATP increases intracellular Na^+ accumulation by the inhibition of Na^+/K^+-ATPase, and the anaerobic glycolysis increases the influx of Na^+ *via* the Na^+/H^+-exchanger. The exchange of Na^+ for Ca^{2+} by the sarcolemmal Na^+/Ca^{2+}-exchanger subsequently induces intracellular Ca^{2+} overload, causing myofibrillar hypercontraction (Tani and Neely, 1989, Ladilov et al., 1995). Increased intracellular lactate produced by anaerobic metabolism causes an accumulation of water and resultant osmotic stress, leading to organelle and cell swelling with sarcolemmal membrane damage (Das et al., 1987, Neill, 1968, Opie, 1990).

Apoptosis is a form of 'programmed cell death' characterized by energy-consuming cell death and characteristic deoxyribonucleic acid strand breaks (Zhang and Xu, 2000, Chiong et al., 2011, Orogo and Gustafsson, 2013). Apoptosis is triggered intrinsically by mitochondrial release of cytochrome C, leading to intracellular proteolysis by a cascade activation, or extrinsically by activation of

sarcolemmal receptors, FAS (TNF receptor superfamily, member 6) and TNF α (tumor necrosis factor alpha) receptors (Kleinbongard et al., 2011). Another form of cell death distinctly regulated by activation of receptor-interacting protein kinases 1 and 3 shares features with necrosis and apoptosis, which is known as necroptosis (Zhou and Yuan, 2014).

Autophagy is a second form of 'programmed cell death' in which activated lysosomal enzymes break down the organelles (Dong et al., 2010). Autophagy is associated with lysosomal degradation and protein recycling and is characterized by the presence of autophagosomes and increased expression of the autophagy-related gene complex, light chain 3, beclin-1, parkin, and p62 (Huang et al., 2011). Activation of lysosomes during ischaemia hydolyses the organelle and cell membranes, leading to osmotic stress and sarcolemmal disruption (see **Figure 1-2**). Autophagy during ischaemia is considered to be protective (Przyklenk et al., 2011). However, the role of autophagy in IR injury remains under debate (Gedik et al., 2014, Singh et al., 2014a).

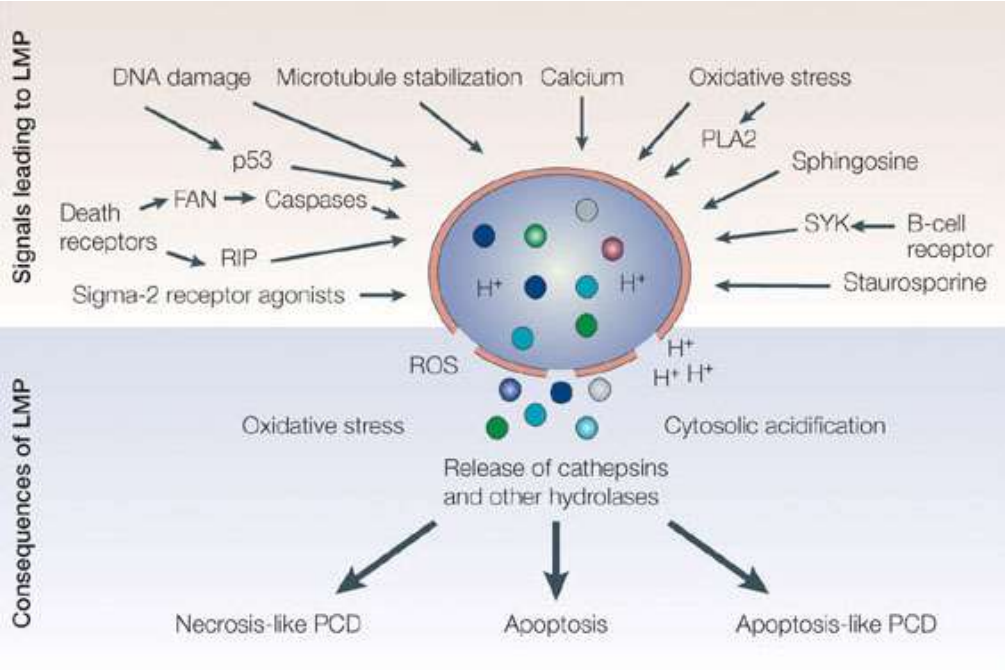

Figure 1-2. Release of lysosomal contents promotes acute cell death. The upper panel shows some of the stimuli and messengers triggering lysosomal-membrane permeabilization (LMP) which results in release of cathepsins and other lysosomal hydrolases, then leads to the release of reactive oxygen species (ROS) and CYTOCHROME C. This results in cell death through classical apoptosis, necrosis-like or caspase-independent apoptosis-like programmed cell death (PCD). Figure taken from Lysosomes and autophagy in cell death control by Guido Kroemer & Marja Jäättelä 2005 (Kroemer and Jaattela, 2005)

The loss of myocardium following MI leads to an abrupt increase of load which results in ventricular remodelling related to the border zone and remote non-infarcted area. Ventricular remodelling is a process which regulates ventricular size, shape, and function by mechanical, neurohormonal, and genetic factors (Pfeffer and Braunwald, 1990, Rouleau et al., 1993), leading to reparative changes such as dilatation, hypertrophy, and formation of collagen scar. Ventricular

remodelling is a predictor of heart failure and negative prognostic value (Kleinbongard et al., 2011). The remodelling process may continue for a prolonged period until the distending force is counterbalanced by the tensile strength of the scar (Warren et al., 1988). The components of the myocardium (cardiomyocytes, extracellular matrix, and capillary microcirculation) play important roles in the remodelling process. The cardiomyocyte is a terminally differentiated cell and develops mechanical shortening (Woodcock and Matkovich, 2005). The extracellular matrix generates a stress-tolerant, viscoelastic scaffold consisting of type I and III collagen that maintains the spatial relations between the myofilaments and the capillary microcirculation. The collagen framework couples adjacent cardiomyocytes and aligns myofilaments to optimize and distribute force evenly to the ventricular walls (Erlebacher et al., 1984, Weber, 1997). Following MI, the macrophages, monocytes, and neutrophils migrate into the infarct zone, which initiates intracellular signaling, neurohormonal activation, and local inflammatory responses. In the early phase of post-infarct remodelling (within 72 hours), the expansion of the infarct zone may result in cardiac rupture or aneurysm formation (Erlebacher et al., 1984). The late phase of remodelling (beyond 72 hours) involves the left ventricle globally with time-dependent dilatation, wall thinning, distortion of ventricular shape, and mural hypertrophy (see **Figure 1-3**). The failure to normalize increased wall stresses related to late remodelling leads to progressive dilatation, deterioration in contractile function, and recruitment of border zone myocardium into the scar (White et al., 1987).

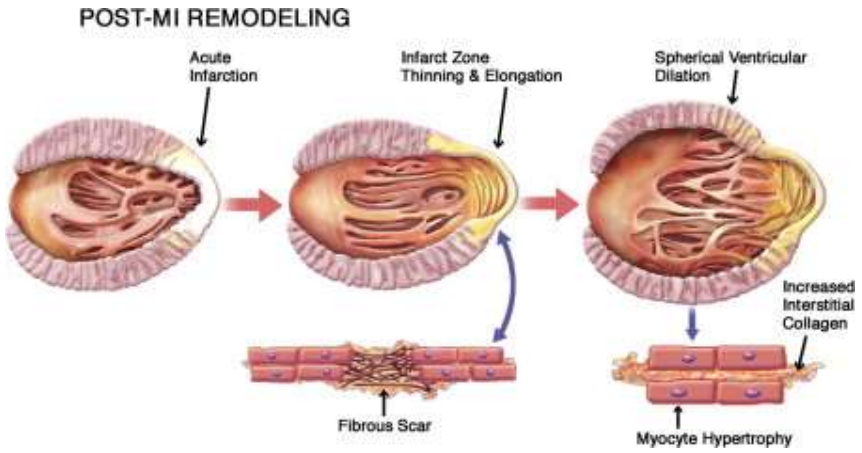

Figure 1-3. Schematic representation of post MI LV remodeling. The early phase of remodeling is thinning and elongating of the fibrous scar in the infarcted area. Subsequent myocyte hypertrophy leads to LV dilation and transition to spherical configuration. Myocyte hypertrophy is associated with increased interstitial collagen formation. Taken from Left Ventricular Remodeling in Heart Failure Current Concepts in Clinical Significance and Assessment by Marvin A. Konstam (Konstam et al., 2011)

Hypertrophy resulting from post-infarction remodelling is an adaptive response to increased workload, progressive dilatation, and contractile dysfunction. To maintain a normal stroke volume, the healthy myocardium has to produce a greater pressure with a reduced number of cardiomyocytes (Opie et al., 2006). The increase in afterload on these cardiomyocytes leads to hypertrophy by myocardial stretch, neurohormonal activation, paracrine/autocrine factors, and the activation of the local tissue renin-angiotensin system (RAS). The type of hypertrophy in post MI is often eccentric, which is characterised by lengthening of the cardiomyocytes in the border zone surrounding the infarct scar and in remote myocardium. Post MI eccentric hypertrophy is associated with increased risk of major adverse cardiac events, such as re-infarction, heart failure, and cardiac arrest (Verma et al., 2008). Hypertrophy is stimulated by both biochemical

and mechanical stimuli involving the activation of protein kinase cascades. Genes for transcriptional factors including c-fos, c-jun, c-myc, Egr-1, natriuretic peptides (ANP, BNP), enzymes including angiotensin-converting enzyme (ACE), Beta adrenergic receptor kinase (βARK), and growth factors including endothelin-1 (ET-1), insulin-like growth factor-1, transforming growth factor (TGF)-β1 are induced and involved in hypertrophic stimulation (Sadoshima and Izumo, 1993, Bogoyevitch et al., 1994, Yamazaki et al., 1995). Intracellular calcium handling plays a role in the activation of protein kinases in myocytes by Ang II and other hypertrophic stimuli before the fetal gene program is switched on for protein synthesis (Sadoshima et al., 1995, Hempel et al., 2002). Transcriptional activity of cardiomyocytes is modified during remodelling, causing reactivation of fetal gene expression which is normally silenced in adults (Machackova et al., 2006). The fetal genes encode structural proteins, which contributes to the lengthening of the cardiomyocyte by adding new sarcomeres (Grossman and Paulus, 2013). The cardiomyocytes reduce production of alpha-MHC (alpha-myosin heavy chain) and increase synthesis of beta-MHC, which is associated with reduced energetic requirement and reduced contractility of sarcomeres (Krenz and Robbins, 2004, Miyata et al., 2000). The decrease in mean number of myofibrils per sarcomere further reduces the contractile force generated by each sarcomere (Koitabashi and Kass, 2012). `

1.2.2 Ischaemia-reperfusion (IR) injury

Reperfusion therapy is the most effective treatment for STEMI, however, cardiac reperfusion has been viewed as “a double-edged sword” due to the existence of IR injury (Braunwald and Kloner, 1985). Cardiac IR injury is the myocardial injury and cardiomyocyte death which occurs during the reperfusion of ischaemic myocardium (Hausenloy and Yellon, 2016). IR injury paradoxically reduces the benefits of reperfusion therapy for patients presenting with STEMI. Cardiac IR injury was first observed in dog hearts undergoing coronary artery ligation where reperfusion led to acceleration of necrosis formation (Jennings et al., 1960). However, the importance of IR injury was not fully recognized until myocardial reperfusion techniques, such as thrombolysis and percutaneous coronary intervention (PCI), were utilized in the treatment of patients with MI about three decades ago. In the clinical setting, the current fundamental treatment for an

acute myocardial infarction is re-establishment of blood flow by using either thrombolytic therapy or primary percutaneous coronary intervention (PPCI) (Zimarino et al., 2008). Reperfusion of the ischaemic myocardium restores the supply of oxygen and nutrients and therefore salvages the reversibly injured myocardium. However, cardiac IR injury paradoxically causes additional injury which contributes to up to 50% of the tissue damage after myocardial infarction and reduces the beneficial effect of PPCI treatment (see **Figure 1-4**) (Braunwald and Kloner, 1985, Piper et al., 1998, Yellon and Hausenloy, 2007). There is still no effective treatment for the irreversible forms of IR injury. A number of new therapeutic strategies, which show the potential for preventing IR injury to improve clinical outcomes in MI patients, are currently under investigation (Hausenloy and Yellon, 2013, Hausenloy and Yellon, 2016).

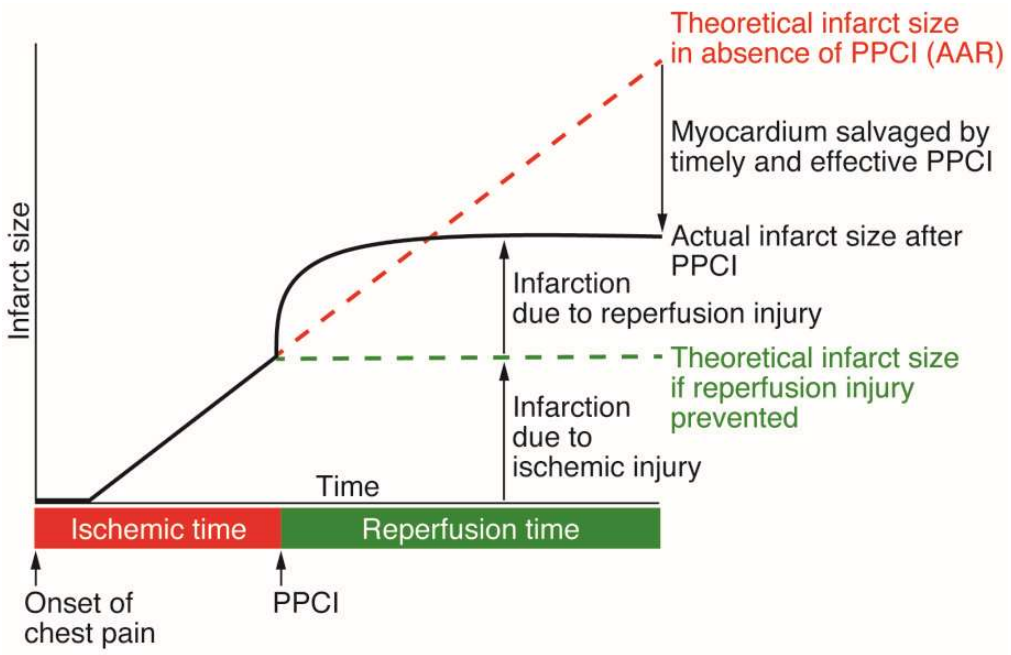

Figure 1-4. Contributions of ischaemic injury and reperfusion injury to final MI size in STEMI patients following PPCI. The final MI size is depicted by the black solid line. The theoretical MI size in the absence of PPCI is depicted by the red dashed line. The theoretical MI size following PPCI in the absence of reperfusion injury is depicted by the green dashed line. IR injury attenuates the benefit of reperfusion treatment in terms of reducing infarct size. Therefore, applying a treatment that is capable of reducing ischaemia-reperfusion injury could result in a smaller infarct size. Figure taken from Myocardial ischaemia-reperfusion injury: a neglected therapeutic target by Derek J. Hausenloy, Derek M. Yellon (Hausenloy and Yellon, 2013).

There are four recognized forms of IR injury, two reversible (IR-induced arrhythmias and myocardial stunning) and two irreversible (microvascular obstruction and lethal myocardial reperfusion injury) (Hausenloy and Yellon, 2013, Hausenloy and Yellon, 2016, Yellon and Hausenloy, 2007). The ventricular arrhythmias are usually induced after the onset of reperfusion in ischaemic myocardium. In STEMI patients undergoing PPCI the IR-induced arrhythmias

normally self-terminate or can be treated (Hearse and Tosaki, 1987). The reversible contractile dysfunction that occurs during reperfusion following myocardial ischaemia is known as myocardial stunning which results from the intracellular calcium overload and oxidative stress (Kloner et al., 1998a). Microvascular obstruction, also known as "no-flow phenomenon", refers to the inability to reperfuse the ischaemic region. Microvascular obstruction was first described by Krug et al. in 1966 (Krug et al., 1966). A number of major factors contribute to microvascular obstruction including micro-embolization, capillary damage and capillary compression. (Ito, 2006, Luo and Wu, 2006, Heusch et al., 2009). The microvascular obstruction leads to larger MI size, worse LV remodelling and lower LV ejection fraction (Ito et al., 1996, Wu et al., 1998, Hombach et al., 2005). Whether microvascular obstruction is an independent causative factor of cell death or a biomarker of IR remains unclear (Hausenloy and Yellon, 2013). Lethal myocardial reperfusion injury refers to the reperfusion-induced cardiomyocyte death after ischaemia (Piper et al., 1998) and is the form of IR injury on which this thesis focuses (referred to therefore hereon as IR injury). The factors that contribute to lethal myocardial reperfusion injury include oxidative stress, calcium overload, opening of the mitochondrial permeability transition pore (MPTP), and hypercontracture. The studies in both experimental MI and in patients with STEMI suggest that lethal myocardial reperfusion injury may contribute to up to 50% of the final MI size (Yellon and Hausenloy, 2007).

Experimental studies have identified several factors that mediate IR injury. The first is oxidative stress. The detrimental oxidative stress produced in the first few minutes of reperfusion mediates myocardial injury and cell death by inducing the opening of the MPTP, mediating dysfunction of the SR and acting as a neutrophil chemoattractant. The second is intracellular Ca^{2+} overload which begins during myocardial ischaemia and is exacerbated during reperfusion due to oxidative stress-induced SR damage, the disruption of the plasma membrane, and the mitochondrial re-energization. Experimental studies have shown that the administration of pharmacologic antagonists of the mitochondrial Ca^{2+} uniporter or the sarcolemmal Ca^{2+} channel at the onset of reperfusion can reduce MI size by up to 50% (Miyamae et al., 1996, Herzog et al., 1997). However, clinical studies have not shown positive results for administering calcium channel blockers at the

onset of reperfusion (Bar et al., 2006). The third factor is the rapid restoration of physiological pH. During ischaemia the intracellular pH decreases, whereas upon the onset of reperfusion, the physiological pH is rapidly restored by washout of lactate and activation of the Na^+-H^+ exchanger and the Na^+-HCO^- symporter. The pH shift leads to cardiomyocyte death by permitting mPTP opening and cardiomyocyte rigor hypercontracture (Lemasters et al., 1996). The fourth is opening of the mPTP, a nonselective channel of the inner mitochondrial membrane. The opening of mPTP leads to ATP depletion and cardiomyocyte death by uncoupling of oxidative phosphorylation and depolarization of the mitochondrial membrane (Hausenloy and Yellon, 2003, Heusch et al., 2010). The mPTP has been shown to remain closed during ischaemia and only open during reperfusion due to the mitochondrial Ca^{2+} and phosphate overload, ATP depletion, oxidative stress, and rapid pH restoration (Griffiths and Halestrap, 1995). Experimental studies in small and large animal MI models have shown that preventing mPTP opening by administering mPTP inhibitors at the onset of myocardial reperfusion can reduce infarct size by up to 50% (Hausenloy et al., 2003, Argaud et al., 2005, Skyschally et al., 2010).

Infarct size is a major factor affecting the clinical outcomes in STEMI patients with reperfusion treatment. Reduction of infarct size is the benefit of reperfusion therapy and is associated with the improvement of cardiac function (White et al., 1994). During reperfusion, the normalization of pH and re-energization causes oscillatory release and reuptake of Ca^{2+} into the SR, leading to uncontrolled myofibrillar hypercontraction (Ladilov et al., 1995, Piper et al., 2003, Piper et al., 2004, Garcia-Dorado et al., 2012). Calpain, a calcium-dependent non-lysosomal cysteine protease, is activated by normalization of pH, which digests the sarcolemma and cytoskeleton (Inserte et al., 2012). The increased intracellular Na^+ and Ca^{2+} contribute to cellular oedema because the extracellular osmolality is normalized by reperfusion and the excess reactive oxygen species (ROS) result in sarcolemma disruption (Schluter et al., 1996). The opening of mPTP in IR injury results in apoptosis. Formation and opening of mPTP cause mitochondrial matrix swelling, rupture of the outer membrane, release of cytochrome C to the cytosol, and eventually activation of the caspase cascade (Heusch et al., 2010). Recent studies have shown that autophagy, a type II programmed cell death, is activated

during ischaemia and further enhanced by reperfusion (Matsui et al., 2007, Gurusamy et al., 2009). However, the role of autophagy during IR injury is contentious. Several studies have demonstrated that inhibition of autophagy increases cardiomyocyte survival and reduces infarct size in IR injury (Matsui et al., 2007, Valentim et al., 2006), while other experiments have shown that autophagy has a protective effect during IR (Hamacher-Brady et al., 2006, Sala-Mercado et al., 2010). These studies relating to the modes of cell death during IR injury may suggest potential targets for reducing infarct size in STEMI patients undergoing reperfusion treatment.

1.3 Therapeutic strategies for MI

STEMI, which results from complete occlusion of a coronary artery, is the most severe form of acute coronary syndrome (Shin et al., 2003). Therefore, patients presenting with STEMI require immediate therapy. Recent advances in the treatment of STEMI have improved survival rate for patients. The mortality of STEMI is influenced by many factors, such as age, cardiac function, type of treatment, delay of treatment, prior MI history, diabetes, renal failure, and the number of affected coronary arteries. Recent studies have shown that the short-term and long-term mortality following STEMI is decreased with application of reperfusion therapy (Fox et al., 2007, Widimsky et al., 2010, Jernberg et al., 2011, McManus et al., 2011). Six-month mortality rates remain substantial at approximately 12% of STEMI patients with higher rates in higher-risk patients (Fox et al., 2006, Fox et al., 2010). However, the reduced mortality and increased number of STEMI patients surviving after acute MI leads to a greater number of patients at risk of developing heart failure due to post MI remodelling (Go et al., 2014).

1.3.1 Treatment of acute MI

The most effective treatment for STEMI patients is the timely restoration of coronary flow by myocardial reperfusion. Patients with persistent ST-segment elevation and within 12 h after symptom onset should undergo reperfusion therapy as early as possible to salvage myocardium (Schomig et al., 2005, Van de Werf et al., 2008). Different reperfusion strategies are used in clinical practice, such as

PCI, fibrinolytic treatment and coronary bypass surgery. The types of PCIs are then divided into primary PCI, facilitated PCI, and rescue PCI.

Primary PCI (PPCI) is the therapy of angioplasty or stenting performed without prior or concomitant fibrinolytic treatment. PPCI is the preferred therapeutic choice for patients presenting with the signs and symptoms of STEMI (Steg et al., 2012). However, performing PPCI requires an experienced team and only hospitals with established interventional cardiology programme can use PPCI as a routine therapy, which limits the timely application of PPCI. PPCI is effective in restoring coronary flow and can avoid the bleeding risk of fibrinolytic therapy. Randomized clinical trials have shown PPCI is more effective in securing and maintaining coronary patency, improving LV function and clinical outcome compared with fibrinolytic therapy (Keeley et al., 2003). When compared with angioplasty, stent implantation decreases the need for coronary revascularization but does not reduce death or re-infarction rates (Grines et al., 1999, Stone et al., 2002). Some recent clinical trials have shown drug-eluting stents produce a significant reduction in the risk of re-intervention when compared with bare-metal stents (Laarman et al., 2006, Spaulding et al., 2006, Kastrati et al., 2007). Importantly, PPCI should be performed within 2 h after first medical contact and the delay time to PPCI is associated with worse clinical outcome, which diminishes the advantages of PPCI over fibrinolytic treatment (Van de Werf et al., 2008). In order to bridge the time delay, pharmacological reperfusion therapy can be given prior to a planned PCI, which is called facilitated PCI. If a primary fibrinolytic therapy fails to restore the coronary flow, a rescue PCI can be performed on the occluded vessel. Rescue PCI is relatively feasible and safe. A recent meta-analysis has shown that rescue PCI significantly reduced the incidence of heart failure (Wijeysundera et al., 2007).

Fibrinolytic therapy has been an important method of reperfusion treatment for decades. However, PPCI has emerged as the preferred strategy of establishing reperfusion due to the limitations of fibrinolytic therapy such as the inability to establish Thrombosis In Myocardial Infarction (TIMI-3) flow in many cases, high rates of re-occlusion, high rates of recurrent ischaemia, and intracranial bleeding (Armstrong and Collen, 2001b, Armstrong and Collen, 2001a, Aversano et al., 2002). There are three fundamental components for pharmacological reperfusion including the core fibrinolytic agent, the accompanying antiplatelet therapy and

the antithrombotic conjunctive therapy. The tissue plasminogen activator congeners tenecteplase (TNK-tPA) and reteplase (rPA) constitute the most conveniently administered fibrinolytic agents (Van De Werf et al., 1999), whereas conjunctive therapy with intravenous antithrombotics (such as GPIIb/IIIa inhibitors) improves myocardial perfusion (Group, 2000, Antman et al., 1999). However, the increase in systemic and intracranial bleeding in fibrinolytic therapy has led to the reassessment of combination GPIIb/IIIa inhibitors (Topol and Investigators, 2001). Recent studies have shown that the combination of fibrinolysis with antiplatelet therapy by using low molecular weight heparin is an attractive treatment because of reduced re-occlusion and recurrent ischaemia (Assessment of the and Efficacy of a New Thrombolytic Regimen, 2001, White et al., 2001). However, because PPCI has become the choice of reperfusion therapy, current effort is focused on improving the PPCI technique and many intervention operators are no longer willing to randomize the STEMI patients to fibrinolytic therapy.

Coronary artery bypass surgery, also known as coronary artery bypass graft (CABG) surgery, is a surgical procedure connecting a graft vessel to a partially obstructed coronary artery. The graft vessel consists of either the left internal thoracic artery or radial artery or a great saphenous vein harvested from the leg attaching to the aorta. The aim of CABG is to restore normal blood flow to a partially obstructed coronary artery. Therefore, the use of CABG is for unsatisfactorily controlled angina but not for acute MI, but CABG can be applied in MI patients after failed PCI or with mechanical complications such as mitral regurgitation and septal defects (Lee et al., 2003, Thielmann et al., 2006).

A number of new technologies such as coronary thrombectomy and systemic cooling have been tested in catheterization laboratory to improve reperfusion therapy and have been shown to reduce infarct size (Dixon et al., 2002, Geng et al., 2016).

1.3.2 Treatment of post MI remodelling

Post MI remodelling leads to enlargement of the LV chamber and precedes the clinical manifestations of heart failure with reduced ejection fraction. Notwithstanding that reperfusion therapy significantly reduces the mortality rate and infarct size in patients experiencing STEMI. Heart failure develops within 5 years of a first MI in 18% of women and 8% of men between 45 and 64 years of age

(Go et al., 2014). Animal models of MI and clinical studies on ischaemic cardiomyopathy indicate that heart failure is preceded by post MI remodelling with increased ventricular volumes (Konstam et al., 2011, Verma et al., 2008).

There are mechanical and pharmacological approaches for the treatment of post MI remodelling. Mechanical approaches require surgery and are normally reserved for heart failure patients with conduction abnormalities such as left bundle branch block (LBBB) or mitral regurgitation (Takeda et al., 2012). Therefore, pharmacological therapies are the preferred strategy for treating mild heart failure or for preventing post MI remodelling. Chronic ß adrenergic stimulation and renin-angiotensin system activation contribute to post MI remodelling. Pharmacological agents that inhibit these two pathways can prevent post MI heart failure by preventing post MI remodelling.

Angiotensin-converting enzyme inhibitors (ACEi) and angiotensin receptor blockers (ARBs) have consolidated effects for preventing ventricular remodelling, because of their antagonism of the renin-angiotensin-aldosterone system (RAAS) which plays a major role in the regulation of ventricular fibrosis (Foster et al., 1998, Solomon et al., 2005). Using ACEi or ARBs combined with an antialdosterone diuretic is more effective than a monotherapy for reversing ventricular remodelling (Foster et al., 1998).

Adrenergic stimulation increases the contractility of viable myocardium following acute MI and contributes to the maintenance of adequate global cardiac function after infarct. However, chronic and excess ß-adrenergic stimulation leads to LV dilatation and contractile dysfunction (Zhang et al., 2013, Whelan et al., 2013). Therefore, together with ACEi, ARBs and antialdosterone diuretics, ß-blockers are used for preventing post MI remodelling (Cohn et al., 2000). ß-blockers might enhance autonomic control in heart failure by increasing the number of ß-receptors and regulating ß-receptor activity (Koitabashi and Kass, 2012, Leineweber et al., 2005). Long-term use of ß-blockers post MI also reduces mortality by reducing the risk of lethal arrhythmia (Hjalmarson, 1997).

Nitric oxide (NO) donors such as nitrates have shown beneficial effects in heart failure patients (Koitabashi and Kass, 2012, Taylor et al., 2004) and therefore might induce reverse remodelling by reducing preload and increasing cyclic guanosine monophosphate (cGMP) which protects against apoptosis in cardiomyocytes (Jones and Bolli, 2006, Koitabashi and Kass, 2012).

Recently, some novel approaches such as stem cell therapy and gene therapy have shown promising results in pre-clinical and pilot trials in treatment of MI and thus these approaches might reverse post MI remodelling (Hong and Bolli, 2014, Thakker and Yang, 2014, Scimia et al., 2014). Because infarct size is the major risk factor for post MI remodelling (Lund et al., 2007), therapies targeting IR injury that improve myocardial salvage such as ischaemic post-conditioning and cyclosporine have shown therapeutic effect in maintenance of LV volumes (Kloner, 2013). Therefore, therapies targeting IR injury during reperfusion therapy of acute MI might also be expected to prevent post MI remodelling.

1.4 Therapeutic strategies for IR injury

Currently there are no reliable therapies for reducing lethal IR injury in patients with STEMI undergoing PPCI (Hausenloy and Yellon, 2016). Therefore, developing novel therapies that can be administered adjunctive to PPCI to reduce infarct size and improve cardiac contractile function post MI are needed to improve survival and prevent the onset of heart failure in patients with STEMI. A number of new therapeutic strategies for preventing IR injury have shown promise in pre-clinical studies and clinical trials. These therapeutic strategies include mechanical interventions and pharmacologic drugs.

1.4.1 Mechanical interventions

A major breakthrough for reducing IR injury is a mechanical intervention method, known as ischaemic preconditioning. In 1986, Murry et al. reported that in the dog model of coronary artery occlusion, brief cycles of ischaemia and reperfusion before the ischaemia could significantly reduce final infarct size (Murry et al., 1986). Ischaemic preconditioning has been intensively studied over the past three decades and believed to be a powerful intervention for reducing infarct size in IR injury (Hausenloy and Yellon, 2016). However, clinical application of ischaemic pre-conditioning is not possible because the intervention should be performed before the occurrence of ischaemia. Therefore, an alternative method, ischaemic post-conditioning, has been discovered.

Ischaemic post-conditioning refers to the methods of performing intermittent reperfusion before prolonged reperfusion of the ischaemic myocardium. A study in dog IR model shown ischaemic post-conditioning could reduce infarct size by 44% (Zhao et al., 2003). This study also shown a myriad of protective effects of ischaemic post-conditioning, such as reduced levels of oxidative stress, myocardial oedema, polymorphonuclear neutrophil accumulation, and endothelial dysfunction, suggesting ischaemic post-conditioning reduces IR injury. The ability of performing the procedure at the onset of reperfusion in STEMI patients has facilitated the translation of ischaemic post-conditioning into the clinical setting. Investigators have shown in a pilot trial that ischaemic post-conditioning reduced enzymatic infarct size (assessed by total creatine kinase) by 36% and improved myocardial perfusion when compared with control (Staat et al., 2005). However, some studies including the largest clinical trial with 700 patients included have failed to show the beneficial effect of ischaemic post-conditioning (Freixa et al., 2012, Tarantini et al., 2012, Hahn et al., 2013). The reasons for the mixed results might be related to the selection criteria and not the ischaemic post-conditioning protocol itself. Therefore, whether ischaemic post-conditioning can improve clinical outcomes is unclear, and is being studied in an ongoing trial (Hofsten et al., 2015).

Remote ischaemic conditioning is a method of applying IR to another organ or tissue to protect against cardiac IR injury (Przyklenk et al., 1993). Because a major limitation of ischaemic post-conditioning is that the intervention needs to be applied directly to the heart, which is not always possible. The remote ischaemic conditioning, which protects from IR injury by applying intervention to a remote organ or tissue, becomes attractive in clinical application. In the clinical setting, remote ischaemic conditioning can be induced noninvasively by pressing a blood pressure cuff on the upper arm. This approach has been shown to be beneficial in patients undergoing cardiac surgery and elective PPCI (Hoole et al., 2009, Thielmann et al., 2010). Whether remote ischaemic conditioning can improve clinical outcomes in STEMI patients undergoing PPCI is currently being investigated in a clinical trial (Hausenloy et al., 2015).

Other mechanical interventions, such as hyperoxemia and hypothermia, have been reported to be protective against IR injury. Treatment with hyperoxemic

reperfusion with aqueous oxygen in patients with anterior acute myocardial infarction reperfused for less than 6 h shown an improvement in regional wall motion, smaller infarct size, and improved ST-segment resolution (O'Neill et al., 2007). Lowering myocardial temperature during ischaemia can reduce infarct size as experimental studies have shown that infarct size is strongly correlated with temperature in IR model (Duncker et al., 1996).

A strategy which might improve the therapeutic effect of reducing IR injury is a combination of different interventions. A study has shown that combining remote ischaemic conditioning with ischaemic post-conditioning has an additive effect for reducing infarct size in experimental studies (Tamareille et al., 2011). Pilot clinical studies have shown that the combination of remote ischaemic conditioning with ischaemic post-conditioning is more effective than ischaemic post-conditioning alone (Eitel et al., 2015). These studies suggest that the therapy of combining different interventions has therapeutic potential in the clinical setting.

1.4.2 Pharmacologic agents

A number of pharmacological therapies targeting IR injury have been shown to reduce MI size in pre-clinical studies, such as antioxidants, magnesium, erythropoietin, atorvastatin, adenosine, glucose modulators, beta-blockers, MPTP blocker cyclosporine-A, natriuretic peptide, exenatide, and anti-inflammatory agents (Lonborg et al., 2012, Alburquerque-Bejar et al., 2016, Monassier et al., 2016, Hausenloy and Yellon, 2016). However, these agents produced disappointing results when attempted to be given as therapy as an adjunctive to reperfusion in clinical trials. The failure of translation has been attributed to several factors including the weak or unclear benefit in the experimental study and poorly designed clinical trials (Hausenloy and Yellon, 2016). Although the translation of cardioprotection studies has been challenging, new therapeutic targets are still needed because currently there is no reliable treatment which can reduce IR injury in STEMI patients undergoing PPCI. Optimizing the design of the experimental and clinical studies might improve the translation from pre-clinical study to the clinical setting.

1.5 Cathepsins in cardiovascular diseases

1.5.1 Biology of cathepsins

Cathepsins are lysosomal proteases, originally discovered in lysosomes and endosomes and which function to degrade unwanted intracellular proteins (Turk et al., 2000, Turk et al., 1997, Turk et al., 2002). Cathepsins consist of a family of 11 members in humans (cathepsin-B, C, F, H, K, L, O, S, V, W, and Z), while 19 types of cathepsins have been discovered in mice (Turk et al., 2001, Sol-Church et al., 2002). Studies have shown that cathepsins play a role in several diseases including atherosclerosis (Sun et al., 2012a, Jaffer et al., 2007), cardiomyopathy (Petermann et al., 2006, Stypmann et al., 2002a), obesity (Yang et al., 2007, Yang et al., 2008), rheumatoid arthritis (Hou et al., 2002, Asagiri et al., 2008), and cancer (Mohamed and Sloane, 2006). Cathepsin expression and activity has been observed altered in failing cardiac tissues and valve tissues from humans and animals, and in cardiomyocytes, cardiac fibroblasts, endothelial cells, vascular smooth muscle cells, and macrophages in cultured media (Cheng et al., 2006, Cheng et al., 2008, Cheng et al., 2012). Furthermore, recent studies have discovered that pharmacological inhibition of cathepsins can leads to cardiovascular protection in animal models (Cheng et al., 2009, Cheng et al., 2008).

Cathepsins have a high homology with members of the papain family (Coulombe et al., 1996).Their primary structure contains a signaling peptide, proregion, heavy chain and light chain. The D-dimensional structures show that all cysteinyl cathepsins share a common fold (Turk et al., 1998). Most types of the cathepsins are endopeptidases breaking peptide bonds in a peptide chain with a few exceptions breaking terminal ones, such as cathepsin-B (exopeptidase) and cathepsin-H (aminopeptidase) (Turk et al., 2000, Musil et al., 1991, Baici, 1998, Brix et al., 2008). Cathepsins are synthesized as proenzymes with an N-terminal signaling peptide that targets the protein to the endoplasmic reticulum (Kominami et al., 1988, Nishimura et al., 1988). Cathepsins are further processed in the Golgi apparatus for modification of mannose residues to mannose-6-phosphate (Reiser et al., 2010). The mannose-6-phosphate enables cathepsin binding to the mannose-6-phosphate receptor for targeting to the lysosome (Nishimura et al., 1990, Kuliawat et al., 1997). Proteolytic activities are activated in lysosomes by

the action of a number of proteases including pepsin, neutrophil elastase, cysteine proteases, and the aspartic protease cathepsin-D (Nishimura et al., 1988, Rowan et al., 1992). Activated cathepsins are recruited from lysosomes or late endosomes for secretion into the extracellular space *via* Ca^{2+}-dependent fusion to the cell membrane (Brix et al., 2008, Cheng et al., 2012, Reiser et al., 2010).

The cathepsins can be regulated at three levels including transcription, activation, and activity. The most important ways to control the activity of cathepsins include mechanisms of the specific precursor activation and the specific regulation of mature enzymes by pH and the endogenous inhibitors (Turk et al., 2000). Activation of cathepsins is an important step for controlling the activity. The activity of cathepsin is controlled intracellularly by stefins (a specific cystatin subgroup) and extracellularly by cystatins and kininogens (Dubin, 2005, Neurath, 1984). The proregion plays an important role in the inhibition of cathepsin activity (Coulombe et al., 1996, Cygler et al., 1996). The stability and the folding of cathepsins can be affected by partial or complete removal of the proregion (Hanewinkel et al., 1987, Cuozzo et al., 1998). The lysosomes and endosomes provide cathepsins with an acidic pH to keep cathepsin activity optimised for degradation of unwanted substrates (Chapman et al., 1997). Alteration of pH from acid to neutral can cause reduced activity of cathepsin-K and cathepsin-L (Novinec et al., 2007).

Transcriptional regulation of cathepsins can be achieved through transcription factors. The Sp1 and Sp3 transcription factors binding to GC boxes can mediate cathepsin-B and cathepsin-L transcription (Yan et al., 2000, Jean et al., 2002). Ets family transcription factors have been shown to play a role in mediation the transcription of cathepsins, MMPs and serine proteases (Mohamed and Sloane, 2006, Yan et al., 2000). On the other hand, recent studies have shown several transcript variants by using alternative promoters and alternative splicing for cathepsin-B and cathepsin-L (Seth et al., 2003, Mohamed and Sloane, 2006, Arora and Chauhan, 2002). The alternative splicing and exon skipping can cause absence of a signaling peptide on cathepsins leading to its accumulation in the nucleus and mitochondrial matrix (Arora and Chauhan, 2002, Muntener et al., 2004, Reiser et al., 2010). Truncation of cathepsin-L can result in losing the integrity of the glomerular filtration barrier due to proteolyzation of dynamin in podocytes (Sever et al., 2007).

Recently, several novel functions of cathepsins have been characterized, such as prohormone processing, neuropeptide regulation, and inactivation of other proteases (Yasothornsrikul et al., 2003, Hwang et al., 2007, Funkelstein et al., 2008, Wartmann et al., 2010). Cathepsin-L has been identified to play a role in cell development and differentiation through histone modification (Adams-Cioaba et al., 2011, Duncan et al., 2008).

1.5.2 The role of cathepsins in cardiac disease

The role of cathepsins in physiologic and pathological processes in the cardiovascular system have been studied in recent years. Specifically, cathepsins have been found involved in many cellular events in the development of atherosclerosis (Lutgens et al., 2007, Liu et al., 2004). Although cathepsins are abundantly present in the cardiac wall and valve tissues, the function and mechanism of each cathepsin in the heart is largely unknown (Cheng et al., 2006, Helske et al., 2006, Rabkin et al., 2001, Balachandran et al., 2010).

Investigation of the role of cathepsin-L (a cysteine protease) in cardiac pathogenesis has been studied in cathepsin-L knockout mice. Recent findings in mice with nonspecific cathepsin-L knockout from birth have shown that 1-year-old cathepsin-L knockout mice develop dilated cardiomyopathy (Petermann et al., 2006, Stypmann et al., 2002a). In these cathepsin-L knockout mice, cathepsin-L transcripts were undetectable, cathepsin-L protein was not present in lysosomes and cathepsin-L activity was undetected (Roth et al., 2000). The complete deficiency of cathepsin-L leads to characteristics of cardiomyopathy such as interstitial myocardial fibrosis, appearance of pleomorphic nuclei, cardiac chamber dilation and impaired contractile function (Stypmann et al., 2002a). Deficiency of cathepsin-L also affects the cardiomyocyte endo-lysosomal system in new born mice with increased numbers of acidic organelles (Stypmann et al., 2002a). These acidic organelles show altered morphology and lack the typical lysosomal storage materials. These defective acidic compartments are subsequently associated with loss of cytoskeletal proteins (at 8-month age) and mitochondrial impairment (at 4-month age) (Petermann et al., 2006). The interstitial fibrosis observed in the dilative cardiomyopathy of cathepsin-L knockout mice is the only defect that cannot be rescued by transgenic reexpression of cathepsin-L in cardiomyocytes of cathepsin-L knockout mice (Spira

et al., 2007b). These results suggest that the cardiac interstitial fibrosis in cathepsin-L knockout mice results from the absence of cathepsin-L in cardiac fibroblasts and not in cardiomyocytes. Keratinocytes from cathepsin-L knockout mice show sustained growth factor signaling with enhanced recycling of nondegraded plasma membrane receptors and ligands (Reinheckel et al., 2005). The altered growth factor signaling within the endolysosomal compartment cause enhanced Ras, Akt, and MAPK activation and proliferation of basal epidermal keratinocytes, leading to epidermal hyperproliferation and tumor progression in mouse epidermis in cathepsin-L knockout mice (Dennemarker et al., 2010b, Dennemarker et al., 2010a).

In transgenic mice overexpressing cathepsin-L, cathepsin-L activity is increased 4 fold of that in wide type mice. This led to a decreased hypertrophic response with reduced cardiomyocyte apoptosis in models of hypertensive heart failure induced by aortic banding and angiotensin II infusion (Tang et al., 2009). The cardioprotective effect of cathepsin-L overexpression was related to inhibition of Akt signaling (Tang et al., 2009). Thus, the overexpression of cathepsin-L in the endolysosomal compartment of cardiomyocytes is likely to cause immediate proteolysis of endocytosed receptors and ligands. As a consequence, the time span available for receptor signaling and the rate of receptor recycling are decreased, leading to reduced activation of Akt and reduced myocardial hypertrophy (Tang et al., 2009).

Extracellular cathepsins also play a role in cardiac remodelling and repair. Cathepsin-L is typically located in the endosome and lysosome, but some of the proenzyme can be secreted and activated by other proteases like MMPs (Everts et al., 2006, Maciewicz and Etherington, 1988). Activated extracellular cathepsin-L can degrade ECM proteins, such as laminin, fibronectin, and collagen, even with neutral pH (Everts et al., 2006, Maciewicz and Etherington, 1988). Cathepsin-B and cathepsin-S are found in abundance in the LV myocardium of patients with hypertensive heart failure and have been implicated in processing of the ECM during ventricular remodelling as they were upregulated with ECM disruption (Schenke-Layland et al., 2009, Cheng et al., 2006).

Endothelial progenitor cells are recruited to ischaemic areas, then differentiate, leading to neovascularization (Chavakis et al., 2008). The endothelial progenitor cells derived from bone marrow exhibit high levels of cathepsin-L expression and

activity, and the neovascularization in experimental hind limb ischaemia is impaired in cathepsin-L knockout mice (Urbich et al., 2005). Interestingly, the specific impaired cathepsin-L activity has been observed in endothelial progenitor cells in diabetic patients with reduced invasion dependent on glucose concentration (Urbich et al., 2008). Therefore, the impairment of cathepsin-L function by hyperglycemia may relate to the poor neovascularization in ischaemic tissues during diabetes. These results imply that extracellular cathepsin-L may have the potential to play a role during cardiac repair mediated by progenitor cells post MI.

Increased activity of lysosomal enzymes is observed in patients with hypertensive heart failure with various cathepsins playing a role (Cheng et al., 2006). Cathepsin-S and Cathepsin-K were found to be increased in animals and in humans with hypertensive heart failure (Cheng et al., 2006). A recent study has shown cathepsin-B functions as a modulator of hypertrophic response through regulation of TNF-α/ASK1/JNK signaling pathway and cathepsin-B inhibition ameliorates the proapoptotic effect of hypertrophic stimuli (Wu et al., 2015). Loss of cathepsin-L by genetic knockout leads to hypertrophy in conditions of stress with accumulation of protein substrates including myosin, α-actinin, H-cadherin and connexin-43 (Sun et al., 2013). Cathepsin-K knockout alleviated hypertrophy induced by pressure overload and high-fat diet with the inhibition of mTOR and ERK pathways (Hua et al., 2013a, Hua et al., 2013b). Cathepsin-K knockout also attenuated aging-induced cardiac dysfunction and remodelling by suppressing age-induced increase in caspase-dependent and caspase-independent apoptosis (Hua et al., 2015).

Cathepsins have been found increased in plasma or serum in a variety of diseases. Plasma cathepsin-B levels were increased in patients with Alzheimer's disease (Sundelof et al., 2010). Cathepsin-L levels in plasma of pancreatic cancer patients were elevated and associated with poor prognosis (Singh et al., 2014b). Plasma Cathepsin-L was associated positively with the severity of abdominal aortic aneurysms (Lv et al., 2013). Plasma Cathepsin-D levels were reduced and negatively associated with severity of liver inflammation (Walenbergh et al., 2015). In term of MI, cathepsin-D was increased in the plasma of patients post MI (Naseem et al., 2005), and cathepsin-L has been detected in plasma (Zhang et al., 2010) and serum (Liu et al., 2009) with a correlation with disease severity (Liu et al., 2009).

Table 1-1. Various cathepsin inhibitors used *in vivo*

References	Targets	Inhibitors	Dose
In vivo inhibition of cathepsin-B by peptidyl (acyloxy)methyl ketones (Wagner et al., 1994)	Cathepsin-B	Z-Phe-Lys-CHzOCO-(2,4,6-Me)Ph	18 mg/kg orally, 5.0 mg/kg intraperitoneally, 2.4 mg/kg subcutaneously
		Acylox	0.1 mg/kg for heart subcutaneously
Treatment with cathepsin-L inhibitor potentiates Th2-type immune response in Leishmania major-infected BALBc mice (Zhang et al., 2001)	Cathepsin-B	CA074	0.25mg/mouse
	Cathepsin-L	CLIK148	0.2mg/mouse
Cathepsin-S inhibitor prevents autoantigen presentation and autoimmunity (Saegusa et al., 2002)	Cathepsin-B	CA074	0.1mg/mouse/day for 4 weeks
	Cathepsin-L	CLIK148	0.1mg/mouse/day for 4 weeks
	Cathepsin-S	CLIK60	0.1mg/mouse/day for 4 weeks
Cathepsin-B inhibition interferes with metastatic potential of human melanoma an *in vitro* and *in vivo* study (Matarrese et al., 2010)	Cathepsin-B	CA074	10mg/kg iv for 8 days
Trial of the cysteine cathepsin inhibitor JPM-OEt on early and advanced mammary cancer stages in the MMTV-PyMT-transgenic mouse model (Schurigt et al., 2008)	Broad cathepsin	JPM-OEt	100 mg/kg/day intraperitoneally
Macrophages and cathepsin proteases blunt chemotherapeutic response in breast cancer (Shree et al., 2011)	Broad cathepsin	JPM-OEt	100 mg/kg/day intraperitoneally
Cathepsin-B inhibition limits bone metastasis in breast cancer (Withana et al., 2012)	Broad cathepsin	JPM-OEt	50mg/kg/day intraperitoneally for 3 days
	Cathepsin-B	CA074	50mg/kg/day intraperitoneally for 3 days
Effect of cathepsin-K inhibitor basicity on *in vivo* off-target activities (Desmarais et al., 2008)	Cathepsin-K	L-006235	10 mg/kg orally
		balicatib	25 mg/kg orally
		L-873724	10 mg/kg orally
		Cmpd A	60mg/kg orally
Cathepsin-L inhibition suppresses drug resistance *in vitro* and *in vivo* a putative mechanism (Zheng et al., 2009)	Cathepsin-L	iCL	20mg/kg/day for 3days
Effects of an inhibitor of cathepsin-L on bone resorption in thyroparathyroidectomized and ovariectomized rats (Millest et al., 1997)	Cathepsin-L	ALLN	100mg/kg intraperitoneally
Novel epoxysuccinyl peptides. A selective inhibitor of cathepsin-B, *in vivo* (Towatari et al., 1991b)	Cathepsin-B	CA074	8mg/100g intraperitoneally
		CA030	8mg/100g intraperitoneally
		E64a	8mg/100g intraperitoneally

Cathepsins have been shown to be involved in post MI remodelling and in dilated cardiomyopathy (Tsuchida et al., 1986, Ge et al., 2006). The degradation of cardiac structural proteins, including myosin heavy chain, alpha-actinin and troponin-I was observed in the infarcted area in a dog MI model (Tsuchida et al., 1986). Treatment with cathepsin inhibitor Ep459 led to reduced protein degradation with reduced activity of cathepsin-B and cathepsin-L in the infarcted tissue (Tsuchida et al., 1986). Although the exact molecular mechanism remains unclear, studies on doxorubicin-induced cardiotoxicity, MI and dilated cardiomyopathy suggested that cathepsin-B modulated cardiomyocyte apoptosis. In patients with heart failure, the expression of cathepsin-B at both mRNA and protein levels were increased in tissue samples taken from transplanted LV (Ge et al., 2006).

Given that cathepsins have been found increased in the blood and involved in LV remodelling in MI, inhibition of cathepsins may have therapeutic potential. A variety of cathepsin inhibitors have been used in experimental studies (**Table 1-1**) but none of the specific cathepsin inhibitors has been used in the clinical setting (Blondelle et al., 2015). A few cathepsin inhibitors have showed protective effect in animal MI models. Inhibition of cathepsin-B with the specific inhibitor CA074Me was shown to ameliorate post MI remodelling in a rat model (Liu et al., 2013), and inhibition of cathepsins-A with inhibitor SAR1 was protective against post MI heart failure in mice (Petrera et al., 2016). Complete loss of cathepsin-L by genetic knockout from birth may not be protective. Cathepsin-L knockout mice demonstrated deteriorated scar dilatation, wall thinning and cardiac dysfunction post MI as reported by Sun et al. (Sun et al., 2011). However, the detrimental effects of cathepsin-L knockout post MI may be due to the persistent deficiency of cathepsin-L from birth, while using a cathepsin inhibitor the inhibition is highly likely to be partial and temporary. Therefore, the effects of cathepsin-L inhibition by pharmacological agents on MI is currently unknown and is investigated in this study by using a specific inhibitor CAA0225 for the first time.

1.6 Role of *Runx1* in the heart

1.6.1 The *Runx1* gene

The *Runx* gene family encode for DNA-binding transcription factors which regulate the expression of genes related to cell cycle progression and cellular differentiation. The mammalian RUNX family includes three members; RUNX1, RUNX2 and RUNX3. The RUNX family are also termed core binding factor-α (CBFα) and they encode DNA-binding α-subunits that partner core binding factor ß (CBFß) to form heterodimeric transcription factors (Blyth et al., 2005). RUNX1 is also known as core-binding factor subunit alpha-2 (CBFA2) or acute myeloid leukemia 1 protein (AML1) (Avramopoulos et al., 1992). RUNX1 plays a role in regulation of the differentiation of hematopoietic stem cells into mature types and in development of neurons for pain transmitting (Okuda et al., 2001, Chen et al., 2006). To date, most studies related to RUNX1 are focused in the hematopoietic system because in different subtypes of leukemia the function of RUNX1 is found corrupted (Cameron and Neil, 2004).

RUNX1 was first cloned from the DNA of a patient with t(8;21)-positive leukemia (Miyoshi et al., 1991). In humans there are at least 12 RUNX1 mRNA isoforms and three major isoforms are RUNX1a, RUNX1b, and RUNX1c (Levanon et al., 2001). These major isoforms of RUNX1 have the Runt domain located at the N-terminal region. RUNX1a and RUNX1b share the same N-terminal region, resulting from alternative splicing (Miyoshi et al., 1995). RUNX1a and RUNX1b are transcribed from the proximal promoter. RUNX1a lacks the transcriptional regulatory domains within the C-terminal region, while RUNX1b and RUNX1c shares the same C-terminal region (Tanaka et al., 1995). The C-terminal domains of RUNX1 are necessary for normal function and over-expression of a RUNX1 isoform lacking C-terminal domains might lead to abnormal hematopoiesis. Because RUNX1a includes the Runt domain lacking C-terminal domains, it may act as a dominant-negative regulator for other isoforms of RUNX1 (Tanaka et al., 1995, Liu et al., 2009a). RUNX1c is the longest isoform of RUNX1 with its transcript transcribed from a distal promoter (Miyoshi et al., 1995). The different RUNX1 isoforms play specific roles in regulating embryonic hematopoiesis and specifying the hematopoietic stem cell (HSC) (Lam and Zhang, 2012).

The promoters of RUNX1 rely on a cis-regulatory element and contain sites for hematopoietic transcription factors such as Gata2, Ets family members, and Lmo2 (Nottingham et al., 2007, Ng et al., 2010). RUNX1 is characterised by its Runt domain in the N-terminal region. The Runt domain play a role in binding to DNA

and interaction with CBFß. Heterodimerization of RUNX1 and CBFß enhances the DNA-binding ability of RUNX1 (Ng et al., 2010, Ogawa et al., 1993, Wang et al., 1993). NMR spectroscopy measurement of the complex of RUNX1, CBFbeta and DNA has shown that the complex resembles an immunoglobulin fold similar to the DNA-binding domains of NF-kappaB, p53, NFAT1, and the STAT proteins (Berardi et al., 1999, Nagata et al., 1999). Crystal structure investigations of complex RUNX1-CBFbeta-DNA have revealed that CBFbeta interacts with RUNX1 to stabilize its DNA-binding capacity and the diseases associated with RUNX1 mutations relate to its DNA-binding site (Warren et al., 2000, Tahirov et al., 2001, Bartfeld et al., 2002).

1.6.2 Regulation of RUNX1

RUNX1 is regulated through interacting with a number of transcription factors and/or transcriptional co-regulators. Deletion studies of full-length RUNX1 have shown that DNA binding of RUNX1 could be inhibited by the N-terminal and C-terminal regions directly adjacent to the Runt domain (Kanno et al., 1998, Gu et al., 2000). Binding to CBF-beta could suppress this inhibition, thus allows RUNX1 to bind to DNA (Kanno et al., 1998). RUNX1 contains a 31 amino acid region in the C-terminal region, a nuclear matrix targeting signal (NMTS), which aids in transcriptional activation (Zeng et al., 1998). A VWRPY motif located at the C-terminal of RUNX1 is conserved among all Runt family members, which mediates the Groucho//TLE-dependent transcriptional repressor activities (Aronson et al., 1997, Levanon et al., 1998). Ets1 is another transcription factor that interacts with RUNX1, which facilitates transcriptional activity of the T cell receptor by interacting with the Runt domain and its adjacent regions of RUNX1 (Gu et al., 2000, Gunther and Graves, 1994, Kim et al., 1999). Many other factors interacting with RUNX1 are not discussed in this thesis, but include PU.1, C/EBPalpha, p300, mSin3a, GATA1, and Fli1 (Zhang et al., 1996, Petrovick et al., 1998, Kitabayashi et al., 1998, Imai et al., 2004, Xu et al., 2006, Huang et al., 2009). These findings suggest that RUNX1 regulates its target genes in a tissue-specific manner through interactions with transcription factors.

RUNX1 is regulated by various post-translational pathways, as revealed by *in vitro* studies. RUNX1 could be phosphorylated by extracellular signal-regulated kinase (ERK), by which the phosphorylated RUNX1 was detected in $CD34^+$ hematopoietic

progenitor cells (Erickson et al., 1996, Tanaka et al., 1996). Serines 249, 266, 273 and threonine 276 are all ERK-associated phosphorylation sites of RUNX1 that regulate its trans-activation ability (Tanaka et al., 1996, Zhang et al., 2004). Serines 249 and 266 are also phosphorylated by the cyclin-dependent kinase (CDK), which regulate the DNA-binding ability of RUNX1 and its degradation by the anaphase-promoting complex (APC) (Zhang et al., 2008, Biggs et al., 2006). In addition, RUNX1 phosphorylated by the homeodomain-interacting protein kinase 2 (HIPK2) could trigger phosphorylation of p300, and the latter is a transcriptional co-activator that interacts with RUNX1 to activate the transcription of target genes (Aikawa et al., 2006). Furthermore, CBFß facilitates recruiting HIPK2 to phosphorylate RUNX1 (Wee et al., 2008), by which the phosphorylated RUNX1 has reduced interaction with histone deacetylases and mSin3A (a transcriptional co-repressor) (Imai et al., 2004, Guo and Friedman, 2011). RUNX1 is a target of the ubiquitin-proteasome system, a system known to regulate transcription, which leads to the degradation of RUNX1 (Muratani and Tansey, 2003). This ubiquitin-mediated degradation is promoted by CDK phosphorylation and suppressed by heterodimerzation with CBFß (Huang et al., 2001, Biggs et al., 2006). In general, phosphorylation of RUNX1 activates transcription by reducing its interaction with transcriptional repressors. Methylation is another post-translational modification of RUNX1, which could be mediated by PRMT1, an arginine methyltransferase, at a region adjacent C-terminal to the Runt domain. Methylation of RUNX1 inhibits its interaction with Sin3A, which therefore increase its activity on transcription of target genes such as PU.1 and CD41 (Zhao et al., 2008).

1.6.3 *Runx1* and disease

Runx1 is extensively studied for haematological diseases, whilst its role in the heart diseases remains relatively unknown.

Roles of *Runx1* in hematopoiesis

RUNX1 regulates activities of HSCs by acting upstream in the hematopoietic lineage tree, involving cells of both myeloid and lymphoid origins. There are two waves of hematopoiesis, the primitive hematopoiesis and the definitive hematopoiesis, during embryonic development (Palis et al., 1999), during which RUNX1 plays an essential role in the specification of the definitive hematopoietic

stem cells (HSCs). During the definitive hematopoiesis, various lineages of mature blood cell types derive from a common definitive HSC. *Runx1* is a marker of the earliest hematopoietic precursor cells (North et al., 1999). In the mouse embryo, HSCs are detected in the aorta-gonad-mesonephros region at 10.5 days' post conception, when HSCs bud off from the ventral aspect of the dorsal aorta and eventually colonize the fetal liver and *Runx1* is detected in both locations during embryogenesis (Medvinsky et al., 1993, Medvinsky and Dzierzak, 1996).

Studies with *Runx1*-null mice provided evidence for the role of *Runx1* in specifying HSCs (Okuda et al., 1996, Wang et al., 1996); the homozygous knockout mice die between 12.5 to 13.5 days' post conception with severe haemorrhage along the central nervous system, although the heterozygous mice are healthy and fertile. It is reported that the expression of angiopoietin-1 is lacked in these knockout mice, which causes defects in angiogenesis that lead to such extensive haemorrhage (Takakura et al., 2000). In these mice they have no major defect in primitive hematopoiesis but lack definitive hematopoiesis. Recently studies have also shown that *Runx1* plays a fundamental role in the derivation of HSCs from hemogenic endothelium, however, once the HSC is defined, RUNX1 is no longer essential for hematopoiesis (Lancrin et al., 2009, Chen et al., 2009).

RUNX1 is a DNA-binding transcription factor, which mediates transcription of a number of genes, for example, the Runt domain of RUNX1 regulates its binding to the TGT/cGGT consensus sequence (Meyers et al., 1993). In addition, RUNX1 directly binds and mediates the promoter activities of genes related to myeloid growth factor signalling including IL-3, M-CSF receptor, GM-CSF, and c-Mpl (Cameron et al., 1994, Takahashi et al., 1995, Zhang et al., 1994, Satoh et al., 2008), and genes essential to the function of myeloid cells including neutrophil elastase, myeloperoxidase, and mast cell protease 6 (Nuchprayoon et al., 1994, Ogihara et al., 1999). Other targets of RUNX1 include promoters and enhancers of T cell receptors and CD11a promoter in T cell lineage (Hsiang et al., 1993, Sun et al., 1995, Puig-Kroger et al., 2000), and Igα promoters, B cell-specific src family tyrosine kinase (blk), and immunoglobulin antigen receptor enhancers in B cell lineage (Libermann et al., 1999, Zhang and Derynck, 2000, Erman et al., 1998). RUNX1 also controls genes regulating hematopoiesis during the stages of stem cell and early progenitor differentiation; for example, RUNX1 regulates the differentiation and function of regulatory T cells by regulating FoxP3 (Kitoh et al.,

2009, Rudra et al., 2009), the transcription activities in myeloid progenitors by targeting PU.1 (Huang et al., 2008), and megakaryopoiesis by interacting with miR-27a (Ben-Ami et al., 2009).

Mutations in RUNX1 were found in patients with various haematological diseases. In a study with 160 patients with acute myeloid leukemia, mutations of *Runx1* were found in eight patients and were all located in the Runt domain; some of these mutations resulted in abnormal DNA binding to the M-CSF promoter thus altering its transactivation (Osato et al., 1999). Although most mutations are in the Runt domain, some patients have mutations in the C-terminal region of RUNX1. Mutations of RUNX1 in the Runt domain could also cause dominant-negative forms of RUNX1, which is associated with myelodysplastic syndrome (Imai et al., 2000); in addition, mutations in the C-terminal region of RUNX1 might lead to progression to the disease (Michaud et al., 2002, Heller et al., 2005, Churpek et al., 2010). Mutations in the C-terminal region is associated with patients with chronic myelomonocytic leukemia, with which patients have faster progression to acute myeloid leukemia as compared to patients without mutations (Gelsi-Boyer et al., 2008, Kuo et al., 2009). Point mutations in RUNX1 are associated with myeloproliferative neoplasms; when this specific mutant RUNX1 was delivered to CD34+ myeloproliferative neoplasm cells *via* retroviral gene delivery it promoted cell proliferation, indicating a role for leukemic transformation in patients with myeloproliferative neoplasm (Ding et al., 2009). Furthermore, the RNA transcript of RUNX1 is over expressed in patients with myeloproliferative neoplasm, and up-regulates NF-E2 which regulates erythropoiesis (Wang et al., 2010).

RUNX1 is the most common target of chromosomal translocations found in patients with acute leukemia. There are three common types of chromosomal translocations associated with acute leukemia, t(8;21), t(12;21), and t(3;21) (Look, 1997). The t(8;21) is found in 12% of acute myeloid leukemia, which results in RUNX1-ETO, also known as AML1-ETO, RUNX1-MTG8, and RUNX1-RUNX1T1 (Peterson and Zhang, 2004)(11). The t(12;21) is found in 25% of patients with paediatric precursor B-cell acute lymphoblastic leukemia, which results in a fusion with the N-terminal HLH domain of the TEL protein and almost the entire RUNX1 protein (i.e. TEL-RUNX1) (Golub et al., 1995). The t(3;21) is in 3% of patients with therapy-related myelodysplastic syndrome or acute myeloid leukemia (Rubin et al., 1987, Rubin et al., 1990), which results in a fusion with the N-terminal portion

of RUNX1 and one of the three genes (i.e. EVI, MDS1, or EAP) on chromosome three (Nucifora et al., 1994). Other types of chromosomal translocations associated with RUNX1 also have been found in patients with different types of haematological neoplasms (Mikhail et al., 2002, Gamou et al., 1998, Chan et al., 2005).

RUNX1 and heart diseases

Although RUNX1 has been relatively well-investigated in patients with haematological diseases, nothing is known about its functional role in adult patients with heart disease. One obstacle for this knowledge gap is that expression of RUNX1 primarily occurs in neonatal cardiomyocytes, whilst it decreases to minimal levels in adult cardiomyocytes (Kubin et al., 2011, Eulalio et al., 2012). In spite of this, researchers have found that *Runx1* is activated in the cardiomyocytes of both animal models and patients with myocardial infarct (Kubin et al., 2011, Gattenlohner et al., 2003). Kubin and colleagues reported that RUNX1 was activated in the border zone adjacent to the infarct in huma patients with MI and mice three weeks after myocardial infarct. RUNX1 expression was also increased in dilated cardiomyocytes in human patients (Kubin et al., 2011). Gattenlöhner et al. reported that *Runx1* was upregulated at both mRNA and protein levels in heart tissues obtained from patients with ischaemic heart disease (Gattenlohner et al., 2003).

In skeletal muscle, *Runx1* expression is increased after denervation and is required for sustaining skeletal muscle by preventing denervated myofibers from undergoing myofibrillar disorganization and autophagy (Wang et al., 2005). These evidence suggests that *Runx1* activation in cardiomyocytes post MI may not only be a marker of ischemic damage but play a functional role post MI as part of the cardiac remodelling pathophysiology.

1.7 Aims

The overall aim of this thesis is to identify whether two novel targets (cathepsin-L and *Runx1*) have the capacity to improve cardiac function post MI and post IR injury. The study involves establishing two separate complex surgically-induced mouse models of MI and IR injury together with the use of either pharmacological inhibition (cathepsin-L) or cardiomyocyte-specific genetic manipulation (*Runx1*) of the targets to investigate their function.

1.7.1 Establishing mice models of MI and IR injury

The first step of my PhD study was to establish two separate mouse models of MI and IR injury. The mouse is the smallest laboratory mammal which can be used to surgically induce MI with open-chest approach (Chimenti et al., 2004). Whilst this model has the advantage of enabling the utilisation of genetic manipulation, their small size demands the use of precise microsurgical skills. Measuring infarct size and cardiac function using echocardiography and pressure-volume loop catheterisation within these models enabled assessment of the therapeutic potential of these two targets post MI and IR injury.

1.7.2 Investigation of the effect of cathepsin-L inhibitor CAA0225 during ischaemia-reperfusion injury

Using the cathepsin-L specific inhibitor CAA0225, the hypothesis that inhibition of cathepsin-L activity has a protective effect against IR injury was tested in *ex vivo* isolated rat hearts and an *in vivo* mouse model of IR injury and MI. Infarct size and cardiac function was assessed in detail within these experimental models.

1.7.3 Investigation of the effect of *Runx1* deficient in mice post myocardial infarction

Using an established cardiomyocyte-specific tamoxifen-inducible *Runx1* deficient mouse, the hypothesis that *Runx1* deficiency protects against adverse cardiac remodelling post MI and post IR injury *in vivo* was tested. Infarct size and cardiac function was assessed by echocardiography and intraventricular pressure-volume loop analysis.

CHAPTER 2.
General methods

2.1 *Ex vivo* Langendorff perfused isolated heart model of ischaemia-reperfusion (IR) injury

2.1.1 Langendorff isolated heart

Langendorff isolated heart preparation was described by Oscar Langendorff in 1897 (Langendorff, 1897). This technique allows for the maintenance of isolated mammalian hearts for a prolonged period by supplying oxygen and nutrients and therefore enables measurements of cardiac function to be performed *ex vivo*. The fundamental methodology of the Langendorff isolated heart is its perfusion through aortic cannulation. There are two approaches to achieve heart perfusion *ex vivo*, constant flow and constant pressure. Constant flow can be achieved by using a peristaltic pump to drive perfusate, and constant pressure can be maintained by positioning a reservoir at a certain height above the perfused heart. In the context of ischaemia-reperfusion (IR) injury, constant flow systems are used for experiments without regional vascular intervention (e.g. singular coronary occlusion leading to regional infarction). This is because constant flow can lead to an increased coronary arterial pressure if regional ischaemia is produced (Bell et al., 2011). If singular coronary artery occlusion is required then a constant pressure system is more useful (Bell et al., 2011).

The heart can be perfused by either blood or crystalloid buffer. Commonly used crystalloid perfusate buffers include the Krebs–Henseleit solution (Krebs and Henseleit, 1932) and Tyrode's solution (Olders et al., 1990). Compared to blood perfusion, crystalloid perfusion may cause accumulation of tissue water content with deterioration of contractile function (Sutherland and Hearse, 2000).

Measuring function within Langendorff perfused isolated hearts can provide data for different physiological parameters including coronary flow, temperature, electrocardiogram (ECG), myocardial contractility, and left ventricular systolic and diastolic function. Ventricular pressure can be measured by inserting a force transducer into the left ventricle within a balloon. The ventricular balloon technique has been successfully applied in small animals such as rats (Curtis et al., 1986) and mice (Sutherland et al., 2003). Without neuro-humoral control, the denervated isolated heart is bradycardic when compared to the heart *in vivo* (Sutherland and Hearse, 2000). The change in heart rate can affect calcium homeostasis and contractile function (Taylor and Cerny, 1976), therefore pacing

isolated hearts at a specific rate can control the variation in heart rate during experiments.

2.1.2 Setting up the Langendorff system

A constant flow Langendorff system was established in our laboratory for rat hearts **(Figure 2-1)**. Tyrodes solution (in mM; 116 NaCl, 20 $NaHCO_3$, 0.4 Na_2HPO_4, 1 $MgSO_4$-$7H_2O$, 5 KCl, 11 glucose, 1.8 $CaCl_2$) was maintained at 37 °C by keeping the glass reservoirs in a temperature controlled water bath. Drugs or substances for testing could be delivered to the heart by adding them into one of the reservoirs and switching between the reservoirs which was controlled by three-way taps. A constant flow rate was achieved by using a peristaltic pump which delivers perfusate (10mL/min) through a heat maintaining glass chamber. A bubble trap was used to extrude air bubbles before the perfusate enters the heart. Immediately after a schedule one kill by concussion and cervical dislocation, hearts were removed and cannulated using a rat aortic cannula (Harvard Apparatus UK) *via* the ascending aorta and a small incision made in the pulmonary artery for outflow of the perfusion buffer. Next the heart was submerged into a glass bath with warmed perfusion buffer and temperature maintained **(Figure 2-1B)**. For temperature control, the perfusion solution was delivered through a heat exchange coil and the reservoirs kept in a warmed water bath (37°C). The temperature of the perfusate was set to 37 °C through the water bath and heat exchange glassware system. A metal cannula with an affixed polyethylene balloon (made from cling film) was inserted into the LV *via* the left atrium. The polyethylene balloon was then filled with double distilled water (ddH_2O) **(Figure 2-1C)**. Air bubbles were extruded from the inside of the balloon and cannula to prevent alteration of pressure signals. The catheter was then calibrated at 37 °C by using set calibration values of 0 and 100 mmHg (using a digital pressure generator) and then ensuring a 0 mmHg reading on the *ADInstruments Labchart 7* software module when putting the sensor just below the surface of double distilled water at 37 °C. The catheter was then pushed down the cannula to enter the balloon through the opening of a haemostat valve. The LV pressure was measured by the catheter and recorded in *ADInstruments Labchart 7* software. By adjusting the inflation extent of the balloon with a fine syringe, the diastolic pressure was set to 5-8 mmHg before starting the protocol.

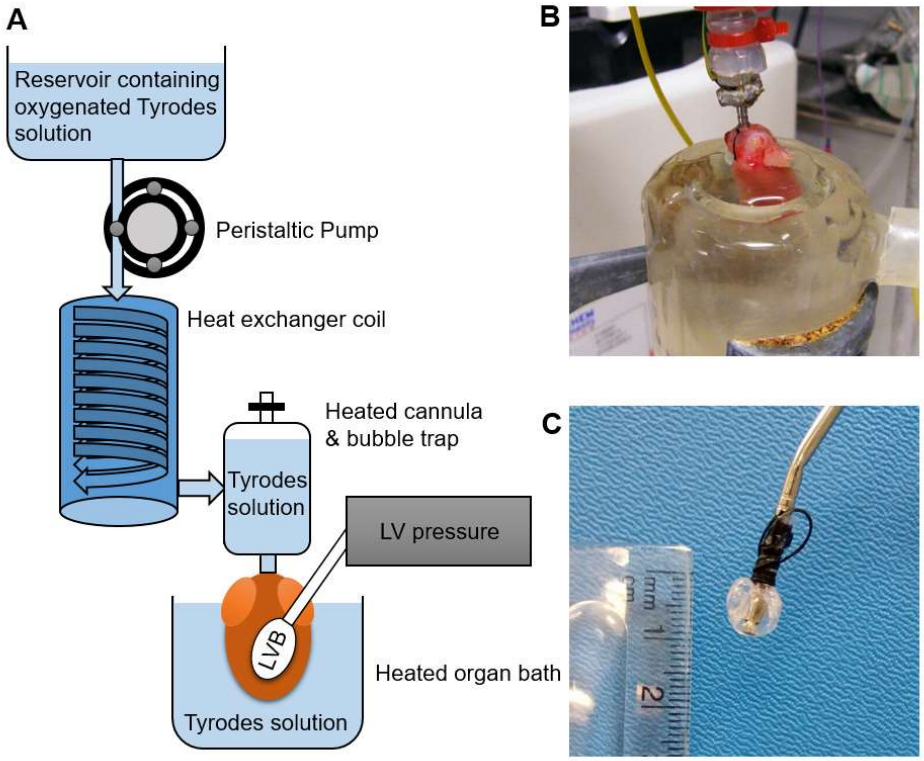

Figure 2-1. Langendorff system for rat isolated heart preparation. (A) A simplified schematic representation of the Langendorff system. A left ventricular balloon (LVB) is inserted into LV, from which LV developed pressure can be measured *via* a pressure transducer within the balloon. Constant flow was maintained by a peristaltic pump. (B) The heart was retrogradely perfused *via* the aorta and placed within a warmed chamber. (C) The LV balloon is made of cling film and is mounted on a metal catheter and inflated with double distilled water.

2.1.3 Heart harvesting and aorta cannulation

Animals were reported in accordance with the ARRIVE guidelines (Kilkenny et al., 2010). Male Wistar rats aged 8-10 weeks (250-300 g) were euthanized in accordance with Schedule 1 of the UK Animal (Scientific Procedures) Act 1986. Rats were first concussed followed by immediate cervical dislocation, which was

confirmed by manual palpation. An incision was then made in the left chest of the animal to break the ribs and create a thoracotomy. The heart was then removed by cutting the descending aorta, inferior vena cava, the ascending aorta and superior vena cava. Next the heart was transferred to a beaker containing ice cold Tyrode's buffer. A small proportion of extra tissue was retained with the heart because this could protect the aorta from damage and thereby be helpful for aortic cannulation. Transferring the heart into the cold Tyrode's solution was required to be done as quickly as possible to prevent the detrimental effects of ischaemia (Bell et al., 2011). Next the heart was transferred directly from the ice cold Tyrode's solution onto the cannula. At this stage the cannula was already in place in the perfusion system and Tyrode's solution was pumped through, preventing air from leaking into the coronary vasculature, which could produce air emboli and cause microvascular obstruction (Bell et al., 2011). The heart was temporarily secured onto the cannula with a vessel clip, and then tied with 2 surgical knots, followed by trimming of the extra tissue. Insertion of the cannula into the aorta was performed carefully to prevent inserting too deeply because this could cause mechanical rupture of the aortic valve leaflets, leading to reduced coronary perfusion and detrimental effect on heart performance (Bell et al., 2011). In contrast, if the cannula was placed above the brachiocephalic artery, perfusate would be drained through the brachiocephalic artery and lead to loss of coronary perfusion pressure.

Once the heart was cannulated and perfused on the Langendorff perfusion system, it began to beat within seconds if it was successfully established. The time taken from sacrifice of the animal to the heart being perfused on the Langendorff system was maintained at less than 5 min to prevent detrimental effects of ischaemia (Awan et al., 1999, Minhaz et al., 1995).

2.1.4 Measuring parameters of cardiac function

Measurement of LV systolic and diastolic function was achieved *via* the inserted LV balloon. This technique has been successfully used in mice (Sutherland et al., 2003) and rats (Awad et al., 1998, Riva and Hearse, 1991). The LV balloon needs to be made of a material that is highly compliant and thin, have no elasticity, and can record signal stably at the range of heart rates (Sutherland et al., 2003, Curtis et al., 1986). The volume of the LV balloon should be able to fill the ventricular cavity

as if it is too small in volume then this would lead to inaccurate estimates of LV function, whereas balloons too large in volume will lead to endocardial necrosis with an altered pre-load diastolic pressure (Bell et al., 2011).

Air bubbles were extruded from the balloon and circuit (because air bubbles are compliant and will dampen the pressure signal). The pressure catheter within the LV balloon was then used to record a range of contractile functional data, including heart rate, maximum pressure, minimum pressure, and derivatives such as the maximum rate of pressure rise (dP/dt_{max}) and fall (dP/dt_{min}). Maintenance of a physiological temperature is important for measuring accurate cardiac functional parameters. Variations in temperature can affect contractility and heart rate (Sutherland and Hearse, 2000, Sutherland et al., 2003, Fukunami and Hearse, 1989). Temperature can also affect myocardial viability following IR injury because lower temperature has a cardioprotective effect (Ferrari et al., 1980, Hale and Kloner, 1999, Hale and Kloner, 1998, Miller and Miller, 1972). The heart temperature was maintained by using a heat exchange column to warm the perfusate combined with submersion of the cannulated heart into warm perfusion solution in a heat exchange organ bath.

Table 2-1. Exclusion criteria for Langendorff isolated hearts

Parameters	From (Bell et al., 2011)	This thesis
Time to perfusion (min)	>3	>5
Arrhythmia Duration (min)	>3	>3
Heart rate (beats per min)	<70 or >400	Maintained at 360
LV developed pressure (mmHg)*	<70 or >130	<60 or >110

* LV pressure is measured with a pre-set diastolic pressure of 5-8 mmHg.

Inclusion and exclusion criteria was used in experiments using Langendorff isolated heart preparations. This was because a number of factors affect the consistency and reproducibility of data, for example, long-time cannulation would lead to myocardial damage and activation of stress signalling pathways (Awan et al., 1999, Minhaz et al., 1995); a damaged aortic wall or aortic valve during dissection or cannulation would lead to high flow rates once perfused (Bell et al., 2011); obstruction of the vasculature would cause low flow rates (Bell et al., 2011); while inadequate perfusion would lead to highly arrhythmogenic and weak

contractile hearts (Bell et al., 2011). These elements could be defined during steady state perfusion ahead of commencing the experimental study as good practice. **Table 2-1** shows exclusion criteria for rats from (Bell et al., 2011) and this thesis. In this thesis the inclusion criteria defined during steady state was as follows: time to perfusion was less than 5 min; arrhythmia duration was less than 3 min; and LV developed pressure was more than 60 mmHg and less than 110 mmHg (with heart rate maintained at 360 beats per min). Because the heart rate was maintained at 360 beats per min, the inclusion criteria of LV developed pressure in this study is lower than the value reported by (Bell et al., 2011).

2.1.5 IR injury in *ex vivo* isolated rat hearts

The Langendorff heart preparation can be used in a variety of studies with the physiological measurements it offers. One of its applications is the isolated heart model of ischaemia–reperfusion (IR) injury. After cannulation, the heart was perfused for a steady-state of 20 min. During the steady-state, it was determined whether the hearts met inclusion criteria as discussed previously. In IR injury studies, pharmacological agents were applied ahead of ischaemia. Global ischaemia was induced by complete cessation of coronary flow (by stopping perfusion completely to the whole heart). An adequate period of ischaemia was crucial for this model as if the period was too short it would not be sufficient to induce infarction whereas if the period was too long it could be detrimental to recovery of contractile function following reperfusion. A 30 min period of ischaemia was sufficient in rat Langendorff model of IR injury (Herr et al., 2015). In current study, we found that a 30 min period of ischaemia was optimal to achieve 25% contractile function recovery and 58% infarction in the control hearts. Reperfusion was initiated by re-establishing coronary flow through switching on the perfusion pump for a total duration of 90 min. Cell death occurs during both the ischaemic period and the reperfusion period (Bell et al., 2011). The duration of reperfusion required for achieving full infarct formation varies between species (Bell et al., 2011). A 30 min period of reperfusion is reported to be sufficient in the mouse heart, due to is high coronary flow rate and no observed differences in infarct size following either 30 or 60 min periods of reperfusion (Sumeray and Yellon, 1998). For rat hearts, studies have shown clear infarct demarcation with 60 min period of reperfusion and no difference in infarct size between 60 or

120 min periods of reperfusion (Schwarz et al., 2000, Ferrera et al., 2009). Therefore, a 90 min period of reperfusion was applied in the studies in this thesis.

2.1.6 Functional data analysis

The LV intraventricular pressure was detected by the pressure catheter within the inflated LV balloon and the pressure traces plotted in Labchart 7 (*ADInstruments*). The developed pressure was defined as the diastolic pressure subtracted from systolic pressure. The dP/dt_{max} and dP/dt_{min} were measured from the derivative of the pressure signal using Labchart 7.

2.1.7 Infarct size analysis

Triphenyltetrazolium chloride (TTC) is the most commonly used biological dye for demarcation of infarct size, which has the ability of crossing cell membranes and binding to intracellular dehydrogenases (Mattson et al., 1947, Schwarz et al., 2000). Viable cells with preserved NADPH (reduced nicotinamide adenine dinucleotide phosphate) are stained red by TTC, while dead cells with NADPH washed out are stained white (Fishbein et al., 1981, Klein et al., 1981). At the end of the reperfusion period, the hearts were removed from the cannula, wrapped in cling film and frozen at -20°C for 45 min. Next, hearts were transversely sectioned into four 2.0 mm slices. TTC (Sigma, Dorset, UK) was dissolved at 1% (m/v) in a phosphate buffer, made by mixing appropriate volumes of 0.1M Na_2HPO_4 and NaH_2PO_4 to achieve a pH of 7.4. The TTC buffer was maintained at 37°C in a water bath. The heart slices were immersed into the TTC solution for 15 min and then fixed in 10% neutral buffered formalin (CellPath, Powys, UK) at 4°C. Photographs of the sections were taken by a Canon camera under a magnifier with ring lights and were converted into JPEG digital images using Adobe Photoshop (Adobe) and converted to a red-green-black image by Image J (National Institute of Health, Maryland, USA). By adjusting the threshold under the green channel, the extent of viable tissue area of each section was determined and the number of pixels counted using Image J. The percent infarct size was calculated using the formula (non-viable pixels/viable and non-viable pixels) × 100%. The final infarct size was expressed as the mean infarct of all 8 faces of the four slices of each heart. This

method for infarct calculation is similar to the commonly used method (Bohl et al., 2009) without weight adjustment.

2.2 *In vivo* mouse models of myocardial infarction (MI) and IR injury

The surgical procedures in this study were performed in accordance with the Animals (Scientific Procedures) Act 1986 and were approved by the University of Glasgow's ethics committee. Animals were reported in accordance with the ARRIVE guidelines (Kilkenny et al., 2010). Animals were given free access to water and food pellets and were housed for a minimum of 7 days to allow an acclimatisation before use.

MI and IR injury were induced in male C57Bl/6 mice aged 9-12 weeks (23-28 g) by performing ligation of the left anterior descending (LAD) coronary artery in open-chest surgery. Due to the small body size of the mouse, inducing MI or IR injury requires experienced microsurgical techniques. Both the open-chest operation and the LAD ligation require rigorous optimisation and refinement to achieve reproducible LAD ligation and infarct size and acceptable survival rates >75%. Each model (MI or IR injury) took ~6 months to achieve these rates.

2.2.1 Establishing microsurgery

The set-up of the microsurgery for MI and IR injury procedures is shown in **Figure 2-2**. These procedures were performed under aseptic conditions. The surgical instruments were autoclaved prior to surgery once per day and decontaminated for each animal during surgery using a dry steriliser (Germinator 500, SouthPointe Surgical Supply Inc, USA). The surgical area was disinfected by spraying 4% chlorhexidine gluconate (Ecolab, U.K.). Sterile surgical drapes were used to cover the surgical table and the animal. Sterile gloves were worn to perform the surgery, one pair for one animal.

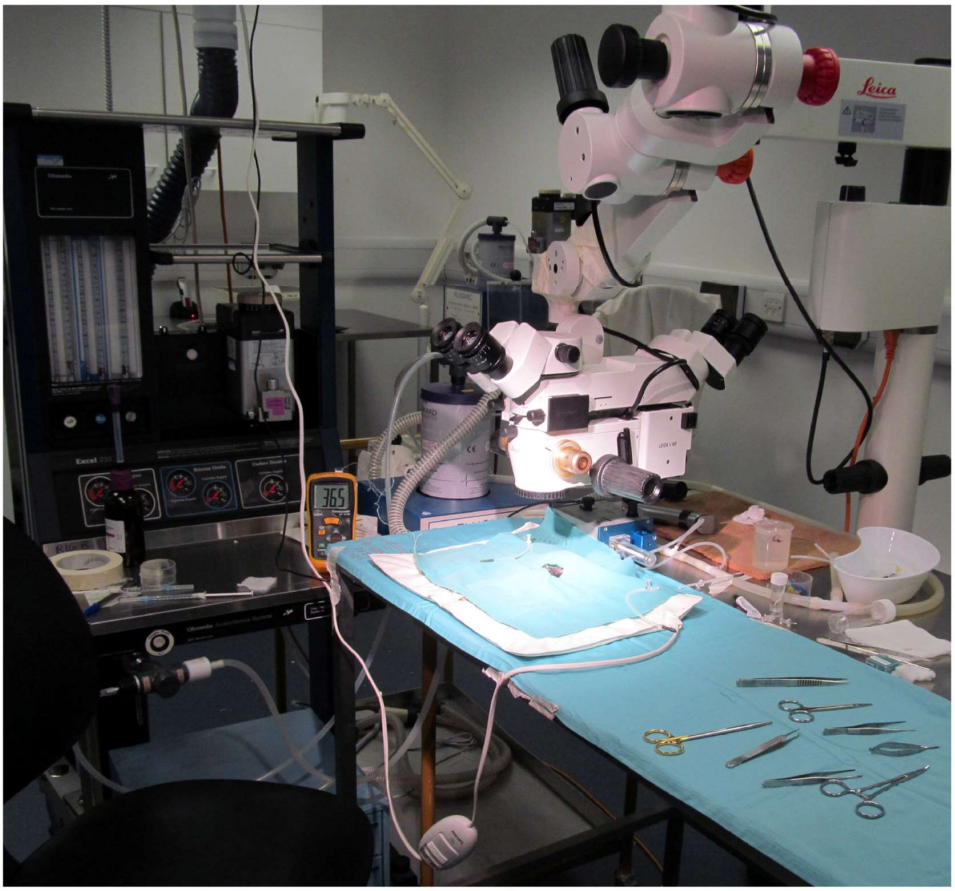

Figure 2-2. The set-up of the microsurgery. The surgical set-up and surgical instruments used for inducing MI and IR injury in mice. The operations were performed under aseptic conditions.

Isofluorane (Isoflo, Abbott Laboratories, USA) mixed with 100% oxygen was used for anaesthesia. Inhalable anaesthetics are easy to control for the depth of anaesthesia and have less depressive effects on the cardiovascular system than other forms of anaesthetics (Richardson and Flecknell, 2005). Anaesthesia was induced by putting the mouse in an induction box. After losing the flexor withdrawal reflex, the animal was moved to a face mask (4% isofluorane; 1.5 L/min). The fur on the entire chest was removed by electric clipper and the skin

disinfected 3 times with 4% chlorhexidine gluconate. The solution was pre-warmed with very minimal wetting of the skin to reduce body heat loss. 5 mg/kg carprofen (Rimadyl, Pfizer Animal Health, U.K.; final volume 20 µl) and 0.1 mg/kg buprenorphine (Vetergesic, Reckitt Benckiser Healthcare Ltd, U.K.; final volume 30 µl) were administered for pre-operative analgesia within 0.4mL normal saline (0.9% sodium chloride w/v) in a single intraperitoneal injection. A sterile ocular lubricant (Lacri-lube ointment, Allergen Inc, USA) was used to protect corneal drying in both eyes during the surgery. Body temperature was maintained at 37 °C during surgery with the use of a heating pad and monitored using a rectal thermometer.

2.2.2 Intubation and ventilation

As the LAD ligation was performed in open chest surgery, respiratory support was needed during the surgery. Therefore, an intubation method with the ability to intubate quickly, reproducibly and with little damage was required. Ventilation was employed by endotracheal intubation, performed through direct visualisation of the endotrachea. To perform intubation, the mouse was anaesthetised and placed under the microscope vertically for visualisation of the tracheal opening (**Figure 2-3)**. The anaesthetised mouse was supported from a suture loop by its front incisors on the vertical side of the L-shaped stand **(Figure 2-3A)**. The tongue was held aside to expose the tracheal opening for insertion of the cannula (**Figure 2-3B**). The stainless steel cannula (25 mm long; 0.8 mm O.D.) (Harvard Apparatus, U.K.) was then carefully inserted into the trachea until the Y-shaped plastic connector entered the mouth. In order to improve the fit within the trachea, a piece of thin silicone tubing was used over the cannula. Once inserted, the Y-shaped plastic tube was connected to a small animal ventilator (Hugo-Sachs, Harvard Apparatus, Germany) and the mouse ventilated at 120 breaths per min with a tidal volume of 120 µl. Chest movements in synchrony with the mechanical ventilation indicated successful intubation and ventilation.

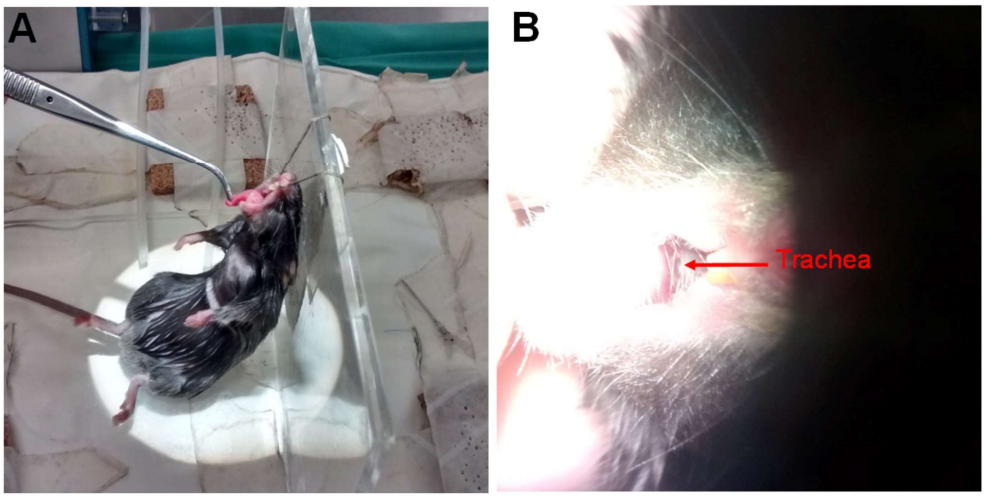

Figure 2-3. Endotracheal intubation of mice. (A) Positioning of the mouse with support of a L-shaped plastic stand and retraction of the tongue for exposure of the trachea. (B) Visualization of the trachea under a surgical microscope for cannula insertion. Arrow indicates trachea.

2.2.3 Opening and closing the chest (Sham surgery)

The mouse models of MI and IR injury were both induced in open-chest surgery. The techniques of opening and closing the chest are fundamental to ensure the mouse can survive following these procedures. The opening and closing chest procedure (including pericardial removal without LAD ligation) was also referred to as sham surgery and was used as a control group.

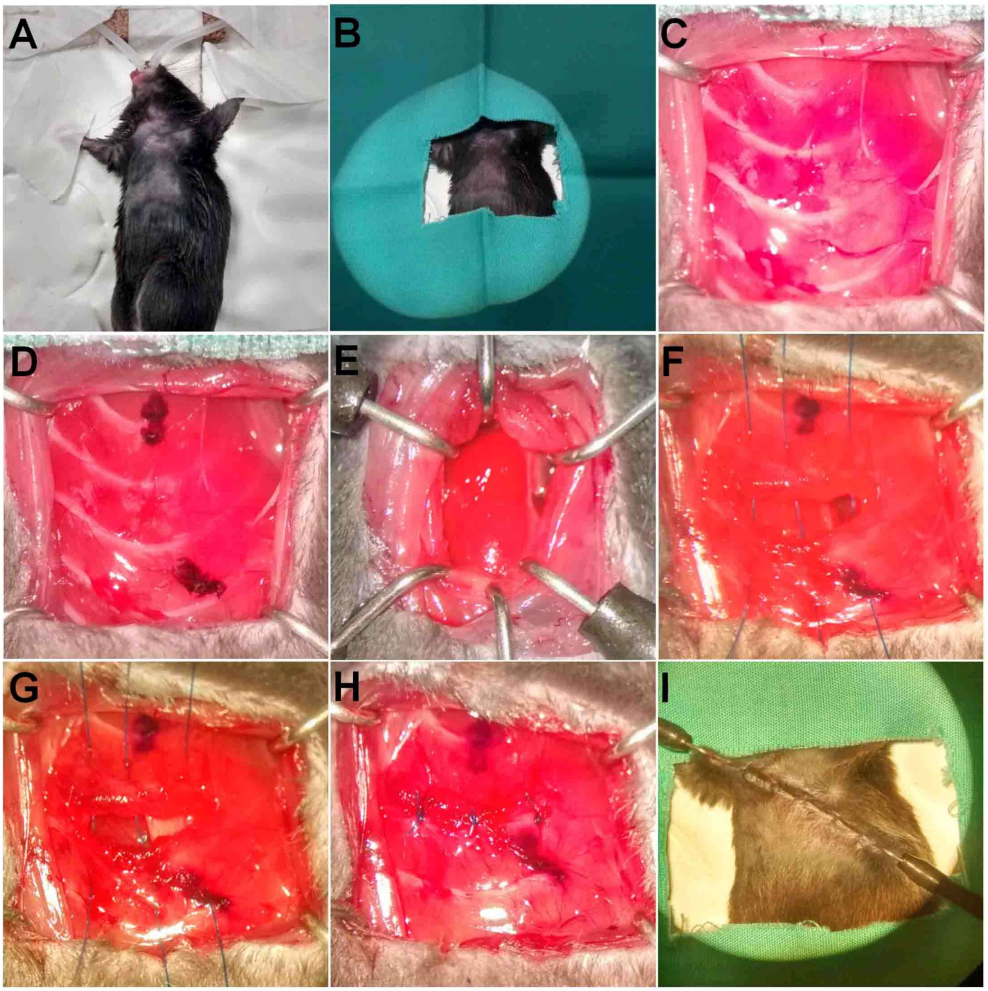

Figure 2-4. The surgical procedure of opening and closing chest of mouse (sham surgery). (A) Positioning of the mouse. (B) Creating a sterile field with surgical drapes. (C) Exposure of the rib cage. (D) Marking the original border of the lung. (E) Opening the thoracic cavity and exposure of the heart with retractors. Following this step, LAD ligation can be applied or pericardium removed without LAD ligation as sham surgery. (F) Closing the chest was started by placing 3 sutures across the incision of the rib cage. (G) Reinflation of the lung to its original place as marked. (H) Closing the thoracic cavity. (I) Sealing the skin. Detailed description of the surgical procedure is in Section 2.2.3.

The mouse was placed on a warm heat pad to maintain body temperature throughout the surgery and positioned in a supine position, slightly turned to the right by retraction of the front left limb. The right front and rear limbs were taped down while the left rear limb was left free for flexor withdrawal (an indicator for the depth of anaesthesia) checks **(Figure 2-4A)**. The mouse was covered by a surgical drape to create a sterile surgical field **(Figure 2-4B)**. The surgery was performed with the aid of a microsurgical microscope. The microscope was set up at the beginning of the surgery by adjusting focus at both the highest magnification and the lowest magnification to ensure it was correctly focused. Prior to incision, flexor withdrawal was checked for sufficient depth of anaesthesia and isofluorane administration was decreased gradually from 4% to 3.5%. Anaesthesia was then continually decreased to a minimum of 1.5% thereafter. A 1.5 cm-long incision was made laterally across the left side of the chest perpendicular to the sternum. The skin and thoracic muscles covering the ribs were retracted by using elastic blunt-hook retractors (Harvard Apparatus, U.K.) **(Figure 2-4C)**. The border of the left lung was marked with a surgical pen **(Figure 2-4D)** and the fourth intercostal space opened with angled forceps *via* penetrating the intercostal muscles. The opening was enlarged carefully by using a battery-operated cauteriser (Harvard Apparatus, U.K.) while preventing damage to the heart or left lung. Blunt-hook retractors were then inserted into the opening to retract the ribs until the heart was fully exposed **(Figure 2-4E)**. After opening the thoracic cavity, the left lung fell down naturally due to having less inflation because of the positioning of the mouse. This ensured that the lung did not need to be manipulated with swabs, which could lead to lung damage. For the sham surgery, the pericardial sac was opened but no LAD ligation was performed, while in MI or IR surgery LAD ligation was performed as stated in section 2.2.4.

To close the chest, the rib retractors were removed and three 6-0 prolene sutures (W8711, Johnson & Johnson, U.K.) placed evenly along the incision **(Figure 2-4F)**. The lungs were re-inflated by pinching the expiration tube until the left lung inflated to the mark of its original place **(Figure 2-4G).** Next the outlet side of the tube was placed underwater in a small beaker containing 100 mL water. The water generated sufficient positive end-expiratory pressure to keep the lungs

inflated while the rib incision was closed. The three pre-placed sutures were then tied to close the thoracic cavity **(Figure 2-4H)**. The thoracic muscles were pulled back with several drops of sterile saline and the skin sutured with absorbable 6-0 vicryl (W9575, Johnson & Johnson, U.K.) **(Figure 2-4I)**. The isofluorane level was gradually decreased before being switched off. Mice were kept incubated until they regained their flexor withdrawal reflex **(Figure 2-5A)**. For some mice that did not regain this reflex in a short time, extubation can be performed to promote them regain spontaneous breath. Mice were placed next to the intubation tube after extubation and given 100% oxygen to allow them to wake up **(Figure 2-5B)**. If the mouse lost spontaneous breath, a rapid re-intubation was performed. After the mouse regained consciousness, it was moved to the recovery cage with soft bedding and heating by a heat pad **(Figure 2-5C)**.

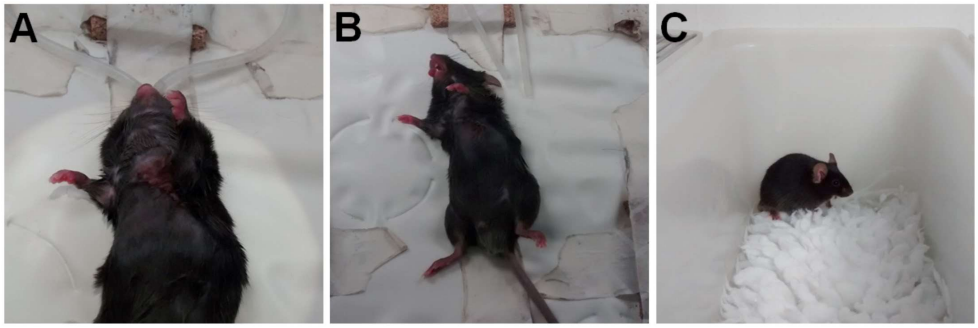

Figure 2-5. Extubation and recovery from open-chest surgery. (A) Mice were kept intubated until regaining flexor withdrawal. (B) Mice were given oxygen before waking up and were prepared for re-intubation in case of respiratory failure. (C) Recovered mice were moved into cages with soft bedding and with maintenance of temperature.

2.2.4 Permanent LAD ligation (inducing MI)

The LAD ligation was performed during the open chest surgery after exposure of the heart. Visualisation of the LAD coronary artery is difficult in mice due to their small body size and deep embedment of the LAD coronary artery in the

myocardium. Therefore, intense lighting and high magnification are important for visualisation of the LAD coronary artery. The LAD coronary artery was visible as a pink vessel running down the LV from the inferior border of the left atrium. For MI surgery the pericardium was removed with forceps and 9-0 nylon non-absorbable suture (W2829 Ethilon, Johnson & Johnson, U.K.) passed around the LAD coronary artery approximately 1.5 mm below the inferior border of the left atrium. A permanent ligation was made to induce infarction. Ligating too close to the left atrium would markedly reduce survival rate. The success of the ligation was determined by the colour changing from red to pale at the apex region of the LV **(Figure 2-6)**.

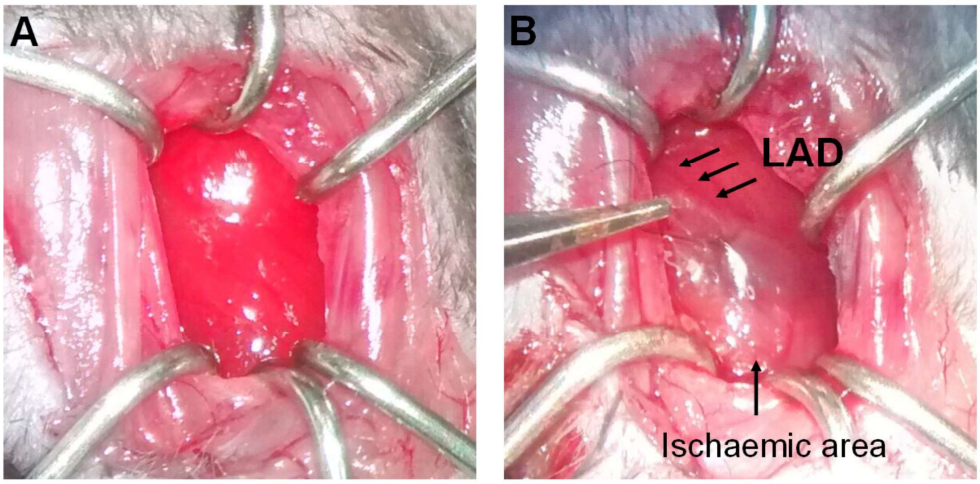

Figure 2-6. Permanent LAD ligation procedure (MI surgery). Permanent LAD ligation was performed following opening of the chest. LAD coronary artery (in pink colour) was visualized under a microscope. Successful LAD ligation led to changing colour of the ischaemic area from red as showed in (A) to pale as indicated in (B).

2.2.5 Temporary LAD ligation (inducing IR injury)

For inducing IR injury, the LAD ligation was temporary. This was achieved by tying the LAD coronary artery against a short section of polyethylene tubing (PE-10; outer diameter, 0.61 mm). After exposure of the heart, a 7-0 polypropylene suture was passed around the LAD coronary approximately 1.5 mm below the inferior border of the left atrium. LAD coronary artery occlusion was induced by ligating the LAD coronary artery against the polyethylene tubing. Once the LAD ligation

had been made, a timer was started to time the ischaemia period for 45 min. During ischaemia, the chest was temporarily closed by releasing the retractors and re-positioning the ribs and muscles. The skin was also temporarily sealed with a vascular clamp. The chest was opened again when the 45min period of ischaemia was almost complete and the polyethylene tubing gently removed when 45min of ischaemia was achieved with the help of a drop of normal saline. The success of ischaemia was determined by the colour changing from deep red to pale red at the apex region of LV, and successful reperfusion indicated by the colour changing back from pale red to deep red **(Figure 2-7)**.

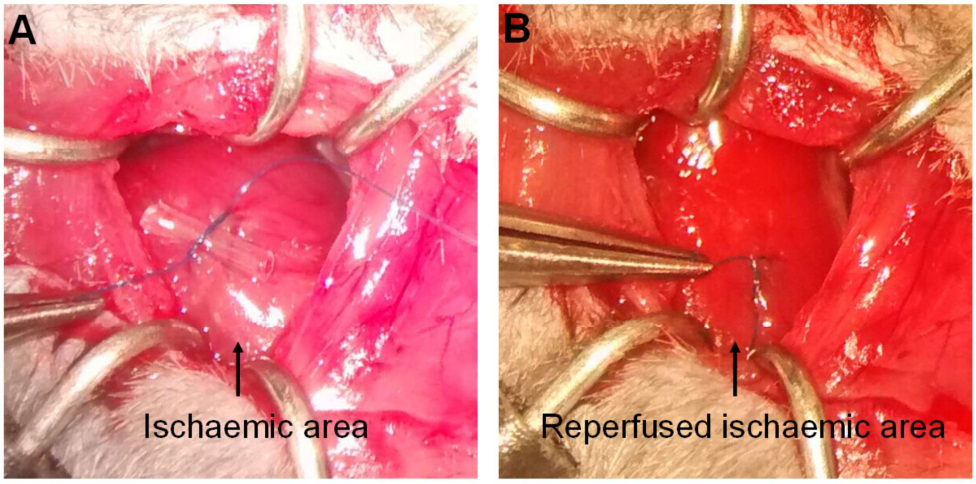

Figure 2-7. Temporary LAD ligation procedure (IR injury surgery). Temporary LAD ligation was performed during the open-chest surgery by tying the LAD coronary artery against a short section of polyethylene tubing. The ischaemic area was visualized under the microscope as pale colored tissue. Reperfusion was induced by removing the polyethylene tubing to release LAD occlusion. The pale ischaemic area indicated in (A) regaining red color (B) indicates successful reperfusion.

2.2.6 Tail vein injection

The cathepsin-L inhibitor was applied by only one injection *via* tail vein following the LAD ligation during the ischaemic period in the surgery **(Figure 2-8)**. An equivalent concentration of DMSO diluted in normal saline was injected in the control group. After the LAD ligation was made, the surgical drape was partly removed and the tail exposed. The tail was slightly rotated until the lateral vein could be visualized. Alcohol (100% ethanol) was applied to the injection site and a 30G needle connected to a 1 mL syringe was inserted into the vein. Once the needle was correctly placed, a flash of blood was observed in the needle hub and the needle was then advanced smoothly into the vein without resistance and the substance injected. During the injection, the blood in the vein was temporarily displaced with the fluid and the vein temporarily display a pale colour. If resistance was felt during injection, the needle was likely to be placed in perivascular space. In this case, the injection was stopped and the needle re-inserted until placed correctly in the vein. Once the substance administration was completed, the needle was removed and a sterile gauze was applied to the injection site with pressure to stop the bleeding.

Figure 2-8. Tail vein injection in surgery. Substances such as the cathepsin-L inhibitor CAA0225 can be delivered *via* tail vein in surgery following LAD ligation, which mimics the clinical setting of pharmacological MI therapy.

The cathepsin-L inhibitor CAA0225 for *in vivo* injection was prepared in normal saline with 15% DMSO. A single dose of 0.25mg CAA0225 (Merck, Darmstadt, Germany) was delivered with 125 μL saline and 15% DMSO (adding DMSO to the compounds first and then saline when making the solution). DMSO was well distributed before injection by shaking the solution. An equivalent amount of DMSO diluted in saline solution without CAA0225 was given to the vehicle control group. The tail vein injection was performed in the 2 min following the LAD ligation.

2.2.7 Post-surgical care

Mice were monitored after surgery by ensuring that sufficient warmth and oxygen were provided. After the mice recovered their mobility they were moved to the recovery room and observed three times a day in the first week after surgery, then daily from the second week. A soft custard was provided in a small dish to feed the mice for one week and post-operative analgesia provided in the form of oral buprenorphine (0.1 mg/kg) administered in *Nutella* for three days after the surgery. Wounds and body weight were monitored according to Home Office regulations. Mice were given the *Nutella* in the week before surgery to improve their interest in it post-surgery. The body weight and eating patterns of each mouse were recorded daily to ensure the food was eaten and the analgesia received. Mice were returned to normal cages and moved back to the housing area after the first week until the time of sacrifice. An autopsy was performed on any mice which died post-surgery.

2.3 Quantification of area at risk and infarct size in the mouse heart following *in vivo* IR injury

The mouse IR injury model mimics the clinical condition of a period of ischaemia followed by reperfusion (Hua et al., 2007). Therefore, the IR injury model provides a good tool to test novel therapeutic strategies for reducing IR injury. The mouse is a good choice as an *in vivo* IR injury model, because of the reduced cost in drug testing than other species and the availability of transgenic mice (Doyle et al., 2012). However, due to the small body size of the mouse, both the open chest surgery and subsequent measurement of infarct size are difficult. Unlike MI where the infarct was transmural, infarction after IR injury was not transmural as shown in **Figure 2-13**. Therefore, the IR injury model allows investigation of the area at risk (AAR) and the infarct size within the AAR. The IR injury demarcates the heart into three regions: the remote myocardium that did not undergo ischaemia; the AAR with ischaemia induced by LAD ligation; and the non-viable area that is dead tissue within the AAR. The ratio of non-viable area to AAR was calculated as the infarct size. The basic methodology was to re-occlude the LAD at the original position, then perfused the heart with Evans blue to stain the remote (perfused)

myocardium. In a second step, TTC was used to delineate viable and nonviable myocardium within the AAR.

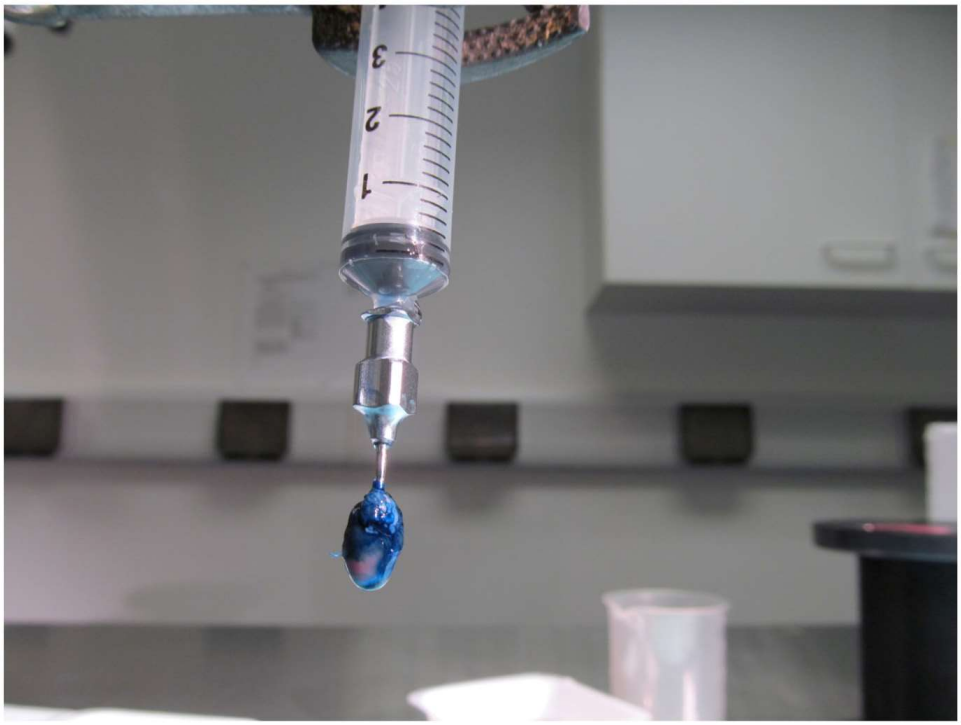

Figure 2-9. Evans blue perfusion demarcating non-ischaemic area. Evans blue solution was perfused into the heart when it is still beating. The dye was distributed after several heart beats. The LAD coronary artery was re-occluded at the place of initial occlusion. The non-ischaemic myocardium was delineated in blue colour but the AAR was left unstained.

2.3.1 Staining the myocardium with Evan's Blue to assess AAR

The mouse was euthanized according to schedule 1 and the heart rapidly excised together with some excess connecting tissue. Care was taken to avoid damaging the aorta and the heart was immersed in saline to extrude the LV blood. The heart

was then transferred to a petri dish and extracardiac tissue trimmed off and the aorta cut proximal to the arch. A 5-mL syringe with a 20-G blunted needle was filled with saline solution and secured by a clamp stand. Air bubbles were extruded from the syringe and needle. The heart was cannulated to the blunt needle through the aorta and secured in position with surgical knot and a 6-0 suture. The needle tip was positioned distal to the aortic valve and the heart perfused with 5 mL saline to rinse out blood from the coronary vasculature. This step improved the demarcation of the border between the red and white coloured tissues (Pitts et al., 2007). The perfusion pressure was carefully controlled to limit the chance that the coronaries could rupture due to the high perfusion pressure and impair dye perfusion. The procedure was completed as soon as possible, normally in 1 or 2 min, to facilitate dye perfusion while the heart was still beating.

Evans blue is the most commonly used dye to stain the remote myocardium (Bohl et al., 2009). A 1% (wt/vol) solution was prepared with 0.9% NaCl and Evans blue powder. The solution was filtered with a 0.2 μm syringe filter (Sartorius Stedim) and air bubbles extruded before use. Since the suture for LAD ligation was left in its original position, re-positioning of the tubing under the knot was performed to re-establish the initial occlusion. Next, 250 μL Evans blue solution was perfused into the heart during beating to distribute the dye. After several heart beats with slow perfusion of Evans blue, the remote myocardium could be delineated but the AAR was left unstained **(Figure 2-9)**.

2.3.2 Preparation of heart sections for measurement of infarct size

The heart was wrapped in cling film and placed at −20°C for 15 min. Next, the heart was placed in a petri dish on ice and sliced into 6–8 parallel transverse sections using a razor blade. The heart sections were then immersed in freshly prepared TTC in a 50 mL Falcon tube at room temperature, and transferred to a water bath at 37°C for 15 min to prevent strong contraction of the heart sections. The Falcon tube was continuously agitated to prevent the tissue from attaching to the tube wall. The heart sections were then removed from the tube, and dried by flattening between tissue paper. Sections were then transferred to 10% neutral-buffered formalin for 90 min, to enhance the red/white contrast between viable and non-viable areas.

2.3.3 Analysis of infarcted tissue

Heart sections were placed on glass and photographed with the help of a glass magnifier and ring light. Both sides of the sections were photographed. The contrast of colour is strongly affected by the light when photographing, therefore the light condition was carefully optimised. Infarct size quantification was performed on digital photographs by contouring the number of pixels of different colours using Photoshop. Areas of non-viable (AON) tissue and the AAR were calculated using the average percent from both sides of each section. The percentage of the sections was then corrected by the weight of the slices:

$$\text{Overall AAR (\% of LV)} = [(\text{Weight}_{\text{Slice 1}} \times \%\ \text{AAR}_{\text{Slice 1}}) + (\text{Weight}_{\text{Slice 2}} \times \%\ \text{AAR}_{\text{Slice 2}}) + \ldots (\text{Weight}_{\text{Slice N}} \times \%\ \text{AAR}_{\text{Slice N}})]/\text{Weight}_{\text{LV}};$$

$$\text{Overall AON (\% of AAR)} = [(\text{Weight}_{\text{Slice 1}} \times \%\ \text{AON}_{\text{Slice 1}}) + (\text{Weight}_{\text{Slice 2}} \times \%\ \text{AON}_{\text{Slice 2}}) + \ldots (\text{Weight}_{\text{Slice N}} \times \%\ \text{AON}_{\text{Slice N}})]/\ [(\text{Weight}_{\text{Slice 1}} \times \%\ \text{AAR}_{\text{Slice 1}}) + (\text{Weight}_{\text{Slice 2}} \times \%\ \text{AAR}_{\text{Slice 2}}) + \ldots (\text{Weight}_{\text{Slice N}} \times \%\ \text{AAR}_{\text{Slice N}})].$$

The final infarct size was expressed as the ratio of overall AON to AAR, which was similar to the method reported by (Bohl et al., 2009).

2.4 Echocardiography

Echocardiography (echo) is extensively used for the evaluation of cardiac function in mouse models of cardiovascular diseases due to its high spatial and temporal resolution.

2.4.1 Mouse echocardiography set up

Anaesthesia was used in mouse echocardiography, because conscious mouse echocardiography requires training of the mouse and two-person operation. Isoflurane was used for anaesthesia because it would cause less depression of cardiac function and was easy to administer (Roth et al., 2002). Using 2% isoflurane as anaesthesia, heart rates of pre-surgical mice were generally 400–500

beats/min and LV fraction shortening (FS) was approximately 40-50%. These values were comparable to the previously published measurements (Stypmann, 2007). The effects of using different anaesthesia on cardiac function are shown in **Table 2-2.**

Echo transducers with frequency higher than 10 MHz are necessary for mice echocardiography because of the small size and rapid heart rate. In our study, a 15 MHz pediatric probe was used (Acuson Sequoia 512, Siemens UK).

To obtain consistent and reproducible echo data, high quality and high resolution images are important for analysis. In addition to good images, the condition of the animals is also crucial, therefore, the mouse body temperature during the echo scanning was carefully controlled and maintained at 37°C and the heart rate was monitored at a similar level. Variation in HR within 100 bpm is considered to be acceptable (Gao et al., 2011). Furthermore, the anaesthetic level and duration as well as the echo measurement time after anaesthesia were controlled at the similar levels between mice.

Table 2-2. Range of normal values for functional cardiac parameters in mice.

Anesthesia	Ket/xyl	Isoflurane	Diazepam
Heart rate (bpm)	320 ± 6	457 ± 17	520 ± 26
Cardiac output (ml/min)	12 ± 1	23 ± 3	17 ± 1
FS (%)	36 ± 1	39 ± 1	50 ± 2
EF (%)	66 ± 2	72 ± 3	82 ± 2

Ket/xyl: Ketamine xylazine i.p.; Isoflurane: isoflurane inhalation 2%; Diazepam: diazepam 17.5 mg/kg i.p.; FS: fraction shortening; EF: ejection fraction. Values of functional cardiac parameters are reported by (Stypmann, 2007).

2.4.2 Echocardiographic measurements

Each mouse was anesthetized in the induction chamber and then maintained *via* facemask on 0.5-1% isofluorane in 1.0 L/min oxygen. The chest hair was shaved before the mouse was positioned on a warm heat pad and body temperature monitored with a rectal thermometer and maintained at 37°C. A shallow left-sided position was used for echo examination. Echo gel was pre-warmed and placed on the chest and the probe placed on the chest contacting the gel and the echo images recorded saved to the echo machine. The probe was placed along the long-axis of the LV to obtain the two-dimensional LV long-axis view. By rotating the probe clockwise by 90º, the LV short-axis view was visualized. The LV M-mode was recorded from the short-axis view at the papillary muscle level. Once scanning was complete, the echo gel was removed with tissue paper and the mouse

recovered on the heat pad with an oxygen supply before being returned to the cage.

LV internal dimensions (LVID), interventricular septal thicknesses (IVS) and posterior wall thicknesses (PW) at diastole and systole (LVIDd, IVSd, PWd and LVIDs, IVSs, PWs, respectively) were measured from transverse M-mode echocardiography images at the papillary muscle level. LV FS was calculated by using the following formula:

FS (%) = 100 × [(LVIDd-LVIDs)/LVIDd]

Due to the LV geometry change in MI/IR injury models, EF calculated by the cubic assumption of LV volume may not be accurate (Gao et al., 2011). Therefore, in this study FS was used to express LV function and FS was found significantly reduced following MI or IR injury. Echocardiography demonstrated that cardiac function was reduced at 2 wk post MI and IR injury in C57Bl/6 mice (**Figure 2-10**). the FS at 2 wk post-surgery was significantly reduced by inducing MI (25 ± 2 *vs.* 44 ± 2 %, MI+DMSO [n = 5] *vs.* Sham+DMSO [n = 9], $P < 0.05$, **Figure 2-10B**) or IR injury (27 ± 3 *vs.* 44 ± 2 %, IR+DMSO [n = 7] *vs.* Sham+DMSO [n = 9], $P < 0.05$, **Figure 2-10B**). The decreased FS was paralleled with increased LVID in hearts with MI and IR injury as showed in **Figure 2-10C, D**.

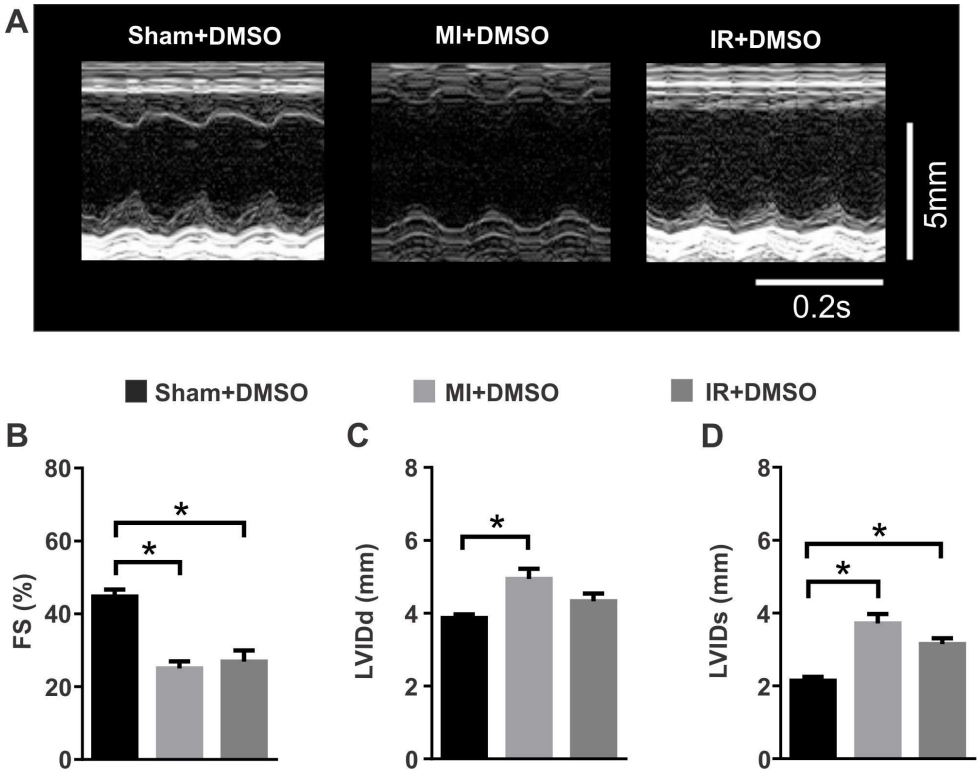

Figure 2-10. M-mode echocardiography demonstrated cardiac dysfunction in hearts underwent MI and IR injury. (A) Typical M-mode echocardiographic images of Sham+DMSO, MI+DMSO and IR+DMSO at 2 wk post-surgery. (B) Mean fractional shortening (FS) data obtained at 2 wk post-surgery for Sham+DMSO (n = 9), MI+DMSO (n = 5) and IR+DMSO (n = 7). Mean echo data at 2 wk post-surgery for (C) Left ventricular internal diameter at systole (LVIDs) and (D) LVID at diastole (LVIDd) (* $P < 0.05$).

2.5 Pressure-volume (PV) loop measurements

The LV PV loop is a measurement of cardiac function, which plots LV pressure against LV volume to generate the loop. The PV loop proceeds in an anticlockwise direction to illustrate instantaneous points throughout the cardiac contraction and relaxation cycle (Lips et al., 2004). The volume of blood in the heart is measured by an electric field. The change of LV volume is correlated to the change of

electrical resistance of the blood pool within the LV (Baan et al., 1984). There are four electrodes located along the axis of the conductance catheter; two outer excitation electrodes and two inner sensing electrodes. The two outer electrodes produce a local electric field by applying a low-amplitude constant current which then passes the blood, the cardiac wall and the surrounding tissues. The two inner electrodes measure the voltage change which is inversely proportional to the conductance. A pressure transducer is located between the two inner electrodes of the catheter for direct pressure measurements within the ventricle.

2.5.1 Surgical procedure for insertion of PV catheter into the LV

Inserting the PV catheter into the LV can be achieved by two main surgical approaches in the rodent heart *in vivo*. The first is an open-chest approach whereby the catheter is inserted into the LV *via* an incision made by thoracotomy to directly expose the heart (Lips et al., 2004). The second is a closed-chest approach where the catheter is inserted into the LV *via* the right common carotid artery and the aortic valve (Lips et al., 2004). The open-chest approach is quicker but it can cause lung collapse and myocardial injury which may influence haemodynamic function (Lips et al., 2004). The open-chest approach is not suitable for MI and IR models as the apical region of the heart with the infarct means there is no stable hold for the catheter. The closed-chest approach is less invasive than the open-chest method, as the lungs are not exposed and the LV is not penetrated by the catheter. The closed-chest therefore provides better haemodynamic stability over a long period of time than the open-chest approach. For this reason, the closed-chest approach was used.

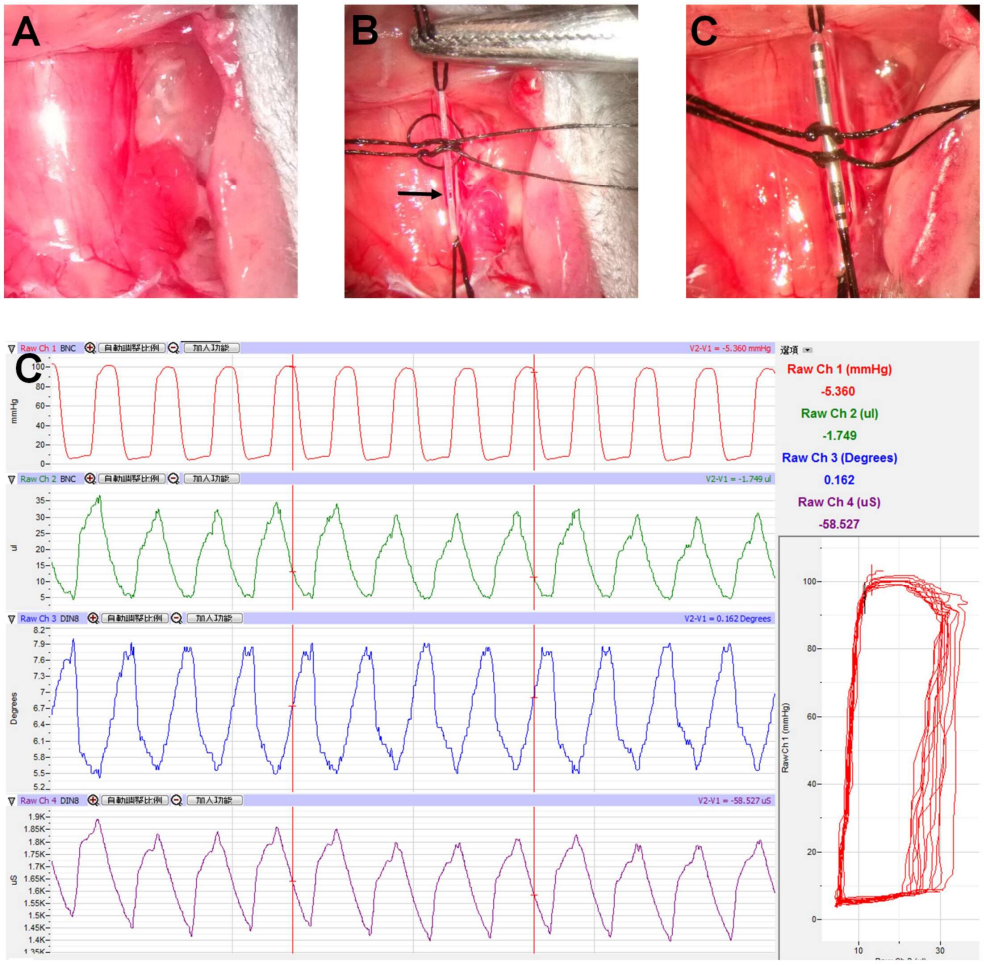

Figure 2-11. Photographs of various steps of mouse LV PV loop performed by close-chest approach. (A) Visualizing the right common carotid artery (RCA) under a microscope. The RCA is inside the carotid sheath with internal jugular vein and vagus nerve. (B) The RCA was dissected and fixed by sutures. A tiny cut (arrow) was made in the RCA at the proximal end to allow insertion of the catheter. (C) The catheter was inserted into the RCA, pushed to the end and tied by sutures to allow advancement into the LV. (D) PV loop data were acquired using LabScribe2 software and loops were generated by plotting pressure against volume.

PV loop experiments were performed using the ADVantage Pressure-Volume System with 1.2F 4.5mm PV catheter (ADV500, Transonic). A 45 min equilibration at 37°C was applied to the catheter before measurement. The catheter was also calibrated for pressure and volume before experimentation by using the pre-set calibration function with the ADV500 system.

Mice were anaesthetised with 4% isoflurane in an induction chamber and maintained on a face-mask. The skin from the neck and upper abdominal areas was shaved and cleaned with chlorohexidine (Hibiscrub, Ecolab Ltd, U.K.). Mice were intubated (via the endotracheal pathway) with a 0.8 mm metal intubation cannula (Harvard Apparatus, U.K.) and ventilated with 1.5% isofluorane at a respiratory rate of 120 per min and a tidal volume of 120 µL (Hugo Sachs Elektronic MiniVent Type 845, Germany). Mice were placed supine on a thermostatically-controlled heat pad with a rectal probe to monitor body temperature at 37°C (Harvard Apparatus, U.K.). The limbs were taped to the heat pad. A cervical incision was made at midline and the muscles retracted to expose the right common carotid artery (**Figure 2-11A**). The carotid artery was dissected to avoid damage to the vagal nerve and blood vessels. Four silk sutures (6-0) were placed around the right common carotid artery and the distal suture at the cranial end was firmly tied to allow anchorage and manipulation of the vessel. The proximal suture at the caudal end was retracted with haemostats to occlude blood flow during cannulation but not tied (**Figure 2-11B**). The other two sutures were loosely placed in the middle of the carotid artery to secure the catheter in place after inserted (**Figure 2-11C**). The inferior vena cava was exposed through an upper abdominal incision at the level of the xiphoid cartilage. Warm swabs were then soaked with saline and placed on the incision sites to avoid heat loss. The catheter was then rebalanced to zero to correct the electrical drift before insertion. A tiny cut was made in the right common carotid artery at the proximal end to allow the insertion of the catheter. The catheter was then inserted into the artery and pushed to the end closest to the junction to the heart and the middle sutures tied to hold it in place. The caudal end suture was then released to allow the catheter to advance to the heart. The pressure was recorded during advancement of the catheter and the diastolic pressure drop (~80 to ~5mmHg)

was used as an indicator that the catheter had entered the LV. The position of the catheter was optimised by fine movements to obtain the tallest and widest loop with the straightest edges achievable. Once this was done, the catheter was secured into place with the sutures. Baseline measurements were recorded for 10 min in a steady state.

2.5.2 Data acquisition and analysis

PV data were acquired using LabScribe2 software (iWorx, New Hampshire, USA) on a Dell laptop. Data were analysed offline using LabScribe2 (iWorx, New Hampshire, USA). A 5 min period of beats in the steady-state after a10 min stabilisation period was used for analysis with exclusion of the loops that displayed interference due to respiratory breaths.

2.6 Organ harvest and weighing

Mice were killed using a Schedule 1 method (cervical dislocation) and the heart, lungs and liver harvested. Organs were weighed using an electronic balance.

2.6.1 Weighing organs

The heart was excised and washed in ice-cold saline (0.9% NaCl). Excess tissues were removed and the aorta mounted to a cannula attached to a syringe. The heart was then perfused retrogradely with 5 mL ice-cold saline to rinse out blood from the coronary arteries. The heart was blotted dry on tissue paper, photographed and weighed. Heart tissue was then fixed in formalin for histological experiments. The lung and liver were removed, blotted dry and weighed but not stored for any further experiments.

2.6.2 Normalisation of organ weights by using ratios of organ weights/body weight or organ weights/tibial length

Organ weight was compared between groups by using ratios of organ weights/body weight or organ weights/tibial length. The length of the mouse tibia was measured through making an incision along the length of the rear left limb and dissecting

the tibia out from surrounding tissues. The distance from the medial condyle to the medial malleolus was measured as the tibial length. Organs harvested at 4 wk post-surgery showed MI or IR injury caused increased heart (**Figure 2-12A, D**) and liver weights (**Figure 2-12B, E**), while there was no significant change in lung weights (**Figure 2-12C, F**).

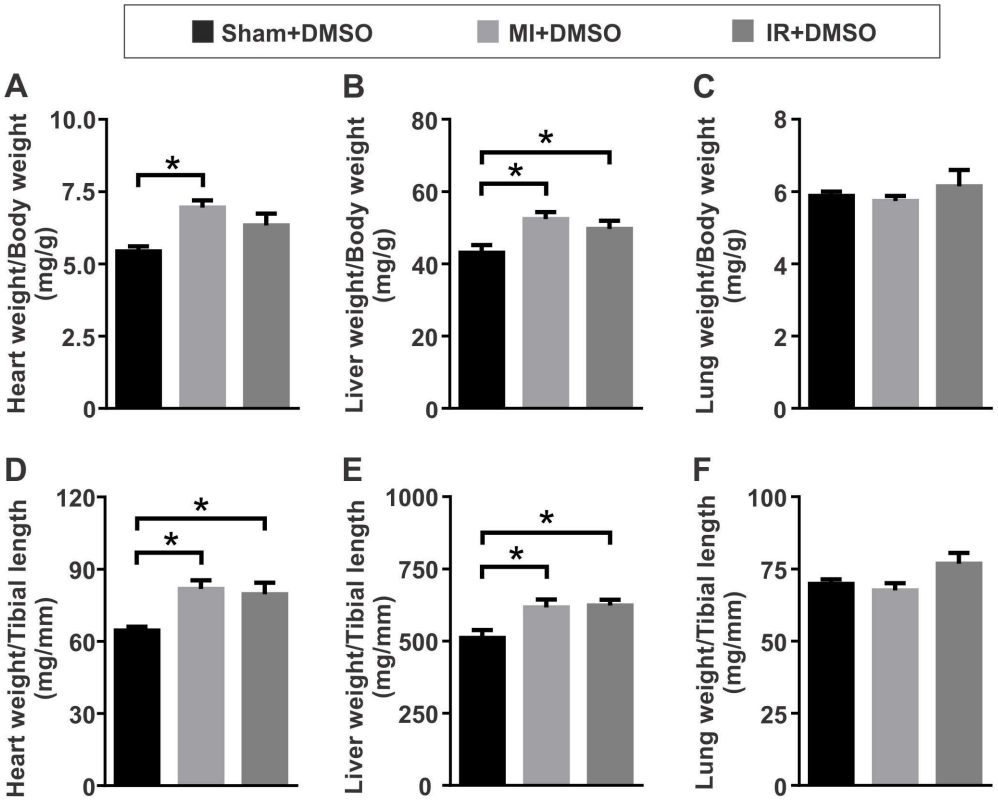

Figure 2-12. Organ weights in mice with MI and IR injury. Mean organ weights ratios obtained at 4 wk post-surgery in three groups: Sham+DMSO (n = 4), MI+DMSO (n = 5) and IR+DMSO (n = 5) for ratios of (A) heart weight/body weight, (B) liver weight/body weight, (C) lung weight/body weight, (D) heart weight/tibial length, (E) liver weight/tibial length, and (F) lung weight/tibial length (* $P < 0.05$).

2.7 Histological studies of MI and IR hearts

2.7.1 Preparation of heart sections

Histological sectioning and staining for mouse hearts were performed by Mrs Lynn Stevenson at the University of Glasgow. Hearts were fixed for a minimum time of 24 hr in 10% neutral buffered formalin (CellPath, U.K.) before being embedded into a wax block until required for sectioning. The heart was sliced parallel to the long axis to produce 1μm thick serial sections at an interval of 250-300 μm. Two adjacent sections were taken at each interval, one for Haematoxylin and Eosin (H&E), a stain in which the haematoxylin stains cell nuclei blue and the eosin stains other intracellular and extracellular structure in pink/red (Fischer et al., 2008), the other for Sirius red, a collagen-specific dye that stains nuclei black, muscle and red blood cells yellow and collagen in red (Malkusch et al., 1995, Cleutjens et al., 1995).

2.7.2 Histological staining of heart sections

Heart sections were deparaffinised in a clearing agent (Citroclear; TSC Biosciences, U.K.) and rehydrated by decreasing concentrations of ethanol: 2 min100% ethanol, 1 min 70% ethanol followed by 1 min cold tap water.

For H&E staining, the sections were submerged in Gill's haematoxylin for 5 min to stain nuclei blue, washed in tap water, differentiated in 1% acid alcohol, and rinsed in water again. Sections were then immersed into Scott's Tap Water Substitute (STWS; a blueing reagent) to arrest differentiation and turn nuclei blue. Next, a 5 min treatment with Eosin was applied to stain the eosinophilic structures including intracellular and extracellular proteins. Sections were then washed in water.

For Sirius red staining, the sections were submerged in Celestine blue for 5 min to stain nuclei. After washed in tap water, the sections were placed in Gill's haematoxylin for 5 min to further stain nuclei, and then washed again with water. The sections were placed in STWS to arrest differentiation and turn nuclei blue. After another wash in water the sections were stained with Sirius red for 6 min to

stain collagen red/orange and muscle/cytoplasm yellow. Finally, the sections were washed in water.

After the completion of the H&E or Sirius red staining, the sections were dehydrated in an ethanol gradient: 1 min 70% ethanol and 2 min 100% ethanol. After the ethanol was cleared, the sections were mounted with dibutyl phthalate xylene (DPX) mounting medium.

2.7.3 Histological morphometry of the mouse heart

The sections were examined and photographed with an EVOS digital microscope (EVOS, USA). The scar was stained red by the Sirius red. In MI hearts the infarction was transmural **(Figure 2-13A)** while in hearts with IR injury the scar was non-transmural **(Figure 2-13B)**. Images were analysed using Adobe Photoshop (Adobe, USA) software. The infarct size of the MI heart was measured using a length based approach (Takagawa et al., 2007). Epicardial and endocardial infarct ratios were calculated by dividing the sum of epicardial or endocardial infarct lengths by the sum of all epicardial or endocardial circumferences from all sections, respectively. The epicardial and endocardial infarct ratios were then averaged to give a mean value for MI infarct size. The infarct size of the IR injury hearts was measured using a pixel-based approach. The number of pixels in a given LV area and red scar area was measured from all sections respectively and the IR infarct size was calculated by dividing the sum of scar pixels by the sum of all LV pixels from all sections, respectively.

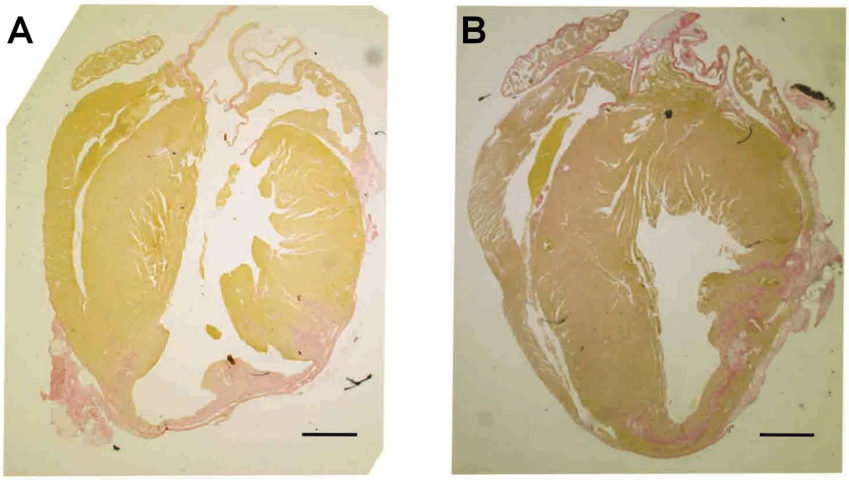

Figure 2-13. Representative MI and IR injury heart slides stained with Sirius red staining. (A) Infarction was transmural in MI hearts showing red color. (B) Scar stained in red color was non-transmural in heart with IR injury. (scale bar: 1mm)

2.8 Statistical Analysis

Statistics were performed in Excel. Comparison between two groups was tested using unpaired, two-tailed Student's t-test. Normality were tested by Shapiro-Wilk test and Kolmogorov-Smirnov test using Prism5 (GraphPad Software, Inc, California). Shapiro-Wilk test has better power than Kolmogorov-Smirnov test, but Shapiro-Wilk test can not apply to groups with small n value (less than 6). So Kolmogorov-Smirnov test were also used in this thesis. For multigroup experiments, ANOVAs were applied using Prism5. Ordinary two-way ANOVA was used to compare the functional measurements in the Langendorff experiments because several treatments were tested for multiple times. Data was represented as averages ± SEM and a value of $P < 0.05$ was considered statistically significant.

CHAPTER 3

The effects of the cathepsin-L inhibitor CAA0225 on LV function in isolated Langendorff perfused rat hearts during IR injury

3.1 Introduction

3.1.1 IR injury in Langendorff perfused isolated hearts

Langendorff perfused isolated hearts can be used to study the pathophysiology of cardiac ischaemia-reperfusion injury. In the isolated heart model of ischaemia-reperfusion injury, cardiac function can be measured during ischaemia-reperfusion and infarct size can be measured at the end of the reperfusion period. This model provides a reliable tool to investigate the effect of pharmacological agents on ischaemia-reperfusion injury (Bell et al., 2011). There are two methods to induce ischaemia, one is stopping the perfusion of the aorta (and therefore all coronary arteries) which induces global ischaemia and the other is occluding a single coronary artery *via* a ligature in order to induce regional ischaemia. The duration of ischaemia and reperfusion are both essential for the ischaemia-reperfusion model. A short period of ischaemia with subsequent reperfusion may induce inadequate sized infarction while a long period of ischaemia can cause complete death of the ischaemic area even though reperfused. A period of 30 minutes' normothermic ischaemia is adequate to induce approximately 50% infarction within the area at risk (Bell et al., 2011). The required duration of reperfusion is related to the species. For rat heart, a recent study demonstrated that 60 min is sufficient to assess function and infarct size (Ferrera et al., 2009). For mouse heart, due to the high coronary flow rate per gram heart, 30 min of reperfusion is sufficient to induce 60% infarct within the AAR (Sumeray and Yellon, 1998). Maintenance of normothermia is critical during ischaemia-reperfusion because hypothermia may attenuate injury (Hale and Kloner, 1999).

Infarct size can be demarcated at the end of reperfusion by using triphenyltetrazolium chloride (TTC) staining. TTC is a cell-permeable dye which can stain viable tissue with preserved NADPH in red colour while non-viable tissue remains unstained (pale) (Mattson et al., 1947). There are two protocols to perform TTC staining. The first is single staining with TTC to determine viable tissue during global ischaemia protocols (Ferrera et al., 2009). The other protocol is a double-dye staining for regional ischaemia protocols (Sumeray and Yellon, 1998, Schwarz et al., 2000). In the latter case, following regional ischaemia, the LAD ligation is re-tied at the end of the reperfusion. Evan's blue dye, which is

made up with saline, is infused into aorta through cannula. The dye will colour the non-risk area of the ventricular wall *via* the coronary system, while the area at risk without dye access remains pink, then subsequent staining of heart slices with TTC to determine viable tissue (red) within the area at risk. Thereafter the TTC staining is performed on heart slices to stain viable tissue within the area at risk which appears red and non-viable tissue appears pale. The double-dye staining technique can be used to express a ratio of infarct as a percentage (%) of area at risk following ischaemia-reperfusion injury.

3.1.2 Cathepsin-L and IR injury

Among the lysosomal proteinases, the cysteine protease cathespin-L and cathepsin-B contribute significantly to non-specific lysosomal proteolysis. The role of these cathepsins in intracellular protein degradation has been demonstrated in mice by the target deletion of cathespin-L (Roth et al., 2000) and cathepsin-B (Deussing et al., 1998). Although cathepsins typically localize in lysosomes and are classically associated with protein degradation, recent studies have shown that several types of cathepsins can be secreted into and function within the extracellular space (Cheng et al., 2012). Recent studies have recognized the function of some cathepsins in cardiovascular diseases, such as cathepsin-F (Oorni et al., 2004), cathepsin-K (Jaffer et al., 2007, Sun et al., 2012b), cathepsin-S (Sasaki et al., 2010), and cathepsin-L (Liu et al., 2006). In ischaemic heart disease, accumulating evidence shows that cathepsin-L plays an important role in pathophysiology. In the mouse model of myocardial infarction induced by left coronary artery ligation, constitutive cathepsin-L knockout mice with a whole body knockout from birth have impaired scar formation and cardiac dilation, which suggests that a basal level of cathepsin-L is necessary to regulate cardiac repairing and remodelling following myocardial infarction (Sun et al., 2011). In the clinical setting, cathepsin-L has been found in plasma (Zhang et al., 2010a) and serum (Liu et al., 2009b) of patients with coronary heart diseases (CHD), and the serum level of cathepsin-L correlated with the severity of coronary heart disease (Liu et al., 2009b). Overall, these observations suggest that whilst complete deficiency of cathepsin-L from birth is deleterious, excess cathepsin-L may be harmful, especially given that the severity of cardiac disease correlates

with cathepsin-L levels in patients with CHD. A study performed in our lab has shown that cathepsin-L was released from *ex vivo* rat hearts during ischaemia-reperfusion injury (unpublished data). The cathepsin-L activity was detected in the coronary artery effluent during reperfusion following 30 min ischaemia in Langendorff perfused hearts but absent in time–control perfused hearts. In separate experiments, application of similar levels of extracellular recombinant cathepsin-L to isolated normal cardiomyocytes led to a reduction in Ca^{2+} release from the sarcoplasmic reticulum, which resulted in a reduction in the calcium transient amplitude and cardiomyocyte contraction. The effect of cathepsin-L inhibition on isolated heart function during ischemia reperfusion is unknown.

3.1.3 A novel cathepsin-L specifical inhibitor: CAA0225

Specific inhibitors of individual cathepsins are useful tools for clarifying different roles of each cathepsin. Hanada *et al*. first isolated an irreversible cathepsin inhibitor E64, which inhibits all cysteine proteases except cathepsin-C (Hanada et al., 1978). Derivatives of L-*trans*-epoxysuccinyl-lle-Pro derivatives, with a modified right side chain of the dipeptide from the leucylagmatine of E64 to isoleucylproline, named CA030 and CA074 showed specific inhibition of cathepsin-B (Towatari et al., 1991a, Turk et al., 1995). CA074 has been widely used in investigations of the specific function of cathepsin-B in lysosomal proteolysis, viral infection and antigen processing (Tohyama et al., 2000, Kominami et al., 1991, Mizuochi et al., 1994, Ebert et al., 2002). Recently, a series of cathepsin-L inhibitors, the cathepsin L inhibitor Katunuma (CLIK) series, have been developed (Tsuge et al., 1999, Katunuma et al., 1999). The CLIK series of inhibitors share an essential structure N-(trans-carbamoyl-oxyrane-2-carbonyl)-L-phenylalanine dimethylamide that can specifically inhibit cathepsin-L activity through establishing a thioester bond with the active site of cathepsin-L, whilst due to N-terminal pyridine part these inhibitors do not fit into the active site of cathepsin-B thus have no effect on it (Tsuge et al., 1999). Kominami *et al*. characterized a novel membrane permeant inhibitor specific for cathepsin-L called compound (2S,3S)-oxirane-2,3-dicarboxylic acid 2-[((S)-1-benzylcarbamoyl-2-phenyl-ethyl)-amide] 3-[[2- (4-hydroxy-phenyl)-ethyl]-amide], also known as CAA0225 (Takahashi et al., 2009). CAA0225 is a cathepsin-L specific inhibitor as it inhibits

rat liver cathepsin-L with IC50 values of 1.9 nM without inhibiting rat liver cathepsin-B (IC50, >1000-5000 nM). CAA0225 is one of the derivatives of E64 and has a structural feature which is similar to the CLIK series (Takahashi et al., 2009). However, CAA0225 has a phenylalanine phenyl-ethyl-amide moiety which substitutes the phenylalanine dimethylamide moiety of the CLIK series, making CAA0225 able to penetrate biological membranes (Takahashi et al., 2009). The cell permeability of CAA0225 can lead to efficient inhibition of cathepsin-L *in vivo* (Takahashi et al., 2009). The concentration of CAA0225 used in this thesis was for inhibition of cathepsin-L without inhibiting cathepsin-B.

3.1.4 Aims of the Chapter

The hypothesis that inhibition of the activity of cathepsin-L or cathepsin-B has a protective effect for ischaemia-reperfusion injury in *ex vivo* isolated hearts will be investigated, by using cathepsin specific inhibitors CAA0225 and CA074Me (membrane permeant form of CA074).

The aims of this chapter are:

i) Explore the effect of the cathepsin-L inhibitor CAA0225 on systolic and diastolic LV function during ischaemia-reperfusion injury.

ii) Explore the effect of the cathepsin-B inhibitor CA074Me on systolic and diastolic LV function during ischaemia-reperfusion injury.

iii) Test if a combination of the cathepsin-L inhibitor CAA0225 and the cathepsin-B inhibitor CA074Me has synergistic effects on cardiac protection during ischaemia-reperfusion injury.

iv) Investigate if the cathepsin-L inhibitor CAA0225 during ischaemia-reperfusion injury alters infarct size.

3.2 Methods

3.2.1 Langendorff retrograde perfusion

Adult male Wistar rats (250 ± 20 g) were sacrificed by Schedule 1 according to the UK Animals (Scientific Procedures) Act 1986. Hearts were collected from the thorax and the adhered lungs and connective tissue were removed. Hearts were

rapidly cannulated *via* the aorta and retrograde perfused with Tyrodes solution (in mM: 116 NaCl, 20 $NaHCO_3$, 0.4 Na_2HPO_4, 5 KCl, 1 $MgSO_4$-$7H_2O$, 11 glucose, 1.8 $CaCl_2$). The Tyrodes solution was bubbled with 95% O_2 and 5% CO_2 to achieve the pH of 7.4 and maintained at 37°C during the experiment. A constant flow rate of 10 mL min^{-1} was applied for retrograde perfusion. Intraventricular pressure was measured by incorporating a fluid-filled cling film balloon coupled with a pressure transducer (Millar Instruments, Houston, Texas) into the left ventricle *via* an incision made on the left atria. The peak left ventricular (LV) pressure (P_{max}), minimum LV pressure (P_{min}), LV developed pressure (P_{dev}) and the maximal rate of LV pressure rise/fall ($dP/dt_{max/min}$) were recorded *via* LabChart7.0 (*ADInstruments*, Oxford, UK). P_{min} before ischemia was started at 5-7 mmHg by adjusting the inflated cling film balloon.

3.2.2 Preparation of cathepsin inhibitors

The cell permeable specific cathepsin-L inhibitor, CAA0225 (Merck, Darmstadt, Germany) and cathepsin-B inhibitor, CA074Me (Merck, Darmstadt, Germany) were dissolved in 100% DMSO (Sigma, Dorset, UK) with a final stock concentration of 10 mM and stored at -20°C. On the experimental day, a 1:10,000 dilution was carried out in Tyrodes solution, producing the final concentrations of 1.0 μM (0.01% DMSO). Non-ischemic control and DMSO vehicle experiments were conducted at 0.01% DMSO.

3.2.3 Protocol of global IR injury

Hearts were perfused for 20 min to reach steady state and next the perfusate was switched to a reservoir containing a known volume. The hearts were perfused for 5 min to regain steady state after which inhibitors/DMSO were added. The hearts were perfused with inhibitors/DMSO for 25 min. Then the global ischaemia was induced by stopping perfusion for 30 min. Following 30 min ischemia, hearts were reperfused with Tyrodes solution for 90 min. The protocol and example traces are shown in **Figure 3-1**.

3.2.4 Infarct staining

Following 90 min reperfusion, infarct size was measured by triphenyltetrazolium

chloride (TTC) staining. At the end of the reperfusion, the hearts were decanulated and wrapped in cling film for 45 min frozen at -20°C before being transversely sectioned into four 2.0 mm slices. The white compound of TTC (Sigma, Dorset, UK) was dissolved at 1% (m/v) in a phosphate buffer, made by mixing the appropriate volumes of 0.1M Na_2HPO_4 and NaH_2PO_4 to achieve a pH of 7.4. The TTC solution was warmed to 37°C in a water bath. The heart slices were submersed in TTC solution for 15.0 min at 37°C. After being in TTC solution for 15min, the heart slices were fixed in 10% neutral buffered formalin (CellPath, Powys, UK) at 4°C. Photographs were taken of the heart sections and converted into planar images by using Adobe Photoshop (Adobe). The images were converted to a red-green-black image by Image J (National Institute of Health, Maryland, USA). By adjusting the threshold under the green channel, the extent of viable tissue area of each section was determined and the number of pixels counted using Image J. The percentage of infarct size was calculated using the formula (viable pixels/non-viable pixels) × 100%. The mean infarct size was calculated from all 8 faces of the four slices of each heart.

3.2.5 Statistics

Data are expressed as mean ± SEM. To compare a particular data set with the control an unpaired two-tailed Student's t-test was performed. Multiple groups measured at several times were compared with two-way ANOVA. A value of $P < 0.05$ was considered statistically significant.

3.3 Results

3.3.1 IR injury caused impaired cardiac function in Langendorff isolated hearts

Experimental procedures of the four groups are summarised in **Figure 3-1A**, including DMSO, IR+DMSO, IR+CAA0225, IR+CAA0225&CA074Me. Representative traces of LV developed pressure at 120 min are showed in **Figure 3-1B**. Another group IR+ CA074Me, which was not shown in Figure 3-1, was tested by Lisa McArthur. In the DMSO group, there was a 13% reduction of P_{dev} following 160 min perfusion (from 74 ± 5 to 64 ± 2mmHg; time point -40 to time point 120; $n = 6$; **Figure 3-2A Green line**). In the IR+DMSO group, the P_{dev} was parallel to that in

the DMSO group before ischaemia and dropped to 0 mmHg during ischaemia, which then started to increase at the onset of reperfusion and by the end of reperfusion recovered to 25 ± 2 % of that at the pre-ischaemic level (90 ± 3 *vs.* 23 ± 2 mmHg; time point 0 *vs.* time point 120; **Figure 3-2A Black line**).

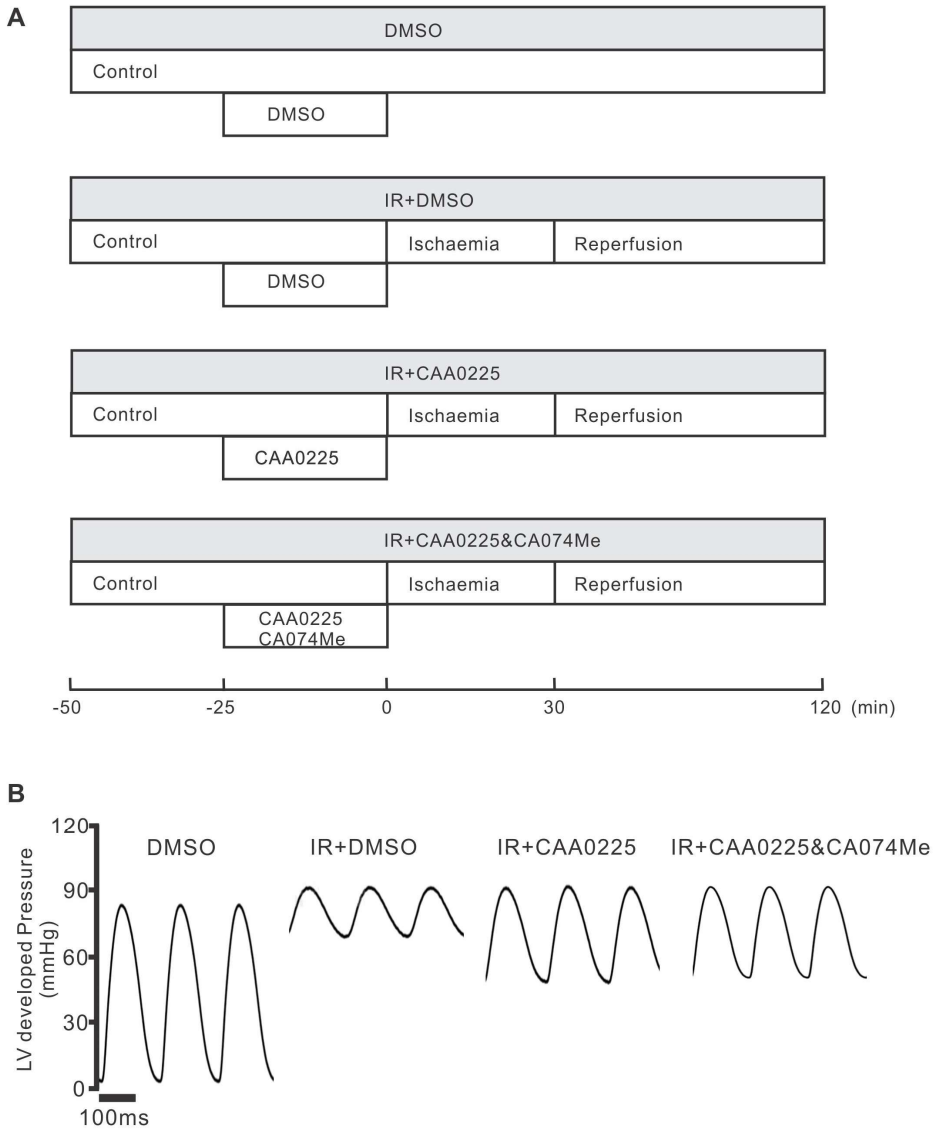

Figure 3-1. Langendorff isolated heart model of IR injury in rats. (A). Protocol of IR injury in isolated hearts. Hearts undergoing IR injury were perfused 25 min for steady state, 25 min for drug/vehicle, 30 min ischaemia and 90 min reperfusion. Four cohorts of hearts were tested: DMSO, IR+DMSO, IR+CAA0225 and IR+CAA0225 & CA074Me. (B). Typical LV pressure traces taken at time point 120 min.

IR injury also impaired other indices of systolic and diastolic cardiac function. By the end of reperfusion, the maximal rate of LV pressure rise (dP/dt_{max}) dropped to 30 ± 2 % of the pre-ischaemic value (**Figure 3-3B Black line**) and the maximal rate of LV pressure fall (dP/dt_{min}) dropped to 32 ± 3 % of the pre-ischaemic value (**Figure 3-3C Black line**). Minimum pressure (P_{min}) increased from 5 ± 0 to 78 ± 5 mmHg (time point 0 *vs.* time point 120 [*n* = 15]; **Figure 3-3D Black line**). In the hearts perfused with no ischaemia,

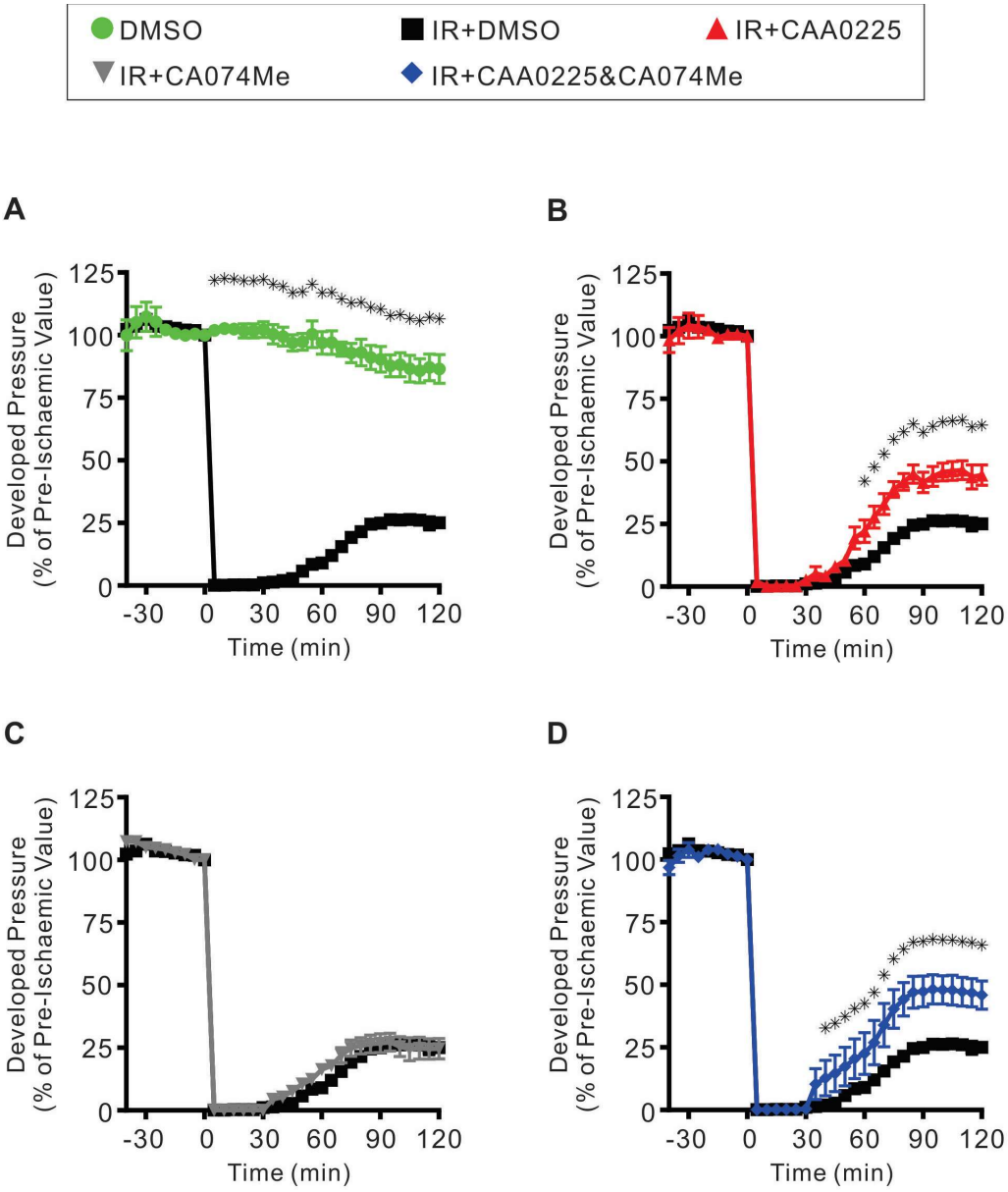

Figure 3-2. Developed pressure change pre/post ischaemia. (A) Mean developed pressure data of DMSO (n = 6) and IR+DMSO (n = 15) (* P < 0.05, DMSO *vs.* IR+DMSO). (B) Mean developed pressure data of IR+DMSO (n = 15) and IR+CAA0225 (n = 6) (* P < 0.05, IR+DMSO *vs.* IR+CAA0225). (C) Mean developed pressure data of IR+DMSO (n = 15) and IR+CA074Me (n = 8) (* P < 0.05, IR+DMSO *vs.* IR+CA074Me). (D) Mean developed pressure data of IR+DMSO (n = 15) and IR+CAA0225&CA074Me (n = 10) (* P < 0.05, IR+DMSO *vs.* IR+CA074Me).

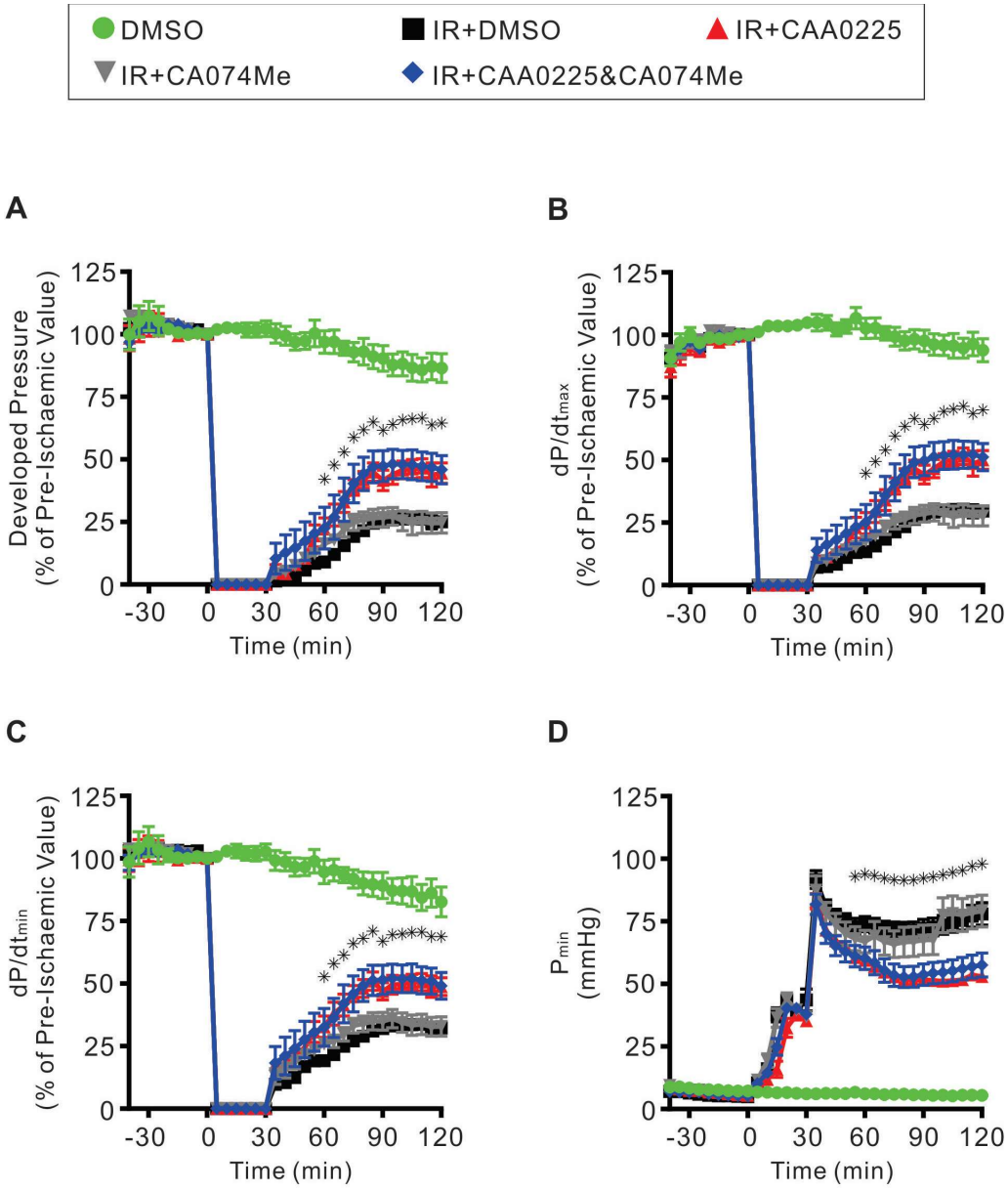

Figure 3-3. Systolic and diastolic parameters pre/post ischaemia. (A) Mean developed pressure data of DMSO (*n* = 6), IR+DMSO (*n* = 15), IR+CAA0225 (*n* = 6), IR+CA074Me (*n* = 8) and IR+CAA0225&CA074Me (*n* = 10). (B) Maximal rate of LV pressure rise (dP/dt_{max}). (C) Maximal rate of LV pressure fall (dP/dt_{min}). (D) Minimum pressure (P_{min}). (* $P < 0.05$, IR+DMSO *vs.* IR+CAA0225).

3.3.2 Cathepsin-L inhibitor CAA0225 improved both systolic and diastolic LV function during IR injury

The treatment of cathepsin-L inhibitor CAA0225 improved overall LV function during IR injury (**Figure 3-2B**). The P_{dev} at 120 min recovered to 45 ± 4 % of the pre-ischemic value (76 ± 7 *vs.* 33 ± 2 mmHg; time point 0 *vs.* time point 120 [*n* = 6]; **Figure 3-2B**), which was 177% of that in the IR+DSMO group (25 ± 2 *vs.* 45 ± 4 % of pre-ischaemia value; IR+DSMO [*n* = 15] *vs.* IR+CAA0225 [*n* = 6]; *P* < 0.05; **Figure 3-2B**). Other systolic and diastolic parameters, dP/dt_{max} dP/dt_{min}, respectively and P_{min} were also improved by CAA0225 treatment. In the IR-CAA0225 group, the dP/dt_{max} at 120 min recovered to 50 ± 4 % of pre-ischaemic value (**Figure 3-3B**) and the dP/dt_{min} at 120 min recovered to 49 ± 4 % of pre-ischaemic value (**Figure 3-3C)**, which were of 169% and 151% of those in the IR+DSMO group, respectively. Although there was no significant change of the P_{min} during the ischaemic period between the IR-CAA0225 and the IR+DSMO groups, it was significantly reduced during reperfusion in the IR+CAA0225 group (53 ± 2 mmHg), which was 68% of that in the IR+DSMO group (78 ± 5 mmHg; *P* < 0.05; **Figure 3-3D**). There was no significant difference in half-time recovery to maximum P_{dev} between these groups (68 ± 2 *vs.* 61 ± 2 min of time point; IR+DSMO [*n* = 13] *vs.* IR+CAA0225 [*n* = 6]; *P* > 0.05; **Figure 3-4A**). It was also noted that CAA0225 didn't change LV developed pressure before induction of ischaemia (78 ± 5 *vs.* 76 ± 7 mmHg [*n* = 15]; pre-CAA0225 treatment *vs.* 25 min post-CAA0225 treatment; *P* > 0.05; **Figure 3-4B**)

3.3.3 Effects of Cathepsin-B inhibitor CA074Me on LV function during IR injury

The cathepsin-B inhibitor CA074Me did not improve overall LV function (**Figure 3-2C**). In the IR-CA074Me group, the P_{dev} at 120 min recovered to 24 ± 4 % of pre-ischaemic value (101 ± 4 *vs.* 24 ± 4 mmHg; time point 0 *vs.* time point 120 [*n* = 8]; **Figure 3-2C Grey line**). The dP/dt_{max} at 120 min recovered to 28 ± 4 % of pre-ischaemic value (**Figure 3-3B Grey line**) and the dP/dt_{min} recovered to 33 ± 4 % of pre-ischaemic value (**Figure 3-3C Grey line**). The P_{min} increased from 6 ± 1 to 79 ± 6 mmHg (time point 0 *vs.* time point 120 [*n* = 8]; **Figure 3-3D Grey line**). However, CA074Me did improved the rate of recovery as it significantly reduced the duration to half maximal P_{dev} recovery (68 ± 2 *vs.* 54 ± 4 min of time point; IR+DSMO [*n* =

13] *vs.* IR+CA074Me [*n* = 8]; *P* < 0.05; **Figure 3-4A**).

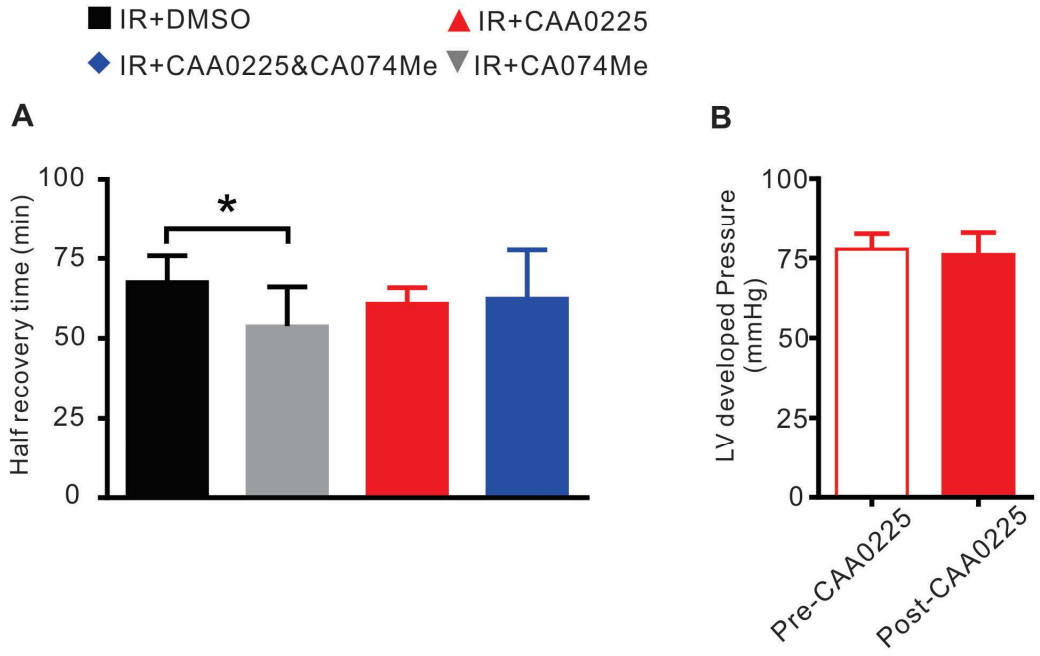

Figure 3-4. Effects of cathepsins inhibitors during IR injury. (A). Time point of recovery with 50% developed pressure. Mean data of IR+DMSO (*n* = 13), IR+CAA0225 (*n* = 6), IR+CA074Me (*n* = 8) and IR+CAA0225&CA074Me (*n* = 10) (* *P* < 0.05). (B) Effect of CAA0225 treatment on developed pressure. There was no difference between pre-CAA0225 treatment and 25 min post-CAA0225 treatment (*n* = 6, *P* > 0.05)

3.3.4 Combined treatment of CAA0225 and CA074Me on LV function during IR injury

Compared to the IR-DSMO group, the combined treatment of CAA0225 and CA074Me improved the overall LV function. However, there was no significant difference in this improvement between the IR+CAA0225&CA074Me group and the IR+CAA0225 group (**Figure 3-3**). In the IR+CAA0225&CA074Me group, the P_{dev} at 120 min recovered to 46 ± 6 % of pre-ischemic value (83 ± 4 *vs.* 37 ± 4 mmHg; time point 0 *vs.* time point 120 [n = 10]; **Figure 3-2D**) and was 184% of that in the IR+DSMO group. The dP/dt_{max} at 120 min recovered to 51 ± 5 % of pre-ischaemic

value (**Figure 3-3B**) and the dP/dt_{min} at 120 min recovered to 49 ± 5 % of pre-ischaemic value (**Figure 3-3C**), which were 176% and 153% of those in the IR+DSMO group, respectively. The P_{min} at 120 min was higher than the pre-ischaemic level (58 ± 5 *vs.* 5 ± 1 mmHg; time point 0 *vs.* time point 120 [*n* = 10]; **Figure 3-2D**) and 73% of the DSMO level (78.0 *vs.* 57.0 mmHg; IR+DSMO [*n* = 15] *vs.* IR+CAA0225&CA074Me [*n* = 10]; $P < 0.05$; **Figure 3-3D**). Combined treatment of CAA0225 and CA074Me showed no significant improvement in recovery rate (68 ± 2 *vs.* 63 ± 5 min of time point; IR+DSMO [*n* = 13] *vs.* IR+ CAA0225&CA074Me [*n* = 8]; $P > 0.05$; **Figure 3-4A**).

3.3.5 Infarct size was reduced by cathepsin-L inhibitor CAA225 following IR injury

Infarct size was assessed by TTC staining by the end of reperfusion, where the red area demonstrated viable tissue and the white area demonstrated non-viable tissue (**Figure 3-5A**). CAA0225 decreased infarct size to 69% of that in the IR-DSMO group (58 ± 2 *vs.* 40 ± 1 %; IR+DSMO [*n* = 11] *vs.* IR+CAA0225 [*n* = 6]; $P < 0.05$; **Figure 3-5B**) and decreased to 62% of that in the IR-DSMO group by the combination-treatment of CAA0225 and CA074Me (58 ± 2 *vs.* 36 ± 3 %; IR+DSMO [*n* = 11] *vs.* IR+CAA0225&CA074Me [*n* = 10]; $P < 0.05$; **Figure 3-5B**). There was no significant difference in the effect on the reduction of infarct size between the IR+CAA0225 and the IR+CAA0225 & CA074Me groups.

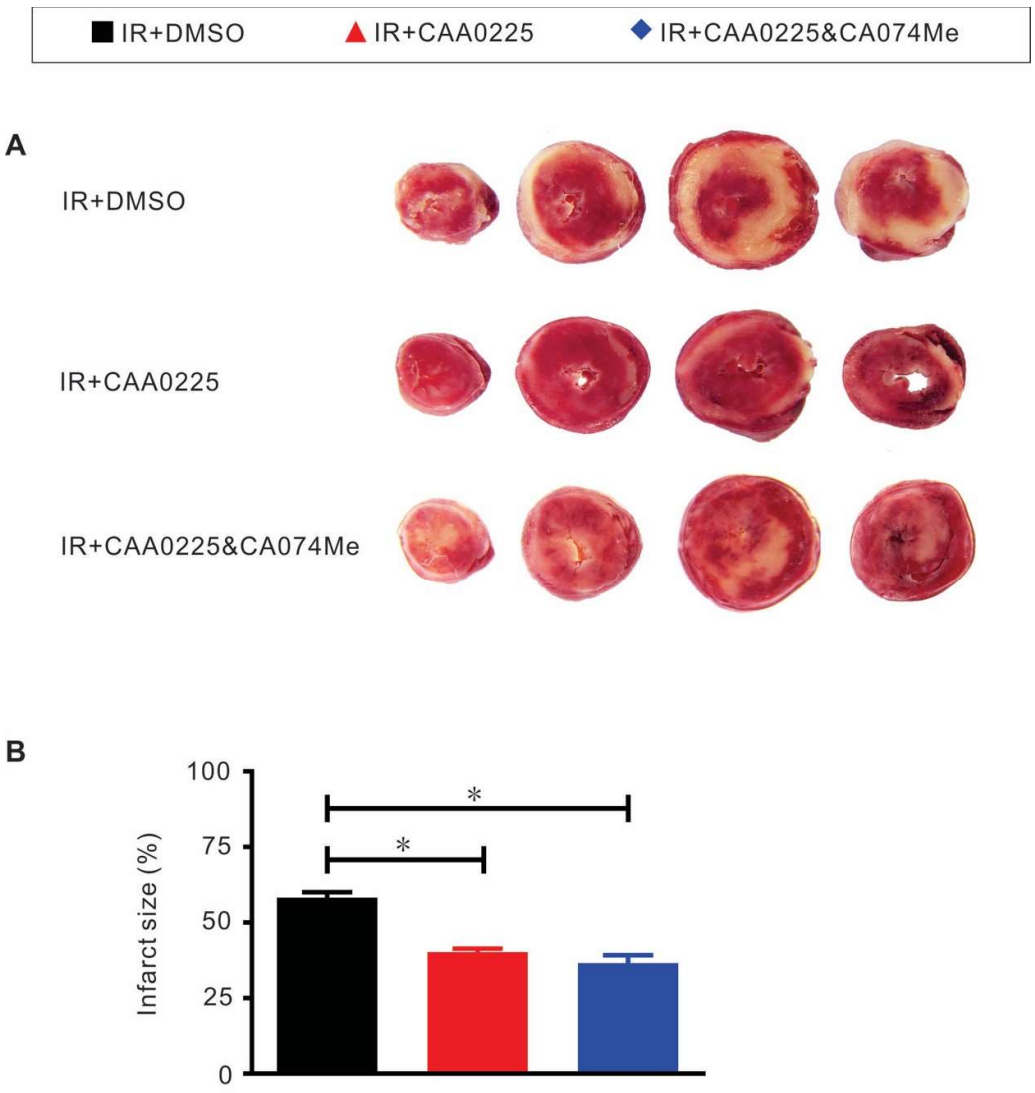

Figure 3-5. Infarct size following ischaemia-reperfusion. (A) Typical images of TTC stained heart slices. (B) Mean infarct size of IR+DMSO (n = 11), CAA0225 (n = 6), and IR+CAA0225&CA074Me (n = 10) (* P < 0.05).

3.4 Discussion

This chapter shows the improvement in LV function following IR injury as well as the reduction in infarct size in the isolated Langendorff perfused rat hearts, by the treatment of CAA0225 and its combination with CA074Me, respectively. The

treatment of CA074Me improved the rate of recovery but not overall LV function. In addition, the combination with CA074Me did not lead to additional significant improvement in LV function to the CAA0225 treatment alone.

3.4.1 CAA0225 improved cardiac function during IR injury

The present study demonstrates that the cathepsin-L inhibitor CAA0225 improves systolic and diastolic heart function post IR injury injury. Reversible contractile dysfunction (myocardial stunning) and irreversible contractile dysfunction occurs during IR injury (Kloner et al., 1998b), and has been observed in various forms of IR injury, including regional ischaemia and global ischaemia, *in vitro* and *in vivo (Bolli, 1990, Kim et al., 2001)*. In the present study, the LV developed pressure (P_{dev}), an index for LV contractibility, was used as a measure for the overall cardiac function. It dropped to 0 mmHg during ischaemia as hearts cannot beat without perfusion and recovered during reperfusion but still lower than the pre-ischaemic level by the end of reperfusion, indicating the impaired cardiac function due to irreversible IR injury. The treatment of CAA0225 led to an increase in the cardiac function by the end of reperfusion as compared to the IR-DMSO group.

Cathepsin-L is a ubiquitously expressed cysteine endopeptidase mainly located in the endosomes and lysosomes (Reiser et al., 2010). A basal level of cathepsin-L is necessary as complete deficiency of cathepsin-L results in dilated cardiomyopathy (Stypmann et al., 2002a), which is characterised by interstitial fibrosis in myocardium, appearance of pleomorphic nuclei in cardiomyocytes, impaired cardiac contraction and cardiac chamber dilation (Stypmann et al., 2002b). These previously published data suggest that basal levels of cathepsin-L are important for normal heart function by the maintenance of lysosomes in order to prevent alterations in cardiac structure and function that lead to dilated cardiomyopathy.

Cathepsins are not only found exclusively within lysosomes but are also secreted into the extracellular space in considerable amounts by both fusions of lysosomal organelles with the plasma membrane and exocytosis (Appelqvist et al., 2013). Lysosomal cathepsins have been found secreted into and function within extracellular space (such as degradation of extracellular matrix (ECM) proteins) by lysosome exocytosis (Lakka et al., 2004, Tu et al., 2008). Inhibition of the

exocytosis of cathepsins from cancer cell lysosomes has shown therapeutic effect for cancer invasion (Lakka et al., 2004, Liu et al., 2012). During cardiac diseases in animal models and human patients there is overwhelming evidence that elevated levels of cathepsin-L occur within the heart and serum. Furthermore, the increased level of cathepsin-L in serum is correlated with the severity of cardiac diseases. In separate studies involving several hundred patients, cathepsin-L was increased in the serum in patients with coronary artery stenosis and coronary heart disease (CHD) even when adjusted for major confounders (Liu et al., 2006, Liu et al., 2009b, Zhang et al., 2010b). These studies also reported that: (i) patients with unstable angina pectoris had higher serum cathepsin-L levels than those with stable angina pectoris (Liu et al., 2009b), (ii) of patients with an acute coronary syndrome, those with acute MI had higher serum cathepins-L than those with unstable angina pectoris (Liu et al., 2009b), (iii) patients with previous chronic MI had the highest cathepsin-L levels as compared to those with acute MI and those with angina pectoris (Liu et al., 2009b), (iv) there was a strong positive correlation between serum cathepsin-L concentrations and the percentage of stenosis of the left anterior descending coronary artery in individual patients (Liu et al., 2006), (v) the cathepsin-L concentration was positively associated with the number of coronary artery branch luminal narrowings (Liu et al., 2009b), and (vi) the cathepsin-L concentration was independently correlated with the coronary collateral formation (Liu et al., 2009b). In summary, these findings implicate the role of cathepsin-L in the pathophysiology of acute and chronic CHD.

During cardiovascular diseases, inflammatory cells, vascular endothelium, and smooth muscles have been identified as sources of human cathepsin-L (Liu et al., 2006). However, cardiomyocytes and myofibroblasts may also contribute to increased serum cathepsin L (Liu et al., 2009b). In a mouse model of MI, cathepsin-L activity within the myocardium was increased after permanent coronary artery ligation (Sun et al., 2011). Release of cathepsin-L from lysosomes during cell death post MI may also lead to the local increase of extracellular cathepsin-L levels in the heart. Our *ex vivo* data presented in this chapter and unpublished data demonstrate that the heart is an important source of cathepsin-L during IR injury independent of inflammatory cells. Under *in vivo* conditions, the increase of extracellular cathepsin-L levels may be compounded by inflammatory cells

migrating to particular cardiac regions post MI e.g. the border zone.

The present study shows inhibition the activity of cathepsin-L improves cardiac contractile function during reperfusion. The inhibitor CAA0225 itself does not alter cardiac function of hearts before ischaemia as systolic and diastolic parameters are not different between groups before ischaemia, so the protective effect of the inhibitor and the improvement of cardiac function is associated with IR injury. These novel data presented in this chapter suggests that cathepsin-L is more than simply a reflection of cell death during IR injury, but may be intrinsically involved in pathophysiology of cardiac dysfunction following IR injury. Together these findings provide convincing evidence supporting our hypothesis that the use of a cathepsin-L inhibitor is beneficial to cardiac function during IR.

Higher concentrations of CAA0225 (not used in this study) have been reported to inhibit cathepsin-B as well as cathepsin-L (Takahashi et al., 2009). To ensure that the protective effect of CAA0225 was not due to an effect on cathepsin-B we utilised a cathepsin-B inhibitor CA074Me. CA074Me did not improve the overall cardiac systolic or diastolic function, which confirmed that the protective effect of CAA0225 was not due to the inhibition of cathepsin-B. Furthermore, whilst combined CAA0225 and CA074Me treatment improved overall cardiac function, there was no significant difference from the CAA0255 treatment alone. These data suggest inhibition of cathepsin-L rather than cathepsin-B has protective effect against IR injury.

3.4.2 CAA0225 reduced infarct size following IR injury

In the present study utilization of the cathepsin-L inhibitor CAA0225 reduced infarct size by 69% of that in the IR-DSMO control. There was no difference between the CAA0225 treatment alone and the combined CAA225 & CA074Me treatment. It is highly likely that the improved cardiac function with CAA0225 was related to the reduced infarct size. Lethal cardiomyocyte death in IR injury is caused by several mediators. The first is oxidative stress which is produced both in cardiomyocytes and neutrophils (Hearse et al., 1973). The overproduction of reactive oxygen species (ROS) mediates myocardial injury and cardiomyocyte death through different mechanisms, including damage to DNA, mitochondrial membranes and sarcoplasmic reticulum (SR) (Zweier et al., 1987, Hausenloy and

Yellon, 2013). The second mediator is intracellular Ca^{2+} overload. The ROS-induced damage of mitochondrial membrane and SR results in intracellular and mitochondrial Ca^{2+} overload (Corretti et al., 1991). Ca^{2+} overload causes hypercontracture of cardiomyocyte and permitting MPTP open which leads to cardiomyocyte death (Piper et al., 1998). The third mediator is rapid pH restoration at reperfusion, which contributes to cardiomyocyte death by opening of MPTP and hence leading to a state of hypercontracture (Lemasters et al., 1996). The fourth mediator is the MPTP, a nonselective channel of the inner mitochondrial membrane, which causes ATP depletion and cell death (Hausenloy and Yellon, 2003, Heusch et al., 2010). However, the role of cathepsins in lethal myocardial reperfusion injury remains unclear. Several studies relate to lysosomal dysfunction suggested the translocation of lysosomal cathespins into the cytoplasm contributes to cell death (Li and Yuan, 2004, Tiwari et al., 2008, Turski and Zaslonka, 2000).

Studies in different organs have shown that inhibition of specific cathepsins can reduce cell death following IR injury. Cathepsin-B contributes to TNF-α-induced hepatocyte apoptosis and, during liver IR injury, inhibition of cathepsin-B can attenuate hepatocyte apoptosis through inactivation of caspase-3 (Guicciardi et al., 2000, Ben-Ari et al., 2005). Also knockout of cathepsin-G results in 70% decrease in tubular cell apoptosis as cathepsin-G causes neutrophil-mediated tissue damage during IR in the kidney (Shimoda et al., 2007). In addition, treatment with the cathepsin-B inhibitor CA074Me protected against programmed necrosis during global IR injury in the brain (Xu et al., 2016). Furthermore, treatment with the cathepsin inhibitor E64d reduces cerebral infarction following transient focal cerebral ischaemia by inhibiting matrix metalloproteinase-9 activity (Tsubokawa et al., 2006). The present study suggests inhibition of cathepsin-L contributes to the cardioprotective effect. Recent unpublished work performed in our laboratory demonstrates that in *ex vivo* isolated rat cardiomyocytes IR injury increased Ca^{2+} influx through L-type calcium channels, reduced sarcolemmal NCX extrusion and decreased SERCA activity culminating in an increase in diastolic $[Ca^{2+}]_i$. This calcium overload promoted adverse spontaneous SR-mediated Ca^{2+} release (Ca^{2+} waves) in cardiomyocytes and irreversible cell contraction. When the same experiments were performed with

CAA0225 treatment the abnormalities in intracellular Ca^{2+} handling parameters were normalised to control levels thus reducing irreversible cell contraction and therefore cell death. These data suggest a potential cellular mechanism for improving cardiac function and reducing infarct size *via* CAA0225 administration during IR injury.

3.4.3 Summary

The present study demonstrates for the first time that the cathepsin-L inhibitor CAA0225 improved both systolic and diastolic cardiac function during IR injury in *ex vivo* isolated rat hearts and the improvement of cardiac function is paralleled with reduction of infarct size. This study has also shown that the cathepsin-B inhibitor CA074Me improved the rate of recovery during IR injury but not overall cardiac function. Combined CAA0225 and CA074Me treatment did not show any synergistic effect on cardiac protection following IR injury. Therefore, cathepsin-L is a potential therapeutic target in IR injury and the cathepsin-L inhibitor CAA0225 is a candidate pharmacological intervention.

CHAPTER 4.

The *in vivo* effect of CAA0225 on LV function in murine models of MI and IR injury

4.1 Introduction

4.1.1 Application of mouse models in drug development of MI and IR injury

Developing new pharmacological agents for treating MI and myocardial IR injury are urgently required as MI is the leading cause of mortality in developed countries (Hausenloy and Yellon, 2013). As outlined in chapter 1, *In vivo* mouse models have particular advantages for testing new pharmacological therapies for MI and IR injury (Vidavalur et al., 2008). The mouse is established as one of the smallest mammals which can be used to reproducibly perform coronary ligation in open chest surgery with subsequent phenotype analysis. In an experimental setting, a mouse normally needs one-tenth amount of drug compared to a rat. Therefore, the mouse model of MI or IR injury is an economical model when testing expensive drugs such as novel chemical inhibitors or gene products. However, due to the small size of this species, performing coronary occlusion in the mouse is a difficult surgical procedure requiring extensive training and therefore limits the widespread application of mouse models of MI and IR injury in drug testing. The mouse model of MI induced by permanent coronary artery ligation has been used for four decades (Zolotareva and Kogan, 1978, Patten and Hall-Porter, 2009). Compared to the permanent coronary ligation model, temporary coronary occlusion can be used to test the protective effect of novel therapies following IR injury (Vidavalur et al., 2008). Surgical induction of IR injury is more difficult than MI because the animal needs to be exposed to open chest surgery throughout the ischaemia period which increases the duration of the surgical anaesthetic period and therefore increases the potential for mortality. Furthermore, IR injury can cause fatal arrhythmias at the onset of reperfusion. The mouse model of IR injury was first described two decades ago (Michael et al., 1995) and a refined approach has been reported by Bohl *et al*. recently (Bohl et al., 2009). Tail vein injection of agents in mice is also a difficult technique (due to the small size of mice) which requires experience but it is the quickest way to delivery most types of drugs into circulation following MI (Turner et al., 2011). Combination of tail vein injection with the mouse models of MI and IR injury allows testing the effects of pharmacological agents on LV function and structure. In this study the effects of

a cathepsin-L inhibitor CAA0225 is investigated in mouse MI and IR injury models with intravenous injection.

A critical step in developing new pharmacological therapies for MI and IR injury is measuring the effects of the drug on heart cardiac function and infarct size. Measurement of cardiac function following MI or IR injury in mice can be achieved by using non-invasive or invasive methods such as echocardiography or cardiac pressure-volume loop (PV loop). Echocardiography is a widely used non-invasive method which can visualize the cardiac structure and evaluate the left ventricular function in mice (Rottman et al., 2007). During echo measurements, LV interventricular septal thicknesses, LV internal dimensions and posterior wall thicknesses at systole and diastole are measured in M-mode at the level of the papillary muscles. LV fractional shortening (FS) and LV ejection fraction (EF) are measured from above parameters to evaluate LV systolic function. Following MI, EF calculated by the cubic assumption of LV volume may not be accurate due to the change of the LV geometry. Therefore, FS is preferable in MI models (Gao et al., 2011). Pressure-volume (PV) loop analysis enables measurement of LV function (Clark and Marber, 2013). PV loop analysis has been used in large mammals and humans for the last three decades and more recently progress in microsurgical catheters allows the application of the PV loop in mice (Abraham and Mao, 2015). Combined application of the PV loop and echocardiography measurements is preferable in a drug testing study, because PV loop measurement is normally performed prior to sacrifice while echocardiography can be performed at multiple time points. PV loops provide blood volume measurements which cannot be determined using echocardiographic images without geometrical assumptions. Infarct size can be demarcated in IR injury by using a double-dye staining technique, which demarcates the area at risk by Evans blue and the area of infarct by triphenyltetrazolium chloride (TTC) (Bohl et al., 2009). While in MI hearts, infarct size can be measured following Sirius red staining by a length-based approach (Takagawa et al., 2007).

4.1.2 Cathepsin-L and ischaemic heart disease

In patients with ischaemic heart disease, cathepsin-L has been detected in plasma (Zhang et al., 2010a) and serum (Liu et al., 2009b) with a correlation of disease

severity (Liu et al., 2009b). However, whether cathepsin-L is only a marker of cardiomyocyte damage or it plays a critical functional role following ischaemic heart disease is unknown. Studies in cathepsin-L knockout mice with persistent cathepsin-L deficiency from birth have demonstrated that cathepsin-L plays a significant role in cardiac morphology. Cathepsin-L deficiency in mice exhibited significant ventricular and atrial enlargement with a comparatively small increase in heart weight (Stypmann et al., 2002a) and a late onset of dilated cardiomyopathy which is characterized by cardiac chamber dilation and impaired cardiac contraction (Petermann et al., 2006, Spira et al., 2007a). In the mouse model of aortic banding, deficiency of cathepsin-L significantly exacerbated cardiac hypertrophy with worsened cardiac function and increased mortality (Sun et al., 2013). In the setting of MI, cathepsin-L deficient mice showed worse cardiac dysfunction with greater scar dilatation and wall thinning following coronary artery ligation. The diminished activity of cardiac matrix metallopeptidase-9 (MMP-9) and decreased mobilization of natural killer cells, c-kit-positive cells, monocytes, and fibrocytes to infarcted myocardium in cathepsin-L deficient mice indicated that cathepsin-L regulates cardiac repair and remodelling following MI (Sun et al., 2011).

Given that levels of cathepsin-L increased in the hearts and serum of patients during cardiac disease and that severity of cardiac disease correlated with cathepsin-L levels, cathepsin-L inhibition may have effect of on cardiac function during ischaemic heart disease. A study by Sun et al. (Sun et al., 2011) found that the induction of MI *via* permanent LAD coronary artery ligation in the complete absence of cathepsin-L in all cell types increased infarct size at day 14 post MI. Sun et al. suggested two possible mechanisms for the increased infarct size in cathepsin-L deficient MI mice: one possibility is that the deficit of cathepsin-L secretion from cells reduces the degradation of extracellular matrix components, which therefore prevents the mobilisation of blood/bone marrow-derived accessory cells to the site of injury to participate in cardiac repair; the other explanation is a reduced level of myofibroblasts and circulating fibroblasts that limit infarct dilatation. It is important to recognise that the knockout mice used by Sun et al. (Sun et al., 2011) were deficient for cathepsin-L from the beginning of development. Cathepsin-L deficiency in all cell types from birth could cause

complex compensatory biochemical changes and alterations of cellular structure, thus these cathepsin-L knockout hearts are highly likely to respond differently to the induction of MI compared with hearts in physiological conditions. Such recognition has become apparent when investigating the effect of cathepsin inhibitors in other body systems, which showed that in contrast to transgenic studies, inactivation of cathepsins by specific inhibitors caused only partial and temporary deficiency and might therefore result in different effects with knockout mice (Lankelma et al., 2010). Sun et al. (Sun et al., 2011) suggest that there is potential benefit provided by partial or temporary cathepsin-L inhibition, which may reduce cardiac fibrosis (a known contributor to increased cardiac stiffness, diastolic dysfunction and arrhythmogenesis) and inflammatory responses (a known contributor to myocardial necrosis). In summary, these observations combined with the results shown in the previous chapter suggest that although complete deficiency of cathepsin-L from birth is deleterious, excess cathepsin-L may also be harmful, given that the severity of cardiac disease correlates with serum levels cathepsin-L in patients with CHD (Liu et al., 2009b).

4.1.3 Aims

In the previous chapter, I found that the cathepsin-L inhibitor CAA0225 improved cardiac function during IR injury in *ex vivo* rat hearts, however the effect of CAA0225 on *in vivo* models of MI and IR injury remains unknown. The application of the tail vein injection in the mouse models of MI and IR injury would allow the investigation of these effects of cathepsin-L inhibitor CAA0225 *in vivo*.

The aims of this chapter are:

v) To investigate the effects of the cathepsin-L inhibitor CAA0225 on cardiac function and infarct size following IR injury induced by temporary coronary artery ligation *in vivo*.

vi) To investigate the effects of the cathepsin-L inhibitor CAA0225 on cardiac function following MI induced by permanent coronary artery ligation *in vivo*.

4.2 Methods

4.2.1 Inducing MI and IR injury in mice by coronary ligation

Male C57Bl/6 mice (9-12 weeks old) were anaesthetised in an induction chamber with 4% isofluorane and 100% oxygen. The anaesthetised mouse was intubated and ventilated *via* a small animal respirator (Harvard Apparatus, Germany) with 1.5% isofluorane. Pre-operative analgesia was administered though the intraperitoneal route (5 mg/Kg carprofen and 0.1 mg/Kg buprenorphine). The chest was opened *via* the bluntly dissected pectoral muscles following a skin incision. The heart was exposed *via* the intercostal space between the 3rd and 4th ribs. MI was induced by permanent LAD coronary ligation using a 9-0 nylon suture and ischaemia-reperfusion injury (IR) was induced by temporarily tying the LAD coronary artery against a short section of polyethylene tubing (PE-10; outer diameter, 0.61 mm) with a 7-0 polypropylene suture. A single dose of 0.25mg CAA0225 (Merck, Darmstadt, Germany) was delivered with 125μL vehicle (normal saline with 15% DMSO) *via* intra-venous (I.V.) injection within 2 min post LAD ligation. Temporary LAD ligation was released following 45 min ischaemia by removing the polyethylene tubing. The lungs were fully inflated by applying positive end-expiratory pressure and the chest was closed in layers. The mouse was extubated after regaining spontaneous breathing. Four separate *in vivo* studies were performed in this chapter using 4 separate cohorts of mice: 2-wk MI, 2-wk IR injury, 4-wk IR injury and 3-hr IR injury. The 2-wk, 4-wk and 3-hr refer to the duration of the study following MI or IR injury. To evaluate the cardiac function following MI or IR injury, the mice recovered from surgery were kept alive for several weeks. Non-invasive echocardiography was performed weekly on these mice and invasive PV loop examination was performed before sacrifice. The 2-wk and 4-wk duration allowed serial echocardiography before sacrifice and obtaining PV loop data at 2-wk and 4-wk following MI and IR injury. The 3-hr IR injury study was performed to investigate the AAR and infarct size. Measuring AAR requires re-occluding of the original LAD ligation, so this cohort of mice were sacrificed at 3-hr post IR injury to assess AAR and infarct size by using double-dye staining.

4.2.2 Echocardiography

Mouse was anesthetized in an induction chamber with 4% isofluorane and 100% oxygen and maintained *via* facemask on 0.5-1% isofluorane in 1.0 L/min oxygen. The chest hair was shaved and the mouse was positioned on a warm heat pad and body temperature was monitored and generally maintained at 37ºC. The mouse was placed at a shallow left-sided position. Warmed echo gel was placed on the chest and the heart was imaged with a 15 MHz pediatric ultrasound probe (Acuson Sequoia 512, Siemens UK). The probe was paced along the long-axis of LV to obtain the two-dimensional LV long-axis view. Then by rotating the probe clock wisely by 90º, the LV short-axis view was visualized. The LV M-mode was recorded from the short-axis view at the papillary muscle level. The echo gel was removed after scanning and the mouse was recovered on the heat pad with oxygen before being returned to the cage. Three separate cohorts of mice were phenotyped by echocardiography, the first cohort underwent a 2 wk study post MI, the second cohort underwent a 2 wk study post IR injury and the third cohort underwent a separate longer 4 wk study post IR injury.

4.2.3 Pressure-Volume loop measurements

Mouse was anesthetized as described above, and endotracheally intubated with artificial ventilation. Body temperature was maintained at 37 ºC h a heat pad controlled by rectal thermometer. PV loop measurements were recorded using the ADVantage Pressure-Volume System (ADV500, Transonic) in a closed chest surgery. The right common carotid artery (RCA) was surgically exposed and A 1.2F 4.5 mm spaced PV catheter was inserted into RCA and then advanced to the LV chamber. The intra-LV pressure and volume was recorded and PV loops were generated by plotting pressure against volume. Two separate cohorts of mice were studied by PV loop measurement: i) 2 wk study post IR injury and ii) 4 wk study post IR injury.

4.2.4 Organ harvest and weighing

Mice were weighed and killed using a Schedule 1 method (cervical dislocation). The heart was excised and washed in a beaker of ice-cold normal saline and excess tissue was trimmed off. The aorta was cut transversely and mounted on to a cannula attached to a syringe. The heart was perfused retrograde with 5mL ice-cold normal saline to rinse blood out of the chambers and vessels. Hearts then

either underwent double-dye staining for AAR measurements or were stored in formalin for further experiments Lungs and liver were removed, blotted dry and then weighed but not stored. The length of the mouse tibia was measured for normalisation of organ weights and the heart, lungs and liver were weighed using a precision electronic balance (precision 0.00001g).

4.2.5 Measurement of area at risk and infarct size by double-dye staining

The double-dye staining was applied in IR hearts following 3 hr reperfusion. The heart was cannulated and perfused with normal saline to rinse out blood. Re-occlusion of the LAD coronary artery was obtained by re-tying a knot onto the polyethylene tubing at the initial place. The perfused myocardium was stained by perfusion of 250 µl 1% Evans blue. The area not stained by Evans blue is the area at risk (AAR). Then the heart was wrapped in cling film and placed at -20℃ for 15 min before being transversely sectioned into 5–8 parallel short-axis slices. The white compound of Triphenyltetrazolium chloride (TTC) (Sigma, Dorset, UK) was dissolved at 1% (m/v) in a phosphate buffer, made by mix of appropriate volumes of 0.1M NaH_2PO_4 and Na_2HPO_4 to achieve a pH of 7.4. The TTC solution was warmed to 37 °C on a heater. The heart slices were submersed in the solution for 15 min then fixed in 10% neutral buffered formalin (CellPath, Powys, UK) overnight at 4°C. Photographs of the heart slices were taken and made into a plane image. The number of pixels was counted by contouring the differentially coloured left ventricle subsets using Adobe Photoshop (Adobe). The infarct size is worked out as percentage of the AAR and the absolute infarct size corrected to the slice weight.

4.2.6 Measurement of infarct size by Sirius red staining of heart sections

The hearts following 2-wk MI and IR injury were taken for histological analysis. Hearts were fixed in 10% neutral buffered formalin (CellPath, U.K.) for a minimum of 24 hr and then embedded into a wax block. The heart was sliced parallel to the long axis of the heart every 250 µm to produce serial sections 1µm thick per heart until the aorta level was reached and stained with Sirius red. The sections were

examined and photographed with an EVOS digital microscope. Images were analysed using Adobe Photoshop (Adobe, USA) software. The infarct size of the MI heart was measured using a length based approach. Epicardial and endocardial infarct ratios were calculated by dividing the sum of epicardial or endocardial infarct lengths from all sections by the sum of all epicardial or endocardial circumferences from all sections respectively. The epicardial and endocardial infarct ratios were then averaged to give a mean value of MI infarct size. The infarct size of the hearts following 2-wk IR injury was measured using a pixel based approach. The numbers of pixels in LV area and red scar area were measured from all sections respectively and the IR infarct size was calculated by dividing the sum of scar pixels from all sections by the sum of all LV pixels from all sections respectively.

4.2.7 Data recording and statistical analysis

Echo images were captured by the echo machine and analysed offline using ImageJ. PV loop data were recorded on a laptop using LabScribe2.0 software at a sampling rate of 1KHz and analysed offline using LabScribe2.0 software. Double-dye staining slices were photographed using a Canon camera. Sirius red sections were photographed using EVOS digital microscope. All data in the text and figures are expressed as mean ± SEM. Unpaired student's t-test (two-tailed) was used for the comparison of a particular data set with control. A critical value of statistical significance was set as P <0.05.

4.3 Results

4.3.1 Effect of CAA0225 on cardiac function measured by echocardiography in 2 weeks post MI cohort

The permanent LAD ligation was made during open chest surgery and the mice were recovered after the MI surgery for a 2 wk study period. CAA0225 or vehicle was injected into MI mice *via* tail vein after the permanent LAD ligation. Cardiac function was assessed using M-mode echocardiography before MI (Time 0) and weekly after the induction of MI (**Figure 4-1A**). As expected, fractional shortening (an index of LV contractility) decreased in MI mice treated with vehicle (40.5 ± 2.3 [n = 5] *vs.* 25.0 ± 1.9 % [n = 5], 0 *vs.* 2 wk post IR injury, P < 0.05, **Figure 4-1B**).

By contrast, the mice treated with CAA0225 demonstrated significantly preserved fractional shortening, which was 139% of vehicle control at 2 wk post MI (34.8 ± 3.3 [*n* = 6] *vs.* 25.0 ± 1.9 % [*n* = 5], CAA0225 *vs.* Vehicle, $P < 0.05$, **Figure 4-1B**). LV internal dimension measured at systole (an inverse index of contractility, i.e. the larger it is the worse the contractility) was significantly different between CAA0225 and vehicle treated mice at 2 wk post MI (2.85 ± 0.27 [*n* = 6] *vs.* 3.71 ± 0.30 mm [*n* = 5], CAA0225 *vs.* Vehicle, $P < 0.05$, **Figure 4-1C**), while no significant difference was found in LV internal dimension at diastole (an index of LV dilation) at 2 wk post MI (4.33 ± 0.22 [*n* = 6] *vs.* 4.94 ± 0.28 mm [*n* = 5], CAA0225 *vs.* Vehicle, $P > 0.05$, **Figure 4-1D**). There was no significant difference in LV posterior (free) wall thickness measured at systole at 2 wk post MI (1.32 ± 0.06 [n = 6] *vs.* 1.24 ± 0.10 mm [*n* = 5], CAA0225 *vs.* Vehicle, $P > 0.05$, **Figure 4-1E**), nor in LV posterior wall thickness measured at diastole at 2 wk post MI (0.90 ± 0.09 [*n* = 6] *vs.* 0.97 ± 0.06 mm [*n* = 5], CAA0225 *vs.* Vehicle, $P > 0.05$, **Figure 4-1F**).

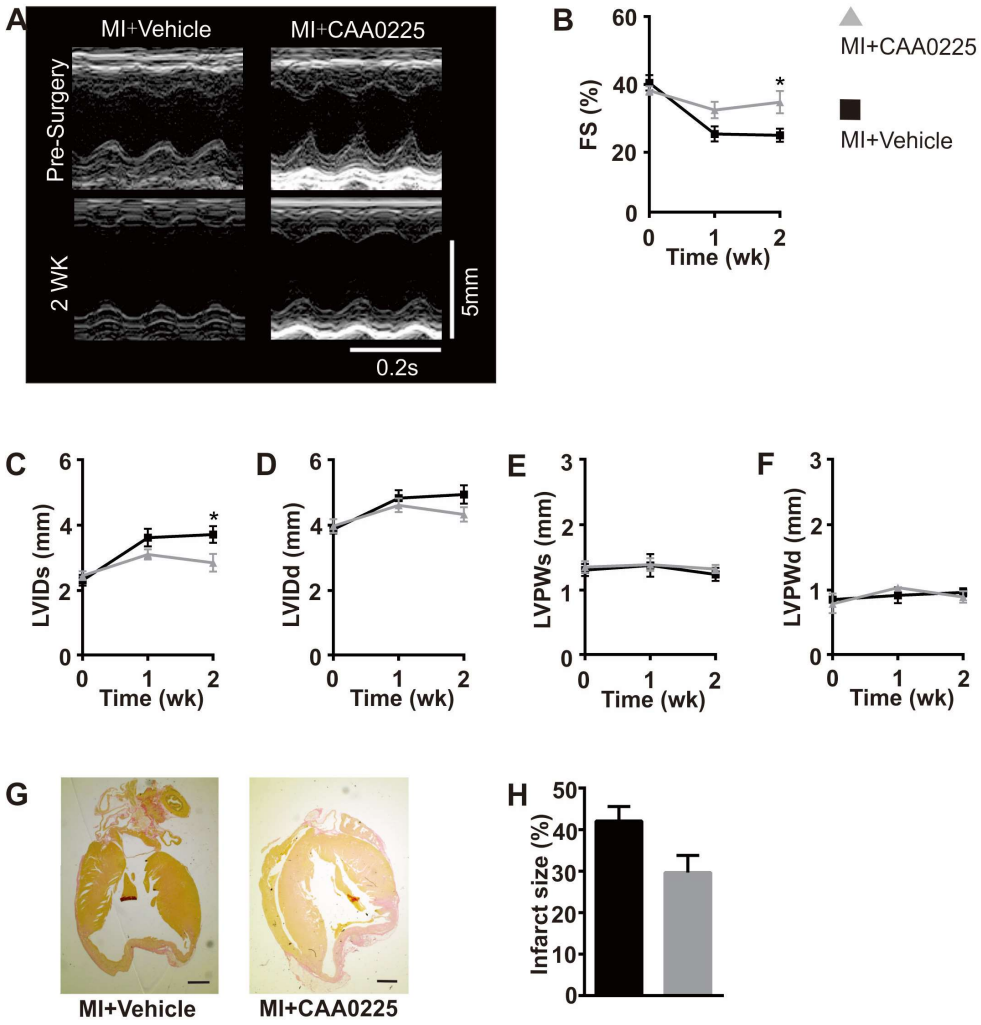

Figure 4-1. Cardiac function and infarct size in MI hearts with CAA0225. (A) Typical M-mode echocardiographic images of MI+Vehicle and MI+CAA0225 at pre-MI and 2 wk post MI. (B) Mean echocardiographic data obtained from a 2 wk study of MI+Vehicle (n = 5) and MI+CAA0225 (n = 6) for Fractional shortening (FS) and (C) Left ventricular internal diameter at systole (LVIDs), (D) LVID at diastole (LVIDd), (E) LV posterior wall thickness at systole (LVPWs) and (F) LVPW thickness at diastole (LVPWd). (G) Representative sirius red staining images of MI+Vehicle and MI+CAA0225 at 2 wk post MI (scale bars: 1mm). (H) Mean infarct size of MI+Vehicle (n = 5) and MI+CAA0225 (n = 4) at 2 wk post MI. (* P < 0.05 IR+Vehicle *vs.* IR+CAA0225)

4.3.2 Effect of CAA0225 on infarct size at 2 weeks post MI

Infarct size was analysed from images of the 5 serial sections using a length based approach. The MI infarct size was calculated by averaging the epicardial and endocardial infarct length ratios. Representative heart images are shown in **Figure 4-1G**. There was no significant difference in infarct size between CAA0225 and vehicle treated mice at 2 wk post MI (29.7 ± 4.1 *vs.* 42.0 ± 3.5 %; CAA0225 [*n* = 4] *vs.* control [*n* = 5]; *P* > 0.05; **Figure 4-1H**).

4.3.3 Effect of CAA0225 on cardiac function measured by echocardiography at 2 weeks post IR injury

The left anterior descending coronary artery (LAD) was temporarily tied *in vivo* for 45 min followed by reperfusion. CAA0225 was delivered to IR mice by intravenous injection after the LAD was tied. Two separate cohorts of mice were used for different lengths of study duration (2 wk and 4 wk). Echocardiography was performed before and post IR in both cohorts. Internal dimension and wall thickness of left ventricle (LV) were measured and fractional shortening (FS) was assessed using M-mode echocardiography (**Figure 4-2A**). In the 2 wk study cohort, FS decreased in vehicle-control mice over the 2 wk period as expected (38.2 ± 1.6 [*n* = 7] *vs.* 26.9 ± 3.0 % [*n* = 7], 0 *vs.* 2 wk post IR injury, **Figure 4-2B**) whereas CAA0225 treated mice demonstrated a preserved FS (40.3 ± 1.7 [*n* = 8] to 35.8 ± 2.0 % [*n* = 8], 0 *vs.* 2 wk post IR injury, **Figure 4-2B**). CAA0225 treated mice demonstrated markedly preserved fractional shortening, which was 146% of vehicle-control at 1 wk post IR injury (34.5 ± 1.6 [*n* = 8] *vs.* 23.6 ± 2.4 % [*n* = 7], CAA0225 *vs.* Vehicle, *P* < 0.05, **Figure 4-2B**) and 133% of vehicle-control at 2 wk post IR injury (35.8 ± 2.0 [n = 8] *vs.* 26.9 ± 3.0 % [*n* = 7], CAA0225 *vs.* Vehicle, *P* < 0.05, **Figure 4-2B**). There was no significant difference in LV internal dimension at systole at 2 wk post IR injury (2.88 ± 0.18 [*n* = 8] *vs.* 3.15 ± 0.16 mm [*n* = 7], CAA0225 *vs.* Vehicle, *P* > 0.05, **Figure 4-2C**), nor in LV internal dimension diastole at 2 wk post IR injury (4.47 ± 0.17 [*n* = 8] *vs.* 4.32 ± 0.22 mm [*n* = 7], CAA0225 *vs.* Vehicle, *P* > 0.05, **Figure 4-2D**). No significant difference was found in LV posterior wall thickness systole at 2 wk post IR injury (1.31 ± 0.12 [*n* = 8] *vs.* 1.11 ± 0.09

mm [*n* = 7], CAA0225 *vs.* Vehicle, *P* > 0.05, **Figure 4-2E**), nor in LV posterior wall thickness diastole at 2 wk post IR injury (0.86 ± 0.09 [n = 8] *vs.* 0.72 ± 0.10 mm [*n* = 7], CAA0225 *vs.* Vehicle, *P* > 0.05, **Figure 4-2F**).

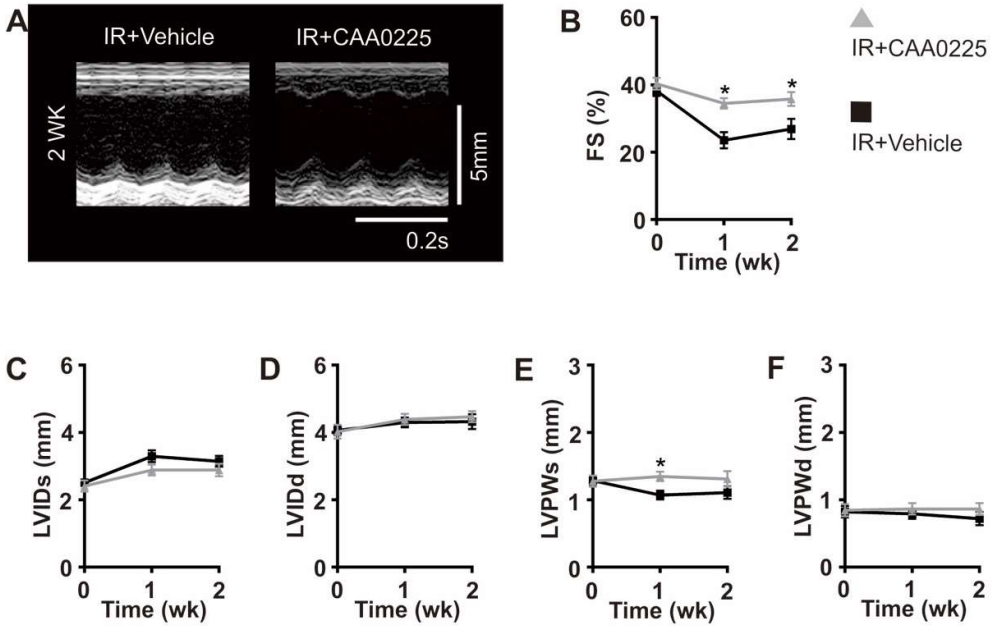

Figure 4-2. Cardiac function in IR hearts with CAA0225. (A) Typical M-mode echocardiographic images of IR+Vehicle and IR+CAA0225 at 2 wk post IR injury. (B) Mean echocardiographic data obtained from a 2 wk study of IR+Vehicle (*n* = 7) and IR+CAA0225 (*n* = 8) for Fractional shortening (FS) and (C) Left ventricular internal diameter at systole (LVIDs), (D) LVID at diastole (LVIDd), (E) LV posterior wall thickness at systole (LVPWs) and (F) LVPW thickness at diastole (LVPWd). (* *P* < 0.05 IR+Vehicle *vs.* IR+CAA0225)

4.3.4 Effect of CAA0225 on cardiac function measured by echocardiography at 4 weeks post IR injury

In order to establish whether the beneficial effects observed at 2 weeks post IR injury injury were maintained to 4 weeks post IR injury injury a separate cohort

of mice was used for a 4 wk study period. Fractional shortening (FS) was significantly preserved at 4 wk post IR injury in CAA0225 treated mice compared with vehicle control (31.4 ± 2.0 [*n* = 6] *vs.* 26.4 ± 1.0 % [*n* = 8], CAA0225 *vs.* Vehicle, *P* < 0.05, **Figure 4-3B**). No significant difference was found in LV internal dimension systole at 4 wk post IR injury (3.19 ± 0.22 [*n* = 6] *vs.* 3.17 ± 0.10 mm [*n* = 8], CAA0225 *vs.* Vehicle, *P* > 0.05, **Figure 4-3C**), nor in LV internal dimension diastole at 4 wk post IR injury (4.64 ± 0.23 [*n* = 6] *vs.* 4.31 ± 0.10 mm [*n* = 8], CAA0225 *vs.* Vehicle, *P* > 0.05, **Figure 4-3D**). There was no significant difference in LV posterior wall thickness systole at 4 wk post IR injury (1.44 ± 0.20 [*n* = 6] *vs.* 1.31 ± 0.09 mm [*n* = 8], CAA0225 *vs.* Vehicle, *P* > 0.05, **Figure 4-3E**), nor in LV posterior wall thickness diastole at 4 wk post IR injury (0.99 ± 0.12 [*n* = 6] *vs.* 0.93 ± 0.09 mm [*n* = 8], CAA0225 *vs.* Vehicle, *P* > 0.05, **Figure 4-3F**).

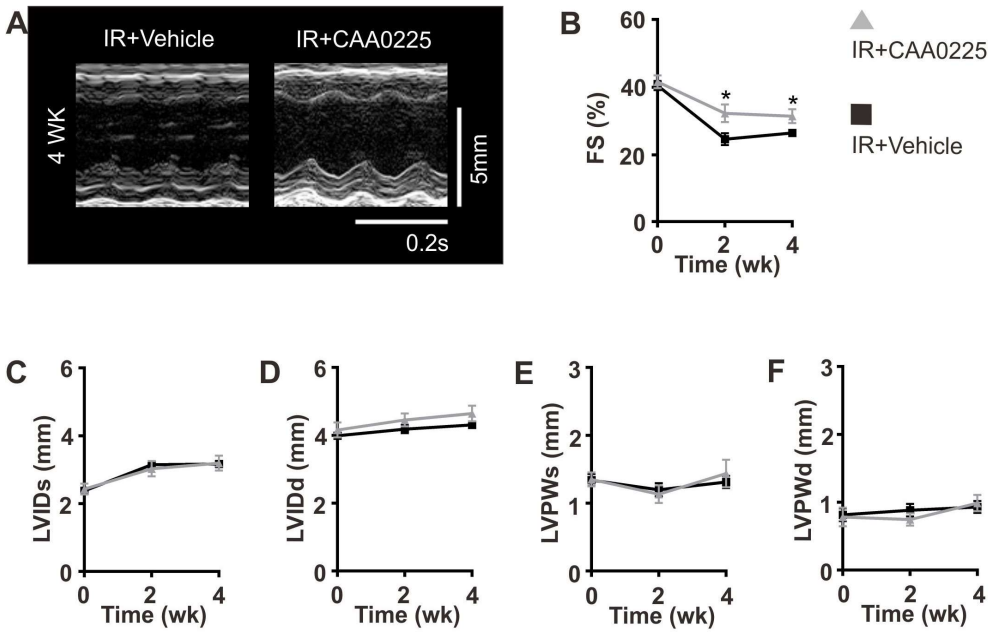

Figure 4-3. Cardiac function in IR hearts with CAA0225. (A) Typical M-mode echocardiographic images of IR+Vehicle and IR+CAA0225 at 4 wk post IR injury. (B) Mean echocardiographic data obtained from a 4 wk study of IR+Vehicle (n = 8) and IR+CAA0225 (n = 6) for Fractional shortening (FS) and (C) Left ventricular internal diameter at systole (LVIDs), (D) LVID at diastole (LVIDd), (E) LV posterior wall thickness at systole (LVPWs) and (F) LVPW thickness at diastole (LVPWd). (* P < 0.05 IR+Vehicle *vs.* IR+CAA0225)

4.3.5 Effect of CAA0225 on cardiac function measured by PV loops at 2 and 4 weeks post IR injury

Pressure-volume (PV) loop measurements were performed in IR mice at the end of the 2 and 4 wk studies, respectively. The loops were generated by plotting intra-LV pressure *vs.* LV volume (**Figure 4-4A and Figure 4-5A**). In the 2 wk study, CAA0225 treated mice demonstrated significantly increased intra-LV parameters at 2 wk post IR injury including developed pressure (101.3 ± 2.0 [n = 4] *vs.* 92.2 ± 3.1 mmHg [n = 5], CAA0225 *vs.* Vehicle, P < 0.05, **Figure 4-4B**), intra-LV maximum

pressure (101.3 ± 1.4 [*n* = 4] *vs.* 92.6 ± 3.2 mmHg [*n* = 5], CAA0225 *vs.* Vehicle, *P* < 0.05, **Figure 4-4B**), maximum rate of intra-LV pressure rise (11065 ± 928 [*n* = 4] *vs.* 8812 ± 642 mmHg/s [*n* = 5], CAA0225 *vs.* Vehicle, *P* < 0.05, **Figure 4-4D**) and minimum rate of intra-LV pressure fall (-9923 ± 744 [*n* = 4] *vs.* -7436 ± 661 mmHg/s [*n* = 5], CAA0225 *vs.* Vehicle, *P* < 0.05, **Figure 4-4D**). No significant difference was found between groups in end systolic pressure (93.2 ± 3.0 [*n* = 4] *vs.* 86.1 ± 4.3 mmHg [*n* = 5], CAA0225 *vs.* Vehicle, *P* > 0.05, **Figure 4-4B**) and end diastolic pressure (5.9 ± 0.6 [*n* = 4] *vs.* 6.9 ± 1.9 mmHg [*n* = 5], CAA0225 *vs.* Vehicle, *P* > 0.05, **Figure 4-4B**). There was no significant difference in end systolic volume (14.2 ± 3.6 [*n* = 4] *vs.* 12.1 ± 2.2 μL [*n* = 5], CAA0225 *vs.* Vehicle, *P* > 0.05, **Figure 4-4E**) and end diastolic volume (34.9 ± 9.7 [*n* = 4] *vs.* 26.2 ± 3.9 μL [*n* = 5], CAA0225 *vs.* Vehicle, *P* > 0.05, **Figure 4-4E**). No significant difference was found in ejection fraction (57.3 ± 2.5 [*n* = 4] *vs.* 53.7 ± 1.7 % [*n* = 5], CAA0225 *vs.* Vehicle, *P* > 0.05, **Figure 4-4C**) and cardiac output (12.5 ± 4.1 [*n* = 4] *vs.* 8.3 ± 0.9 mL [*n* = 5], CAA0225 *vs.* Vehicle, *P* > 0.05, **Figure 4-4F**).

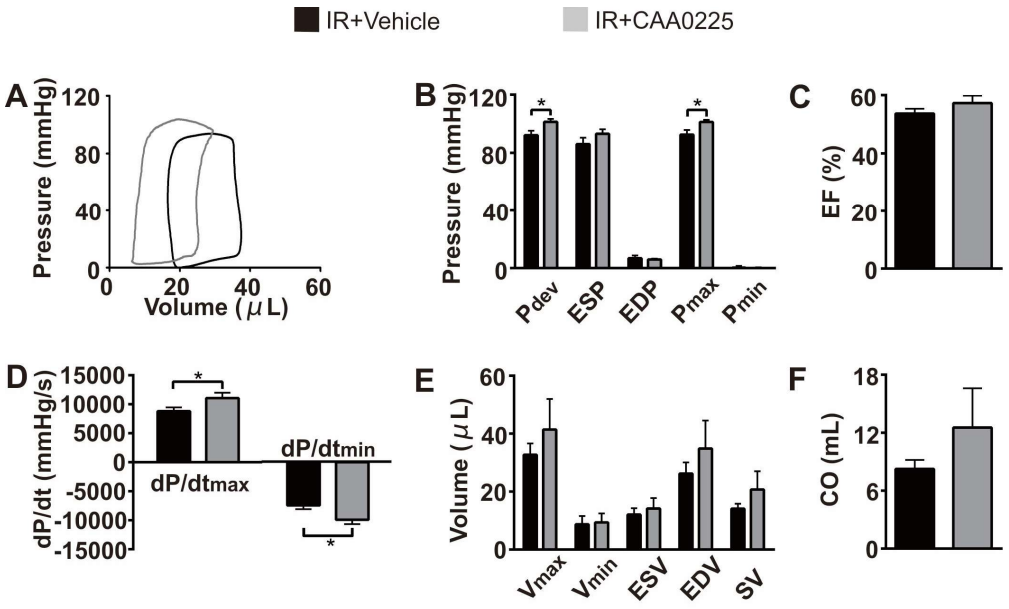

Figure 4-4. Cardiac function in IR hearts with CAA0225. (A) Representative PV loops of IR+Vehicle and IR+CAA0225 at 2 wk post IR injury. (B) Mean PV loop data obtained from a 2 wk study of IR+Vehicle (*n* = 5) and IR+CAA0225 (*n* = 4) for intra-LV pressure and (C) Ejection fraction (EF), (D) rate of intro-LV pressure change (dP/dt), (E) intra-LV volume and (F) Cardiac output (CO). (* *P* < 0.05 IR+Vehicle *vs.* IR+CAA0225)

At the end of the 4 wk period study, no significant difference was found between CAA0225 treated mice and control mice at 4 wk post IR injury in intra-LV developed pressure (97.9 ± 9.0 [*n* = 3] *vs.* 89.9 ± 4.1 mmHg [*n* = 4], CAA0225 *vs.* Vehicle, *P* > 0.05, **Figure 4-5B**), intra-LV maximum pressure (100.8 ± 7.7 [*n* = 3] *vs.* 90.7 ± 4.0 mmHg [n = *4*], CAA0225 *vs.* Vehicle, *P* > 0.05, **Figure 4-5B**), end systolic pressure (88.5 ± 10.0 [*n* = 3] *vs.* 82.6 ± 4.9 mmHg [*n* = 4], CAA0225 *vs.* Vehicle, *P* > 0.05, **Figure 4-5B**), and end diastolic pressure (8.7 ± 0.8 [*n* = 3] *vs.* 6.6 ± 1.3 mmHg [*n* = 4], CAA0225 *vs.* Vehicle, *P* > 0.05, **Figure 4-5B**). There was no significant difference between groups in maximum rate of intra-LV pressure change (8598 ± 1222 [*n* = 3] *vs.* 7884 ± 607 mmHg/s [*n* = 4], CAA0225 *vs.* Vehicle, *P* > 0.05, **Figure 4-5D**) and minimum rate of intro-LV pressure change (-6856 ± 734 [*n* = 3]

vs. -7072 ± 714 mmHg/s [*n* = 4], CAA0225 *vs.* Vehicle, *P* > 0.05, **Figure 4-5D**). No significant difference was found in end systolic volume (18.7 ± 7.0 [*n* = 3] *vs.* 19.4 ± 4.2 μL [*n* = 4], CAA0225 *vs.* Vehicle, *P* > 0.05, **Figure 4-5E**) and end diastolic volume (35.2 ± 7.5 [*n* = 3] *vs.* 37.1 ± 6.0 μL [*n* = 4], CAA0225 *vs.* Vehicle, *P* > 0.05, **Figure 4-5E**). No significant difference was found in ejection fraction (50.0 ± 10.0 [*n* = 3] *vs.* 47.2 ± 5.3 % [*n* = 4], CAA0225 *vs.* Vehicle, *P* > 0.05, **Figure 4-5C**) and cardiac output (8.6 ± 1.0 [*n* = 3] *vs.* 9.5 ± 1.9 mL [*n* = 4], CAA0225 *vs.* Vehicle, *P* > 0.05, **Figure 4-5F**).

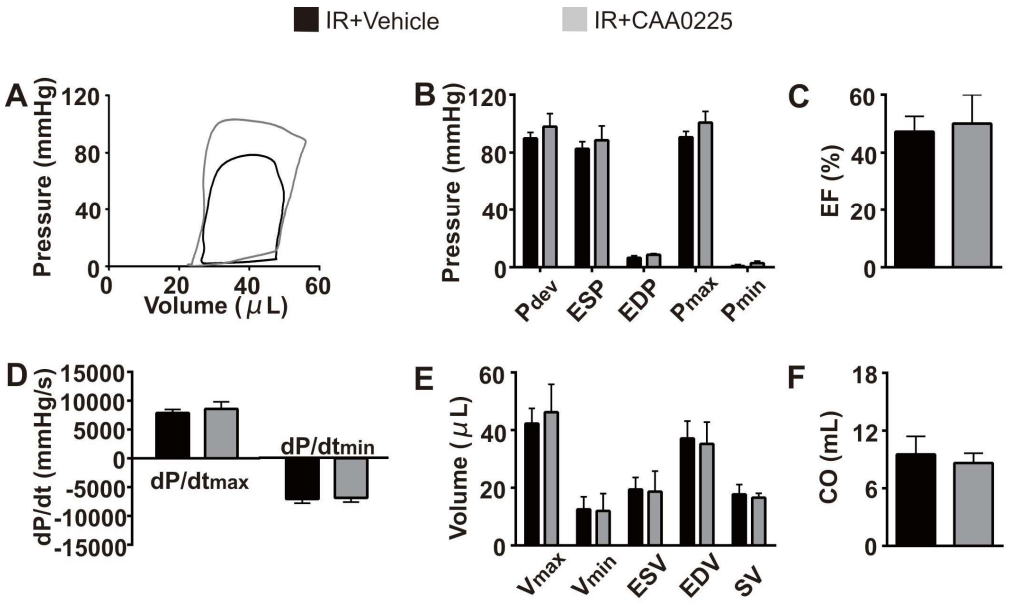

Figure 4-5. Cardiac function in IR hearts with CAA0225. (A) Representative PV loops of IR+Vehicle and IR+CAA0225 at 4 wk post IR injury. (B) Mean PV loop data obtained from a 4 wk study of IR+Vehicle (*n* = 4) and IR+CAA0225 (*n* = 3) for intra-LV pressure and (C) Ejection fraction (EF), (D) rate of intro-LV pressure change (dP/dt), (E) intra-LV volume and (F) Cardiac output (CO). (* *P* < 0.05 IR+Vehicle *vs.* IR+CAA0225)

4.3.6 Effect of CAA0225 on infarct size at 2 weeks post IR injury

Double-dye staining is not possible at the 2 wk stage due to adhesions which

prevent the retying of the suture to occlude the coronary artery. The hearts at 2 wk post IR injury were therefore fixed and Sirius staining performed for infarct size measurement. Area of LV and red-stained scar were measured from 5 images/heart and the overall IR infarct size was calculated by dividing the sum of scar pixels by the sum of LV pixels. Representative heart sections are shown in **Figure 4-6A**. CAA0225 treatment significantly reduced infarct size by 53% at 2 wk post IR injury (6.0 ± 1.6 *vs.* 12.8 ± 3.2 %; CAA0225 [n = 9] *vs.* control [n = 7]; $P < 0.05$; **Figure 4-6B**).

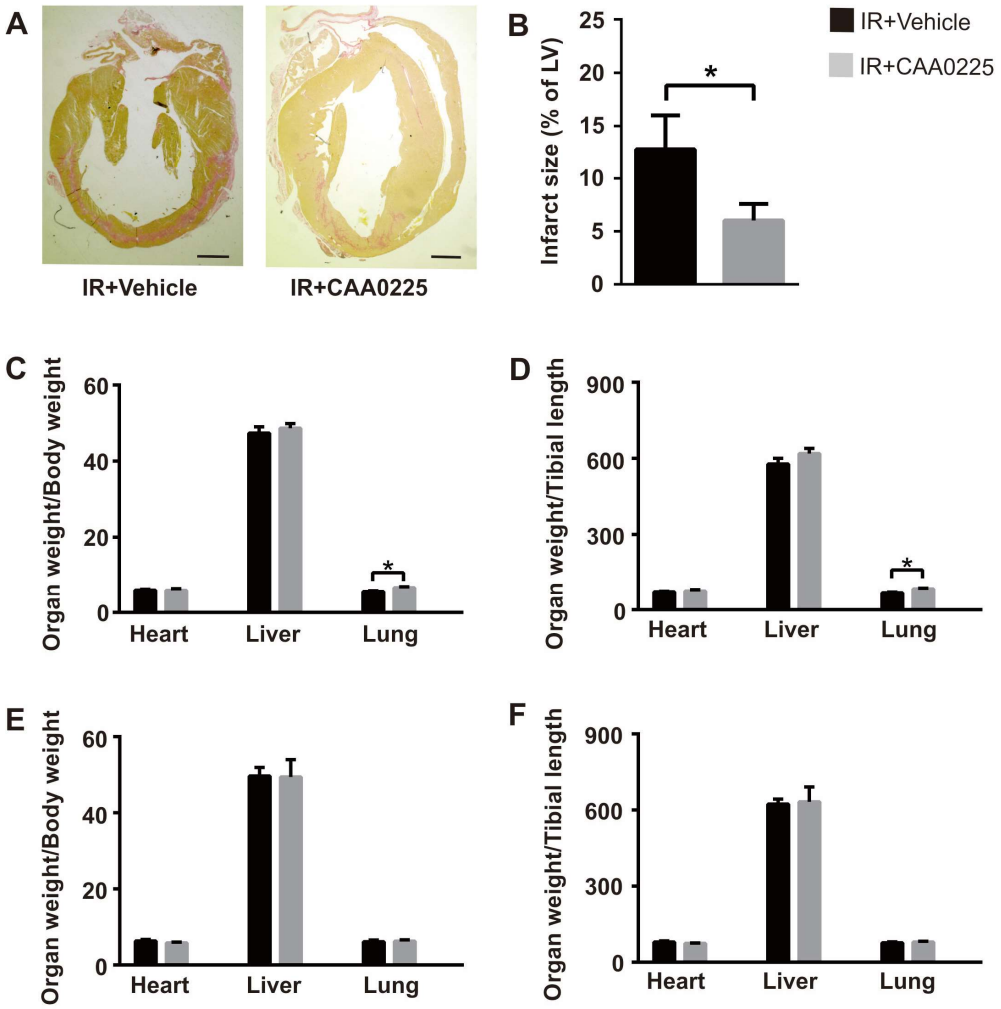

Figure 4-6. Infarct size and organ weights in IR mice with CAA0225. (A) Representative sirius red staining images of IR+Vehicle and IR+CAA0225 at 2 wk post IR injury (scale bars: 1mm). **(B)** Mean infarct size of IR+Vehicle (n = 7) and IR+CAA0225 (n = 9) at 2 wk post IR injury. **(C)** Mean organ weights obtained in a 2 wk study of IR+Vehicle (n = 9) and IR+CAA0225 (n = 7) *vs.* body weight and **(D)** *vs.* tibial length. **(E)** Mean organ weights obtained in a 4 wk study of IR+Vehicle (n = 5) and IR+CAA0225 (n = 6) *vs.* body weight and **(F)** *vs.* tibial length. (* $P < 0.05$ IR+Vehicle *vs.* IR+CAA0225)

4.3.7 Effect of CAA0225 on organ weights at 2 and 4 weeks post IR injury

Mice with IR induced by temporary LAD ligation were recovered from the surgery and sacrificed at 2 and 4 wk post IR injury. Organs including heart, liver and lung were weighed and the organ weights normalised by body weight and tibial length respectively. CAA0225 treated mice showed a small but significant increase of lung weight compared with control mice for lung-weight/body-weight (6.7 ± 0.3 *vs.* 5.7 ± 0.2; CAA0225 [*n* = 7] *vs.* control [*n* = 9]; *P* < 0.05; **Figure 4-6C**), and for lung-weight/tibial-length (85.2 ± 3.3 *vs.* 69.8 ± 3.3; CAA0225 [*n* = 7] *vs.* control [*n* = 9]; *P* < 0.05; **Figure 4-6D**). There was no significant difference between CAA0225 and control groups in lung weight at 4 wk post IR injury for lung-weight/body-weight (6.3 ± 0.3 *vs.* 6.1± 0.5; CAA0225 [*n* = 6] *vs.* control [*n* = 5]; *P* > 0.05; **Figure 4-6E**), nor for lung-weight/tibial-length (80.2 ± 3.0 *vs.* 76.8 ± 3.8; CAA0225 [*n* = 6] *vs.* control [*n* = 5]; *P* > 0.05; **Figure 4-6F**). There was no significant difference between CAA0225 treated mice and control mice in heart weight at 2 wk post IR injury for heart-weight/body-weight (6.0 ± 0.4 *vs.* 6.1 ± 0.3; CAA0225 [*n* = 7] *vs.* control [*n* = 9]; *P* > 0.05; **Figure 4-6C**), nor for heart-weight/tibial length (76.8 ± 5.5 *vs.* 73.6 ± 2.6; CAA0225 [*n* = 7] *vs.* control [*n* = 9]; *P* > 0.05; **Figure 4-6D**). There was no significant difference in heart weight at 4 wk post IR injury for heart-weight/body-weight (5.8 ± 0.2 *vs.* 6.3 ± 0.4; CAA0225 [*n* = 6] *vs.* control [*n* = 5]; *P* > 0.05; **Figure 4-6E**) and for heart-weight/tibial length (74 ± 2 *vs.* 80 ± 5; CAA0225 [*n* = 6] *vs.* control [*n* = 5]; *P* > 0.05; **Figure 4-6F**). There was no significant difference between CAA0225 and control groups in liver weight at 2 wk post IR injury for liver-weight/body-weight (48.7 ± 1.2 *vs.* 47.4 ± 1.7; CAA0225 [*n* = 7] *vs.* control [*n* = 9]; *P* > 0.05; **Figure 4-6C**) and for liver-weight/tibial length (619 ± 20 *vs.* 578 ± 23; CAA0225 [*n* = 7] *vs.* control [*n* = 9]; *P* > 0.05; **Figure 4-6D**). No significant difference in liver weight was found at 4 wk post IR injury liver-weight/body-weight (49 ± 5 *vs.* 50 ± 2; CAA0225 [*n* = 6] *vs.* control [*n* = 5]; *P* > 0.05; **Figure 4-6E**) and for liver-weight/tibial length (632 ± 59 *vs.* 623 ± 20; CAA0225 [*n* = 6] *vs.* control [*n* = 5]; *P* > 0.05; **Figure 4-6F**).

4.3.8 Effect of CAA0225 on area at risk (AAR) and infarct size at 3 hours post IR injury

Representative heart slices are shown in **Figure 4-7A**. Area at risk was comparable between the IR+CAA0225 group and the IR+Vehicle group at a relative size of 22-24% of LV (23.8 ± 4.0 *vs.* 22.2 ± 1.8 %; CAA0225 [*n* = 14] *vs.* control [*n* = 13]; *P* > 0.05; **Figure 4-7B**), while mice treated with CAA0025 had an infarct size which was 73% of that in the vehicle control (46.9 ± 5.2 *vs.* 64.1 ± 3.8 %; CAA0225 [*n* = 14] *vs.* control [n = 13]; *P* < 0.05; **Figure 5-1C**).

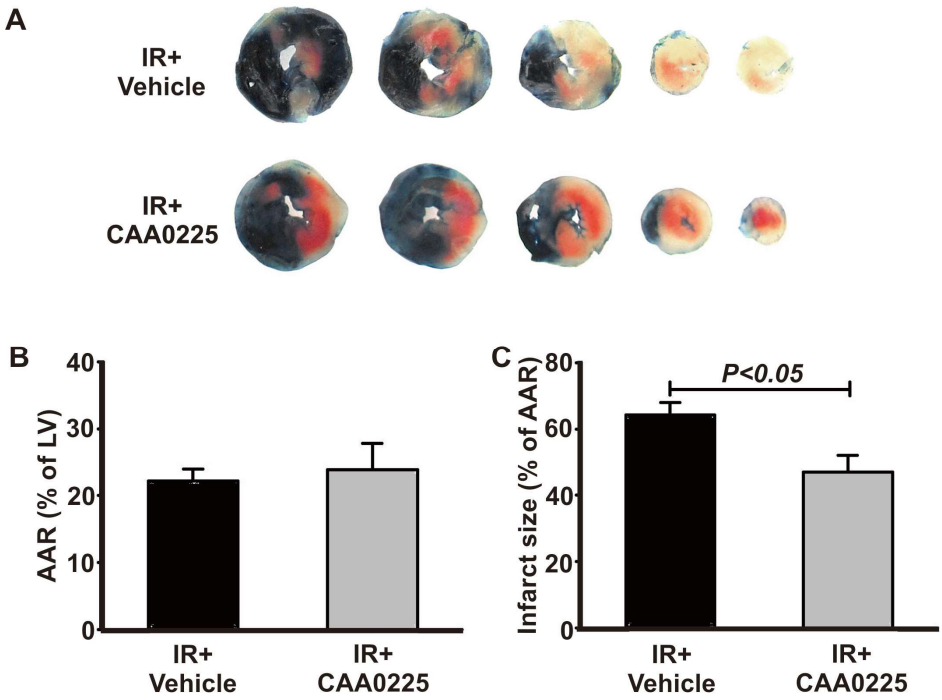

Figure 4-7. Area at risk (AAR) and infarct size in IR hearts with CAA0225. (A) Representative double-dye staining images of IR+Vehichle and IR+CAA0225 at 3 hours post IR injury injury. (B) Mean AAR (% of LV) and (C) infarct size (% of AAR) of IR+Vehicle (*n* = 13) and IR+CAA0225 (*n* = 14) at 3 hours post IR injury injury (data presented as mean ± SEM; **P* < 0.05 IR+Vehicle *vs.* IR+CAA0225)

4.4 Discussion

4.4.1 CAA0225 reduced infarct size in *in vivo* mouse model of IR injury

The fundamental treatment for an acute MI in the clinical setting is to re-establish blood flow by primary percutaneous coronary intervention (PPCI) (Zimarino et al., 2008). However, the process of restoring blood flow to ischaemic areas paradoxically causes additional injury, i.e. reperfusion injury, which contributes to up to 50% of tissue damage after MI (Frohlich et al., 2013). In the clinical setting infarct size is an important index of clinical outcomes, where smaller infarct size indicates less damage and better ejection fraction (Rakowski et al., 2014, Bethke et al., 2015), but currently there are no reliable therapies which can clinically reduce IR injury by rescuing or preserving areas at risk and thus ultimately limit infarct size following PPCI treatment. Therefore, exploring new targets with strong clinical relevance that can reduce infarct size following MI and reperfusion is of great interest in pre-clinical studies. Using the *in vivo* mouse models of MI and IR injury, our data showed for the first time that inhibition of cathepsin-L with a cathepsin-specific inhibitor CAA0225 can reduce infarct size following IR injury. Area at risk (AAR) can be demarcated by double-dye staining after acute ischaemic injury with reperfusion (Bohl et al., 2009). The area at risk was not significantly different between groups post IR injury injury indicating that the surgical induced coronary artery ligation was performed consistently between groups. In the IR mouse with 3 hr reperfusion, infarct size was expressed as the percentage of AAR. CAA0225 significantly reduced infarct size to 73% of control level at 3 hr post IR injury without change in AAR size. A significant difference was also found in infarct size expressed in the percentage of LV at 2 wk following IR, where mice treated with CAA0225 had an infarct size of 47% of that of the control mice. These findings are consistent with our results of the isolated rat heart with IR injury, where we found the infarct size was decreased to 69% of control level by CAA0225. In the present study, there was no significant difference in infarct size at 2 wk post MI with a single dose of inhibitor mediated cathepsin-L inhibition. Although the difference is not significant, in these MI hearts CAA0225 treatment showed smaller infarct than DMSO control. Further work on this particular result is required with

in order to measure the AAR, which we have shown in our IR injury model. In the MI model induced by permanent coronary artery ligation, we would not expect differences to occur between groups unless changes in angiogenesis/myocardial regeneration/resistance to hypoxia occurred, as in the permanent MI model there is no reperfusion and the infarct size represents the full AAR. Collectively these data are in contrast to the setting of complete cathepsin-L deficiency (knockout) where the cathepsin-L deficient mice exhibited a significantly larger infarct than control mice at 2 wk and 4 wk post MI with permanent LAD ligation (Sun et al., 2011). The difference may result from the pattern of cathepsin-L inhibition, as in cathepsin-L knockout mouse the deficiency is complete and from birth while using inhibitor the inhibition is highly likely to be temporary and incomplete.

Cathepsin-L, which typically localizes in endosomes and lysosomes, is a key member of the lysosomal proteases participating in the lysosomal proteolytic processes in the heart. The role of lysosomal proteases in MI and IR injury is still not well understood. Studies about lysosomal cathespins suggest that the translocation of cathespins from lysosomes into the cytoplasm contributes to cell death (Li and Yuan, 2004, Tiwari et al., 2008, Turski and Zaslonka, 2000). A previous study *in vitro* has demonstrated that the expression and activity of cathepsin-L were significantly increased in the heart in response to stress such as hypertrophic stimulation (phenylephrine-induced cardiac hypertrophy), and cathepsin-L deficient myocytes showed reduced lysosomal activity with impaired autophagosomal function (Sun et al., 2013). The alteration of lysosomal activity in cathepsin-L deficient myocytes resulted in impaired protein processing with aggregation of cellular filaments and decrease of cellular protein degradation. In mice with cathepsin-L deficiency, an accelerated response to pathological stress resulted in exacerbated cardiac hypertrophy and dysfunction. These alternations were associated with impaired lysosomal function, which led to the defective of autophagy–lysosomal pathway, and finally resulted in impaired intracellular protein degradation and homeostatic remodelling (Sun et al., 2013). These findings showed an imbalance of protein homeostasis caused by dysfunction of the autophagy–lysosomal pathway system, which may lead to pathological hypertrophy and dysfunction.

Autophagy has recently been recognized to play an important role in

cardiomyocyte death (Chiong et al., 2011). Increased autophagy is related to the acceleration of cell death in response to stress (McCormick et al., 2012). In recent years, studies have shown that autophagy is induced by myocardial ischaemia and further enhanced during reperfusion (Matsui et al., 2007, Gurusamy et al., 2009). However, the role of autophagy in cardiac IR injury remains inconclusive. Studies have reported that autophagy induced by lack of blood supply is beneficial during the period of ischaemia and protects myocardium from apoptosis in the ischaemic area (Yan et al., 2005). However, whether autophagy is protective or detrimental during reperfusion remains controversial. A recent study has shown that inhibition of autophagy by the treatment of 3-methyladenine (an inhibitor of autophagosome formation) or by knockdown of Beclin1 (a key regulator of autophagy) can increase the survival of cardiomyocytes following IR injury *in vitro* (Valentim et al., 2006). In an *in vivo* model of IR injury, autophagy is increased in mouse hearts with IR and the infarct size was reduced *via* down-regulation of autophagy in Beclin1 knockout mice (Matsui et al., 2007). These evidence suggests that autophagy plays a critical role during IR injury. As cathepsin-L is involved in the autophagy process as a key member of lysosomal proteases, whether CAA0225 has altered the ability of cathepsin-L to regulate the autophagy–lysosomal pathway during IR injury remains unknown and requires future investigation.

4.4.2 CAA0225 preserved cardiac function in *in vivo* mouse models of MI and IR injury

Our data have shown in the *in vivo* mouse models of MI and IR, treatment with the cathepsin-L inhibitor CAA0225 significantly preserved cardiac function in both mice with MI and IR injury. The improvement in cardiac function most likely relates to the reduction in infarct size, which was observed by double-dye staining at 3 hr post IR injury and Sirius red staining at 2 wk post IR injury. However, although there was no significant difference in infarct size at 2 wk post MI, cardiac function was improved in mice treated with CAA0225. Therefore, cathepsin-L may also play a role in pathways that relate to cardiac contractile function or post infarct remodelling.

A number of significantly changed functional parameters were observed in mice treated with CAA0225. These significant improved parameters include fractional

shortening, intra-LV developed pressure, maximum pressure, maximum rate of pressure rise and fall. These parameters indicate that CAA0225 increased cardiac contractility following MI and IR. Fractional shortening measured by M-mode echocardiography was found to be significantly improved at 2 wk post MI, 2 wk and 4 wk post IR injury. The LV internal dimension and wall thickness measured from M-mode echo showed that treatment with CAA0225 did not lead to LV dilation or changes in wall thickness. The PV loop parameters such as developed pressure, maximum pressure, maximum and minimum rate of pressure change were also found to be significantly improved at 2 wk post IR injury, but no significant differences were found at 4 wk post IR injury. A possible explanation for this is that only a single dose of cathepsin-L inhibitor was used when the LAD ligation was made, therefore the effect of the inhibitor on cardiac function may diminish over time. It is also possible that the *n* values for the PV loops experiments are too low to detect significant differences.

Compared to temporary inhibition with CAA0225, cathepsin-L was completely and persistently deficient in the cathepsin-L knockout mouse and the one-year-old cathepsin-L knockout mice showed impaired cardiac contraction and LV hypertrophy (Stypmann et al., 2002a). In the *in vivo* model of aortic banding in mice, cathepsin-L deficiency significantly exacerbated cardiac hypertrophy and worsened cardiac function (Sun et al., 2013). Worsened cardiac function was also observed in cathepsin-L deficient mice post MI when compared with wild type mice (Sun et al., 2011). A recent study has shown that cathepsin-L activity was significantly increased in myocardium from 24 h post MI in mice with a peak at 3 d post MI (Sun et al., 2011). Increased heart weight and liver weight were also shown in the cathepsin-L knockout mice post MI. These results suggest that complete deficiency of cathepsin-L can lead to cardiac remodelling and heart failure post MI (Sun et al., 2011). In our IR injury mice with CAA0225 treatment, no increase was found in heart and liver weight compared with mice treated with vehicle. Our functional measurements also showed use of the cathepsin-L inhibitor did not cause hypertrophy or heart failure. Interestingly, the lung weight was found significantly increased in mice with CAA0225 at 2 wk post IR injury, but no difference was found in lung weight at 4 wk post IR injury. The lung weight change might have been due to the inhibition of cathepsin function in the lung that might

temporarily impair the matrix remodelling and protein degradation in lungs (Buhling et al., 2004). A limitation of the current study is that it is unknown how long the inhibitor lasts *in vivo* as just one injection was given. However, the injection was given during ischaemia before reperfusion, which is an important therapeutic period to apply therapies to prevent IR injury with clinical applicability. The cathepsin activity measurement in different organs at different time points post IR injury may be included in further work.

4.4.3 A potential mechanistic explanation for the effects of extracellular cathepsin-L on IR injury

Lysosomal exocytosis is a secretory function of lysosomes leading to release of contents such as cathepsins into extracellular spaces (Appelqvist et al., 2013). Lysosomal exocytosis is involved in several physiological processes and activation of lysosomal exocytosis is considered to be beneficial for cellular clearance (Medina et al., 2011). Exocytosis can be promoted by insufficient autophagy as Lee et al. demonstrated that inefficient clearance of α-synuclein aggregates caused by reduced autophagic activity led to elevated α-synuclein exocytosis and subsequently caused α-synuclein deposition and cell death in neighbouring neurons (Lee et al., 2013). Our data demonstrated that cathepsin-L released from isolated heart during IR injury (unpublished data) and increased serum levels of cathepsin-L was also observed in MI patients (Liu et al., 2009). The extracellular cathepsin-L may come from lysosomal exocytosis following IR injury and then functions within the extracellular space and causes detrimental effects to the heart. Our group demonstrated that extracellular cathepsin-L derived from Trypanosoma brucei can cause cardiac dysfunction by changing sarcoplasmic reticulum function (Elliott et al., 2013). The recent work in our group has also demonstrated that IR injury leads to increased Ca^{2+} influx through L-type calcium channels, reduced sarcolemmal NCX extrusion and SERCA activity in *ex vivo* isolated rat cardiomyocytes. These alterations increased diastolic $[Ca^{2+}]i$ and promoted adverse spontaneous SR-mediated Ca^{2+} release (Ca^{2+} waves) in cardiomyocytes. These changes can lead to cell death and contractile dysfunction of the whole heart while treatment with CAA0225 can normalise these Ca^{2+} handling abnormalities following IR injury (unpublished data). This evidence

indicates that the beneficial effects of CAA0225 may be associated with normalization of cathepsin-L-induced abnormal calcium handling in cardiomyocytes following IR injury.

A limitation of this study is that it is not known whether extracellular inhibition or intracellular inhibition of cathepsin-L contributes to the beneficial effects. The cathepsin inhibitor utilized in this study is CAA0225, a cell-permeable compound, which inhibits both intracellular and extracellular cathepsin-L (Takahashi et al., 2009). The specific inhibition of cathepsin-L by CAA0225 can lead to depressed degradation of long-lived proteins in HeLa and Huh-7 cells cultured under nutrient-deprived conditions as reported by Takahashi et al. (Takahashi et al., 2009). Therefore, a non-permeable inhibitor which cannot enter the cell may be used to further assess the effects of extracellular cathepsin-L on cardiomyocytes without inhibition of intracellular cathepsin-L. Nevertheless, the function of intracellular cathepsin-L following IR injury is still not fully understood and requires future investigation.

4.4.4 A potential mechanistic explanation of the effects of intracellular cathepsin-L during IR injury

Recent evidence demonstrated that lysosomal enzymes, including cathepsin-B and cathepsin-L, are released into cytosol through lysosomes in some diseases, such as atherosclerosis and type 2 diabetes, causing inflammasome activation, and inhibition of cathepsins prevents the NLRP3 inflammasome activation (Masters et al., 2010, Masters et al., 2011, Guo et al., 2015). In the rat model of MI, Liu et al. have demonstrated that the cathepsin inhibitor CA074Me caused attenuated cardiac dysfunction by inhibiting NLRP3 activation (Liu et al., 2013). It's important to note that the cathepsin inhibitor used in these studies is a cell-permeable inhibitor CA074Me which is capable of specifically inhibiting both cathepsin-B and cathepsin-L with IC50 of 2.2 nM and 1.5 μM respectively (Steverding, 2011). The concentration of CA074Me used for the type 2 diabetes study is 10 μM (Masters et al., 2010), and for the rat MI study is 10 mg/kg per day (Liu et al., 2013). In the study of atherogenesis with cholesterol crystals activation, acute inflammation induced by cholesterol crystals is impaired in knockout mice with deficiency of NLRP3, cathepsin-B, or cathepsin-L (Duewell et al., 2010). The above evidence

suggests that the intracellular function of cathesin-L and the beneficial effects of CAA0225 in IR injury, as demonstrated in this thesis, may be related to the NLRP3 inflammasome activation.

NLRP3 inflammasome is a large multiprotein complex that is formed in the cytosol in response to injury and plays a central role in the inflammatory response by activation of caspase-1 and mediation of the processing and releasing of the proinflammatory cytokine IL-1ß (Baroja-Mazo et al., 2014). The NLRP3 inflammasome was found to be activated by increased caspase-1 activity and cytoplasmic aggregates of its components (apoptosis-associated speck-like protein containing a caspase recruitment domain (ASC), cryopyrin, and caspase-1) within cardiomyocytes located at the BZ. The formation of the inflammasome in the heart post MI caused additional loss of cells and led to heart failure (Kawaguchi et al., 2011). Inhibition of the inflammasome component cryopyrin by using silencing RNA or a pharmacologic inhibitor prevented the formation of the inflammasome and limited infarct size and post MI remodelling (Mezzaroma et al., 2011). Activation of the NRLP3 inflammasome by a calcium sensing receptor (CaSR) contributes to post MI remodelling by accelerating cardiac fibroblast phenotypic transversion, increase of collagen and extracellular matrix (ECM) secretion (Liu et al., 2015). During IR injury, the inflammatory response also plays an important role by the release of inflammatory cytokines and chemokines that recruit circulating leukocytes into ischaemic regions (Frangogiannis et al., 2002, Steffens et al., 2009, Hausenloy and Yellon, 2016), and inhibition of inflammatory responses by inhibition leukocyte or cell adhesion can reduce infarct size, preserve cardiac function and prevent remodelling (Litt et al., 1989, Ma et al., 1991, Zhao et al., 1997). Recent evidence indicates that inflammasome activation in cardiac fibroblasts is involved in the initial inflammatory response during IR injury. In mice deficient of the inflammasome component ASC, the inflammatory responses and subsequent injuries, including cardiac dysfunction and post-infarct remodelling were diminished (Kawaguchi et al., 2011). However, the molecular events triggering the inflammatory response during cardiac IR injury are incompletely understood. Future work needs to look into the NLRP3 inflammasome activation as a potential mechanistic explanation of the therapeutic effect of CAA0225.

CHAPTER 5.

Cardiac function in *Runx1* deficient mice following MI and IR injury

5.1 Introduction

5.1.1 Application of transgenic mice in cardiovascular research

The heart is composed of several types of cells. Each type has specific functions based on gene expression patterns, which responds to cellular and physiological environments (Doetschman et al., 2012, Gittenberger-de Groot et al., 2005). It is important to identify these functions at the animal level because the physiological and pathophysiological complexity cannot be recapitulated *in vitro* (Doetschman and Azhar, 2012). Mice models are optimal choices for investigating the genetic basis of cardiovascular diseases as they have four chambered hearts and are cost- and time-effective compared with other mammals (Snider and Conway, 2011). Tamoxifen and tetracycline-inducible strategies have been successful applied to demonstrate gene functions in cardiac structure, function, physiology and pathophysiology (Yutzey and Robbins, 2007, Molkentin and Robbins, 2009, Moga et al., 2008). Human α-myosin heavy chain (αMHC) and rat troponin T (Tnnt2) promoters with Tamoxifen and Tetracycline-inducible genes are two commonly used targeting strategies for the heart (Sohal et al., 2001, Sanbe et al., 2003, Minamino et al., 2001, Passman and Fishman, 1994, Wu et al., 2010). Both αMHC and Tnnt2 are expressed in the heart during the embryonic stage, whilst Cre or rtTA-inducible genes are applied in the postnatal heart (Ng et al., 1991, Jiao et al., 2003). Tamoxifen-regulated αMHC-CreERT2 (also called αMHC-MerCreMer) is the most extensively used strategy by far to target cardiomyocytes (Sohal et al., 2001). An alternative method is RU486 (anti-progestin)-inducible αMHC-CrePR1, which can also induce myocardial gene targeting in adult hearts (Minamino et al., 2001). However, αMHC-MerCreMer is more extensively used than αMHC-CrePR1, as tamoxifen is better tolerated than RU486 in mice (Doetschman and Azhar, 2012). There are some inherent pitfalls in using these strategies in the postnatal heart because the αMHC promoter can cause excess Cre levels that lead to temporary cardiac dysfunction, which, although, can resolve in 1 to 2 weeks post tamoxifen induction. (Molkentin and Robbins, 2009, Agah et al., 1997) Furthermore, these problems can be avoided by using proper control groups and have been found to be minimal in our lab (unpublished data).

5.1.2 Role of *Runx1* in cardiac remodelling post MI

Improvements in the treatment of myocardial infarction (MI), especially the application of PPCI, have increased the survival rate in patients with MI. Use of reperfusion therapy can salvage injured myocardial and reduce cardiac damage. However, the survivors who have survived with substantial left ventricular injury are facing a later risk of developing heart failure. Heart failure has become a frequent complication of MI which increases the risk of death by at least 3 to 4 fold (Minicucci et al., 2011) and heart failure post MI is associated with extremely high mortality despite optimised medical interventions (Roger, 2013, Chen et al., 2013). LV remodelling post MI plays a major role in the progression to heart failure (Mann and Taegtmeyer, 2001, Mann, 1999). Post MI cardiomyocyte death initiates a reparative process in the heart, which is associated with the generation of scar tissue composed predominately of fibrillary collagen (Sun and Weber, 2000). The surviving cardiomyocytes post MI undergo eccentric hypertrophy, which is characterised by thinning and lengthening of cardiomyocytes (Kehat and Molkentin, 2010). These post MI cellular changes can lead to adverse cardiac remodelling, including left ventricular (LV) wall thinning, dilation and contractile dysfunction (McMurray et al., 2012), which can cause systolic heart failure. Physiological cardiac function is regulated by intracellular calcium ions ($[Ca^{2+}]i$) and EC coupling. Abnormal calcium handling in cardiomyocyte plays an important role in cardiac contractile dysfunction and hypertrophy during heart failure (Luo and Anderson, 2013). Recent studies have shown that, post MI, *Runx1* expression is switched on in cardiomyocytes in the border zone (BZ) region adjacent to the infarct in both MI patients and animal models (Kubin et al., 2011, Gattenlohner et al., 2003). Given that *Runx1* expression is presented in neonatal cardiomyocytes but decreases to negligible levels in adult as discussed in Chapter 1, the re-activation of *Runx1* in adult cardiomyocytes post MI may play a role in regulation of the cardiac function and remodelling post MI.

5.1.3 Aims

To understand whether activation of *Runx1* is only a marker of ischaemic damage or plays a functional role post MI, MI was induced in mice where exon 4 of *Runx1* had been specifically excised in cardiomyocytes using Cre-LoxP technology.

The aims of this chapter are:

i) To investigate the effects of *Runx1* deficiency on LV function serially up to 8 weeks post MI, by using M-mode echocardiography with measurements of LV fractional shortening, wall thickness and LV dimension.

ii) To investigate the effects of *Runx1* deficiency on LV function 2 weeks post MI in a separate cohort of mice, by using intra-ventricular pressure volume loops.

iii) To investigate the effects of *Runx1* deficiency on LV function post IR injury in a separate cohort of mice, by using M-mode echocardiography.

5.2 Methods

5.2.1 Inducing myocardial infarction and ischaemia-reperfusion injury in mice by coronary ligation

MI and IR injury were induced in three groups of mice: $Runx1^{\Delta/\Delta}$ mice (αMHC-MerCreMer: $Runx1^{fl/fl}$); litter-mate $Runx1^{fl/fl}$ mice controlling for the insertion of the LoxP sites and $Runx1^{wt/wt}$ mice controlling for insertion of the tamoxifen-inducible Cre recombinase. *Runx1* deficiency mice ($Runx1^{\Delta/\Delta}$) and their littermate control mice ($Runx1^{fl/fl}$ and $Runx1^{wt/wt}$) aged 10–12 weeks (25–30 g) were induced with anesthesia by inhalation of 4% isofluorane gas (Isoflo, Abbott Laboratories, USA) with oxygen at 1.5 L/min followed by preoperative analgesia of 0.1 mg/kg buprenorphine (Vetergesic, Reckitt Benckiser Healthcare Ltd, UK) and 5 mg/kg carprofen (Rimadyl, Pfizer Animal Health, U.) delivered in 0.4 mL of sterile saline i.p. Endotracheal intubation was performed for the anesthetized mice and artificial ventilation was maintained with a tidal volume of 120 μL at 120 breaths/min on 1% isofluorane in 0.5 L/min oxygen. Mice were placed in a left lateral oblique position on a heat pad covered by surgical drape and their skin was incised in parallel with the ribs perpendicular to the sternum 5 mm proximal to the xyphoid process. The intercostal space was exposed through carefully

retracted thoracic muscles and the intercostal muscle was cut by an electrocautery pen, and then the ribs were retracted to expose the heart. The pericardial sac was removed to provide access to the left anterior descending (LAD) coronary artery. MI was induced by permanent ligation of the LAD coronary artery using a 9-0 nylon suture (W2829 Ethilon, Johnson & Johnson, UK). Ischaemia-reperfusion injury (IR) was induced by temporary tying of the LAD coronary artery (for 45 minutes) against a short section of polyethylene tubing (PE-10; outer diameter, 0.61 mm) with a 7-0 polypropylene suture.

To close the chest, three 6-0 metric non-absorbable prolene sutures (W8711, Johnson & Johnson, UK) were evenly pre-placed along the ribs. The lungs were reinflated and the pre-placed sutures were tied. The thoracic muscles were returned to their original place and skin was closed with 6-0 metric absorbable vicryl (W9575, Johnson & Johnson, UK). Mice that underwent the sham procedure had a thoracotomy without LAD ligation. Post-operatively, mice were given buprenorphine (0.1mg/kg) orally for 3 days.

5.2.2 Echocardiography

Anaesthesia was induced with 4% isofluorane gas (Isoflo, Abbott Laboratories, USA) with oxygen at 1.5 L/min and maintained *via* facemask with 0.5-1% isofluorane with 1.0 L/min oxygen. On a warmed heat pad, chest hair of mice was shaved and their body temperature was monitored and maintained at 37 °C with a rectal thermometer and the feedback-controlled heat pad. Mice were placed in a left lateral oblique position and warmed echo gel was applied on their chest and echocardiography obtained with a 15 MHz paediatric probe (Acuson Sequoia 512, Siemens UK). The two-dimensional LV long-axis view was obtained by placing the probe along the long-axis and then the LV short-axis view was obtained by rotating the probe clockwise by 90. The LV M-mode echocardiography was recorded from the short-axis view at the papillary muscle level. After scanning the echo gel was removed and the mice were recovered on the heat pad with oxygen supply before being returned to the cage.

5.2.3 Pressure-Volume loop measurements

Mice were anesthetized, endotracheally intubated, artificially ventilated and

body temperature maintained as described above. The PV loop measurement was performed using a closed chest surgical approach. A 1.2F 4.5 mm spaced PV catheter was inserted into the RCA in order to enter the LV chamber through the ascending thoracic aorta. The intra-LV pressure and volume were measured and PV loops were generated by plotting the pressure against the volume. These PV loop measurements were recorded with the ADVantage Pressure-Volume System (ADV500, Transonic).

5.2.4 Organ harvest and weighing

Mice were weighed and killed complying with the Schedule 1 method (cervical dislocation). The heart was excised and washed in ice-cold normal saline. Excess tissue was trimmed off. Aortas were cut transversely and cannulated with an aortic cannula attached to a syringe. The heart was perfused retrograde with 5 mL ice-cold normal saline to rinse out blood from the chambers and vessels. Hearts were weighed and stored. Lungs and liver were removed, blotted dry and then weighed but not stored. The mouse tibia length was measured for normalisation of organ weights. The heart, lungs and liver were weighed using a precision electronic balance (precision 0.00001g).

5.2.5 Measurement of infarct size by Sirius red staining

The hearts were fixed in 10% neutral buffered formalin (CellPath, U.K.) for a minimum of 24 hour before embedding into wax blocks. Each heart was sliced parallel to the long axis of the heart every 250 μm to produce serial sections until the aorta level was reached. The sections were stained with Sirius red (detailed protocol is described in Chapter 2). An EVOS digital microscope was used for photography. Images obtained were analysed using Adobe Photoshop (Adobe, USA) software, by which the infarct size of the post IR injury heart was measured with a pixel based approach and the number of pixels in LV area and red scar area were measured from all sections, respectively. The IR infarct size was calculated by dividing the sum of scar pixels from all sections by the sum of all LV pixels from all sections of the same heart.

5.2.6 Data recording and statistical analysis

Echo images were captured by the echo machine and analysed offline using ImageJ. PV loop data was recorded at a sampling rate of 1KHz and analysed offline using LabScribe2.0 software. Raw data in this thesis are expressed as mean ± SEM. Comparisons between MI and sham groups were performed using the Student's t test. Comparisons between more than two groups were conducted using ANOVA. In cases where the two control groups were combined, comparison was performed between the data of *Runx1*$^{\Delta/\Delta}$ mice and the pooled data of the two control groups using the Student's t test.

5.3 Results

5.3.1 Echocardiographic assessment of cardiac function in *Runx1*$^{\Delta/\Delta}$ mice post MI

One week after tamoxifen injection i.p., MI was induced in *Runx1* deficient mice (*Runx1*$^{\Delta/\Delta}$ MI mice), as well as two control groups (*Runx1*$^{fl/fl}$ MI mice and *Runx1*$^{wt/wt}$ MI mice). *Runx1*$^{\Delta/\Delta}$ sham mice were undergone sham surgical procedures without the ligation of right descending coronary artery. **Figure 5-1** shows the cardiac contractile function (measured by fractional shortening, of which the higher value indicates better cardiac function) recorded by M-mode echocardiography immediately prior to MI and every other week thereafter till 8 weeks. Fractional shortening decreased post MI in both control groups (i.e. *Runx1*$^{fl/fl}$ MI and *Runx1*$^{wt/wt}$ MI mice). By contrast, *Runx1*$^{\Delta/\Delta}$ mice demonstrated significantly preserved fractional shortening, of which the mean value of fractional shortening was 158% of that of the control groups at 8 weeks post MI (39.5 ± 0.7% *vs.* 24.9 ± 1.9%; $P < 0.05$; **Figure 5-1A and B**). *Runx1*$^{\Delta/\Delta}$ sham mice showed no change in fractional shortening during the equivalent 8-week time course post-surgery. There was no significant difference in fractional shortening between the *Runx1*$^{\Delta/\Delta}$ sham mice and *Runx1*$^{\Delta/\Delta}$ MI mice after surgery until at 8 weeks, when *Runx1*$^{\Delta/\Delta}$ MI mice had lower value of fractional shortening but still higher than that of control mice (**Figure 5-1B**).

At two weeks post MI, *Runx1*$^{\Delta/\Delta}$ mice showed smaller LV internal dimension measured at systole (LVIDs), of which the mean value was 77% of that of the two control groups post MI (2.5 ± 0.2 mm *vs.* 3.3 ± 0.1 mm; $P < 0.05$) (**Figure 5-1B**). The LVID measured at diastole (LVIDd) indicated that the hearts of *Runx1*$^{\Delta/\Delta}$ MI

mice and both control groups dilated at the level of the infarct border zone albeit to a lesser degree in *Runx1*$^{\Delta/\Delta}$ MI mice (**Figure 5-1C**). *Runx1*$^{\Delta/\Delta}$ sham mice demonstrated no change in either LVIDs or LVIDd during the equivalent 8-week time course post-surgery (**Figure 5-1C and D**).

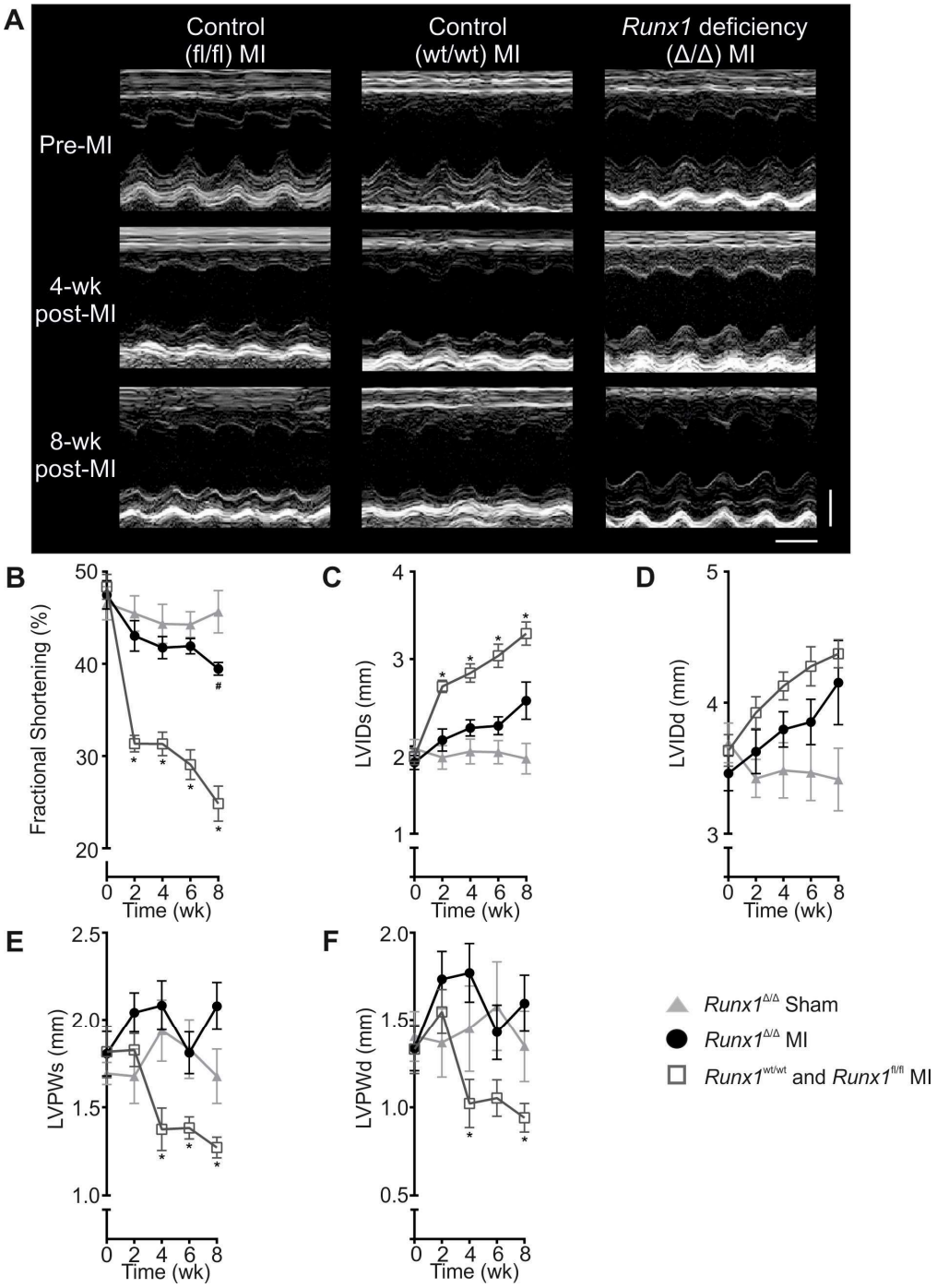

Figure 5-1. Cardiac function assessed by echocardiography in *Runx1*$^{\Delta/\Delta}$ mice. (A) Typical M-mode images (scale bar: x = 0.1 s; y = 2 mm). (B) Mean data obtained from an 8 wk study of control *Runx1*$^{fl/fl}$ MI and control *Runx1*$^{wt/wt}$ MI mice combined (n = 11), *Runx1*$^{\Delta/\Delta}$ MI mice (n = 9) and *Runx1*$^{\Delta/\Delta}$ sham mice (n = 5) (# P < 0.05 *Runx1*$^{\Delta/\Delta}$ MI mice *vs.* *Runx1*$^{\Delta/\Delta}$ sham mice and * P < 0.05 *Runx1*$^{\Delta/\Delta}$ mice *vs.* control *Runx1*$^{fl/fl}$ MI and control *Runx1*$^{wt/wt}$ MI mice combined) for Fractional shortening and (C) LVIDs, (D) LVIDd, (E) LVPWs and (F) LVPWd.

5.3.2 Echocardiographic assessment of cardiac structure in *Runx1*$^{\Delta/\Delta}$ mice post MI

As a result of the cardiac remodelling process, LV posterior wall thickness during systole (LVPWs) measured at the border zone level of the control group (*Runx1*$^{fl/fl}$ and *Runx1*$^{wt/wt}$) thinned at 2 weeks post MI. By contrast, *Runx1*$^{\Delta/\Delta}$ MI mice displayed preserved wall thickness that was 164% of control groups (*Runx1*$^{fl/fl}$ and *Runx1*$^{wt/wt}$) at 8 wk post MI (2.07 ± 0.14 *vs.* 1.27 ± 0.06 mm; $P < 0.05$; **Figure 5-1D**). Similarly, patterns of wall-thickness changes during diastole was consistent with those during systole in both *Runx1*$^{\Delta/\Delta}$ MI mice and control mice at 8-week post MI (**Figure 5-1E**). The wall-thickness data were confirmed at diastole 8 wk post MI (**Figure 5-1F**).

5.3.3 Blinded echocardiographic assessment of *Runx1*$^{\Delta/\Delta}$ mice post MI

A separate blinded study was performed to repeat the measurements and verify the robustness of data at the 2 wk time-point, where I was blinded to the genotypes during surgery and echo measurements (**Figure 5-2A-E**). Results of the echocardiography measurements of contractility and wall-thickness at the 2 week time point in this blinded study was consistent with those in the echocardiography study described above.

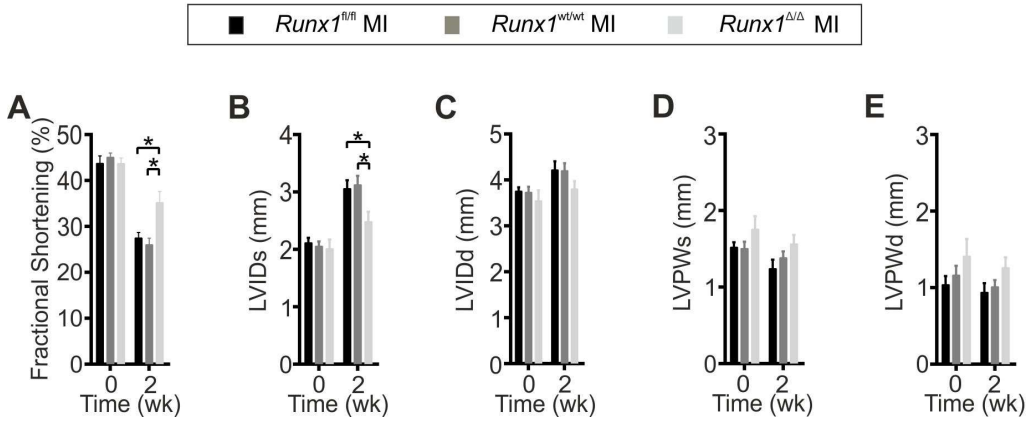

Figure 5-2. Cardiac function assessed by echocardiography in *Runx1*$^{\Delta/\Delta}$ mice (blinded study). 2 wk post MI blinded study (control 2 wk post MI blinded-study (control *Runx1*$^{fl/fl}$ MI (*n* = 8), control *Runx1*$^{wt/wt}$ MI (*n* = 11) and *Runx1*$^{\Delta/\Delta}$ mice MI (*n* = 7)) for the following functional parameters: (A) Fractional shortening, (B) Left ventricular internal diameter at systole (LVIDs), (C) LVID at diastole (LVIDd), (D) LV posterior wall thickness at systole (LVPWs), (E) LVPW thickness at diastole (LVPWd).

5.3.4 Organ weights in *Runx1*$^{\Delta/\Delta}$ mice post MI

Heart, liver and lung were harvest at 8-week post MI. These organs were weighed and normalised by body weight and tibial length, respectively. *Runx1*$^{\Delta/\Delta}$ MI mice (*n* = 9) demonstrated an increase of heart weight compared with that of *Runx1*$^{\Delta/\Delta}$ sham mice (*n* = 5) with normalisation by tibial length (83 ± 4 *vs.* 67 ± 2 mg/mm; *P* < 0.05; **Figure 5-3A**). However, there was no significant difference in heart weight when normalized to body weight (**Figure 5-3B**). No significant difference was found in liver and lung weight (**Figure 5-3C, D**).

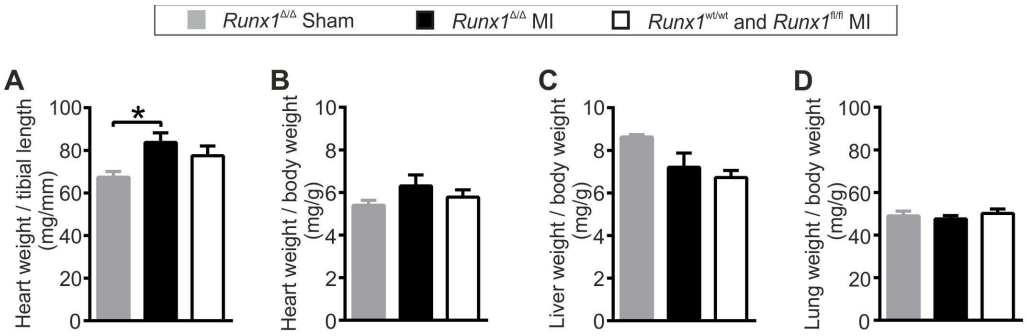

Figure 5-3. Organ weights post MI in *Runx1*$^{\Delta/\Delta}$ mice. Mean weight data obtained from the 8 wk study of control *Runx1*$^{fl/fl}$ MI and control *Runx1*$^{wt/wt}$ MI mice combined (n = 11), *Runx1*$^{\Delta/\Delta}$ MI mice (n = 9) and *Runx1*$^{\Delta/\Delta}$ sham mice (n = 5) (* P < 0.05) for the following ratios: (A) Heart weight to tibial length, (B) Heart weight to body weight, (C) Liver weight to body weight, and (D) Lung weight to body weight.

5.3.5 PV loop assessment of *Runx1*$^{\Delta/\Delta}$ mice post MI

An LV intraventricular pressure volume (PV) loop was utilized to assess the luminal volume of the *Runx1*$^{\Delta/\Delta}$ MI mice and the control mice *in vivo* in a separate study at 2 weeks post MI (**Figure 5-4A**). A proportion of the PV loop measurement were performed by Caroline Fattah. The end diastolic volume (EDV) in the *Runx1*$^{\Delta/\Delta}$ MI mice was decreased to 82% of that in the control mice (*Runx1*$^{fl/fl}$ and *Runx1*$^{wt/wt}$), indicating reduced LV dilation (36.3 ± 3.00 µL *vs.* 44.5 ± 2.47 µL; P < 0.05; **Figure 5-4A and C**). The end systolic volume (ESV) in *Runx1*$^{\Delta/\Delta}$ MI mice was decreased to 54% of that of the control mice, showing a greater level of emptying of LV blood volume (12.9 ± 2.98 µL *vs.* 23.7 ± 2.51 µL; P < 0.05; **Figure 5-4A and D**). This leftward shift in the PV loop in the *Runx1*$^{\Delta/\Delta}$ MI mice resulted in an increased ejection fraction (EF) that was 138% of the control mice (66.3% ± 5.69% *vs.* 48.0% ± 3.18%; P < 0.05; **Figure 5-4A and B**)

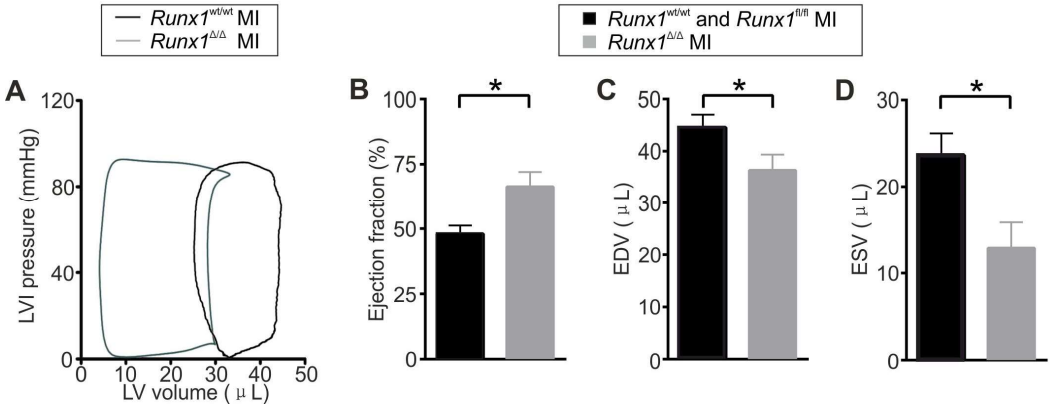

Figure 5-4. Cardiac function assessed by intraventricular pressure-volume (PV) loops in *Runx1*$^{\Delta/\Delta}$ mice. (A) Typical PV loops of control *Runx1*$^{wt/wt}$ and *Runx1*$^{\Delta/\Delta}$ mice at 2 wk post MI. Mean PV data obtained from a 2 wk post MI study of control *Runx1*$^{fl/fl}$ MI and control *Runx1*$^{wt/wt}$ MI mice combined (n = 11), *Runx1*$^{\Delta/\Delta}$ MI mice (n = 8) for the following functional parameters: (B) Ejection fraction, (C) End diastolic volume (EDV) (D) End systolic volume (ESV).

5.3.6 Echocardiographic assessment of *Runx1*$^{\Delta/\Delta}$ mice post IR injury injury

Next, it was tested whether *Runx1*$^{\Delta/\Delta}$ mice maintain preserved LV contractile function in a model of ischemia with IR injury. Fractional shortening decreased in control *Runx1*$^{fl/fl}$ mice post IR injury injury (**Figure 5-5A and B**). By contrast, *Runx1*$^{\Delta/\Delta}$ mice exhibited significantly preserved fractional shortening, which was 154% of control *Runx1*$^{fl/fl}$ mice at 8 weeks post IR injury injury (42.7 ± 1.5% *vs.* 27.7 ± 2.13%; P < 0.05; **Figure 5-5A and B**). Infarct size did not differ between *Runx1*$^{\Delta/\Delta}$ mice and *Runx1*$^{fl/fl}$ 8 weeks post IR injury injury (**Figure 5-5C**).

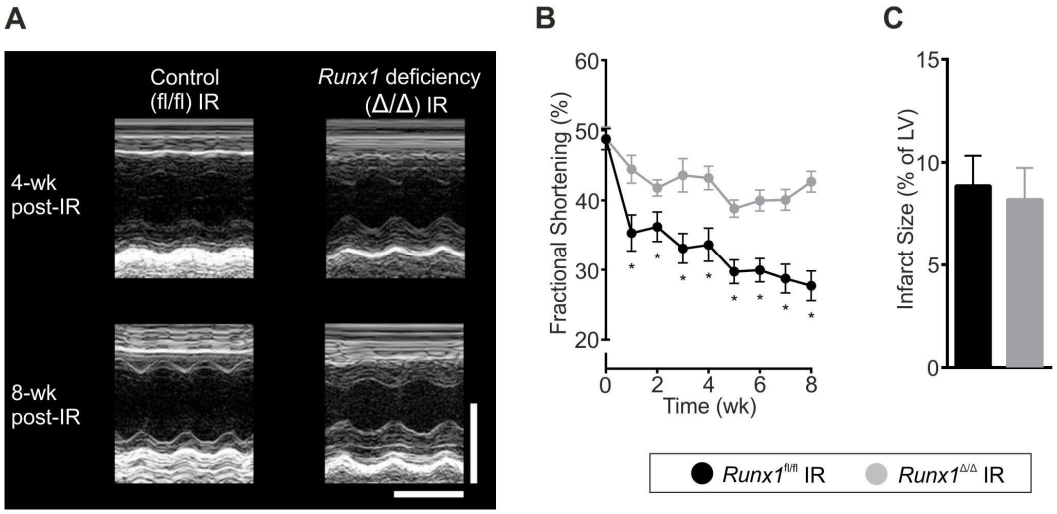

Figure 5-5. Cardiac function in *Runx1*$^{\Delta/\Delta}$ mice after IR injury. (A) Typical M-mode echocardiographic images of control *Runx1*$^{fl/fl}$ and *Runx1*$^{\Delta/\Delta}$ mice at 0, 4 and 8 wk post IR injury (scale bar: x = 0.1 s; y = 2 mm). (B) Mean echocardiographic fractional shortening data obtained from an 8 wk study of control *Runx1*$^{fl/fl}$ IR mice (n = 9) and *Runx1*$^{\Delta/\Delta}$ IR mice (n = 8) [* P < 0.05 *Runx1*$^{\Delta/\Delta}$ mice *vs.* control *Runx1*$^{fl/fl}$]. (C) Mean infarct size (control *Runx1*$^{fl/fl}$ IR mice [n = 9] and *Runx1*$^{\Delta/\Delta}$ IR mice [n = 7]).

5.4 Discussion

5.4.1 *Runx1* deficiency preserved cardiac contractility following myocardial infarction

The current study shows that *Runx1*-deficient mice had preserved contractile function post MI which is presented as higher value of fractional shortening, smaller LVIDs, smaller ESV and increased ejection function as compared to control mice. The *Runx1*-deficient mice also exhibited a smaller diastolic LV volume (LVIDd and EDV) and thicker LV wall compared with control, which suggests that the characteristics of eccentric hypertrophy were present in control mice but absent

in *Runx1*-deficient mice post MI. The heart weight was heavier in *Runx1*-deficient MI mice than that of *Runx*-deficient sham mice, indicating that reducing *Runx1* function might not completely prevent hypertrophy post MI. However, the cardiac function post MI is persistently preserved as long as 8 weeks without transition to systolic heart failure. Furthermore, *Runx1*-deficient mice also showed preserved cardiac function upon ischaemia-reperfusion injury.

MI has taken the place of hypertension or valvular diseases to become the most common cause of heart failure (Gheorghiade and Bonow, 1998). Loss of cardiomyocytes post MI induces profound alterations of LV architecture, such as scar formation, ventricular dilatation, and hypertrophy of the surviving cardiomyocytes (Cohn et al., 2000). Adverse LV remodelling mediated by biomechanical stress and humoral growth factors post MI is a major cause of heart failure (Mann, 1999, Force et al., 2002). LV remodelling post MI includes infarct expansion and hypertrophy of remote non-infarcted myocardium, fibrosis formation, LV dilatation, deterioration of cardiac function and progression to heart failure (Pfeffer and Braunwald, 1990, Braunwald and Pfeffer, 1991, Sutton and Sharpe, 2000). At the cellular level, the maladaptive hypertrophy of the remote myocardium includes progressive cell lengthening without a proportional widening of the cell (Zimmer et al., 1990, Gerdes et al., 1992). The mechanism and pathophysiological process in post MI remodelling and hypertrophy, and the progression to heart failure is not fully understood but does involve modulation at the cellular level including altered contractile function and gene expression.

Runx1 gene is known to regulate lineage differentiation and function within the hematopoietic system. In 2011, Kubin et al. (Kubin et al., 2011) reported that *Runx1* is activated in BZ cardiomyocytes in mice 3 wk post MI. This indicated that *Runx1* gene might play a role in post MI remodelling. This leads to the investigation of the *Runx1* mRNA and protein levels by our group, and we found that *Runx1* mRNA and RUNX1 protein levels are increased at 3-4 wk and 8 wk post MI time points within the BZ myocardium (unpublished data). Additionally, our group has demonstrated that *Runx1* expression is sustained until at least 8 wk post MI, at which time point *Runx1* expression is also increased within the remote LV myocardium (unpublished data). This detailed quantification of *Runx1* expression levels enabled our group to show a substantial inverse correlation between *Runx1*

expression level in myocardial tissue and the ability of cardiac contractility and relaxation. This relationship is important because changes in *Runx1* expression post MI not only occur in rodent models but also occur in humans as Gattenlöhner et al. (Gattenlohner et al., 2003) have demonstrated that RUNX1 is upregulated in the heart at the mRNA and protein level in patients with ischemic heart disease. To investigate the role of *Runx1* in the inverse correlation between *Runx1* expression level and cardiac function, models of MI and IR within tamoxifen-inducible cardiomyocyte-specific *Runx1* deficiency transgenic mice were utilised in this study. Induction of MI in control transgenic mice led to reduced contractility 8 wk post MI; however, the cardiac contractile function was preserved in *Runx1* deficient mice at this time point. The data were confirmed in a blinded study where I was blinded to the genotype of the mice during the surgery and functional measurements. Although reduced infarct size can be a possible explanation for the preservation of cardiac function as previous studies have shown that the infarct size correlated with systolic function (Takagawa et al., 2007), our analysis has shown no significant difference in infarct size or fibrosis between *Runx1* deficient mice and the control mice post MI (unpublished data). The echocardiography and PV loop data also provided information related to cardiac remodelling including LV wall thickness and cardiac dilation. Control mice demonstrated the characteristics of eccentric hypertrophy such as LV wall thinning and cardiac dilation at 8 wk post MI; however, these characteristics were absent in *Runx1* deficient mice. WGA staining performed on the heart slides from the MI mice (I induced) showed cardiomyocyte lengthening and thinning in control mice at 8 wk post MI, and an absence of these changes in *Runx1* deficient mice (Katrin Nather and Dr. Christopher Loughrey, unpublished data). These data indicated that post MI eccentric hypertrophy was prevented by *Runx1* deficiency, finally leading to preserved contractile function. In the clinical setting, patients with MI normally receive reperfusion therapy such as PPCI. Therefore, we further tested the cardiac function in *Runx1* deficient mice with our IR mice which has additional clinical relevance. We found that *Runx1* deficiency also showed a beneficial effect on cardiac function post IR injury injury. The IR injury data further support the MI data and implicates the translational potential of targeting *Runx1*.

5.4.2 *Runx1* deficiency regulates cardiac function post MI *via* modulating cardiac calcium handling

At cellular level, the contractile function of cardiomyocyte is regulated by EC coupling which is modulated by calcium handling. To establish the mechanism underlying the beneficial effects on cardiac function, I induced MI in *Runx1* deficient mice and Dr. Charlotte McCarroll investigated calcium handling in cardiomyocytes isolated from these mice at 2 wk post MI. At the 2 wk post MI time point, we found the contractility of isolated cardiomyocytes was significantly improved in *Runx1* deficient mice, however, the wall thickness in *Runx1* deficient mice was comparable to that of the control mice. This indicated that regulation of cardiac function post MI happened before progression to eccentric hypertrophy. The fluorescence based calcium imaging technique allowed us to investigate the calcium release from the intra-cardiomyocyte calcium store (the SR) by the calcium transient induced by electrical stimulation and subsequent cell shortening. MI typically leads to calcium transients with lower amplitude and a slower rate of decay than control or healthy cardiomyocytes in patients and animals. These changes of the calcium transients are largely attributed to reduced SR-mediated calcium uptake through SERCA (Piacentino et al., 2003). We found that *Runx1* deficient mice post MI had increased Ca^{2+} transient amplitudes and a reduced time of $[Ca^{2+}]_i$ decline as compared to control mice post MI. These changes in calcium transient amplitude paralleled an increased cell shortening. The enhanced calcium transient amplitude in *Runx1* deficient mice post MI can be explained by higher SR calcium content (Elliott et al., 2012, Trafford et al., 2000). The caffeine-induced calcium transient showed no detectable change in NCX activity in *Runx1* deficient mice post MI as compared to control mice post MI, while enhanced SR-mediated calcium uptake through SERCA was observed in the *Runx1* deficient mice post MI. SERCA activity is a major determinant of the SR calcium content, which is regulated by the inhibitory protein phospholamban (PLB). Although expression of PLB was not altered in *Runx1* deficient mice post MI, we found PKA-mediated phosphorylation of PLB increased, and this change was possibly due to reduced levels of PP1. PLB-mediated inhibition of SERCA is controlled through phosphorylation by PKA and CaMKII (which relieves inhibition of SERCA) and dephosphorylation by PP1 (which returns PLB to an inhibitory state (Haghighi et

al., 2014)). Therefore, these findings suggest that PLB phosphorylation stimulates SERCA activity in *Runx1* deficient mice post MI, and results in increased calcium content, which in turn increases SR-mediated calcium release induced by electrical stimulation and thus leading to increased cardiomyocyte contraction. This mechanism was supported by the complete blockade of the enhanced calcium transient in cardiomyocytes from *Runx1* deficient mice at 2 wk post MI by inhibition of PKA. The increased rate of removal of calcium from the cytosol following enhanced SERCA activity is sufficient to reduce the end diastolic $[Ca^{2+}]i$, which may improve whole heart relaxation and also limit the hypertrophic stimulation (Kehat and Molkentin, 2010).

The novel mechanism we identified in this study is supported by previous studies. We have demonstrated that *Runx1* deficiency preserves cardiac contractile function in mice post MI *via* regulation of cardiac calcium handling. These findings are similar to previous evidence that improved SR function contributes to better cardiac function while reduced SR function has been observed among patients with HF (Piacentino et al., 2003), and enhanced SR-mediated calcium cycling significantly preserved contractile function with decreased adverse cardiac remodelling and delayed progression to heart failure (Haghighi et al., 2014, He et al., 2014, Fish et al., 2013, Ishikawa et al., 2014). A recent study by Zhang et al. demonstrated increased SR calcium uptake and increased the calcium transient lead to increased contractile amplitude, enhanced cardiomyocyte contraction and relaxation increased heart weight (Zhang et al., 2015). These changes are similar to our findings as heart weight increased post MI in *Runx1* deficiency mice with enhanced SR function. The increase of heart weight might be a condition of physiological hypertrophy after the cell loss post MI as increased contraction and relaxation were observed in cardiomyocyte post MI and persistent preserved LV contractile function was exhibited over 8 weeks post MI in our experiment.

In conclusion, I have produced essential phenotypic characterisation of post MI *Runx1* deficient mice which has been critical in leading subsequent experiments performed by other members of the group to understand how *Runx1* deficiency improves cardiac function post MI. In this study, I have demonstrated that *Runx1* deficiency leads to preserved cardiac contractile function post MI. The improved contractility is driven by a novel mechanism we identified in which *Runx1*

regulates cardiac SR calcium uptake through modulation of phospholamban phosphorylation. In addition, the *Runx1* deficient mice limited eccentric hypertrophy post MI. As demonstrated by clinical studies, preserving cardiac contractile function and preventing adverse cardiac remodelling are important factors to limiting progression to heart failure post MI (Konstam et al., 2011). The *Runx1* deficiency mediated improvement of contractile function post MI may have therapeutic potential and clinical implications.

CHAPTER 6.
General discussion

6.1 Establishing an *in vivo* mouse model for investigation of potential therapies targeting MI and cardiac IR injury

In recent decades, the application of PPCI technique has become the fundamental strategy to treat MI by reperfusion of the ischaemic myocardium (Keeley and Hillis, 2007). The application of PPCI enables salvaging the injured myocardium by restoring the blood flow to the ischaemic area and thereby has led to an increased survival rate in patients undergoing MI (Keeley and Hillis, 2007). However, although a larger proportion of patients can survive from MI with the PPCI treatment, the substantial left ventricular (LV) injury caused by prolonged ischaemia leads to a later risk of developing heart failure (Minicucci et al., 2011). Therefore, post MI heart failure has become a frequent complication of MI and is associated with extremely high mortality rates (Minicucci et al., 2011). Novel therapies which can limit progression to heart failure post MI are urgently required. To achieve this object, treatments can be applied to two phases in MI patients undergoing PPCI. The first phase is in the acute MI phase, where targeting IR injury during PPCI may reduce infarct size and thus improve cardiac function. The second phase is in the chronic stage of post MI remodelling, where therapies targeting the adverse LV remodelling may prevent progression to heart failure. In this thesis, two potential therapeutic strategies, targeting IR injury or post MI remodelling (albeit immediately post MI rather than chronic stage), were both investigated by using *in vivo* mouse models of MI and IR injury.

In vivo mouse models have two particular advantages for investigation of new therapeutic targets. The first advantage is that mouse models can reduce the cost when testing expensive biochemical compounds due to the relatively smaller quantities of drug for a small species compared to larger species. Although the price of most biochemical drugs can be reduced after industrialised production, at the stage of laboratory research their price is extremely high, such as the cathepsin-L inhibitors used in current study. Secondly, the widespread availability of knockout and transgenic mice provides tools for investigating the genetic basis of the diseases and therapies. However, due to the small size of mice, the surgical procedures for MI and IR models are complex and challenging and require experienced microsurgical techniques to be acquired in order to generate high

quality models of MI and IR with a good survival rate. The IR model has more clinical relevance than MI as it mimics the PPCI treatment post MI. However, induction of IR is much more difficult than MI due to the prolonged duration of the open chest operation and death due to reperfusion arrhythmias. In the current study, I have learnt the mouse models of MI and IR injury, and successful established these models. The survival rate was increasing during my PhD study as I have become increasingly experienced, and I have reached my highest monthly survival rate, which was 100%, in July 2015 (26 mice all survived post open-chest surgery). In addition, this was the first time the IR injury mouse model was used in the laboratory. I have also learnt the techniques to characterise the cardiac function using echocardiography and PV loops, and I have successfully applied these techniques into my MI and IR injury models. The high quality mouse models I induced and characterised in this study were used not only to independently determine the therapeutic effects of two novel targets as demonstrated in this thesis but also to generate MI and IR injury heart tissue which was important for experiments performed by other lab members to further explore underlying mechanisms of action.

6.2 The cathepsin-L inhibitor CAA0225 protected against IR injury

While restoring blood flow *via* PPCI salvages the cells within the ischaemic area, reperfusion of this area also leads to IR injury, which paradoxically causes additional cell death with cardiac dysfunction (Hausenloy and Yellon, 2016). Currently there is no reliable therapy for IR injury, therefore discovering novel treatment which can effectively prevent IR injury is of great benefit to MI patients undergoing PPCI (Hausenloy and Yellon, 2016). In the current study, a potential therapeutic target, cathepsin-L, was investigated by using a cathepsin-L inhibitor CAA0225 in both *ex vivo* rat isolated heart model and in an *in vivo* mouse model of IR injury. Both models demonstrated that the beneficial effects of cathepsin-L inhibitor CAA0225 on improving cardiac function and reducing infarct size against IR injury. A limitation of this study is that we did not show what degree cathepsin-L activity was inhibited *in vivo*, therefore the degree of cathepsin-L inhibition in various organs at different time points post MI and IR injury when using the

inhibitor will be investigated in future study.

Recent studies demonstrated that cathepsins play a functional role following MI and inhibition of cathepsin activity by using specific inhibitors exhibited promising beneficial effects. A study performed by Liu et al. demonstrated that application of the cathepsin-B inhibitor CA074Me can significantly attenuate cardiac dysfunction in a rat MI model by inhibiting NLRP3 activation (Liu et al., 2013). A recent study by Petrera et al. found that the cathepsin-A inhibitor SAR1 protects against post MI heart failure in mice (Petrera et al., 2016). In contrast, Sun et al. demonstrated that cathepsin-L is involved in post MI remodelling as cathepsin-L knockout mice demonstrated scar dilatation, wall thinning and worse cardiac function post MI (Sun et al., 2011). However, it's important to note that the patterns of cathepsin-L deficiency are different between knockout mice and inhibitor inactivation, because in the cathepsin-L knockout mice the deficiency is persistent from birth while using an inhibitor means the inhibition is highly likely to be partial and temporary. As cathepsin-L is a key member of the lysosomal protease family (Lutgens et al., 2007), the pathophysiological changes of lysosomal function in response to IR injury should be considered to be one of the underlying mechanisms and needs to be explored in future studies.

The key function of the lysosome is degradation of intracellular proteins and organelles (Turk et al., 2000, Lutgens et al., 2007). An intracellular degradative process mediated by the lysosome is known as autophagy which occurs in healthy myocardium but it can substantially increase in response to injury such as ischaemia (Yan et al., 2005). Autophagy can act in a recycling pathway to trigger cell death in the absence of nutrients or in a quality-control pathway to eliminate damaged organelles (Tooze et al., 2014). Lysosomes and autophagosomes were observed in necrotic cardiomyocytes within the infarcted area post MI (Kanamori et al., 2011). This indicates that autophagy is activated and function within the ischaemic area in response to ischaemia, and autophagic cell death may be the outcome of ischaemic damage. Evidence showed that autophagy was enhanced and had beneficial effects against MI (Matsui et al., 2007, Gurusamy et al., 2009), however, during IR injury the role of autophagy is controversial as protective (Yan et al., 2005) and detrimental effects (Valentim et al., 2006, Matsui et al., 2007) were observed in different studies respectively. These controversial findings

(Matsui et al., 2007, Gurusamy et al., 2009) (Yan et al., 2005) (Valentim et al., 2006, Matsui et al., 2007) suggest that there may be a balance in regulation of the autophagy process following IR injury, a certain level of autophagy may be protective but excessive autophagy may lead to autophagic cell death. This hypothesis will be investigated in my future work. Given that autophagy is mediated by lysosomal degradation and cathepsin-L is the key member of lysosomal proteases, during the autophagy process in response to IR injury, cathepsin-L may be released from lysosomes into the cytosol (by increased lysosomal membrane permeability) and extracellular spaces (by lysosomal exocytosis), leading to subsequently cardiac dysfunction and cell death.

A potential pathway of intracellular cathepsin-L is activation of NLRP3 inflammasome. Recent evidences demonstrated that cathepsin-B and cathepsin-L are released into cytosol through lysosomes in atherosclerosis and type 2 diabetes, causing inflammasome activation, and inhibition of cathepsins prevents the NLRP3 inflammasome activation (Masters et al., 2010, Masters et al., 2011, Guo et al., 2015, Duewell et al., 2010). This evidence suggests that the intracellular cathepsin-L released from lysosomes in IR injury may initiate inflammation *via* NLRP3 inflammasome activation and thereby cause cardiac dysfunction and deteriorate injury, and the beneficial effects of cathepsin-L inhibition in IR injury by using CAA0225, as demonstrated in this thesis, may be related to the NLRP3 inflammasome activation. This hypothesis can be investigated in the future by testing if NLRP3 inhibitors show similar effect of CAA0225 and if CAA0225 loses its beneficial effects in NLRP3 knockout mice during IR injury.

6.3 *Runx1* deficiency preserved cardiac function and prevented dilation post MI

Although the application of PPCI has successfully increased the survival rate in patients with MI, the patients surviving from the acute MI facing a later risk of progression to post MI heart failure which leads to extremely high mortality despite optimised medical interventions (Roger, 2013, Chen et al., 2013). Therefore, developing effective therapies to prevent post MI heart failure is urgently required. In this thesis, I have demonstrated the functional role of *Runx1* in post MI remodelling and found *Runx1* deficiency led to preserved cardiac

contractile function post MI with limitation of cardiac LV dilation. The preserved cardiac function in *Runx1* deficient mice is likely to be regulated at the cellular level *via* a number of process including increased cellular contractility *via* enhanced SERCA function. SERCA activity is a major modulator of intracellular calcium handling in cardiomyocytes and thereby regulates cellular contraction and relaxation. Although we have found that increased SERCA activity parallels PLB inhibition and reduced PP1, whether there are direct links between *Runx1* deficiency and PP1 is currently unclear and needs further investigation.

One limitation of this study is that using the conditional knockout technology the *Runx1* cannot be switched back on once it has been knocked out. The *Runx1* knockout is beneficial for an 8-wk period post MI, however, increased contractile function can sometimes be a double-edged sword as persistent increased contraction has a risk to cause concentric hypertrophy (Katholi and Couri, 2011), which may subsequently progress to heart failure. However, the risk of concentric hypertrophy may be avoided by adjusting the level and duration of *Runx1* deficiency. Therefore, the translational application of *Runx1* deficiency requires further investigating, in particular to determine the optimum level and duration of *Runx1* deficiency. To achieve this goal, clinically applicable approaches, such as viral vectors delivering interfering RNA or pharmacological *Runx1* inhibitors (e.g. Ro5-3335 (Cunningham et al., 2012)), can be utilized to search for the best condition for the *Runx1* deficiency therapy and to achieve the best outcome for the treatment of post MI heart failure.

6.4 Future work

In my future career, I will continue working on novel targets for MI and IR injury. I will fully support my supervisor Dr. Christopher Loughrey for his future work on the cathepsin-L and *Runx1* projects and I will also start to investigate other potential targets. As I have started my postdoc at Virginia Commonwealth University, the group with which I am currently working with has found that coronary arteritis can increase lysosomal membrane permeability and trigger release of lysosomal cathepsin-B into the cytosol in coronary arterial endothelium and also that treatment with the cathepsin inhibitor CA074Me can inhibit

endothelial inflammasome activation in a murine model of coronary arteritis (Chen et al., 2015). As I have demonstrated the beneficial effect of the cathepsin-L inhibitor CAA0225 on IR injury in this thesis and as discussed the underlying mechanism may be related to lysosomal dysfunction and NLRP3 inflammasome activation. This evidence will inform my future work on investigation of NLRP3 inflammasome activation during IR injury. I will investigate the hypothesis that the NLRP3 inflammasome activation contributes to tissue inflammation during IR injury and I will explore the underlying mechanisms by using NLRP3 and ASC knockout mice and NLRP3 inhibitors with my MI and IR injury mouse models. Meanwhile, I will also test the effects of some pharmacologic compounds such as short chain fatty acid (SCFA) on IR injury during my postdoc at Virginia.

References

ABRAHAM, D. & MAO, L. 2015. Cardiac Pressure-Volume Loop Analysis Using Conductance Catheters in Mice. Jove-Journal of Visualized Experiments.

ADAMS-CIOABA, M. A., KRUPA, J. C., XU, C., MORT, J. S. & MIN, J. 2011. Structural basis for the recognition and cleavage of histone H3 by cathepsin L. Nat Commun, 2, 197.

AGAH, R., FRENKEL, P. A., FRENCH, B. A., MICHAEL, L. H., OVERBEEK, P. A. & SCHNEIDER, M. D. 1997. Gene recombination in postmitotic cells. Targeted expression of Cre recombinase provokes cardiac-restricted, site-specific rearrangement in adult ventricular muscle in vivo. J Clin Invest, 100, 169-79.

AIKAWA, Y., NGUYEN, L. A., ISONO, K., TAKAKURA, N., TAGATA, Y., SCHMITZ, M. L., KOSEKI, H. & KITABAYASHI, I. 2006. Roles of HIPK1 and HIPK2 in AML1- and p300-dependent transcription, hematopoiesis and blood vessel formation. EMBO J, 25, 3955-65.

ALBURQUERQUE-BEJAR, J. J., BARBA, I., RUIZ-MEANA, M., VALLS-LACALLE, L., RODRIGUEZ-SINOVAS, A. & GARCIA-DORADO, D. 2016. Additive Effects of Exenatide, Glucose-insulin-potassium, and Remote Ischemic Conditioning Against Reperfusion Ventricular Arrhythmias in Pigs. Rev Esp Cardiol (Engl Ed), 69, 620-2.

ANTMAN, E. M., GIUGLIANO, R. P., GIBSON, C. M., MCCABE, C. H., COUSSEMENT, P., KLEIMAN, N. S., VAHANIAN, A., ADGEY, A. A., MENOWN, I., RUPPRECHT, H. J., VAN DER WIEKEN, R., DUCAS, J., SCHERER, J., ANDERSON, K., VAN DE WERF, F. & BRAUNWALD, E. 1999. Abciximab facilitates the rate and extent of thrombolysis: results of the thrombolysis in myocardial infarction (TIMI) 14 trial. The TIMI 14 Investigators. Circulation, 99, 2720-32.

APPELQVIST, H., WASTER, P., KAGEDAL, K. & OLLINGER, K. 2013. The lysosome: from waste bag to potential therapeutic target. J Mol Cell Biol, 5, 214-26.

ARGAUD, L., GATEAU-ROESCH, O., MUNTEAN, D., CHALABREYSSE, L., LOUFOUAT, J., ROBERT, D. & OVIZE, M. 2005. Specific inhibition of the mitochondrial permeability transition prevents lethal reperfusion injury. J Mol Cell Cardiol, 38, 367-74.

ARMSTRONG, P. W. & COLLEN, D. 2001a. Fibrinolysis for acute myocardial infarction: current status and new horizons for pharmacological reperfusion, part 1. Circulation, 103, 2862-6.

ARMSTRONG, P. W. & COLLEN, D. 2001b. Fibrinolysis for acute myocardial infarction: current status and new horizons for pharmacological reperfusion, part 2. Circulation, 103, 2987-92.

ARONSON, B. D., FISHER, A. L., BLECHMAN, K., CAUDY, M. & GERGEN, J. P. 1997. Groucho-dependent and -independent repression activities of Runt domain proteins. Mol Cell Biol, 17, 5581-7.

ARORA, S. & CHAUHAN, S. S. 2002. Identification and characterization of a novel human cathepsin L splice variant. Gene, 293, 123-31.

ASAGIRI, M., HIRAI, T., KUNIGAMI, T., KAMANO, S., GOBER, H. J., OKAMOTO, K., NISHIKAWA, K., LATZ, E., GOLENBOCK, D. T., AOKI, K., OHYA, K., IMAI, Y., MORISHITA, Y., MIYAZONO, K., KATO, S., SAFTIG, P. & TAKAYANAGI, H. 2008. Cathepsin K-dependent toll-like receptor 9 signaling revealed in experimental arthritis. Science, 319, 624-7.

ASSESSMENT OF THE, S. & EFFICACY OF A NEW THROMBOLYTIC REGIMEN, I. 2001. Efficacy and safety of tenecteplase in combination with enoxaparin, abciximab, or unfractionated heparin: the ASSENT-3 randomised trial in acute myocardial infarction. Lancet, 358, 605-13.

AVERSANO, T., AVERSANO, L. T., PASSAMANI, E., KNATTERUD, G. L., TERRIN, M. L., WILLIAMS, D. O., FORMAN, S. A. & ATLANTIC CARDIOVASCULAR PATIENT OUTCOMES RESEARCH, T. 2002. Thrombolytic therapy vs primary percutaneous

coronary intervention for myocardial infarction in patients presenting to hospitals without on-site cardiac surgery: a randomized controlled trial. JAMA, 287, 1943-51.

AVRAMOPOULOS, D., COX, T., BLASCHAK, J. E., CHAKRAVARTI, A. & ANTONARAKIS, S. E. 1992. Linkage mapping of the AML1 gene on human chromosome 21 using a DNA polymorphism in the 3' untranslated region. Genomics, 14, 506-7.

AWAD, W. I., SHATTOCK, M. J. & CHAMBERS, D. J. 1998. Ischemic preconditioning in immature myocardium. Circulation, 98, II206-13.

AWAN, M. M., TAUNYANE, C., AITCHISON, K. A., YELLON, D. M. & OPIE, L. H. 1999. Normothermic transfer times up to 3 min will not precondition the isolated rat heart. J Mol Cell Cardiol, 31, 503-11.

BAAN, J., VAN DER VELDE, E. T., DE BRUIN, H. G., SMEENK, G. J., KOOPS, J., VAN DIJK, A. D., TEMMERMAN, D., SENDEN, J. & BUIS, B. 1984. Continuous measurement of left ventricular volume in animals and humans by conductance catheter. Circulation, 70, 812-23.

BAICI, A. 1998. Inhibition of extracellular matrix-degrading endopeptidases: problems, comments, and hypotheses. Biol Chem, 379, 1007-18.

BALACHANDRAN, K., SUCOSKY, P., JO, H. & YOGANATHAN, A. P. 2010. Elevated cyclic stretch induces aortic valve calcification in a bone morphogenic protein-dependent manner. Am J Pathol, 177, 49-57.

BAR, F. W., TZIVONI, D., DIRKSEN, M. T., FERNANDEZ-ORTIZ, A., HEYNDRICKX, G. R., BRACHMANN, J., REIBER, J. H., AVASTHY, N., TATSUNO, J., DAVIES, M., HIBBERD, M. G., KRUCOFF, M. W. & GROUP, C. S. 2006. Results of the first clinical study of adjunctive CAldaret (MCC-135) in patients undergoing primary percutaneous coronary intervention for ST-Elevation Myocardial Infarction: the randomized multicentre CASTEMI study. Eur Heart J, 27, 2516-23.

BARTFELD, D., SHIMON, L., COUTURE, G. C., RABINOVICH, D., FROLOW, F., LEVANON, D., GRONER, Y. & SHAKKED, Z. 2002. DNA recognition by the RUNX1 transcription factor is mediated by an allosteric transition in the RUNT domain and by DNA bending. Structure, 10, 1395-407.

BELL, R. M., MOCANU, M. M. & YELLON, D. M. 2011. Retrograde heart perfusion: the Langendorff technique of isolated heart perfusion. J Mol Cell Cardiol, 50, 940-50.

BEN-AMI, O., PENCOVICH, N., LOTEM, J., LEVANON, D. & GRONER, Y. 2009. A regulatory interplay between miR-27a and Runx1 during megakaryopoiesis. Proc Natl Acad Sci U S A, 106, 238-43.

BEN-ARI, Z., MOR, E., AZAROV, D., SULKES, J., TOR, R., CHEPORKO, Y., HOCHHAUSER, E. & PAPPO, O. 2005. Cathepsin B inactivation attenuates the apoptotic injury induced by ischemia/reperfusion of mouse liver. Apoptosis, 10, 1261-1269.

BERARDI, M. J., SUN, C., ZEHR, M., ABILDGAARD, F., PENG, J., SPECK, N. A. & BUSHWELLER, J. H. 1999. The Ig fold of the core binding factor alpha Runt domain is a member of a family of structurally and functionally related Ig-fold DNA-binding domains. Structure, 7, 1247-56.

BERS, D. M. 2002. Cardiac excitation-contraction coupling. Nature, 415, 198-205.

BERS, D. M. & PEREZ-REYES, E. 1999. Ca channels in cardiac myocytes: structure and function in Ca influx and intracellular Ca release. Cardiovasc Res, 42, 339-60.

BETHKE, A., HALVORSEN, S., BOHMER, E., ABDELNOOR, M., ARNESEN, H. & HOFFMANN, P. 2015. Myocardial perfusion grade predicts final infarct size and left ventricular function in patients with ST-elevation myocardial infarction treated with a pharmaco-invasive strategy (thrombolysis and early angioplasty). EuroIntervention, 11, 518-24.

BIGGS, J. R., PETERSON, L. F., ZHANG, Y., KRAFT, A. S. & ZHANG, D. E. 2006. AML1/RUNX1 phosphorylation by cyclin-dependent kinases regulates the degradation of AML1/RUNX1 by the anaphase-promoting complex. Mol Cell Biol, 26, 7420-9.

BLAUSTEIN, M. P. & LEDERER, W. J. 1999. Sodium/calcium exchange: its physiological implications. Physiol Rev, 79, 763-854.

BLONDELLE, J., LANGE, S., GREENBERG, B. H. & COWLING, R. T. 2015. Cathepsins in heart disease-chewing on the heartache? Am J Physiol Heart Circ Physiol, 308, H974-6.

BLYTH, K., CAMERON, E. R. & NEIL, J. C. 2005. The RUNX genes: gain or loss of function in cancer. Nat Rev Cancer, 5, 376-87.

BOGOYEVITCH, M. A., GLENNON, P. E., ANDERSSON, M. B., CLERK, A., LAZOU, A., MARSHALL, C. J., PARKER, P. J. & SUGDEN, P. H. 1994. Endothelin-1 and fibroblast growth factors stimulate the mitogen-activated protein kinase signaling cascade in cardiac myocytes. The potential role of the cascade in the integration of two signaling pathways leading to myocyte hypertrophy. J Biol Chem, 269, 1110-9.

BOHL, S., MEDWAY, D. J., SCHULZ-MENGER, J., SCHNEIDER, J. E., NEUBAUER, S. & LYGATE, C. A. 2009. Refined approach for quantification of in vivo ischemia-reperfusion injury in the mouse heart. Am J Physiol Heart Circ Physiol, 297, H2054-8.

BOLLI, R. 1990. Mechanism of myocardial "stunning". Circulation, 82, 723-38.

BRAUNWALD, E. & KLONER, R. A. 1985. Myocardial reperfusion: a double-edged sword? J Clin Invest, 76, 1713-9.

BRAUNWALD, E. & PFEFFER, M. A. 1991. Ventricular enlargement and remodeling following acute myocardial infarction: mechanisms and management. Am J Cardiol, 68, 1D-6D.

BRIX, K., DUNKHORST, A., MAYER, K. & JORDANS, S. 2008. Cysteine cathepsins: cellular roadmap to different functions. Biochimie, 90, 194-207.

BUHLING, F., WALDBURG, N., REISENAUER, A., HEIMBURG, A., GOLPON, H. & WELTE, T. 2004. Lysosomal cysteine proteases in the lung: role in protein processing and immunoregulation. Eur Respir J, 23, 620-8.

CAMERON, E. R. & NEIL, J. C. 2004. The Runx genes: lineage-specific oncogenes and tumor suppressors. Oncogene, 23, 4308-14.

CAMERON, S., TAYLOR, D. S., TEPAS, E. C., SPECK, N. A. & MATHEY-PREVOT, B. 1994. Identification of a critical regulatory site in the human interleukin-3 promoter by in vivo footprinting. Blood, 83, 2851-9.

CAVE, A. C., INGWALL, J. S., FRIEDRICH, J., LIAO, R., SAUPE, K. W., APSTEIN, C. S. & EBERLI, F. R. 2000. ATP synthesis during low-flow ischemia: influence of increased glycolytic substrate. Circulation, 101, 2090-6.

CHAN, E. M., COMER, E. M., BROWN, F. C., RICHKIND, K. E., HOLMES, M. L., CHONG, B. H., SHIFFMAN, R., ZHANG, D. E., SLOVAK, M. L., WILLMAN, C. L., NOGUCHI, C. T., LI, Y., HEIBER, D. J., KWAN, L., CHAN, R. J., VANCE, G. H., RAMSEY, H. C. & HROMAS, R. A. 2005. AML1-FOG2 fusion protein in myelodysplasia. Blood, 105, 4523-6.

CHAPMAN, H. A., RIESE, R. J. & SHI, G. P. 1997. Emerging roles for cysteine proteases in human biology. Annu Rev Physiol, 59, 63-88.

CHAVAKIS, E., URBICH, C. & DIMMELER, S. 2008. Homing and engraftment of progenitor cells: a prerequisite for cell therapy. J Mol Cell Cardiol, 45, 514-22.

CHEN, C. L., BROOM, D. C., LIU, Y., DE NOOIJ, J. C., LI, Z., CEN, C., SAMAD, O. A., JESSELL, T. M., WOOLF, C. J. & MA, Q. 2006. Runx1 determines nociceptive sensory neuron phenotype and is required for thermal and neuropathic pain. Neuron, 49, 365-77.

CHEN, J., HSIEH, A. F., DHARMARAJAN, K., MASOUDI, F. A. & KRUMHOLZ, H. M. 2013. National trends in heart failure hospitalization after acute myocardial infarction for Medicare beneficiaries: 1998-2010. Circulation, 128, 2577-84.

CHEN, M. J., YOKOMIZO, T., ZEIGLER, B. M., DZIERZAK, E. & SPECK, N. A. 2009. Runx1 is required for the endothelial to haematopoietic cell transition but not thereafter. Nature, 457, 887-91.

CHEN, Y., LI, X., BOINI, K. M., PITZER, A. L., GULBINS, E., ZHANG, Y. & LI, P. L. 2015. Endothelial Nlrp3 inflammasome activation associated with lysosomal destabilization during coronary arteritis. Biochim Biophys Acta, 1853, 396-408.

CHENG, X. W., MUROHARA, T., KUZUYA, M., IZAWA, H., SASAKI, T., OBATA, K., NAGATA, K., NISHIZAWA, T., KOBAYASHI, M., YAMADA, T., KIM, W., SATO, K., SHI, G. P., OKUMURA, K. & YOKOTA, M. 2008. Superoxide-dependent cathepsin activation is associated with hypertensive myocardial remodeling and represents a target for angiotensin II type 1 receptor blocker treatment. Am J Pathol, 173, 358-69.

CHENG, X. W., OBATA, K., KUZUYA, M., IZAWA, H., NAKAMURA, K., ASAI, E., NAGASAKA, T., SAKA, M., KIMATA, T., NODA, A., NAGATA, K., JIN, H., SHI, G. P., IGUCHI, A., MUROHARA, T. & YOKOTA, M. 2006. Elastolytic cathepsin induction/activation system exists in myocardium and is upregulated in hypertensive heart failure. Hypertension, 48, 979-87.

CHENG, X. W., OKUMURA, K., KUZUYA, M., JIN, Z., NAGATA, K., OBATA, K., INOUE, A., HIRASHIKI, A., TAKESHITA, K., UNNO, K., HARADA, K., SHI, G. P., YOKOTA, M. & MUROHARA, T. 2009. Mechanism of diastolic stiffening of the failing myocardium and its prevention by angiotensin receptor and calcium channel blockers. J Cardiovasc Pharmacol, 54, 47-56.

CHENG, X. W., SHI, G. P., KUZUYA, M., SASAKI, T., OKUMURA, K. & MUROHARA, T. 2012. Role for cysteine protease cathepsins in heart disease: focus on biology and mechanisms with clinical implication. Circulation, 125, 1551-62.

CHIMENTI, S., CARLO, E., MASSON, S., BAI, A. & LATINI, R. 2004. Myocardial infarction: animal models. Methods Mol Med, 98, 217-26.

CHIONG, M., WANG, Z. V., PEDROZO, Z., CAO, D. J., TRONCOSO, R., IBACACHE, M., CRIOLLO, A., NEMCHENKO, A., HILL, J. A. & LAVANDERO, S. 2011. Cardiomyocyte death: mechanisms and translational implications. Cell Death Dis, 2, e244.

CHURPEK, J. E., GARCIA, J. S., MADZO, J., JACKSON, S. A., ONEL, K. & GODLEY, L. A. 2010. Identification and molecular characterization of a novel 3′ mutation in RUNX1 in a family with familial platelet disorder. Leuk Lymphoma, 51, 1931-5.

CLARK, J. E. & MARBER, M. S. 2013. Advancements in pressure-volume catheter technology - stress remodelling after infarction. Exp Physiol, 98, 614-21.

CLEUTJENS, J. P., VERLUYTEN, M. J., SMITHS, J. F. & DAEMEN, M. J. 1995. Collagen remodeling after myocardial infarction in the rat heart. Am J Pathol, 147, 325-38.

COHN, J. N., FERRARI, R. & SHARPE, N. 2000. Cardiac remodeling--concepts and clinical implications: a consensus paper from an international forum on cardiac remodeling. Behalf of an International Forum on Cardiac Remodeling. J Am Coll Cardiol, 35, 569-82.

CORRETTI, M. C., KORETSUNE, Y., KUSUOKA, H., CHACKO, V. P., ZWEIER, J. L. & MARBAN, E. 1991. Glycolytic Inhibition and Calcium Overload as Consequences of Exogenously Generated Free-Radicals in Rabbit Hearts. Journal of Clinical Investigation, 88, 1014-1025.

COULOMBE, R., GROCHULSKI, P., SIVARAMAN, J., MENARD, R., MORT, J. S. & CYGLER, M. 1996. Structure of human procathepsin L reveals the molecular basis of inhibition by the prosegment. EMBO J, 15, 5492-503.

CUNNINGHAM, L., FINCKBEINER, S., HYDE, R. K., SOUTHALL, N., MARUGAN, J., YEDAVALLI, V. R., DEHDASHTI, S. J., REINHOLD, W. C., ALEMU, L., ZHAO, L., YEH, J. R., SOOD, R., POMMIER, Y., AUSTIN, C. P., JEANG, K. T., ZHENG, W. & LIU, P. 2012. Identification of benzodiazepine Ro5-3335 as an inhibitor of CBF leukemia through quantitative high throughput screen against RUNX1-CBFbeta interaction. Proc Natl Acad Sci U S A, 109, 14592-7.

CUOZZO, J. W., TAO, K., CYGLER, M., MORT, J. S. & SAHAGIAN, G. G. 1998. Lysine-based structure responsible for selective mannose phosphorylation of cathepsin D and cathepsin L defines a common structural motif for lysosomal enzyme targeting. J Biol Chem, 273, 21067-76.

CURTIS, M. J., MACLEOD, B. A., TABRIZCHI, R. & WALKER, M. J. 1986. An improved perfusion apparatus for small animal hearts. J Pharmacol Methods, 15, 87-94.

CYGLER, M., SIVARAMAN, J., GROCHULSKI, P., COULOMBE, R., STORER, A. C. & MORT, J. S. 1996. Structure of rat procathepsin B: model for inhibition of cysteine protease activity by the proregion. Structure, 4, 405-16.

DAS, D. K., ENGELMAN, R. M., ROUSOU, J. A. & BREYER, R. H. 1987. Aerobic vs anaerobic metabolism during ischemia in heart muscle. Ann Chir Gynaecol, 76, 68-76.

DENNEMARKER, J., LOHMULLER, T., MAYERLE, J., TACKE, M., LERCH, M. M., COUSSENS, L. M., PETERS, C. & REINHECKEL, T. 2010a. Deficiency for the cysteine protease cathepsin L promotes tumor progression in mouse epidermis. Oncogene, 29, 1611-21.

DENNEMARKER, J., LOHMULLER, T., MULLER, S., AGUILAR, S. V., TOBIN, D. J., PETERS, C. & REINHECKEL, T. 2010b. Impaired turnover of autophagolysosomes in cathepsin L deficiency. Biol Chem, 391, 913-22.

DESMARAIS, S., BLACK, W. C., OBALLA, R., LAMONTAGNE, S., RIENDEAU, D., TAWA, P., DUONG, L. T., PICKARSKI, M. & PERCIVAL, M. D. 2008. Effect of cathepsin k inhibitor basicity on in vivo off-target activities. Mol Pharmacol, 73, 147-56.

DEUSSING, J., ROTH, W., SAFTIG, P., PETERS, C., PLOEGH, H. L. & VILLADANGOS, J. A. 1998. Cathepsins B and D are dispensable for major histocompatibility complex class II-mediated antigen presentation. Proc Natl Acad Sci U S A, 95, 4516-21.

DING, Y., HARADA, Y., IMAGAWA, J., KIMURA, A. & HARADA, H. 2009. AML1/RUNX1 point mutation possibly promotes leukemic transformation in myeloproliferative neoplasms. Blood, 114, 5201-5.

DIXON, S. R., WHITBOURN, R. J., DAE, M. W., GRUBE, E., SHERMAN, W., SCHAER, G. L., JENKINS, J. S., BAIM, D. S., GIBBONS, R. J., KUNTZ, R. E., POPMA, J. J., NGUYEN, T. T. & O'NEILL, W. W. 2002. Induction of mild systemic hypothermia with endovascular cooling during primary percutaneous coronary intervention for acute myocardial infarction. J Am Coll Cardiol, 40, 1928-34.

DOETSCHMAN, T. & AZHAR, M. 2012. Cardiac-specific inducible and conditional gene targeting in mice. Circ Res, 110, 1498-512.

DOETSCHMAN, T., BARNETT, J. V., RUNYAN, R. B., CAMENISCH, T. D., HEIMARK, R. L., GRANZIER, H. L., CONWAY, S. J. & AZHAR, M. 2012. Transforming growth factor beta signaling in adult cardiovascular diseases and repair. Cell Tissue Res, 347, 203-23.

DONG, Y., UNDYALA, V. V., GOTTLIEB, R. A., MENTZER, R. M., JR. & PRZYKLENK, K. 2010. Autophagy: definition, molecular machinery, and potential role in myocardial ischemia-reperfusion injury. J Cardiovasc Pharmacol Ther, 15, 220-30.

DOYLE, A., MCGARRY, M. P., LEE, N. A. & LEE, J. J. 2012. The construction of transgenic and gene knockout/knockin mouse models of human disease. Transgenic Res, 21, 327-49.

DUBIN, G. 2005. Proteinaceous cysteine protease inhibitors. Cell Mol Life Sci, 62, 653-69.

DUEWELL, P., KONO, H., RAYNER, K. J., SIROIS, C. M., VLADIMER, G., BAUERNFEIND, F. G., ABELA, G. S., FRANCHI, L., NUNEZ, G., SCHNURR, M., ESPEVIK, T., LIEN, E., FITZGERALD, K. A., ROCK, K. L., MOORE, K. J., WRIGHT, S. D., HORNUNG, V. & LATZ, E. 2010. NLRP3 inflammasomes are required for atherogenesis and activated by cholesterol crystals. Nature, 464, 1357-61.

DUNCAN, E. M., MURATORE-SCHROEDER, T. L., COOK, R. G., GARCIA, B. A., SHABANOWITZ, J., HUNT, D. F. & ALLIS, C. D. 2008. Cathepsin L proteolytically processes histone H3 during mouse embryonic stem cell differentiation. Cell, 135, 284-94.

DUNCKER, D. J., KLASSEN, C. L., ISHIBASHI, Y., HERRLINGER, S. H., PAVEK, T. J. & BACHE, R. J. 1996. Effect of temperature on myocardial infarction in swine. Am J Physiol, 270, H1189-99.

EBERT, D. H., DEUSSING, J., PETERS, C. & DERMODY, T. S. 2002. Cathepsin L and cathepsin B mediate reovirus disassembly in murine fibroblast cells. J Biol Chem, 277, 24609-17.

EISNER, D. A., TRAFFORD, A. W., DIAZ, M. E., OVEREND, C. L. & O'NEILL, S. C. 1998. The control of Ca release from the cardiac sarcoplasmic reticulum: regulation versus autoregulation. Cardiovasc Res, 38, 589-604.

EITEL, I., STIERMAIER, T., ROMMEL, K. P., FUERNAU, G., SANDRI, M., MANGNER, N., LINKE, A., ERBS, S., LURZ, P., BOUDRIOT, E., MENDE, M., DESCH, S., SCHULER, G. & THIELE, H. 2015. Cardioprotection by combined intrahospital remote ischaemic perconditioning and postconditioning in ST-elevation myocardial infarction: the randomized LIPSIA CONDITIONING trial. Eur Heart J, 36, 3049-57.

ELLIOTT, E. B., KELLY, A., SMITH, G. L. & LOUGHREY, C. M. 2012. Isolated rabbit working heart function during progressive inhibition of myocardial SERCA activity. Circ Res, 110, 1618-27.

ERICKSON, P. F., DESSEV, G., LASHER, R. S., PHILIPS, G., ROBINSON, M. & DRABKIN, H. A. 1996. ETO and AML1 phosphoproteins are expressed in CD34+ hematopoietic progenitors: implications for t(8;21) leukemogenesis and monitoring residual disease. Blood, 88, 1813-23.

ERLEBACHER, J. A., WEISS, J. L., WEISFELDT, M. L. & BULKLEY, B. H. 1984. Early dilation of the infarcted segment in acute transmural myocardial infarction: role of infarct expansion in acute left ventricular enlargement. J Am Coll Cardiol, 4, 201-8.

ERMAN, B., CORTES, M., NIKOLAJCZYK, B. S., SPECK, N. A. & SEN, R. 1998. ETS-core binding factor: a common composite motif in antigen receptor gene enhancers. Mol Cell Biol, 18, 1322-30.

EULALIO, A., MANO, M., DAL FERRO, M., ZENTILIN, L., SINAGRA, G., ZACCHIGNA, S. & GIACCA, M. 2012. Functional screening identifies miRNAs inducing cardiac regeneration. Nature, 492, 376-81.

EVERTS, V., KORPER, W., HOEBEN, K. A., JANSEN, I. D., BROMME, D., CLEUTJENS, K. B., HEENEMAN, S., PETERS, C., REINHECKEL, T., SAFTIG, P. & BEERTSEN, W. 2006. Osteoclastic bone degradation and the role of different cysteine proteinases and matrix metalloproteinases: differences between calvaria and long bone. J Bone Miner Res, 21, 1399-408.

FERRARI, R., BONGRANI, S., RADDINO, R., DI LISA, F. & VISIOLI, O. 1980. [Effect and action mechanism of hypothermia to preserve the ischaemic myocardium (author's transl)]. G Ital Cardiol, 10, 1496-507.

FERRERA, R., BENHABBOUCHE, S., BOPASSA, J. C., LI, B. & OVIZE, M. 2009. One hour reperfusion is enough to assess function and infarct size with TTC staining in Langendorff rat model. Cardiovasc Drugs Ther, 23, 327-31.

FISCHER, A. H., JACOBSON, K. A., ROSE, J. & ZELLER, R. 2008. Hematoxylin and eosin staining of tissue and cell sections. CSH Protoc, 2008, pdb prot4986.

FISH, K. M., LADAGE, D., KAWASE, Y., KARAKIKES, I., JEONG, D., LY, H., ISHIKAWA, K., HADRI, L., TILEMANN, L., MULLER-EHMSEN, J., SAMULSKI, R. J., KRANIAS, E. G. & HAJJAR, R. J. 2013. AAV9.I-1c delivered via direct coronary infusion in a porcine model of heart failure improves contractility and mitigates adverse remodeling. Circ Heart Fail, 6, 310-7.

FISHBEIN, M. C., MEERBAUM, S., RIT, J., LANDO, U., KANMATSUSE, K., MERCIER, J. C., CORDAY, E. & GANZ, W. 1981. Early phase acute myocardial infarct size quantification: validation of the triphenyl tetrazolium chloride tissue enzyme staining technique. Am Heart J, 101, 593-600.

FLACHSKAMPF, F. A., SCHMID, M., ROST, C., ACHENBACH, S., DEMARIA, A. N. & DANIEL, W. G. 2011. Cardiac imaging after myocardial infarction. Eur Heart J, 32, 272-83.

FORCE, T., MICHAEL, A., KILTER, H. & HAQ, S. 2002. Stretch-activated pathways and left ventricular remodeling. J Card Fail, 8, S351-8.

FOSTER, R. E., JOHNSON, D. B., BARILLA, F., BLACKWELL, G. G., ORR, R., RONEY, M., STANLEY, A. W., JR., POHOST, G. M. & DELL'ITALIA, L. J. 1998. Changes in left ventricular mass and volumes in patients receiving angiotensin-converting enzyme inhibitor therapy for left ventricular dysfunction after Q-wave myocardial infarction. Am Heart J, 136, 269-75.

FOX, K. A., CARRUTHERS, K. F., DUNBAR, D. R., GRAHAM, C., MANNING, J. R., DE RAEDT, H., BUYSSCHAERT, I., LAMBRECHTS, D. & VAN DE WERF, F. 2010.

Underestimated and under-recognized: the late consequences of acute coronary syndrome (GRACE UK-Belgian Study). Eur Heart J, 31, 2755-64.

FOX, K. A., DABBOUS, O. H., GOLDBERG, R. J., PIEPER, K. S., EAGLE, K. A., VAN DE WERF, F., AVEZUM, A., GOODMAN, S. G., FLATHER, M. D., ANDERSON, F. A., JR. & GRANGER, C. B. 2006. Prediction of risk of death and myocardial infarction in the six months after presentation with acute coronary syndrome: prospective multinational observational study (GRACE). BMJ, 333, 1091.

FOX, K. A., STEG, P. G., EAGLE, K. A., GOODMAN, S. G., ANDERSON, F. A., JR., GRANGER, C. B., FLATHER, M. D., BUDAJ, A., QUILL, A., GORE, J. M. & INVESTIGATORS, G. 2007. Decline in rates of death and heart failure in acute coronary syndromes, 1999-2006. JAMA, 297, 1892-900.

FREIXA, X., BELLERA, N., ORTIZ-PEREZ, J. T., JIMENEZ, M., PARE, C., BOSCH, X., DE CARALT, T. M., BETRIU, A. & MASOTTI, M. 2012. Ischaemic postconditioning revisited: lack of effects on infarct size following primary percutaneous coronary intervention. Eur Heart J, 33, 103-12.

FROHLICH, G. M., MEIER, P., WHITE, S. K., YELLON, D. M. & HAUSENLOY, D. J. 2013. Myocardial reperfusion injury: looking beyond primary PCI. Eur Heart J, 34, 1714-22.

FUKUNAMI, M. & HEARSE, D. J. 1989. The inotropic consequences of cooling: studies in the isolated rat heart. Heart Vessels, 5, 1-9.

FUNKELSTEIN, L., TONEFF, T., MOSIER, C., HWANG, S. R., BEUSCHLEIN, F., LICHTENAUER, U. D., REINHECKEL, T., PETERS, C. & HOOK, V. 2008. Major role of cathepsin L for producing the peptide hormones ACTH, beta-endorphin, and alpha-MSH, illustrated by protease gene knockout and expression. J Biol Chem, 283, 35652-9.

GAMOU, T., KITAMURA, E., HOSODA, F., SHIMIZU, K., SHINOHARA, K., HAYASHI, Y., NAGASE, T., YOKOYAMA, Y. & OHKI, M. 1998. The partner gene of AML1 in

t(16;21) myeloid malignancies is a novel member of the MTG8(ETO) family. Blood, 91, 4028-37.

GAO, S., HO, D., VATNER, D. E. & VATNER, S. F. 2011. Echocardiography in Mice. Curr Protoc Mouse Biol, 1, 71-83.

GARCIA-DORADO, D., RUIZ-MEANA, M., INSERTE, J., RODRIGUEZ-SINOVAS, A. & PIPER, H. M. 2012. Calcium-mediated cell death during myocardial reperfusion. Cardiovasc Res, 94, 168-80.

GATTENLOHNER, S., WALLER, C., ERTL, G., BULTMANN, B. D., MULLER-HERMELINK, H. K. & MARX, A. 2003. NCAM(CD56) and RUNX1(AML1) are up-regulated in human ischemic cardiomyopathy and a rat model of chronic cardiac ischemia. Am J Pathol, 163, 1081-90.

GE, J., ZHAO, G., CHEN, R., LI, S., WANG, S., ZHANG, X., ZHUANG, Y., DU, J., YU, X., LI, G. & YANG, Y. 2006. Enhanced myocardial cathepsin B expression in patients with dilated cardiomyopathy. Eur J Heart Fail, 8, 284-9.

GEDIK, N., THIELMANN, M., KOTTENBERG, E., PETERS, J., JAKOB, H., HEUSCH, G. & KLEINBONGARD, P. 2014. No evidence for activated autophagy in left ventricular myocardium at early reperfusion with protection by remote ischemic preconditioning in patients undergoing coronary artery bypass grafting. PLoS One, 9, e96567.

GELSI-BOYER, V., TROUPLIN, V., ADELAIDE, J., ACETO, N., REMY, V., PINSON, S., HOUDAYER, C., ARNOULET, C., SAINTY, D., BENTIRES-ALJ, M., OLSCHWANG, S., VEY, N., MOZZICONACCI, M. J., BIRNBAUM, D. & CHAFFANET, M. 2008. Genome profiling of chronic myelomonocytic leukemia: frequent alterations of RAS and RUNX1 genes. BMC Cancer, 8, 299.

GENG, T., ZHANG, J. G., SONG, Z. Y., DAI, S. P., LUO, Y. & XU, Z. S. 2016. Aspiration thrombectomy and intracoronary tirofiban in ST-segment elevation

myocardial infarction : Combination treatment for patients undergoing primary percutaneous coronary intervention. Herz.

GERDES, A. M., KELLERMAN, S. E., MOORE, J. A., MUFFLY, K. E., CLARK, L. C., REAVES, P. Y., MALEC, K. B., MCKEOWN, P. P. & SCHOCKEN, D. D. 1992. Structural remodeling of cardiac myocytes in patients with ischemic cardiomyopathy. Circulation, 86, 426-30.

GHEORGHIADE, M. & BONOW, R. O. 1998. Chronic heart failure in the United States: a manifestation of coronary artery disease. Circulation, 97, 282-9.

GITTENBERGER-DE GROOT, A. C., BARTELINGS, M. M., DERUITER, M. C. & POELMANN, R. E. 2005. Basics of cardiac development for the understanding of congenital heart malformations. Pediatr Res, 57, 169-76.

GO, A. S., MOZAFFARIAN, D., ROGER, V. L., BENJAMIN, E. J., BERRY, J. D., BLAHA, M. J., DAI, S., FORD, E. S., FOX, C. S., FRANCO, S., FULLERTON, H. J., GILLESPIE, C., HAILPERN, S. M., HEIT, J. A., HOWARD, V. J., HUFFMAN, M. D., JUDD, S. E., KISSELA, B. M., KITTNER, S. J., LACKLAND, D. T., LICHTMAN, J. H., LISABETH, L. D., MACKEY, R. H., MAGID, D. J., MARCUS, G. M., MARELLI, A., MATCHAR, D. B., MCGUIRE, D. K., MOHLER, E. R., 3RD, MOY, C. S., MUSSOLINO, M. E., NEUMAR, R. W., NICHOL, G., PANDEY, D. K., PAYNTER, N. P., REEVES, M. J., SORLIE, P. D., STEIN, J., TOWFIGHI, A., TURAN, T. N., VIRANI, S. S., WONG, N. D., WOO, D., TURNER, M. B., AMERICAN HEART ASSOCIATION STATISTICS, C. & STROKE STATISTICS, S. 2014. Heart disease and stroke statistics--2014 update: a report from the American Heart Association. Circulation, 129, e28-e292.

GOLUB, T. R., BARKER, G. F., BOHLANDER, S. K., HIEBERT, S. W., WARD, D. C., BRAY-WARD, P., MORGAN, E., RAIMONDI, S. C., ROWLEY, J. D. & GILLILAND, D. G. 1995. Fusion of the TEL gene on 12p13 to the AML1 gene on 21q22 in acute lymphoblastic leukemia. Proc Natl Acad Sci U S A, 92, 4917-21.

GRIFFITHS, E. J. & HALESTRAP, A. P. 1995. Mitochondrial non-specific pores remain closed during cardiac ischaemia, but open upon reperfusion. Biochem J, 307 (Pt 1), 93-8.

GRINES, C. L., COX, D. A., STONE, G. W., GARCIA, E., MATTOS, L. A., GIAMBARTOLOMEI, A., BRODIE, B. R., MADONNA, O., EIJGELSHOVEN, M., LANSKY, A. J., O'NEILL, W. W. & MORICE, M. C. 1999. Coronary angioplasty with or without stent implantation for acute myocardial infarction. Stent Primary Angioplasty in Myocardial Infarction Study Group. N Engl J Med, 341, 1949-56.

GROSSMAN, W. & PAULUS, W. J. 2013. Myocardial stress and hypertrophy: a complex interface between biophysics and cardiac remodeling. J Clin Invest, 123, 3701-3.

GROUP, S. F. P. E. I. T. E. D. S. 2000. Trial of abciximab with and without low-dose reteplase for acute myocardial infarction. Strategies for Patency Enhancement in the Emergency Department (SPEED) Group. Circulation, 101, 2788-94.

GU, T. L., GOETZ, T. L., GRAVES, B. J. & SPECK, N. A. 2000. Auto-inhibition and partner proteins, core-binding factor beta (CBFbeta) and Ets-1, modulate DNA binding by CBFalpha2 (AML1). Mol Cell Biol, 20, 91-103.

GUICCIARDI, M. E., DEUSSING, J., MIYOSHI, H., BRONK, S. F., SVINGEN, P. A., PETERS, C., KAUFMANN, S. H. & GORES, G. J. 2000. Cathepsin B contributes to TNF-alpha-mediated hepatocyte apoptosis by promoting mitochondrial release of cytochrome c. Journal of Clinical Investigation, 106, 1127-1137.

GUNTHER, C. V. & GRAVES, B. J. 1994. Identification of ETS domain proteins in murine T lymphocytes that interact with the Moloney murine leukemia virus enhancer. Mol Cell Biol, 14, 7569-80.

GUO, H., CALLAWAY, J. B. & TING, J. P. 2015. Inflammasomes: mechanism of action, role in disease, and therapeutics. Nat Med, 21, 677-87.

GUO, H. & FRIEDMAN, A. D. 2011. Phosphorylation of RUNX1 by cyclin-dependent kinase reduces direct interaction with HDAC1 and HDAC3. J Biol Chem, 286, 208-15.

GURUSAMY, N., LEKLI, I., GORBUNOV, N. V., GHERGHICEANU, M., POPESCU, L. M. & DAS, D. K. 2009. Cardioprotection by adaptation to ischaemia augments autophagy in association with BAG-1 protein. J Cell Mol Med, 13, 373-87.

HAGHIGHI, K., BIDWELL, P. & KRANIAS, E. G. 2014. Phospholamban interactome in cardiac contractility and survival: A new vision of an old friend. J Mol Cell Cardiol, 77, 160-7.

HAHN, J. Y., SONG, Y. B., KIM, E. K., YU, C. W., BAE, J. W., CHUNG, W. Y., CHOI, S. H., CHOI, J. H., BAE, J. H., AN, K. J., PARK, J. S., OH, J. H., KIM, S. W., HWANG, J. Y., RYU, J. K., PARK, H. S., LIM, D. S. & GWON, H. C. 2013. Ischemic postconditioning during primary percutaneous coronary intervention: the effects of postconditioning on myocardial reperfusion in patients with ST-segment elevation myocardial infarction (POST) randomized trial. Circulation, 128, 1889-96.

HALE, S. L. & KLONER, R. A. 1998. Myocardial temperature reduction attenuates necrosis after prolonged ischemia in rabbits. Cardiovasc Res, 40, 502-7.

HALE, S. L. & KLONER, R. A. 1999. Myocardial hypothermia: a potential therapeutic technique for acute regional myocardial ischemia. J Cardiovasc Electrophysiol, 10, 405-13.

HAMACHER-BRADY, A., BRADY, N. R. & GOTTLIEB, R. A. 2006. Enhancing macroautophagy protects against ischemia/reperfusion injury in cardiac myocytes. J Biol Chem, 281, 29776-87.

HANADA, K., TAMAI, M., YAMAGISHI, M., OHMURA, S., SAWADA, J. & TANAKA, I. 1978. Isolation and Characterization of E-64, a New Thiol Protease Inhibitor. Agricultural and Biological Chemistry, 42, 523-528.

HANEWINKEL, H., GLOSSL, J. & KRESSE, H. 1987. Biosynthesis of cathepsin B in cultured normal and I-cell fibroblasts. J Biol Chem, 262, 12351-5.

HARRIS, I. S. & BLACK, B. L. 2010. Development of the endocardium. Pediatr Cardiol, 31, 391-9.

HAUSENLOY, D. J., DUCHEN, M. R. & YELLON, D. M. 2003. Inhibiting mitochondrial permeability transition pore opening at reperfusion protects against ischaemia-reperfusion injury. Cardiovasc Res, 60, 617-25.

HAUSENLOY, D. J., KHARBANDA, R., RAHBEK SCHMIDT, M., MOLLER, U. K., RAVKILDE, J., OKKELS JENSEN, L., ENGSTROM, T., GARCIA RUIZ, J. M., RADOVANOVIC, N., CHRISTENSEN, E. F., SORENSEN, H. T., RAMLALL, M., BULLUCK, H., EVANS, R., NICHOLAS, J., KNIGHT, R., CLAYTON, T., YELLON, D. M. & BOTKER, H. E. 2015. Effect of remote ischaemic conditioning on clinical outcomes in patients presenting with an ST-segment elevation myocardial infarction undergoing primary percutaneous coronary intervention. Eur Heart J, 36, 1846-8.

HAUSENLOY, D. J. & YELLON, D. M. 2003. The mitochondrial permeability transition pore: its fundamental role in mediating cell death during ischaemia and reperfusion. J Mol Cell Cardiol, 35, 339-41.

HAUSENLOY, D. J. & YELLON, D. M. 2013. Myocardial ischemia-reperfusion injury: a neglected therapeutic target. J Clin Invest, 123, 92-100.

HAUSENLOY, D. J. & YELLON, D. M. 2016. Ischaemic conditioning and reperfusion injury. Nat Rev Cardiol, 13, 193-209.

HE, Y. Y., LIU, C. L., LI, X., ZHONG, W., LI, S., HE, K. L. & WANG, L. L. 2014. Effects of PP1-12, a novel protein phosphatase-1 inhibitor, on ventricular function and remodeling after myocardial infarction in rats. J Cardiovasc Pharmacol, 64, 360-7.

HEARSE, D. J., HUMPHREY, S. M. & CHAIN, E. B. 1973. Abrupt reoxygenation of the anoxic potassium-arrested perfused rat heart: a study of myocardial enzyme release. J Mol Cell Cardiol, 5, 395-407.

HEARSE, D. J. & TOSAKI, A. 1987. Free radicals and reperfusion-induced arrhythmias: protection by spin trap agent PBN in the rat heart. Circ Res, 60, 375-83.

HELLER, P. G., GLEMBOTSKY, A. C., GANDHI, M. J., CUMMINGS, C. L., PIROLA, C. J., MARTA, R. F., KORNBLIHTT, L. I., DRACHMAN, J. G. & MOLINAS, F. C. 2005. Low Mpl receptor expression in a pedigree with familial platelet disorder with predisposition to acute myelogenous leukemia and a novel AML1 mutation. Blood, 105, 4664-70.

HELSKE, S., SYVARANTA, S., LINDSTEDT, K. A., LAPPALAINEN, J., OORNI, K., MAYRANPAA, M. I., LOMMI, J., TURTO, H., WERKKALA, K., KUPARI, M. & KOVANEN, P. T. 2006. Increased expression of elastolytic cathepsins S, K, and V and their inhibitor cystatin C in stenotic aortic valves. Arterioscler Thromb Vasc Biol, 26, 1791-8.

HEMPEL, P., HOCH, B., BARTEL, S. & KARCZEWSKI, P. 2002. Hypertrophic phenotype of cardiac calcium/calmodulin-dependent protein kinase II is reversed by angiotensin converting enzyme inhibition. Basic Res Cardiol, 97 Suppl 1, I96-101.

HERR, D. J., AUNE, S. E. & MENICK, D. R. 2015. Induction and Assessment of Ischemia-reperfusion Injury in Langendorff-perfused Rat Hearts. J Vis Exp, e52908.

HERZOG, W. R., VOGEL, R. A., SCHLOSSBERG, M. L., EDENBAUM, L. R., SCOTT, H. J. & SEREBRUANY, V. L. 1997. Short-term low dose intracoronary diltiazem administered at the onset of reperfusion reduces myocardial infarct size. Int J Cardiol, 59, 21-7.

HEUSCH, G., BOENGLER, K. & SCHULZ, R. 2010. Inhibition of mitochondrial permeability transition pore opening: the Holy Grail of cardioprotection. Basic Res Cardiol, 105, 151-4.

HEUSCH, G., KLEINBONGARD, P., BOSE, D., LEVKAU, B., HAUDE, M., SCHULZ, R. & ERBEL, R. 2009. Coronary microembolization: from bedside to bench and back to bedside. Circulation, 120, 1822-36.

HJALMARSON, A. 1997. Effects of beta blockade on sudden cardiac death during acute myocardial infarction and the postinfarction period. Am J Cardiol, 80, 35J-39J.

HOFSTEN, D. E., KELBAEK, H., HELQVIST, S., KLOVGAARD, L., HOLMVANG, L., CLEMMENSEN, P., TORP-PEDERSEN, C., TILSTED, H. H., BOTKER, H. E., JENSEN, L. O., KOBER, L., ENGSTROM, T. & INVESTIGATORS, D. 2015. The Third DANish Study of Optimal Acute Treatment of Patients with ST-segment Elevation Myocardial Infarction: Ischemic postconditioning or deferred stent implantation versus conventional primary angioplasty and complete revascularization versus treatment of culprit lesion only: Rationale and design of the DANAMI 3 trial program. Am Heart J, 169, 613-21.

HOMBACH, V., GREBE, O., MERKLE, N., WALDENMAIER, S., HOHER, M., KOCHS, M., WOHRLE, J. & KESTLER, H. A. 2005. Sequelae of acute myocardial infarction regarding cardiac structure and function and their prognostic significance as assessed by magnetic resonance imaging. Eur Heart J, 26, 549-57.

HONG, K. U. & BOLLI, R. 2014. Cardiac stem cell therapy for cardiac repair. Curr Treat Options Cardiovasc Med, 16, 324.

HOOLE, S. P., HECK, P. M., SHARPLES, L., KHAN, S. N., DUEHMKE, R., DENSEM, C. G., CLARKE, S. C., SHAPIRO, L. M., SCHOFIELD, P. M., O'SULLIVAN, M. & DUTKA, D. P. 2009. Cardiac Remote Ischemic Preconditioning in Coronary Stenting (CRISP Stent) Study: a prospective, randomized control trial. Circulation, 119, 820-7.

HOU, W. S., LI, W., KEYSZER, G., WEBER, E., LEVY, R., KLEIN, M. J., GRAVALLESE, E. M., GOLDRING, S. R. & BROMME, D. 2002. Comparison of cathepsins K and S expression within the rheumatoid and osteoarthritic synovium. Arthritis Rheum, 46, 663-74.

HSIANG, Y. H., SPENCER, D., WANG, S., SPECK, N. A. & RAULET, D. H. 1993. The role of viral enhancer "core" motif-related sequences in regulating T cell receptor-gamma and -delta gene expression. J Immunol, 150, 3905-16.

HUA, F., HA, T., MA, J., LI, Y., KELLEY, J., GAO, X., BROWDER, I. W., KAO, R. L., WILLIAMS, D. L. & LI, C. 2007. Protection against myocardial ischemia/reperfusion injury in TLR4-deficient mice is mediated through a phosphoinositide 3-kinase-dependent mechanism. J Immunol, 178, 7317-24.

HUA, Y., ROBINSON, T. J., CAO, Y., SHI, G. P., REN, J. & NAIR, S. 2015. Cathepsin K knockout alleviates aging-induced cardiac dysfunction. Aging Cell, 14, 345-51.

HUA, Y., XU, X., SHI, G. P., CHICCO, A. J., REN, J. & NAIR, S. 2013a. Cathepsin K knockout alleviates pressure overload-induced cardiac hypertrophy. Hypertension, 61, 1184-92.

HUA, Y., ZHANG, Y., DOLENCE, J., SHI, G. P., REN, J. & NAIR, S. 2013b. Cathepsin K knockout mitigates high-fat diet-induced cardiac hypertrophy and contractile dysfunction. Diabetes, 62, 498-509.

HUANG, C., ANDRES, A. M., RATLIFF, E. P., HERNANDEZ, G., LEE, P. & GOTTLIEB, R. A. 2011. Preconditioning involves selective mitophagy mediated by Parkin and p62/SQSTM1. PLoS One, 6, e20975.

HUANG, G., SHIGESADA, K., ITO, K., WEE, H. J., YOKOMIZO, T. & ITO, Y. 2001. Dimerization with PEBP2beta protects RUNX1/AML1 from ubiquitin-proteasome-mediated degradation. EMBO J, 20, 723-33.

HUANG, G., ZHANG, P., HIRAI, H., ELF, S., YAN, X., CHEN, Z., KOSCHMIEDER, S., OKUNO, Y., DAYARAM, T., GROWNEY, J. D., SHIVDASANI, R. A., GILLILAND, D. G., SPECK, N. A., NIMER, S. D. & TENEN, D. G. 2008. PU.1 is a major downstream target of AML1 (RUNX1) in adult mouse hematopoiesis. Nat Genet, 40, 51-60.

HUANG, H., YU, M., AKIE, T. E., MORAN, T. B., WOO, A. J., TU, N., WALDON, Z., LIN, Y. Y., STEEN, H. & CANTOR, A. B. 2009. Differentiation-dependent interactions between RUNX-1 and FLI-1 during megakaryocyte development. Mol Cell Biol, 29, 4103-15.

HWANG, S. R., GARZA, C., MOSIER, C., TONEFF, T., WUNDERLICH, E., GOLDSMITH, P. & HOOK, V. 2007. Cathepsin L expression is directed to secretory vesicles for enkephalin neuropeptide biosynthesis and secretion. J Biol Chem, 282, 9556-63.

IMAI, Y., KUROKAWA, M., IZUTSU, K., HANGAISHI, A., TAKEUCHI, K., MAKI, K., OGAWA, S., CHIBA, S., MITANI, K. & HIRAI, H. 2000. Mutations of the AML1 gene in myelodysplastic syndrome and their functional implications in leukemogenesis. Blood, 96, 3154-60.

IMAI, Y., KUROKAWA, M., YAMAGUCHI, Y., IZUTSU, K., NITTA, E., MITANI, K., SATAKE, M., NODA, T., ITO, Y. & HIRAI, H. 2004. The corepressor mSin3A regulates phosphorylation-induced activation, intranuclear location, and stability of AML1. Mol Cell Biol, 24, 1033-43.

INSERTE, J., HERNANDO, V. & GARCIA-DORADO, D. 2012. Contribution of calpains to myocardial ischaemia/reperfusion injury. Cardiovasc Res, 96, 23-31.

ISHIKAWA, K., FISH, K. M., TILEMANN, L., RAPTI, K., AGUERO, J., SANTOS-GALLEGO, C. G., LEE, A., KARAKIKES, I., XIE, C., AKAR, F. G., SHIMADA, Y. J., GWATHMEY, J. K., ASOKAN, A., MCPHEE, S., SAMULSKI, J., SAMULSKI, R. J., SIGG, D. C., WEBER, T., KRANIAS, E. G. & HAJJAR, R. J. 2014. Cardiac I-1c overexpression with reengineered AAV improves cardiac function in swine ischemic heart failure. Mol Ther, 22, 2038-45.

ITO, H. 2006. No-reflow phenomenon and prognosis in patients with acute myocardial infarction. Nat Clin Pract Cardiovasc Med, 3, 499-506.

ITO, H., MARUYAMA, A., IWAKURA, K., TAKIUCHI, S., MASUYAMA, T., HORI, M., HIGASHINO, Y., FUJII, K. & MINAMINO, T. 1996. Clinical implications of the 'no reflow' phenomenon. A predictor of complications and left ventricular remodeling in reperfused anterior wall myocardial infarction. Circulation, 93, 223-8.

JAFFE, A. S. 2006. Chasing troponin: how low can you go if you can see the rise? J Am Coll Cardiol, 48, 1763-4.

JAFFER, F. A., KIM, D. E., QUINTI, L., TUNG, C. H., AIKAWA, E., PANDE, A. N., KOHLER, R. H., SHI, G. P., LIBBY, P. & WEISSLEDER, R. 2007. Optical visualization of cathepsin K activity in atherosclerosis with a novel, protease-activatable fluorescence sensor. Circulation, 115, 2292-8.

JAMES, P. H., PRUSCHY, M., VORHERR, T. E., PENNISTON, J. T. & CARAFOLI, E. 1989. Primary structure of the cAMP-dependent phosphorylation site of the plasma membrane calcium pump. Biochemistry, 28, 4253-8.

JEAN, D., GUILLAUME, N. & FRADE, R. 2002. Characterization of human cathepsin L promoter and identification of binding sites for NF-Y, Sp1 and Sp3 that are essential for its activity. Biochem J, 361, 173-84.

JENNINGS, R. B., SOMMERS, H. M., SMYTH, G. A., FLACK, H. A. & LINN, H. 1960. Myocardial necrosis induced by temporary occlusion of a coronary artery in the dog. Arch Pathol, 70, 68-78.

JERNBERG, T., JOHANSON, P., HELD, C., SVENNBLAD, B., LINDBACK, J., WALLENTIN, L. & SWEDEHEART/RIKS, H. I. A. 2011. Association between adoption of evidence-based treatment and survival for patients with ST-elevation myocardial infarction. JAMA, 305, 1677-84.

JIAO, K., KULESSA, H., TOMPKINS, K., ZHOU, Y., BATTS, L., BALDWIN, H. S. & HOGAN, B. L. 2003. An essential role of Bmp4 in the atrioventricular septation of the mouse heart. Genes Dev, 17, 2362-7.

JONES, S. P. & BOLLI, R. 2006. The ubiquitous role of nitric oxide in cardioprotection. J Mol Cell Cardiol, 40, 16-23.

KANAMORI, H., TAKEMURA, G., GOTO, K., MARUYAMA, R., ONO, K., NAGAO, K., TSUJIMOTO, A., OGINO, A., TAKEYAMA, T., KAWAGUCHI, T., WATANABE, T., KAWASAKI, M., FUJIWARA, T., FUJIWARA, H., SEISHIMA, M. & MINATOGUCHI, S. 2011. Autophagy limits acute myocardial infarction induced by permanent coronary artery occlusion. Am J Physiol Heart Circ Physiol, 300, H2261-71.

KANNO, T., KANNO, Y., CHEN, L. F., OGAWA, E., KIM, W. Y. & ITO, Y. 1998. Intrinsic transcriptional activation-inhibition domains of the polyomavirus enhancer binding protein 2/core binding factor alpha subunit revealed in the presence of the beta subunit. Mol Cell Biol, 18, 2444-54.

KASTRATI, A., DIBRA, A., SPAULDING, C., LAARMAN, G. J., MENICHELLI, M., VALGIMIGLI, M., DI LORENZO, E., KAISER, C., TIERALA, I., MEHILLI, J., SEYFARTH, M., VARENNE, O., DIRKSEN, M. T., PERCOCO, G., VARRICCHIO, A., PITTL, U., SYVANNE, M., SUTTORP, M. J., VIOLINI, R. & SCHOMIG, A. 2007. Meta-analysis of randomized trials on drug-eluting stents vs. bare-metal stents in patients with acute myocardial infarction. Eur Heart J, 28, 2706-13.

KATHOLI, R. E. & COURI, D. M. 2011. Left ventricular hypertrophy: major risk factor in patients with hypertension: update and practical clinical applications. Int J Hypertens, 2011, 495349.

KATUNUMA, N., MURATA, E., KAKEGAWA, H., MATSUI, A., TSUZUKI, H., TSUGE, H., TURK, D., TURK, V., FUKUSHIMA, M., TADA, Y. & ASAO, T. 1999. Structure based development of novel specific inhibitors for cathepsin L and cathepsin S in vitro and in vivo. Febs Letters, 458, 6-10.

KEELEY, E. C., BOURA, J. A. & GRINES, C. L. 2003. Primary angioplasty versus intravenous thrombolytic therapy for acute myocardial infarction: a quantitative review of 23 randomised trials. Lancet, 361, 13-20.

KEELEY, E. C. & HILLIS, L. D. 2007. Primary PCI for myocardial infarction with ST-segment elevation. N Engl J Med, 356, 47-54.

KEHAT, I. & MOLKENTIN, J. D. 2010. Molecular pathways underlying cardiac remodeling during pathophysiological stimulation. Circulation, 122, 2727-35.

KELLMAN, P. & ARAI, A. E. 2012. Cardiac imaging techniques for physicians: late enhancement. J Magn Reson Imaging, 36, 529-42.

KILKENNY, C., BROWNE, W., CUTHILL, I. C., EMERSON, M., ALTMAN, D. G. & GROUP, N. C. R. R. G. W. 2010. Animal research: reporting in vivo experiments: the ARRIVE guidelines. Br J Pharmacol, 160, 1577-9.

KIM, S. J., KUDEJ, R. K., YATANI, A., KIM, Y. K., TAKAGI, G., HONDA, R., COLANTONIO, D. A., VAN EYK, J. E., VATNER, D. E., RASMUSSON, R. L. & VATNER, S. F. 2001. A novel mechanism for myocardial stunning involving impaired Ca(2+) handling. Circ Res, 89, 831-7.

KIM, W. Y., SIEWEKE, M., OGAWA, E., WEE, H. J., ENGLMEIER, U., GRAF, T. & ITO, Y. 1999. Mutual activation of Ets-1 and AML1 DNA binding by direct interaction of their autoinhibitory domains. EMBO J, 18, 1609-20.

KITABAYASHI, I., YOKOYAMA, A., SHIMIZU, K. & OHKI, M. 1998. Interaction and functional cooperation of the leukemia-associated factors AML1 and p300 in myeloid cell differentiation. EMBO J, 17, 2994-3004.

KITOH, A., ONO, M., NAOE, Y., OHKURA, N., YAMAGUCHI, T., YAGUCHI, H., KITABAYASHI, I., TSUKADA, T., NOMURA, T., MIYACHI, Y., TANIUCHI, I. & SAKAGUCHI, S. 2009. Indispensable role of the Runx1-Cbfbeta transcription

complex for in vivo-suppressive function of FoxP3+ regulatory T cells. Immunity, 31, 609-20.

KLEIN, H. H., SCHAPER, J., PUSCHMANN, S., NIENABER, C., KREUZER, H. & SCHAPER, W. 1981. Loss of canine myocardial nicotinamide adenine dinucleotides determines the transition from reversible to irreversible ischemic damage of myocardial cells. Basic Res Cardiol, 76, 612-21.

KLEINBONGARD, P., SCHULZ, R. & HEUSCH, G. 2011. TNFalpha in myocardial ischemia/reperfusion, remodeling and heart failure. Heart Fail Rev, 16, 49-69.

KLONER, R. A. 2013. Current state of clinical translation of cardioprotective agents for acute myocardial infarction. Circ Res, 113, 451-63.

KLONER, R. A., BOLLI, R., MARBAN, E., REINLIB, L. & BRAUNWALD, E. 1998a. Medical and cellular implications of stunning, hibernation, and preconditioning: an NHLBI workshop. Circulation, 97, 1848-67.

KLONER, R. A., BOLLI, R., MARBAN, E., REINLIB, L., BRAUNWALD, E., REINLIB, L. J., BONOW, R. O., BORGERS, M., DOWNEY, J., FEIGENBAUM, H., GANOTE, C., GROSS, G., JENNINGS, R., LEVITSKY, S., MCCULLY, J. D., MENTZER, R., MILLER, W. P., PRZYKLENK, K., RAHIMTOOLA, S., VATNER, S. & YELLON, D. 1998b. Medical and cellular implications of stunning, hibernation, and preconditioning - An NHLBI Workshop. Circulation, 97, 1848-1867.

KLONER, R. A., ELLIS, S. G., LANGE, R. & BRAUNWALD, E. 1983. Studies of experimental coronary artery reperfusion. Effects on infarct size, myocardial function, biochemistry, ultrastructure and microvascular damage. Circulation, 68, I8-15.

KOITABASHI, N. & KASS, D. A. 2012. Reverse remodeling in heart failure--mechanisms and therapeutic opportunities. Nat Rev Cardiol, 9, 147-57.

KOMINAMI, E., TSUKAHARA, T., HARA, K. & KATUNUMA, N. 1988. Biosyntheses and processing of lysosomal cysteine proteinases in rat macrophages. FEBS Lett, 231, 225-8.

KOMINAMI, E., UENO, T., MUNO, D. & KATUNUMA, N. 1991. The selective role of cathepsins B and D in the lysosomal degradation of endogenous and exogenous proteins. FEBS Lett, 287, 189-92.

KONSTAM, M. A., KRAMER, D. G., PATEL, A. R., MARON, M. S. & UDELSON, J. E. 2011. Left ventricular remodeling in heart failure: current concepts in clinical significance and assessment. JACC Cardiovasc Imaging, 4, 98-108.

KREBS, H. A. & HENSELEIT, K. 1932. Untersuchungen über die Harnstoffbildung im Tierkörper. Klinische Wochenschrift, 11, 757-759.

KRENZ, M. & ROBBINS, J. 2004. Impact of beta-myosin heavy chain expression on cardiac function during stress. J Am Coll Cardiol, 44, 2390-7.

KROEMER, G. & JAATTELA, M. 2005. Lysosomes and autophagy in cell death control. Nat Rev Cancer, 5, 886-97.

KRUG, A., DU MESNIL DE, R. & KORB, G. 1966. Blood supply of the myocardium after temporary coronary occlusion. Circ Res, 19, 57-62.

KUBIN, T., POLING, J., KOSTIN, S., GAJAWADA, P., HEIN, S., REES, W., WIETELMANN, A., TANAKA, M., LORCHNER, H., SCHIMANSKI, S., SZIBOR, M., WARNECKE, H. & BRAUN, T. 2011. Oncostatin M is a major mediator of cardiomyocyte dedifferentiation and remodeling. Cell Stem Cell, 9, 420-32.

KULIAWAT, R., KLUMPERMAN, J., LUDWIG, T. & ARVAN, P. 1997. Differential sorting of lysosomal enzymes out of the regulated secretory pathway in pancreatic beta-cells. J Cell Biol, 137, 595-608.

KUO, M. C., LIANG, D. C., HUANG, C. F., SHIH, Y. S., WU, J. H., LIN, T. L. & SHIH, L. Y. 2009. RUNX1 mutations are frequent in chronic myelomonocytic leukemia

and mutations at the C-terminal region might predict acute myeloid leukemia transformation. Leukemia, 23, 1426-31.

LAARMAN, G. J., SUTTORP, M. J., DIRKSEN, M. T., VAN HEEREBEEK, L., KIEMENEIJ, F., SLAGBOOM, T., VAN DER WIEKEN, L. R., TIJSSEN, J. G., RENSING, B. J. & PATTERSON, M. 2006. Paclitaxel-eluting versus uncoated stents in primary percutaneous coronary intervention. N Engl J Med, 355, 1105-13.

LADILOV, Y. V., SIEGMUND, B. & PIPER, H. M. 1995. Protection of reoxygenated cardiomyocytes against hypercontracture by inhibition of Na+/H+ exchange. Am J Physiol, 268, H1531-9.

LAKKA, S. S., GONDI, C. S., YANAMANDRA, N., OLIVERO, W. C., DINH, D. H., GUJRATI, M. & RAO, J. S. 2004. Inhibition of cathepsin B and MMP-9 gene expression in glioblastoma cell line via RNA interference reduces tumor cell invasion, tumor growth and angiogenesis. Oncogene, 23, 4681-9.

LAM, K. & ZHANG, D. E. 2012. RUNX1 and RUNX1-ETO: roles in hematopoiesis and leukemogenesis. Front Biosci (Landmark Ed), 17, 1120-39.

LANCRIN, C., SROCZYNSKA, P., STEPHENSON, C., ALLEN, T., KOUSKOFF, V. & LACAUD, G. 2009. The haemangioblast generates haematopoietic cells through a haemogenic endothelium stage. Nature, 457, 892-5.

LANGENDORFF, O. 1897. Untersuchungen am überlebenden Säugethierherzen. Archiv für die gesamte Physiologie des Menschen und der Tiere, 66, 355-400.

LANKELMA, J. M., VOOREND, D. M., BARWARI, T., KOETSVELD, J., VAN DER SPEK, A. H., DE PORTO, A. P., VAN ROOIJEN, G. & VAN NOORDEN, C. J. 2010. Cathepsin L, target in cancer treatment? Life Sci, 86, 225-33.

LAYLAND, J., SOLARO, R. J. & SHAH, A. M. 2005. Regulation of cardiac contractile function by troponin I phosphorylation. Cardiovasc Res, 66, 12-21.

LEE, D. C., OZ, M. C., WEINBERG, A. D. & TING, W. 2003. Appropriate timing of surgical intervention after transmural acute myocardial infarction. J Thorac Cardiovasc Surg, 125, 115-9; discussion 119-20.

LEINEWEBER, K., ROHE, P., BEILFUSS, A., WOLF, C., SPORKMANN, H., BRUCK, H., JAKOB, H. G., HEUSCH, G., PHILIPP, T. & BRODDE, O. E. 2005. G-protein-coupled receptor kinase activity in human heart failure: effects of beta-adrenoceptor blockade. Cardiovasc Res, 66, 512-9.

LEMASTERS, J. J., BOND, J. M., CHACON, E., HARPER, I. S., KAPLAN, S. H., OHATA, H., TROLLINGER, D. R., HERMAN, B. & CASCIO, W. E. 1996. The pH paradox in ischemia-reperfusion injury to cardiac myocytes. EXS, 76, 99-114.

LEVANON, D., GLUSMAN, G., BANGSOW, T., BEN-ASHER, E., MALE, D. A., AVIDAN, N., BANGSOW, C., HATTORI, M., TAYLOR, T. D., TAUDIEN, S., BLECHSCHMIDT, K., SHIMIZU, N., ROSENTHAL, A., SAKAKI, Y., LANCET, D. & GRONER, Y. 2001. Architecture and anatomy of the genomic locus encoding the human leukemia-associated transcription factor RUNX1/AML1. Gene, 262, 23-33.

LEVANON, D., GOLDSTEIN, R. E., BERNSTEIN, Y., TANG, H., GOLDENBERG, D., STIFANI, S., PAROUSH, Z. & GRONER, Y. 1998. Transcriptional repression by AML1 and LEF-1 is mediated by the TLE/Groucho corepressors. Proc Natl Acad Sci U S A, 95, 11590-5.

LI, W. & YUAN, X. M. 2004. Increased expression and translocation of lysosomal cathepsins contribute to macrophage apoptosis in atherogenesis. Ann N Y Acad Sci, 1030, 427-33.

LIBERMANN, T. A., PAN, Z., AKBARALI, Y., HETHERINGTON, C. J., BOLTAX, J., YERGEAU, D. A. & ZHANG, D. E. 1999. AML1 (CBFalpha2) cooperates with B cell-specific activating protein (BSAP/PAX5) in activation of the B cell-specific BLK gene promoter. J Biol Chem, 274, 24671-6.

LIPS, D. J., VAN DER NAGEL, T., STEENDIJK, P., PALMEN, M., JANSSEN, B. J., VAN DANTZIG, J. M., DE WINDT, L. J. & DOEVENDANS, P. A. 2004. Left ventricular pressure-volume measurements in mice: comparison of closed-chest versus open-chest approach. Basic Res Cardiol, 99, 351-9.

LIU, A., GAO, X., ZHANG, Q. & CUI, L. 2013. Cathepsin B inhibition attenuates cardiac dysfunction and remodeling following myocardial infarction by inhibiting the NLRP3 pathway. Mol Med Rep, 8, 361-6.

LIU, J., SUKHOVA, G. K., SUN, J. S., XU, W. H., LIBBY, P. & SHI, G. P. 2004. Lysosomal cysteine proteases in atherosclerosis. Arterioscler Thromb Vasc Biol, 24, 1359-66.

LIU, J., SUKHOVA, G. K., YANG, J. T., SUN, J., MA, L., REN, A., XU, W. H., FU, H., DOLGANOV, G. M., HU, C., LIBBY, P. & SHI, G. P. 2006. Cathepsin L expression and regulation in human abdominal aortic aneurysm, atherosclerosis, and vascular cells. Atherosclerosis, 184, 302-11.

LIU, X., ZHANG, Q., ZHANG, D. E., ZHOU, C., XING, H., TIAN, Z., RAO, Q., WANG, M. & WANG, J. 2009a. Overexpression of an isoform of AML1 in acute leukemia and its potential role in leukemogenesis. Leukemia, 23, 739-45.

LIU, Y., LI, X., PENG, D., TAN, Z., LIU, H., QING, Y., XUE, Y. & SHI, G. P. 2009b. Usefulness of serum cathepsin L as an independent biomarker in patients with coronary heart disease. Am J Cardiol, 103, 476-81.

LIU, Y., ZHOU, Y. & ZHU, K. 2012. Inhibition of glioma cell lysosome exocytosis inhibits glioma invasion. PLoS One, 7, e45910.

LONBORG, J., VEJLSTRUP, N., KELBAEK, H., BOTKER, H. E., KIM, W. Y., MATHIASEN, A. B., JORGENSEN, E., HELQVIST, S., SAUNAMAKI, K., CLEMMENSEN, P., HOLMVANG, L., THUESEN, L., KRUSELL, L. R., JENSEN, J. S., KOBER, L., TREIMAN, M., HOLST, J. J. & ENGSTROM, T. 2012. Exenatide reduces reperfusion

injury in patients with ST-segment elevation myocardial infarction. Eur Heart J, 33, 1491-9.

LOOK, A. T. 1997. Oncogenic transcription factors in the human acute leukemias. Science, 278, 1059-64.

LUND, G. K., STORK, A., MUELLERLEILE, K., BARMEYER, A. A., BANSMANN, M. P., KNEFEL, M., SCHLICHTING, U., MULLER, M., VERDE, P. E., ADAM, G., MEINERTZ, T. & SAEED, M. 2007. Prediction of left ventricular remodeling and analysis of infarct resorption in patients with reperfused myocardial infarcts by using contrast-enhanced MR imaging. Radiology, 245, 95-102.

LUO, A. K. & WU, K. C. 2006. Imaging microvascular obstruction and its clinical significance following acute myocardial infarction. Heart Fail Rev, 11, 305-12.

LUO, M. & ANDERSON, M. E. 2013. Mechanisms of altered Ca(2)(+) handling in heart failure. Circ Res, 113, 690-708.

LUTGENS, S. P., CLEUTJENS, K. B., DAEMEN, M. J. & HEENEMAN, S. 2007. Cathepsin cysteine proteases in cardiovascular disease. FASEB J, 21, 3029-41.

LV, B. J., LINDHOLT, J. S., WANG, J., CHENG, X. & SHI, G. P. 2013. Plasma levels of cathepsins L, K, and V and risks of abdominal aortic aneurysms: a randomized population-based study. Atherosclerosis, 230, 100-5.

MACHACKOVA, J., BARTA, J. & DHALLA, N. S. 2006. Myofibrillar remodeling in cardiac hypertrophy, heart failure and cardiomyopathies. Can J Cardiol, 22, 953-68.

MACIEWICZ, R. A. & ETHERINGTON, D. J. 1988. A comparison of four cathepsins (B, L, N and S) with collagenolytic activity from rabbit spleen. Biochem J, 256, 433-40.

MALKUSCH, W., REHN, B. & BRUCH, J. 1995. Advantages of Sirius Red staining for quantitative morphometric collagen measurements in lungs. Exp Lung Res, 21, 67-77.

MANN, D. L. 1999. Mechanisms and models in heart failure: A combinatorial approach. Circulation, 100, 999-1008.

MANN, D. L. & TAEGTMEYER, H. 2001. Dynamic regulation of the extracellular matrix after mechanical unloading of the failing human heart: recovering the missing link in left ventricular remodeling. Circulation, 104, 1089-91.

MASTERS, S. L., DUNNE, A., SUBRAMANIAN, S. L., HULL, R. L., TANNAHILL, G. M., SHARP, F. A., BECKER, C., FRANCHI, L., YOSHIHARA, E., CHEN, Z., MULLOOLY, N., MIELKE, L. A., HARRIS, J., COLL, R. C., MILLS, K. H., MOK, K. H., NEWSHOLME, P., NUNEZ, G., YODOI, J., KAHN, S. E., LAVELLE, E. C. & O'NEILL, L. A. 2010. Activation of the NLRP3 inflammasome by islet amyloid polypeptide provides a mechanism for enhanced IL-1beta in type 2 diabetes. Nat Immunol, 11, 897-904.

MASTERS, S. L., LATZ, E. & O'NEILL, L. A. 2011. The inflammasome in atherosclerosis and type 2 diabetes. Sci Transl Med, 3, 81ps17.

MATARRESE, P., ASCIONE, B., CIARLO, L., VONA, R., LEONETTI, C., SCARSELLA, M., MILEO, A. M., CATRICALA, C., PAGGI, M. G. & MALORNI, W. 2010. Cathepsin B inhibition interferes with metastatic potential of human melanoma: an in vitro and in vivo study. Mol Cancer, 9, 207.

MATSUI, Y., TAKAGI, H., QU, X., ABDELLATIF, M., SAKODA, H., ASANO, T., LEVINE, B. & SADOSHIMA, J. 2007. Distinct roles of autophagy in the heart during ischemia and reperfusion: roles of AMP-activated protein kinase and Beclin 1 in mediating autophagy. Circ Res, 100, 914-22.

MATTSON, A. M., JENSEN, C. O. & DUTCHER, R. A. 1947. Triphenyltetrazolium Chloride as a Dye for Vital Tissues. Science, 106, 294-5.

MCCORMICK, J., KNIGHT, R. A., BARRY, S. P., SCARABELLI, T. M., ABOUNIT, K., LATCHMAN, D. S. & STEPHANOU, A. 2012. Autophagy in the stress-induced myocardium. Front Biosci (Elite Ed), 4, 2131-41.

MCMANUS, D. D., GORE, J., YARZEBSKI, J., SPENCER, F., LESSARD, D. & GOLDBERG, R. J. 2011. Recent trends in the incidence, treatment, and outcomes of patients with STEMI and NSTEMI. Am J Med, 124, 40-7.

MCMURRAY, J. J., ADAMOPOULOS, S., ANKER, S. D., AURICCHIO, A., BOHM, M., DICKSTEIN, K., FALK, V., FILIPPATOS, G., FONSECA, C., GOMEZ-SANCHEZ, M. A., JAARSMA, T., KOBER, L., LIP, G. Y., MAGGIONI, A. P., PARKHOMENKO, A., PIESKE, B. M., POPESCU, B. A., RONNEVIK, P. K., RUTTEN, F. H., SCHWITTER, J., SEFEROVIC, P., STEPINSKA, J., TRINDADE, P. T., VOORS, A. A., ZANNAD, F., ZEIHER, A., TASK FORCE FOR THE, D., TREATMENT OF, A., CHRONIC HEART FAILURE OF THE EUROPEAN SOCIETY OF, C., BAX, J. J., BAUMGARTNER, H., CECONI, C., DEAN, V., DEATON, C., FAGARD, R., FUNCK-BRENTANO, C., HASDAI, D., HOES, A., KIRCHHOF, P., KNUUTI, J., KOLH, P., MCDONAGH, T., MOULIN, C., POPESCU, B. A., REINER, Z., SECHTEM, U., SIRNES, P. A., TENDERA, M., TORBICKI, A., VAHANIAN, A., WINDECKER, S., MCDONAGH, T., SECHTEM, U., BONET, L. A., AVRAAMIDES, P., BEN LAMIN, H. A., BRIGNOLE, M., COCA, A., COWBURN, P., DARGIE, H., ELLIOTT, P., FLACHSKAMPF, F. A., GUIDA, G. F., HARDMAN, S., IUNG, B., MERKELY, B., MUELLER, C., NANAS, J. N., NIELSEN, O. W., ORN, S., PARISSIS, J. T., PONIKOWSKI, P. & GUIDELINES, E. S. C. C. F. P. 2012. ESC guidelines for the diagnosis and treatment of acute and chronic heart failure 2012: The Task Force for the Diagnosis and Treatment of Acute and Chronic Heart Failure 2012 of the European Society of Cardiology. Developed in collaboration with the Heart Failure Association (HFA) of the ESC. Eur J Heart Fail, 14, 803-69.

MEDVINSKY, A. & DZIERZAK, E. 1996. Definitive hematopoiesis is autonomously initiated by the AGM region. Cell, 86, 897-906.

MEDVINSKY, A. L., SAMOYLINA, N. L., MULLER, A. M. & DZIERZAK, E. A. 1993. An early pre-liver intraembryonic source of CFU-S in the developing mouse. Nature, 364, 64-7.

MENDIS, S., DAVIS, S. & NORRVING, B. 2015. Organizational update: the world health organization global status report on noncommunicable diseases 2014; one more landmark step in the combat against stroke and vascular disease. Stroke, 46, e121-2.

MEYERS, S., DOWNING, J. R. & HIEBERT, S. W. 1993. Identification of AML-1 and the (8;21) translocation protein (AML-1/ETO) as sequence-specific DNA-binding proteins: the runt homology domain is required for DNA binding and protein-protein interactions. Mol Cell Biol, 13, 6336-45.

MICHAEL, L. H., ENTMAN, M. L., HARTLEY, C. J., YOUKER, K. A., ZHU, J., HALL, S. R., HAWKINS, H. K., BERENS, K. & BALLANTYNE, C. M. 1995. Myocardial ischemia and reperfusion: a murine model. Am J Physiol, 269, H2147-54.

MICHAUD, J., WU, F., OSATO, M., COTTLES, G. M., YANAGIDA, M., ASOU, N., SHIGESADA, K., ITO, Y., BENSON, K. F., RASKIND, W. H., ROSSIER, C., ANTONARAKIS, S. E., ISRAELS, S., MCNICOL, A., WEISS, H., HORWITZ, M. & SCOTT, H. S. 2002. In vitro analyses of known and novel RUNX1/AML1 mutations in dominant familial platelet disorder with predisposition to acute myelogenous leukemia: implications for mechanisms of pathogenesis. Blood, 99, 1364-72.

MIKHAIL, F. M., SERRY, K. A., HATEM, N., MOURAD, Z. I., FARAWELA, H. M., EL KAFFASH, D. M., COIGNET, L. & NUCIFORA, G. 2002. A new translocation that rearranges the AML1 gene in a patient with T-cell acute lymphoblastic leukemia. Cancer Genet Cytogenet, 135, 96-100.

MILLER, J. A. & MILLER, F. S. 1972. Mechanisms of hypothermic protection against anoxia. Adv Exp Med Biol, 33, 571-86.

MILLEST, A. J., BREEN, S. A., LOVEDAY, B. E., CLARKSON, P. N., SIMPSON, C. A., WATERTON, J. C. & JOHNSTONE, D. 1997. Effects of an inhibitor of cathepsin L on bone resorption in thyroparathyroidectomized and ovariectomized rats. Bone, 20, 465-71.

MINAMINO, T., GAUSSIN, V., DEMAYO, F. J. & SCHNEIDER, M. D. 2001. Inducible gene targeting in postnatal myocardium by cardiac-specific expression of a hormone-activated Cre fusion protein. Circ Res, 88, 587-92.

MINHAZ, U., KOIDE, S., SHOHTSU, A., FUJISHIMA, M. & NAKAZAWA, H. 1995. Perfusion delay causes unintentional ischemic preconditioning in isolated heart preparation. Basic Res Cardiol, 90, 418-23.

MINICUCCI, M. F., AZEVEDO, P. S., POLEGATO, B. F., PAIVA, S. A. & ZORNOFF, L. A. 2011. Heart failure after myocardial infarction: clinical implications and treatment. Clin Cardiol, 34, 410-4.

MIYAMAE, M., CAMACHO, S. A., WEINER, M. W. & FIGUEREDO, V. M. 1996. Attenuation of postischemic reperfusion injury is related to prevention of [Ca2+]m overload in rat hearts. Am J Physiol, 271, H2145-53.

MIYATA, S., MINOBE, W., BRISTOW, M. R. & LEINWAND, L. A. 2000. Myosin heavy chain isoform expression in the failing and nonfailing human heart. Circ Res, 86, 386-90.

MIYOSHI, H., OHIRA, M., SHIMIZU, K., MITANI, K., HIRAI, H., IMAI, T., YOKOYAMA, K., SOEDA, E. & OHKI, M. 1995. Alternative splicing and genomic structure of the AML1 gene involved in acute myeloid leukemia. Nucleic Acids Res, 23, 2762-9.

MIYOSHI, H., SHIMIZU, K., KOZU, T., MASEKI, N., KANEKO, Y. & OHKI, M. 1991. t(8;21) breakpoints on chromosome 21 in acute myeloid leukemia are clustered within a limited region of a single gene, AML1. Proc Natl Acad Sci U S A, 88, 10431-4.

MIZUOCHI, T., YEE, S. T., KASAI, M., KAKIUCHI, T., MUNO, D. & KOMINAMI, E. 1994. Both cathepsin B and cathepsin D are necessary for processing of ovalbumin as well as for degradation of class II MHC invariant chain. Immunol Lett, 43, 189-93.

MOGA, M. A., NAKAMURA, T. & ROBBINS, J. 2008. Genetic approaches for changing the heart and dissecting complex syndromes. J Mol Cell Cardiol, 45, 148-55.

MOHAMED, M. M. & SLOANE, B. F. 2006. Cysteine cathepsins: multifunctional enzymes in cancer. Nat Rev Cancer, 6, 764-75.

MOLKENTIN, J. D. & ROBBINS, J. 2009. With great power comes great responsibility: using mouse genetics to study cardiac hypertrophy and failure. J Mol Cell Cardiol, 46, 130-6.

MONASSIER, L., AYME-DIETRICH, E., AUBERTIN-KIRCH, G. & PATHAK, A. 2016. Targeting myocardial reperfusion injuries with cyclosporine in the CIRCUS Trial - pharmacological reasons for failure. Fundam Clin Pharmacol, 30, 191-3.

MORGAN, J. P., ERNY, R. E., ALLEN, P. D., GROSSMAN, W. & GWATHMEY, J. K. 1990. Abnormal intracellular calcium handling, a major cause of systolic and diastolic dysfunction in ventricular myocardium from patients with heart failure. Circulation, 81, III21-32.

MUNTENER, K., ZWICKY, R., CSUCS, G., ROHRER, J. & BAICI, A. 2004. Exon skipping of cathepsin B: mitochondrial targeting of a lysosomal peptidase provokes cell death. J Biol Chem, 279, 41012-7.

MURATANI, M. & TANSEY, W. P. 2003. How the ubiquitin-proteasome system controls transcription. Nat Rev Mol Cell Biol, 4, 192-201.

MURRY, C. E., JENNINGS, R. B. & REIMER, K. A. 1986. Preconditioning with ischemia: a delay of lethal cell injury in ischemic myocardium. Circulation, 74, 1124-36.

MUSIL, D., ZUCIC, D., TURK, D., ENGH, R. A., MAYR, I., HUBER, R., POPOVIC, T., TURK, V., TOWATARI, T., KATUNUMA, N. & ET AL. 1991. The refined 2.15 A X-ray crystal structure of human liver cathepsin B: the structural basis for its specificity. EMBO J, 10, 2321-30.

NAGATA, T., GUPTA, V., SORCE, D., KIM, W. Y., SALI, A., CHAIT, B. T., SHIGESADA, K., ITO, Y. & WERNER, M. H. 1999. Immunoglobulin motif DNA recognition and heterodimerization of the PEBP2/CBF Runt domain. Nat Struct Biol, 6, 615-9.

NASEEM, R. H., HEDEGARD, W., HENRY, T. D., LESSARD, J., SUTTER, K. & KATZ, S. A. 2005. Plasma cathepsin D isoforms and their active metabolites increase after myocardial infarction and contribute to plasma renin activity. Basic Res Cardiol, 100, 139-46.

NEILL, W. A. 1968. Myocardial hypoxia and anerobic metabolism in coronary heart disease. Am J Cardiol, 22, 507-15.

NEURATH, H. 1984. Evolution of proteolytic enzymes. Science, 224, 350-7.

NG, C. E., YOKOMIZO, T., YAMASHITA, N., CIROVIC, B., JIN, H., WEN, Z., ITO, Y. & OSATO, M. 2010. A Runx1 intronic enhancer marks hemogenic endothelial cells and hematopoietic stem cells. Stem Cells, 28, 1869-81.

NG, W. A., GRUPP, I. L., SUBRAMANIAM, A. & ROBBINS, J. 1991. Cardiac myosin heavy chain mRNA expression and myocardial function in the mouse heart. Circ Res, 68, 1742-50.

NIENHUIS, M. B., OTTERVANGER, J. P., DE BOER, M. J., DAMBRINK, J. H., HOORNTJE, J. C., GOSSELINK, A. T., SURYAPRANATA, H., VAN'T HOF, A. W. & ZWOLLE MYOCARDIAL INFARCTION STUDY, G. 2008. Prognostic importance of creatine kinase and creatine kinase-MB after primary percutaneous coronary intervention for ST-elevation myocardial infarction. Am Heart J, 155, 673-9.

NISHIMURA, Y., KAWABATA, T. & KATO, K. 1988. Identification of latent procathepsins B and L in microsomal lumen: characterization of enzymatic activation and proteolytic processing in vitro. Arch Biochem Biophys, 261, 64-71.

NISHIMURA, Y., KAWABATA, T., YANO, S. & KATO, K. 1990. Inhibition of intracellular sorting and processing of lysosomal cathepsins H and L at reduced

temperature in primary cultures of rat hepatocytes. Arch Biochem Biophys, 283, 458-63.

NORTH, T., GU, T. L., STACY, T., WANG, Q., HOWARD, L., BINDER, M., MARIN-PADILLA, M. & SPECK, N. A. 1999. Cbfa2 is required for the formation of intra-aortic hematopoietic clusters. Development, 126, 2563-75.

NOTTINGHAM, W. T., JARRATT, A., BURGESS, M., SPECK, C. L., CHENG, J. F., PRABHAKAR, S., RUBIN, E. M., LI, P. S., SLOANE-STANLEY, J., KONG, A. S. J. & DE BRUIJN, M. F. 2007. Runx1-mediated hematopoietic stem-cell emergence is controlled by a Gata/Ets/SCL-regulated enhancer. Blood, 110, 4188-97.

NOVINEC, M., GRASS, R. N., STARK, W. J., TURK, V., BAICI, A. & LENARCIC, B. 2007. Interaction between human cathepsins K, L, and S and elastins: mechanism of elastinolysis and inhibition by macromolecular inhibitors. J Biol Chem, 282, 7893-902.

NUCHPRAYOON, I., MEYERS, S., SCOTT, L. M., SUZOW, J., HIEBERT, S. & FRIEDMAN, A. D. 1994. PEBP2/CBF, the murine homolog of the human myeloid AML1 and PEBP2 beta/CBF beta proto-oncoproteins, regulates the murine myeloperoxidase and neutrophil elastase genes in immature myeloid cells. Mol Cell Biol, 14, 5558-68.

NUCIFORA, G., BEGY, C. R., KOBAYASHI, H., ROULSTON, D., CLAXTON, D., PEDERSEN-BJERGAARD, J., PARGANAS, E., IHLE, J. N. & ROWLEY, J. D. 1994. Consistent intergenic splicing and production of multiple transcripts between AML1 at 21q22 and unrelated genes at 3q26 in (3;21)(q26;q22) translocations. Proc Natl Acad Sci U S A, 91, 4004-8.

O'NEILL, W. W., MARTIN, J. L., DIXON, S. R., BARTORELLI, A. L., TRABATTONI, D., OEMRAWSINGH, P. V., ATSMA, D. E., CHANG, M., MARQUARDT, W., OH, J. K., KRUCOFF, M. W., GIBBONS, R. J., SPEARS, J. R. & INVESTIGATORS, A. 2007. Acute Myocardial Infarction with Hyperoxemic Therapy (AMIHOT): a prospective,

randomized trial of intracoronary hyperoxemic reperfusion after percutaneous coronary intervention. J Am Coll Cardiol, 50, 397-405.

OGAWA, E., MARUYAMA, M., KAGOSHIMA, H., INUZUKA, M., LU, J., SATAKE, M., SHIGESADA, K. & ITO, Y. 1993. PEBP2/PEA2 represents a family of transcription factors homologous to the products of the Drosophila runt gene and the human AML1 gene. Proc Natl Acad Sci U S A, 90, 6859-63.

OGIHARA, H., KANNO, T., MORII, E., KIM, D. K., LEE, Y. M., SATO, M., KIM, W. Y., NOMURA, S., ITO, Y. & KITAMURA, Y. 1999. Synergy of PEBP2/CBF with mi transcription factor (MITF) for transactivation of mouse mast cell protease 6 gene. Oncogene, 18, 4632-9.

OKUDA, T., NISHIMURA, M., NAKAO, M. & FUJITA, Y. 2001. RUNX1/AML1: a central player in hematopoiesis. Int J Hematol, 74, 252-7.

OKUDA, T., VAN DEURSEN, J., HIEBERT, S. W., GROSVELD, G. & DOWNING, J. R. 1996. AML1, the target of multiple chromosomal translocations in human leukemia, is essential for normal fetal liver hematopoiesis. Cell, 84, 321-30.

OLDERS, J., TUREK, Z., EVERS, J., HOOFD, L., OESEBURG, B. & KREUZER, F. 1990. Comparison of Tyrode and blood perfused working isolated rat hearts. Adv Exp Med Biol, 277, 403-13.

OORNI, K., SNECK, M., BROMME, D., PENTIKAINEN, M. O., LINDSTEDT, K. A., MAYRANPAA, M., AITIO, H. & KOVANEN, P. T. 2004. Cysteine protease cathepsin F is expressed in human atherosclerotic lesions, is secreted by cultured macrophages, and modifies low density lipoprotein particles in vitro. Journal of Biological Chemistry, 279, 34776-34784.

OPIE, L. H. 1990. Myocardial ischemia--metabolic pathways and implications of increased glycolysis. Cardiovasc Drugs Ther, 4 Suppl 4, 777-90.

OPIE, L. H., COMMERFORD, P. J., GERSH, B. J. & PFEFFER, M. A. 2006. Controversies in ventricular remodelling. Lancet, 367, 356-67.

OROGO, A. M. & GUSTAFSSON, A. B. 2013. Cell death in the myocardium: my heart won't go on. IUBMB Life, 65, 651-6.

OSATO, M., ASOU, N., ABDALLA, E., HOSHINO, K., YAMASAKI, H., OKUBO, T., SUZUSHIMA, H., TAKATSUKI, K., KANNO, T., SHIGESADA, K. & ITO, Y. 1999. Biallelic and heterozygous point mutations in the runt domain of the AML1/PEBP2alphaB gene associated with myeloblastic leukemias. Blood, 93, 1817-24.

PALIS, J., ROBERTSON, S., KENNEDY, M., WALL, C. & KELLER, G. 1999. Development of erythroid and myeloid progenitors in the yolk sac and embryo proper of the mouse. Development, 126, 5073-84.

PASSMAN, R. S. & FISHMAN, G. I. 1994. Regulated expression of foreign genes in vivo after germline transfer. J Clin Invest, 94, 2421-5.

PATTEN, R. D. & HALL-PORTER, M. R. 2009. Small animal models of heart failure: development of novel therapies, past and present. Circ Heart Fail, 2, 138-44.

PETERMANN, I., MAYER, C., STYPMANN, J., BINIOSSEK, M. L., TOBIN, D. J., ENGELEN, M. A., DANDEKAR, T., GRUNE, T., SCHILD, L., PETERS, C. & REINHECKEL, T. 2006. Lysosomal, cytoskeletal, and metabolic alterations in cardiomyopathy of cathepsin L knockout mice. FASEB J, 20, 1266-8.

PETERSON, L. F. & ZHANG, D. E. 2004. The 8;21 translocation in leukemogenesis. Oncogene, 23, 4255-62.

PETRERA, A., GASSENHUBER, J., RUF, S., GUNASEKARAN, D., ESSER, J., SHAHINIAN, J. H., HUBSCHLE, T., RUTTEN, H., SADOWSKI, T. & SCHILLING, O. 2016. Cathepsin A inhibition attenuates myocardial infarction-induced heart failure on the functional and proteomic levels. J Transl Med, 14, 153.

PETROVICK, M. S., HIEBERT, S. W., FRIEDMAN, A. D., HETHERINGTON, C. J., TENEN, D. G. & ZHANG, D. E. 1998. Multiple functional domains of AML1: PU.1 and C/EBPalpha synergize with different regions of AML1. Mol Cell Biol, 18, 3915-25.

PFEFFER, M. A. & BRAUNWALD, E. 1990. Ventricular remodeling after myocardial infarction. Experimental observations and clinical implications. Circulation, 81, 1161-72.

PIACENTINO, V., 3RD, WEBER, C. R., CHEN, X., WEISSER-THOMAS, J., MARGULIES, K. B., BERS, D. M. & HOUSER, S. R. 2003. Cellular basis of abnormal calcium transients of failing human ventricular myocytes. Circ Res, 92, 651-8.

PIPER, H. M., ABDALLAH, Y. & SCHAFER, C. 2004. The first minutes of reperfusion: a window of opportunity for cardioprotection. Cardiovasc Res, 61, 365-71.

PIPER, H. M., GARCIA-DORADO, D. & OVIZE, M. 1998. A fresh look at reperfusion injury. Cardiovascular Research, 38, 291-300.

PIPER, H. M., MEUTER, K. & SCHAFER, C. 2003. Cellular mechanisms of ischemia-reperfusion injury. Ann Thorac Surg, 75, S644-8.

PITTS, K. R., STIKO, A., BUETOW, B., LOTT, F., GUO, P., VIRCA, D. & TOOMBS, C. F. 2007. Washout of heme-containing proteins dramatically improves tetrazolium-based infarct staining. J Pharmacol Toxicol Methods, 55, 201-8.

PRZYKLENK, K., BAUER, B., OVIZE, M., KLONER, R. A. & WHITTAKER, P. 1993. Regional ischemic 'preconditioning' protects remote virgin myocardium from subsequent sustained coronary occlusion. Circulation, 87, 893-9.

PRZYKLENK, K., UNDYALA, V. V., WIDER, J., SALA-MERCADO, J. A., GOTTLIEB, R. A. & MENTZER, R. M., JR. 2011. Acute induction of autophagy as a novel strategy for cardioprotection: getting to the heart of the matter. Autophagy, 7, 432-3.

PUIG-KROGER, A., LOPEZ-RODRIGUEZ, C., RELLOSO, M., SANCHEZ-ELSNER, T., NUEDA, A., MUNOZ, E., BERNABEU, C. & CORBI, A. L. 2000. Polyomavirus

enhancer-binding protein 2/core binding factor/acute myeloid leukemia factors contribute to the cell type-specific activity of the CD11a integrin gene promoter. J Biol Chem, 275, 28507-12.

RABKIN, E., AIKAWA, M., STONE, J. R., FUKUMOTO, Y., LIBBY, P. & SCHOEN, F. J. 2001. Activated interstitial myofibroblasts express catabolic enzymes and mediate matrix remodeling in myxomatous heart valves. Circulation, 104, 2525-32.

RAKOWSKI, T., DZIEWIERZ, A., LEGUTKO, J., KLECZYNSKI, P., BRZOZOWSKA-CZARNEK, A., SIUDAK, Z., URBANIK, A., DUBIEL, J. S. & DUDEK, D. 2014. Creatine kinase-MB assessed in patients with acute myocardial infarction correlates with cardiac magnetic resonance infarct size at 6-month follow up. Hellenic J Cardiol, 55, 4-8.

REIMER, K. A. & JENNINGS, R. B. 1979. The "wavefront phenomenon" of myocardial ischemic cell death. II. Transmural progression of necrosis within the framework of ischemic bed size (myocardium at risk) and collateral flow. Lab Invest, 40, 633-44.

REIMER, K. A., LOWE, J. E., RASMUSSEN, M. M. & JENNINGS, R. B. 1977. The wavefront phenomenon of ischemic cell death. 1. Myocardial infarct size vs duration of coronary occlusion in dogs. Circulation, 56, 786-94.

REINHECKEL, T., HAGEMANN, S., DOLLWET-MACK, S., MARTINEZ, E., LOHMULLER, T., ZLATKOVIC, G., TOBIN, D. J., MAAS-SZABOWSKI, N. & PETERS, C. 2005. The lysosomal cysteine protease cathepsin L regulates keratinocyte proliferation by control of growth factor recycling. J Cell Sci, 118, 3387-95.

REISER, J., ADAIR, B. & REINHECKEL, T. 2010. Specialized roles for cysteine cathepsins in health and disease. J Clin Invest, 120, 3421-31.

RICHARDSON, C. A. & FLECKNELL, P. A. 2005. Anaesthesia and post-operative analgesia following experimental surgery in laboratory rodents: are we making progress? Altern Lab Anim, 33, 119-27.

RINGER, S. 1882a. Concerning the Influence exerted by each of the Constituents of the Blood on the Contraction of the Ventricle. J Physiol, 3, 380-93.

RINGER, S. 1882b. Regarding the Action of Hydrate of Soda, Hydrate of Ammonia, and Hydrate of Potash on the Ventricle of the Frog's Heart. J Physiol, 3, 195-202 6.

RINGER, S. 1883a. A further Contribution regarding the influence of the different Constituents of the Blood on the Contraction of the Heart. J Physiol, 4, 29-42 3.

RINGER, S. 1883b. A third contribution regarding the Influence of the Inorganic Constituents of the Blood on the Ventricular Contraction. J Physiol, 4, 222-5.

RIVA, E. & HEARSE, D. J. 1991. Isolated, perfused neonatal rat heart preparation for studies of calcium and functional stability. Ann Thorac Surg, 52, 987-92.

ROGER, V. L. 2013. Epidemiology of heart failure. Circ Res, 113, 646-59.

ROTH, D. M., SWANEY, J. S., DALTON, N. D., GILPIN, E. A. & ROSS, J., JR. 2002. Impact of anesthesia on cardiac function during echocardiography in mice. Am J Physiol Heart Circ Physiol, 282, H2134-40.

ROTH, W., DEUSSING, J., BOTCHKAREV, V. A., PAULY-EVERS, M., SAFTIG, P., HAFNER, A., SCHMIDT, P., SCHMAHL, W., SCHERER, J., ANTON-LAMPRECHT, I., VON FIGURA, K., PAUS, R. & PETERS, C. 2000. Cathepsin L deficiency as molecular defect of furless: hyperproliferation of keratinocytes and pertubation of hair follicle cycling. FASEB J, 14, 2075-86.

ROTTMAN, J. N., NI, G. & BROWN, M. 2007. Echocardiographic evaluation of ventricular function in mice. Echocardiography, 24, 83-9.

ROULEAU, J. L., DE CHAMPLAIN, J., KLEIN, M., BICHET, D., MOYE, L., PACKER, M., DAGENAIS, G. R., SUSSEX, B., ARNOLD, J. M., SESTIER, F. & ET AL. 1993. Activation of neurohumoral systems in postinfarction left ventricular dysfunction. J Am Coll Cardiol, 22, 390-8.

ROWAN, A. D., MASON, P., MACH, L. & MORT, J. S. 1992. Rat procathepsin B. Proteolytic processing to the mature form in vitro. J Biol Chem, 267, 15993-9.

RUBIN, C. M., LARSON, R. A., ANASTASI, J., WINTER, J. N., THANGAVELU, M., VARDIMAN, J. W., ROWLEY, J. D. & LE BEAU, M. M. 1990. t(3;21)(q26;q22): a recurring chromosomal abnormality in therapy-related myelodysplastic syndrome and acute myeloid leukemia. Blood, 76, 2594-8.

RUBIN, C. M., LARSON, R. A., BITTER, M. A., CARRINO, J. J., LE BEAU, M. M., DIAZ, M. O. & ROWLEY, J. D. 1987. Association of a chromosomal 3;21 translocation with the blast phase of chronic myelogenous leukemia. Blood, 70, 1338-42.

RUDRA, D., EGAWA, T., CHONG, M. M., TREUTING, P., LITTMAN, D. R. & RUDENSKY, A. Y. 2009. Runx-CBFbeta complexes control expression of the transcription factor Foxp3 in regulatory T cells. Nat Immunol, 10, 1170-7.

SADOSHIMA, J. & IZUMO, S. 1993. Molecular characterization of angiotensin II--induced hypertrophy of cardiac myocytes and hyperplasia of cardiac fibroblasts. Critical role of the AT1 receptor subtype. Circ Res, 73, 413-23.

SADOSHIMA, J., QIU, Z., MORGAN, J. P. & IZUMO, S. 1995. Angiotensin II and other hypertrophic stimuli mediated by G protein-coupled receptors activate tyrosine kinase, mitogen-activated protein kinase, and 90-kD S6 kinase in cardiac myocytes. The critical role of Ca(2+)-dependent signaling. Circ Res, 76, 1-15.

SAEGUSA, K., ISHIMARU, N., YANAGI, K., ARAKAKI, R., OGAWA, K., SAITO, I., KATUNUMA, N. & HAYASHI, Y. 2002. Cathepsin S inhibitor prevents autoantigen presentation and autoimmunity. J Clin Invest, 110, 361-9.

SALA-MERCADO, J. A., WIDER, J., UNDYALA, V. V., JAHANIA, S., YOO, W., MENTZER, R. M., JR., GOTTLIEB, R. A. & PRZYKLENK, K. 2010. Profound cardioprotection with chloramphenicol succinate in the swine model of myocardial ischemia-reperfusion injury. Circulation, 122, S179-84.

SANBE, A., GULICK, J., HANKS, M. C., LIANG, Q., OSINSKA, H. & ROBBINS, J. 2003. Reengineering inducible cardiac-specific transgenesis with an attenuated myosin heavy chain promoter. Circ Res, 92, 609-16.

SASAKI, T., KUZUYA, M., NAKAMURA, K., CHENG, X. W., HAYASHI, T., SONG, H., HU, L., OKUMURA, K., MUROHARA, T., IGUCHI, A. & SATO, K. 2010. AT1 blockade attenuates atherosclerotic plaque destabilization accompanied by the suppression of cathepsin S activity in apoE-deficient mice. Atherosclerosis, 210, 430-7.

SATOH, Y., MATSUMURA, I., TANAKA, H., EZOE, S., FUKUSHIMA, K., TOKUNAGA, M., YASUMI, M., SHIBAYAMA, H., MIZUKI, M., ERA, T., OKUDA, T. & KANAKURA, Y. 2008. AML1/RUNX1 works as a negative regulator of c-Mpl in hematopoietic stem cells. J Biol Chem, 283, 30045-56.

SCANLON, P. J., FAXON, D. P., AUDET, A. M., CARABELLO, B., DEHMER, G. J., EAGLE, K. A., LEGAKO, R. D., LEON, D. F., MURRAY, J. A., NISSEN, S. E., PEPINE, C. J., WATSON, R. M., RITCHIE, J. L., GIBBONS, R. J., CHEITLIN, M. D., GARDNER, T. J., GARSON, A., JR., RUSSELL, R. O., JR., RYAN, T. J. & SMITH, S. C., JR. 1999. ACC/AHA guidelines for coronary angiography: executive summary and recommendations. A report of the American College of Cardiology/American Heart Association Task Force on Practice Guidelines (Committee on Coronary Angiography) developed in collaboration with the Society for Cardiac Angiography and Interventions. Circulation, 99, 2345-57.

SCHENKE-LAYLAND, K., STOCK, U. A., NSAIR, A., XIE, J., ANGELIS, E., FONSECA, C. G., LARBIG, R., MAHAJAN, A., SHIVKUMAR, K., FISHBEIN, M. C. & MACLELLAN, W. R. 2009. Cardiomyopathy is associated with structural remodelling of heart valve extracellular matrix. Eur Heart J, 30, 2254-65.

SCHLUTER, K. D., JAKOB, G., RUIZ-MEANA, M., GARCIA-DORADO, D. & PIPER, H. M. 1996. Protection of reoxygenated cardiomyocytes against osmotic fragility by nitric oxide donors. Am J Physiol, 271, H428-34.

SCHOMIG, A., MEHILLI, J., ANTONIUCCI, D., NDREPEPA, G., MARKWARDT, C., DI PEDE, F., NEKOLLA, S. G., SCHLOTTERBECK, K., SCHUHLEN, H., PACHE, J., SEYFARTH, M., MARTINOFF, S., BENZER, W., SCHMITT, C., DIRSCHINGER, J., SCHWAIGER, M., KASTRATI, A. & BEYOND 12 HOURS REPERFUSION ALTERNATIVE EVALUATION TRIAL, I. 2005. Mechanical reperfusion in patients with acute myocardial infarction presenting more than 12 hours from symptom onset: a randomized controlled trial. JAMA, 293, 2865-72.

SCHUIJF, J. D., SHAW, L. J., WIJNS, W., LAMB, H. J., POLDERMANS, D., DE ROOS, A., VAN DER WALL, E. E. & BAX, J. J. 2005. Cardiac imaging in coronary artery disease: differing modalities. Heart, 91, 1110-7.

SCHURIGT, U., SEVENICH, L., VANNIER, C., GAJDA, M., SCHWINDE, A., WERNER, F., STAHL, A., VON ELVERFELDT, D., BECKER, A. K., BOGYO, M., PETERS, C. & REINHECKEL, T. 2008. Trial of the cysteine cathepsin inhibitor JPM-OEt on early and advanced mammary cancer stages in the MMTV-PyMT-transgenic mouse model. Biol Chem, 389, 1067-74.

SCHWARZ, E. R., SOMOANO, Y., HALE, S. L. & KLONER, R. A. 2000. What is the required reperfusion period for assessment of myocardial infarct size using triphenyltetrazolium chloride staining in the rat? J Thromb Thrombolysis, 10, 181-7.

SCIMIA, M. C., GUMPERT, A. M. & KOCH, W. J. 2014. Cardiovascular gene therapy for myocardial infarction. Expert Opin Biol Ther, 14, 183-95.

SETH, P., MAHAJAN, V. S. & CHAUHAN, S. S. 2003. Transcription of human cathepsin L mRNA species hCATL B from a novel alternative promoter in the first intron of its gene. Gene, 321, 83-91.

SEVER, S., ALTINTAS, M. M., NANKOE, S. R., MOLLER, C. C., KO, D., WEI, C., HENDERSON, J., DEL RE, E. C., HSING, L., ERICKSON, A., COHEN, C. D., KRETZLER, M., KERJASCHKI, D., RUDENSKY, A., NIKOLIC, B. & REISER, J. 2007. Proteolytic

processing of dynamin by cytoplasmic cathepsin L is a mechanism for proteinuric kidney disease. J Clin Invest, 117, 2095-104.

SHIMODA, N., FUKAZAWA, N., NONOMURA, K. & FAIRCHILD, R. L. 2007. Cathepsin G is required for sustained inflammation and tissue injury after reperfusion of ischemic kidneys. American Journal of Pathology, 170, 930-940.

SHIN, J., EDELBERG, J. E. & HONG, M. K. 2003. Vulnerable atherosclerotic plaque: clinical implications. Curr Vasc Pharmacol, 1, 183-204.

SHREE, T., OLSON, O. C., ELIE, B. T., KESTER, J. C., GARFALL, A. L., SIMPSON, K., BELL-MCGUINN, K. M., ZABOR, E. C., BROGI, E. & JOYCE, J. A. 2011. Macrophages and cathepsin proteases blunt chemotherapeutic response in breast cancer. Genes Dev, 25, 2465-79.

SINGH, K. K., YANAGAWA, B., QUAN, A., WANG, R., GARG, A., KHAN, R., PAN, Y., WHEATCROFT, M. D., LOVREN, F., TEOH, H. & VERMA, S. 2014a. Autophagy gene fingerprint in human ischemia and reperfusion. J Thorac Cardiovasc Surg, 147, 1065-1072 e1.

SINGH, N., DAS, P., GUPTA, S., SACHDEV, V., SRIVASATAVA, S., DATTA GUPTA, S., PANDEY, R. M., SAHNI, P., CHAUHAN, S. S. & SARAYA, A. 2014b. Plasma cathepsin L: a prognostic marker for pancreatic cancer. World J Gastroenterol, 20, 17532-40.

SKYSCHALLY, A., SCHULZ, R. & HEUSCH, G. 2010. Cyclosporine A at reperfusion reduces infarct size in pigs. Cardiovasc Drugs Ther, 24, 85-7.

SNIDER, P. & CONWAY, S. J. 2011. Probing human cardiovascular congenital disease using transgenic mouse models. Prog Mol Biol Transl Sci, 100, 83-110.

SOHAL, D. S., NGHIEM, M., CRACKOWER, M. A., WITT, S. A., KIMBALL, T. R., TYMITZ, K. M., PENNINGER, J. M. & MOLKENTIN, J. D. 2001. Temporally regulated

and tissue-specific gene manipulations in the adult and embryonic heart using a tamoxifen-inducible Cre protein. Circ Res, 89, 20-5.

SOL-CHURCH, K., PICERNO, G. N., STABLEY, D. L., FRENCK, J., XING, S., BERTENSHAW, G. P. & MASON, R. W. 2002. Evolution of placentally expressed cathepsins. Biochem Biophys Res Commun, 293, 23-9.

SOLOMON, S. D., SKALI, H., ANAVEKAR, N. S., BOURGOUN, M., BARVIK, S., GHALI, J. K., WARNICA, J. W., KHRAKOVSKAYA, M., ARNOLD, J. M., SCHWARTZ, Y., VELAZQUEZ, E. J., CALIFF, R. M., MCMURRAY, J. V. & PFEFFER, M. A. 2005. Changes in ventricular size and function in patients treated with valsartan, captopril, or both after myocardial infarction. Circulation, 111, 3411-9.

SOUDERS, C. A., BOWERS, S. L. & BAUDINO, T. A. 2009. Cardiac fibroblast: the renaissance cell. Circ Res, 105, 1164-76.

SPAULDING, C., HENRY, P., TEIGER, E., BEATT, K., BRAMUCCI, E., CARRIE, D., SLAMA, M. S., MERKELY, B., ERGLIS, A., MARGHERI, M., VARENNE, O., CEBRIAN, A., STOLL, H. P., SNEAD, D. B., BODE, C. & INVESTIGATORS, T. 2006. Sirolimus-eluting versus uncoated stents in acute myocardial infarction. N Engl J Med, 355, 1093-104.

SPIRA, D., STYPMANN, J., TOBIN, D. J., PETERMANN, I., MAYER, C., HAGEMANN, S., VASILJEVA, O., G NTHER, T., SCH LE, R., PETERS, C. & REINHECKEL, T. 2007a. Cell type-specific functions of the lysosomal protease cathepsin L in the heart. J Biol Chem, 282, 37045-52.

SPIRA, D., STYPMANN, J., TOBIN, D. J., PETERMANN, I., MAYER, C., HAGEMANN, S., VASILJEVA, O., GUNTHER, T., SCHULE, R., PETERS, C. & REINHECKEL, T. 2007b. Cell type-specific functions of the lysosomal protease cathepsin L in the heart. J Biol Chem, 282, 37045-52.

STAAT, P., RIOUFOL, G., PIOT, C., COTTIN, Y., CUNG, T. T., L'HUILLIER, I., AUPETIT, J. F., BONNEFOY, E., FINET, G., ANDRE-FOUET, X. & OVIZE, M. 2005. Postconditioning the human heart. Circulation, 112, 2143-8.

STEG, P. G., JAMES, S. K., ATAR, D., BADANO, L. P., BLOMSTROM-LUNDQVIST, C., BORGER, M. A., DI MARIO, C., DICKSTEIN, K., DUCROCQ, G., FERNANDEZ-AVILES, F., GERSHLICK, A. H., GIANNUZZI, P., HALVORSEN, S., HUBER, K., JUNI, P., KASTRATI, A., KNUUTI, J., LENZEN, M. J., MAHAFFEY, K. W., VALGIMIGLI, M., VAN 'T HOF, A., WIDIMSKY, P. & ZAHGER, D. 2012. ESC Guidelines for the management of acute myocardial infarction in patients presenting with ST-segment elevation. Eur Heart J, 33, 2569-619.

STONE, G. W., GRINES, C. L., COX, D. A., GARCIA, E., TCHENG, J. E., GRIFFIN, J. J., GUAGLIUMI, G., STUCKEY, T., TURCO, M., CARROLL, J. D., RUTHERFORD, B. D., LANSKY, A. J., CONTROLLED, A. & DEVICE INVESTIGATION TO LOWER LATE ANGIOPLASTY COMPLICATIONS, I. 2002. Comparison of angioplasty with stenting, with or without abciximab, in acute myocardial infarction. N Engl J Med, 346, 957-66.

STYPMANN, J. 2007. Doppler ultrasound in mice. Echocardiography, 24, 97-112.

STYPMANN, J., GL SER, K., ROTH, W., TOBIN, D. J., PETERMANN, I., MATTHIAS, R., M NNIG, G., HAVERKAMP, W., BREITHARDT, G., SCHMAHL, W., PETERS, C. & REINHECKEL, T. 2002a. Dilated cardiomyopathy in mice deficient for the lysosomal cysteine peptidase cathepsin L. Proc Natl Acad Sci U S A, 99, 6234-9.

STYPMANN, J., GLASER, K., ROTH, W., TOBIN, D. J., PETERMANN, I., MATTHIAS, R., MONNIG, G., HAVERKAMP, W., BREITHARDT, G., SCHMAHL, W., PETERS, C. & REINHECKEL, T. 2002b. Dilated cardiomyopathy in mice deficient for the lysosomal cysteine peptidase cathepsin L. Proceedings of the National Academy of Sciences of the United States of America, 99, 6234-6239.

SUMERAY, M. S. & YELLON, D. M. 1998. Characterisation and validation of a murine model of global ischaemia-reperfusion injury. Mol Cell Biochem, 186, 61-8.

SUN, J., SUKHOVA, G. K., ZHANG, J., CHEN, H., SJOBERG, S., LIBBY, P., XIA, M., XIONG, N., GELB, B. D. & SHI, G. P. 2012a. Cathepsin K deficiency reduces elastase perfusion-induced abdominal aortic aneurysms in mice. Arterioscler Thromb Vasc Biol, 32, 15-23.

SUN, J. S., SUKHOVA, G. K., ZHANG, J., CHEN, H., SJOBERG, S., LIBBY, P., XIA, M. C., XIONG, N., GELB, B. D. & SHI, G. P. 2012b. Cathepsin K Deficiency Reduces Elastase Perfusion-Induced Abdominal Aortic Aneurysms in Mice. Arteriosclerosis Thrombosis and Vascular Biology, 32, 15-U68.

SUN, M., CHEN, M., LIU, Y., FUKUOKA, M., ZHOU, K., LI, G., DAWOOD, F., GRAMOLINI, A. & LIU, P. P. 2011. Cathepsin-L contributes to cardiac repair and remodelling post-infarction. Cardiovasc Res, 89, 374-83.

SUN, M., OUZOUNIAN, M., DE COUTO, G., CHEN, M., YAN, R., FUKUOKA, M., LI, G., MOON, M., LIU, Y., GRAMOLINI, A., WELLS, G. J. & LIU, P. P. 2013. Cathepsin-L ameliorates cardiac hypertrophy through activation of the autophagy-lysosomal dependent protein processing pathways. J Am Heart Assoc, 2, e000191.

SUN, W., GRAVES, B. J. & SPECK, N. A. 1995. Transactivation of the Moloney murine leukemia virus and T-cell receptor beta-chain enhancers by cbf and ets requires intact binding sites for both proteins. J Virol, 69, 4941-9.

SUN, Y. & WEBER, K. T. 2000. Infarct scar: a dynamic tissue. Cardiovasc Res, 46, 250-6.

SUNDELOF, J., SUNDSTROM, J., HANSSON, O., ERIKSDOTTER-JONHAGEN, M., GIEDRAITIS, V., LARSSON, A., DEGERMAN-GUNNARSSON, M., INGELSSON, M., MINTHON, L., BLENNOW, K., KILANDER, L., BASUN, H. & LANNFELT, L. 2010. Higher cathepsin B levels in plasma in Alzheimer's disease compared to healthy controls. J Alzheimers Dis, 22, 1223-30.

SUTHERLAND, F. J. & HEARSE, D. J. 2000. The isolated blood and perfusion fluid perfused heart. Pharmacol Res, 41, 613-27.

SUTHERLAND, F. J., SHATTOCK, M. J., BAKER, K. E. & HEARSE, D. J. 2003. Mouse isolated perfused heart: characteristics and cautions. Clin Exp Pharmacol Physiol, 30, 867-78.

SUTTON, M. G. & SHARPE, N. 2000. Left ventricular remodeling after myocardial infarction: pathophysiology and therapy. Circulation, 101, 2981-8.

TAHIROV, T. H., INOUE-BUNGO, T., MORII, H., FUJIKAWA, A., SASAKI, M., KIMURA, K., SHIINA, M., SATO, K., KUMASAKA, T., YAMAMOTO, M., ISHII, S. & OGATA, K. 2001. Structural analyses of DNA recognition by the AML1/Runx-1 Runt domain and its allosteric control by CBFbeta. Cell, 104, 755-67.

TAKAGAWA, J., ZHANG, Y., WONG, M. L., SIEVERS, R. E., KAPASI, N. K., WANG, Y., YEGHIAZARIANS, Y., LEE, R. J., GROSSMAN, W. & SPRINGER, M. L. 2007. Myocardial infarct size measurement in the mouse chronic infarction model: comparison of area- and length-based approaches. J Appl Physiol (1985), 102, 2104-11.

TAKAHASHI, A., SATAKE, M., YAMAGUCHI-IWAI, Y., BAE, S. C., LU, J., MARUYAMA, M., ZHANG, Y. W., OKA, H., ARAI, N., ARAI, K. & ET AL. 1995. Positive and negative regulation of granulocyte-macrophage colony-stimulating factor promoter activity by AML1-related transcription factor, PEBP2. Blood, 86, 607-16.

TAKAHASHI, K., UENO, T., TANIDA, I., MINEMATSU-IKEGUCHI, N., MURATA, M. & KOMINAMI, E. 2009. Characterization of CAA0225, a novel inhibitor specific for cathepsin L, as a probe for autophagic proteolysis. Biol Pharm Bull, 32, 475-9.

TAKAKURA, N., WATANABE, T., SUENOBU, S., YAMADA, Y., NODA, T., ITO, Y., SATAKE, M. & SUDA, T. 2000. A role for hematopoietic stem cells in promoting angiogenesis. Cell, 102, 199-209.

TAKEDA, K., SAKAGUCHI, T., MIYAGAWA, S., SHUDO, Y., KAINUMA, S., MASAI, T., TANIGUCHI, K. & SAWA, Y. 2012. The extent of early left ventricular reverse remodelling is related to midterm outcomes after restrictive mitral annuloplasty

in patients with non-ischaemic dilated cardiomyopathy and functional mitral regurgitation. Eur J Cardiothorac Surg, 41, 506-11.

TAMAREILLE, S., MATEUS, V., GHABOURA, N., JEANNETEAU, J., CROUE, A., HENRION, D., FURBER, A. & PRUNIER, F. 2011. RISK and SAFE signaling pathway interactions in remote limb ischemic perconditioning in combination with local ischemic postconditioning. Basic Res Cardiol, 106, 1329-39.

TANAKA, T., KUROKAWA, M., UEKI, K., TANAKA, K., IMAI, Y., MITANI, K., OKAZAKI, K., SAGATA, N., YAZAKI, Y., SHIBATA, Y., KADOWAKI, T. & HIRAI, H. 1996. The extracellular signal-regulated kinase pathway phosphorylates AML1, an acute myeloid leukemia gene product, and potentially regulates its transactivation ability. Mol Cell Biol, 16, 3967-79.

TANAKA, T., TANAKA, K., OGAWA, S., KUROKAWA, M., MITANI, K., NISHIDA, J., SHIBATA, Y., YAZAKI, Y. & HIRAI, H. 1995. An acute myeloid leukemia gene, AML1, regulates hemopoietic myeloid cell differentiation and transcriptional activation antagonistically by two alternative spliced forms. EMBO J, 14, 341-50.

TANG, Q., CAI, J., SHEN, D., BIAN, Z., YAN, L., WANG, Y. X., LAN, J., ZHUANG, G. Q., MA, W. Z. & WANG, W. 2009. Lysosomal cysteine peptidase cathepsin L protects against cardiac hypertrophy through blocking AKT/GSK3beta signaling. J Mol Med (Berl), 87, 249-60.

TANI, M. & NEELY, J. R. 1989. Role of intracellular Na+ in Ca2+ overload and depressed recovery of ventricular function of reperfused ischemic rat hearts. Possible involvement of H+-Na+ and Na+-Ca2+ exchange. Circ Res, 65, 1045-56.

TARANTINI, G., FAVARETTO, E., MARRA, M. P., FRIGO, A. C., NAPODANO, M., CACCIAVILLANI, L., GIOVAGNONI, A., RENDA, P., DE BIASIO, V., PLEBANI, M., MION, M., ZANINOTTO, M., ISABELLA, G., BILATO, C. & ILICETO, S. 2012. Postconditioning during coronary angioplasty in acute myocardial infarction: the POST-AMI trial. Int J Cardiol, 162, 33-8.

TASK FORCE ON THE MANAGEMENT OF, S. T. S. E. A. M. I. O. T. E. S. O. C., STEG, P. G., JAMES, S. K., ATAR, D., BADANO, L. P., BLOMSTROM-LUNDQVIST, C., BORGER, M. A., DI MARIO, C., DICKSTEIN, K., DUCROCQ, G., FERNANDEZ-AVILES, F., GERSHLICK, A. H., GIANNUZZI, P., HALVORSEN, S., HUBER, K., JUNI, P., KASTRATI, A., KNUUTI, J., LENZEN, M. J., MAHAFFEY, K. W., VALGIMIGLI, M., VAN 'T HOF, A., WIDIMSKY, P. & ZAHGER, D. 2012. ESC Guidelines for the management of acute myocardial infarction in patients presenting with ST-segment elevation. Eur Heart J, 33, 2569-619.

TAYLOR, A. L., ZIESCHE, S., YANCY, C., CARSON, P., D'AGOSTINO, R., JR., FERDINAND, K., TAYLOR, M., ADAMS, K., SABOLINSKI, M., WORCEL, M., COHN, J. N. & AFRICAN-AMERICAN HEART FAILURE TRIAL, I. 2004. Combination of isosorbide dinitrate and hydralazine in blacks with heart failure. N Engl J Med, 351, 2049-57.

TAYLOR, P. B. & CERNY, F. J. 1976. Evaluation of the isolated paced rat heart. J Appl Physiol, 41, 328-31.

THAKKER, R. & YANG, P. 2014. Mesenchymal stem cell therapy for cardiac repair. Curr Treat Options Cardiovasc Med, 16, 323.

THIELMANN, M., KOTTENBERG, E., BOENGLER, K., RAFFELSIEPER, C., NEUHAEUSER, M., PETERS, J., JAKOB, H. & HEUSCH, G. 2010. Remote ischemic preconditioning reduces myocardial injury after coronary artery bypass surgery with crystalloid cardioplegic arrest. Basic Res Cardiol, 105, 657-64.

THIELMANN, M., MASSOUDY, P., NEUHAUSER, M., TSAGAKIS, K., MARGGRAF, G., KAMLER, M., MANN, K., ERBEL, R. & JAKOB, H. 2006. Prognostic value of preoperative cardiac troponin I in patients undergoing emergency coronary artery bypass surgery with non-ST-elevation or ST-elevation acute coronary syndromes. Circulation, 114, I448-53.

THYGESEN, K., ALPERT, J. S., JAFFE, A. S., SIMOONS, M. L., CHAITMAN, B. R., WHITE, H. D. & WRITING GROUP ON BEHALF OF THE JOINT, E. S. C. A. A. H. A. W.

H. F. T. F. F. T. U. D. O. M. I. 2012. Third universal definition of myocardial infarction. Glob Heart, 7, 275-95.

THYGESEN, K., ALPERT, J. S., WHITE, H. D. & JOINT, E. S. C. A. A. H. A. W. H. F. T. F. F. T. R. O. M. I. 2007. Universal definition of myocardial infarction. J Am Coll Cardiol, 50, 2173-95.

TIWARI, M., HEMALATHA, T., GANESAN, K., NAYEEM, M., MURALI MANOHAR, B., BALACHANDRAN, C., VAIRAMUTHU, S., SUBRAMANIAM, S. & PUVANAKRISHNAN, R. 2008. Myocardial ischemia and reperfusion injury in rats: lysosomal hydrolases and matrix metalloproteinases mediated cellular damage. Mol Cell Biochem, 312, 81-91.

TOHYAMA, T., KIYOCHI, H., NARUMOTO, K., HONDA, K., KOBAYASHI, N., KANOH, M., SAIBARA, T. & KATUNUMA, N. 2000. Inhibitory effect of cathepsin B inhibitor CA 074 on mouse anti-rat mixed lymphocyte reaction: novel immunosuppressive strategy for indirect xenoantigen recognition. Transplant Proc, 32, 944-5.

TOOZE, S. A., ABADA, A. & ELAZAR, Z. 2014. Endocytosis and autophagy: exploitation or cooperation? Cold Spring Harb Perspect Biol, 6, a018358.

TOPOL, E. J. & INVESTIGATORS, G. V. 2001. Reperfusion therapy for acute myocardial infarction with fibrinolytic therapy or combination reduced fibrinolytic therapy and platelet glycoprotein IIb/IIIa inhibition: the GUSTO V randomised trial. Lancet, 357, 1905-14.

TOWATARI, T., NIKAWA, T., MURATA, M., YOKOO, C., TAMAI, M., HANADA, K. & KATUNUMA, N. 1991a. Novel Epoxysuccinyl Peptides - a Selective Inhibitor of Cathepsin-B, Invivo. Febs Letters, 280, 311-315.

TOWATARI, T., NIKAWA, T., MURATA, M., YOKOO, C., TAMAI, M., HANADA, K. & KATUNUMA, N. 1991b. Novel epoxysuccinyl peptides. A selective inhibitor of cathepsin B, in vivo. FEBS Lett, 280, 311-5.

TRAFFORD, A. W., DIAZ, M. E., SIBBRING, G. C. & EISNER, D. A. 2000. Modulation of CICR has no maintained effect on systolic Ca2+: simultaneous measurements of sarcoplasmic reticulum and sarcolemmal Ca2+ fluxes in rat ventricular myocytes. J Physiol, 522 Pt 2, 259-70.

TSUBOKAWA, T., SOLAROGLU, I., YATSUSHIGE, H., CAHILL, J., YATA, K. & ZHANG, J. H. 2006. Cathepsin and calpain inhibitor E64d attenuates matrix metalloproteinase-9 activity after focal cerebral ischemia in rats. Stroke, 37, 1888-1894.

TSUCHIDA, K., AIHARA, H., ISOGAI, K., HANADA, K. & SHIBATA, N. 1986. Degradation of myocardial structural proteins in myocardial infarcted dogs is reduced by Ep459, a cysteine proteinase inhibitor. Biol Chem Hoppe Seyler, 367, 39-45.

TSUGE, H., NISHIMURA, T., TADA, Y., ASAO, T., TURK, D., TURK, V. & KATUNUMA, N. 1999. Inhibition mechanism of cathepsin L-specific inhibitors based on the crystal structure of papain-CLIK148 complex. Biochemical and Biophysical Research Communications, 266, 411-416.

TU, C., ORTEGA-CAVA, C. F., CHEN, G., FERNANDES, N. D., CAVALLO-MEDVED, D., SLOANE, B. F., BAND, V. & BAND, H. 2008. Lysosomal cathepsin B participates in the podosome-mediated extracellular matrix degradation and invasion via secreted lysosomes in v-Src fibroblasts. Cancer Res, 68, 9147-56.

TURK, B., TURK, D. & SALVESEN, G. S. 2002. Regulating cysteine protease activity: essential role of protease inhibitors as guardians and regulators. Curr Pharm Des, 8, 1623-37.

TURK, B., TURK, D. & TURK, V. 2000. Lysosomal cysteine proteases: more than scavengers. Biochim Biophys Acta, 1477, 98-111.

TURK, B., TURK, V. & TURK, D. 1997. Structural and functional aspects of papain-like cysteine proteinases and their protein inhibitors. Biol Chem, 378, 141-50.

TURK, D., GUNCAR, G., PODOBNIK, M. & TURK, B. 1998. Revised definition of substrate binding sites of papain-like cysteine proteases. Biol Chem, 379, 137-47.

TURK, D., PODOBNIK, M., POPOVIC, T., KATUNUMA, N., BODE, W., HUBER, R. & TURK, V. 1995. Crystal structure of cathepsin B inhibited with CA030 at 2.0-A resolution: A basis for the design of specific epoxysuccinyl inhibitors. Biochemistry, 34, 4791-7.

TURK, V., TURK, B. & TURK, D. 2001. Lysosomal cysteine proteases: facts and opportunities. EMBO J, 20, 4629-33.

TURNER, P. V., BRABB, T., PEKOW, C. & VASBINDER, M. A. 2011. Administration of substances to laboratory animals: routes of administration and factors to consider. J Am Assoc Lab Anim Sci, 50, 600-13.

TURSKI, W. A. & ZASLONKA, J. 2000. Activity of cathepsin D and L in the heart muscle of coronary patients during coronary--aortal bypass graft operation. Med Sci Monit, 6, 853-60.

URBICH, C., DERNBACH, E., ROSSIG, L., ZEIHER, A. M. & DIMMELER, S. 2008. High glucose reduces cathepsin L activity and impairs invasion of circulating progenitor cells. J Mol Cell Cardiol, 45, 429-36.

URBICH, C., HEESCHEN, C., AICHER, A., SASAKI, K., BRUHL, T., FARHADI, M. R., VAJKOCZY, P., HOFMANN, W. K., PETERS, C., PENNACCHIO, L. A., ABOLMAALI, N. D., CHAVAKIS, E., REINHECKEL, T., ZEIHER, A. M. & DIMMELER, S. 2005. Cathepsin L is required for endothelial progenitor cell-induced neovascularization. Nat Med, 11, 206-13.

VALENTIM, L., LAURENCE, K. M., TOWNSEND, P. A., CARROLL, C. J., SOOND, S., SCARABELLI, T. M., KNIGHT, R. A., LATCHMAN, D. S. & STEPHANOU, A. 2006. Urocortin inhibits Beclin1-mediated autophagic cell death in cardiac myocytes exposed to ischaemia/reperfusion injury. J Mol Cell Cardiol, 40, 846-52.

VAN DE WERF, F., ADGEY, J., ARDISSINO, D., ARMSTRONG, P. W., AYLWARD, P., BARBASH, G., BETRIU, A., BINBREK, A. S., CALIFF, R., DIAZ, R., FANEBUST, R., FOX, K., GRANGER, C., HEIKKILA, J., HUSTED, S., JANSKY, P., LANGER, A., LUPI, E., MASERI, A., MEYER, J., MLCZOCH, J., MOCCETI, D., MYBURGH, D., OTO, A., PAOLASSO, E., PEHRSSON, K., SEABRA-GOMES, R., SOARES-PIEGAS, L., SUGRUE, D., TENDERA, M., TOPOL, E., TOUTOUZAS, P., VAHANIAN, A., VERHEUGT, F., WALLENTIN, L. & WHITE, H. 1999. Single-bolus tenecteplase compared with front-loaded alteplase in acute myocardial infarction: the ASSENT-2 double-blind randomised trial. Lancet, 354, 716-22.

VAN DE WERF, F., BAX, J., BETRIU, A., BLOMSTROM-LUNDQVIST, C., CREA, F., FALK, V., FILIPPATOS, G., FOX, K., HUBER, K., KASTRATI, A., ROSENGREN, A., STEG, P. G., TUBARO, M., VERHEUGT, F., WEIDINGER, F., WEIS, M. & GUIDELINES, E. S. C. C. F. P. 2008. Management of acute myocardial infarction in patients presenting with persistent ST-segment elevation: the Task Force on the Management of ST-Segment Elevation Acute Myocardial Infarction of the European Society of Cardiology. Eur Heart J, 29, 2909-45.

VERMA, A., MERIS, A., SKALI, H., GHALI, J. K., ARNOLD, J. M., BOURGOUN, M., VELAZQUEZ, E. J., MCMURRAY, J. J., KOBER, L., PFEFFER, M. A., CALIFF, R. M. & SOLOMON, S. D. 2008. Prognostic implications of left ventricular mass and geometry following myocardial infarction: the VALIANT (VALsartan In Acute myocardial iNfarcTion) Echocardiographic Study. JACC Cardiovasc Imaging, 1, 582-91.

VIDAVALUR, R., SWARNAKAR, S., THIRUNAVUKKARASU, M., SAMUEL, S. M. & MAULIK, N. 2008. Ex vivo and in vivo approaches to study mechanisms of cardioprotection targeting ischemia/reperfusion (i/r) injury: useful techniques for cardiovascular drug discovery. Curr Drug Discov Technol, 5, 269-78.

VOSS, J., JONES, L. R. & THOMAS, D. D. 1994. The physical mechanism of calcium pump regulation in the heart. Biophys J, 67, 190-6.

WAGNER, B. M., SMITH, R. A., COLES, P. J., COPP, L. J., ERNEST, M. J. & KRANTZ, A. 1994. In vivo inhibition of cathepsin B by peptidyl (acyloxy)methyl ketones. J Med Chem, 37, 1833-40.

WALENBERGH, S. M., HOUBEN, T., HENDRIKX, T., JEURISSEN, M. L., VAN GORP, P. J., VREUGDENHIL, A. C., ADRIAANSE, M. P., BUURMAN, W. A., HOFKER, M. H., MOSCA, A., LINDSEY, P. J., ALISI, A., LICCARDO, D., PANERA, N., KOEK, G. H., NOBILI, V. & SHIRI-SVERDLOV, R. 2015. Plasma cathepsin D levels: a novel tool to predict pediatric hepatic inflammation. Am J Gastroenterol, 110, 462-70.

WANG, Q., STACY, T., MILLER, J. D., LEWIS, A. F., GU, T. L., HUANG, X., BUSHWELLER, J. H., BORIES, J. C., ALT, F. W., RYAN, G., LIU, P. P., WYNSHAW-BORIS, A., BINDER, M., MARIN-PADILLA, M., SHARPE, A. H. & SPECK, N. A. 1996. The CBFbeta subunit is essential for CBFalpha2 (AML1) function in vivo. Cell, 87, 697-708.

WANG, S., WANG, Q., CRUTE, B. E., MELNIKOVA, I. N., KELLER, S. R. & SPECK, N. A. 1993. Cloning and characterization of subunits of the T-cell receptor and murine leukemia virus enhancer core-binding factor. Mol Cell Biol, 13, 3324-39.

WANG, W., SCHWEMMERS, S., HEXNER, E. O. & PAHL, H. L. 2010. AML1 is overexpressed in patients with myeloproliferative neoplasms and mediates JAK2V617F-independent overexpression of NF-E2. Blood, 116, 254-66.

WANG, X., BLAGDEN, C., FAN, J., NOWAK, S. J., TANIUCHI, I., LITTMAN, D. R. & BURDEN, S. J. 2005. Runx1 prevents wasting, myofibrillar disorganization, and autophagy of skeletal muscle. Genes Dev, 19, 1715-22.

WARREN, A. J., BRAVO, J., WILLIAMS, R. L. & RABBITTS, T. H. 2000. Structural basis for the heterodimeric interaction between the acute leukaemia-associated transcription factors AML1 and CBFbeta. EMBO J, 19, 3004-15.

WARREN, S. E., ROYAL, H. D., MARKIS, J. E., GROSSMAN, W. & MCKAY, R. G. 1988. Time course of left ventricular dilation after myocardial infarction: influence of

infarct-related artery and success of coronary thrombolysis. J Am Coll Cardiol, 11, 12-9.

WARTMANN, T., MAYERLE, J., KAHNE, T., SAHIN-TOTH, M., RUTHENBURGER, M., MATTHIAS, R., KRUSE, A., REINHECKEL, T., PETERS, C., WEISS, F. U., SENDLER, M., LIPPERT, H., SCHULZ, H. U., AGHDASSI, A., DUMMER, A., TELLER, S., HALANGK, W. & LERCH, M. M. 2010. Cathepsin L inactivates human trypsinogen, whereas cathepsin L-deletion reduces the severity of pancreatitis in mice. Gastroenterology, 138, 726-37.

WEBER, K. T. 1997. Extracellular matrix remodeling in heart failure: a role for de novo angiotensin II generation. Circulation, 96, 4065-82.

WEE, H. J., VOON, D. C., BAE, S. C. & ITO, Y. 2008. PEBP2-beta/CBF-beta-dependent phosphorylation of RUNX1 and p300 by HIPK2: implications for leukemogenesis. Blood, 112, 3777-87.

WHELAN, R. S., KAPLINSKIY, V. & KITSIS, R. N. 2010. Cell death in the pathogenesis of heart disease: mechanisms and significance. Annu Rev Physiol, 72, 19-44.

WHELAN, R. S., KONSTANTINIDIS, K., XIAO, R. P. & KITSIS, R. N. 2013. Cardiomyocyte life-death decisions in response to chronic beta-adrenergic signaling. Circ Res, 112, 408-10.

WHITE, H., HIRULOG & EARLY REPERFUSION OR OCCLUSION -2 TRIAL, I. 2001. Thrombin-specific anticoagulation with bivalirudin versus heparin in patients receiving fibrinolytic therapy for acute myocardial infarction: the HERO-2 randomised trial. Lancet, 358, 1855-63.

WHITE, H. D., CROSS, D. B., ELLIOTT, J. M., NORRIS, R. M. & YEE, T. W. 1994. Long-term prognostic importance of patency of the infarct-related coronary artery after thrombolytic therapy for acute myocardial infarction. Circulation, 89, 61-7.

WHITE, H. D., NORRIS, R. M., BROWN, M. A., BRANDT, P. W. T., WHITLOCK, R. M. L. & WILD, C. J. 1987. Left-Ventricular End-Systolic Volume as the Major Determinant of Survival after Recovery from Myocardial-Infarction. Circulation, 76, 44-51.

WIDIMSKY, P., WIJNS, W., FAJADET, J., DE BELDER, M., KNOT, J., AABERGE, L., ANDRIKOPOULOS, G., BAZ, J. A., BETRIU, A., CLAEYS, M., DANCHIN, N., DJAMBAZOV, S., ERNE, P., HARTIKAINEN, J., HUBER, K., KALA, P., KLINCEVA, M., KRISTENSEN, S. D., LUDMAN, P., FERRE, J. M., MERKELY, B., MILICIC, D., MORAIS, J., NOC, M., OPOLSKI, G., OSTOJIC, M., RADOVANOVIC, D., DE SERVI, S., STENESTRAND, U., STUDENCAN, M., TUBARO, M., VASILJEVIC, Z., WEIDINGER, F., WITKOWSKI, A., ZEYMER, U. & EUROPEAN ASSOCIATION FOR PERCUTANEOUS CARDIOVASCULAR, I. 2010. Reperfusion therapy for ST elevation acute myocardial infarction in Europe: description of the current situation in 30 countries. Eur Heart J, 31, 943-57.

WIJEYSUNDERA, H. C., VIJAYARAGHAVAN, R., NALLAMOTHU, B. K., FOODY, J. M., KRUMHOLZ, H. M., PHILLIPS, C. O., KASHANI, A., YOU, J. J., TU, J. V. & KO, D. T. 2007. Rescue angioplasty or repeat fibrinolysis after failed fibrinolytic therapy for ST-segment myocardial infarction: a meta-analysis of randomized trials. J Am Coll Cardiol, 49, 422-30.

WITHANA, N. P., BLUM, G., SAMENI, M., SLANEY, C., ANBALAGAN, A., OLIVE, M. B., BIDWELL, B. N., EDGINGTON, L., WANG, L., MOIN, K., SLOANE, B. F., ANDERSON, R. L., BOGYO, M. S. & PARKER, B. S. 2012. Cathepsin B inhibition limits bone metastasis in breast cancer. Cancer Res, 72, 1199-209.

WOODCOCK, E. A. & MATKOVICH, S. J. 2005. Cardiomyocytes structure, function and associated pathologies. Int J Biochem Cell Biol, 37, 1746-51.

WU, B., ZHOU, B., WANG, Y., CHENG, H. L., HANG, C. T., PU, W. T., CHANG, C. P. & ZHOU, B. 2010. Inducible cardiomyocyte-specific gene disruption directed by the rat Tnnt2 promoter in the mouse. Genesis, 48, 63-72.

WU, K. C., ZERHOUNI, E. A., JUDD, R. M., LUGO-OLIVIERI, C. H., BAROUCH, L. A., SCHULMAN, S. P., BLUMENTHAL, R. S. & LIMA, J. A. 1998. Prognostic significance of microvascular obstruction by magnetic resonance imaging in patients with acute myocardial infarction. Circulation, 97, 765-72.

WU, Q. Q., XU, M., YUAN, Y., LI, F. F., YANG, Z., LIU, Y., ZHOU, M. Q., BIAN, Z. Y., DENG, W., GAO, L., LI, H. & TANG, Q. Z. 2015. Cathepsin B deficiency attenuates cardiac remodeling in response to pressure overload via TNF-α/ASK1/JNK pathway. Am J Physiol Heart Circ Physiol, 308, H1143-54.

XU, G., KANEZAKI, R., TOKI, T., WATANABE, S., TAKAHASHI, Y., TERUI, K., KITABAYASHI, I. & ITO, E. 2006. Physical association of the patient-specific GATA1 mutants with RUNX1 in acute megakaryoblastic leukemia accompanying Down syndrome. Leukemia, 20, 1002-8.

XU, Y., WANG, J. Y., SONG, X. H., WEI, R. L., HE, F. P., PENG, G. P. & LUO, B. Y. 2016. Protective mechanisms of CA074-me (other than cathepsin-B inhibition) against programmed necrosis induced by global cerebral ischemia/reperfusion injury in rats. Brain Research Bulletin, 120, 97-105.

YAMAZAKI, T., KOMURO, I., KUDOH, S., ZOU, Y., SHIOJIMA, I., MIZUNO, T., TAKANO, H., HIROI, Y., UEKI, K., TOBE, K. & ET AL. 1995. Angiotensin II partly mediates mechanical stress-induced cardiac hypertrophy. Circ Res, 77, 258-65.

YAN, L., VATNER, D. E., KIM, S. J., GE, H., MASUREKAR, M., MASSOVER, W. H., YANG, G., MATSUI, Y., SADOSHIMA, J. & VATNER, S. F. 2005. Autophagy in chronically ischemic myocardium. Proc Natl Acad Sci U S A, 102, 13807-12.

YAN, S., BERQUIN, I. M., TROEN, B. R. & SLOANE, B. F. 2000. Transcription of human cathepsin B is mediated by Sp1 and Ets family factors in glioma. DNA Cell Biol, 19, 79-91.

YANG, M., SUN, J., ZHANG, T., LIU, J., ZHANG, J., SHI, M. A., DARAKHSHAN, F., GUERRE-MILLO, M., CLEMENT, K., GELB, B. D., DOLGNOV, G. & SHI, G. P. 2008.

Deficiency and inhibition of cathepsin K reduce body weight gain and increase glucose metabolism in mice. Arterioscler Thromb Vasc Biol, 28, 2202-8.

YANG, M., ZHANG, Y., PAN, J., SUN, J., LIU, J., LIBBY, P., SUKHOVA, G. K., DORIA, A., KATUNUMA, N., PERONI, O. D., GUERRE-MILLO, M., KAHN, B. B., CLEMENT, K. & SHI, G. P. 2007. Cathepsin L activity controls adipogenesis and glucose tolerance. Nat Cell Biol, 9, 970-7.

YASOTHORNSRIKUL, S., GREENBAUM, D., MEDZIHRADSZKY, K. F., TONEFF, T., BUNDEY, R., MILLER, R., SCHILLING, B., PETERMANN, I., DEHNERT, J., LOGVINOVA, A., GOLDSMITH, P., NEVEU, J. M., LANE, W. S., GIBSON, B., REINHECKEL, T., PETERS, C., BOGYO, M. & HOOK, V. 2003. Cathepsin L in secretory vesicles functions as a prohormone-processing enzyme for production of the enkephalin peptide neurotransmitter. Proc Natl Acad Sci U S A, 100, 9590-5.

YELLON, D. M. & HAUSENLOY, D. J. 2007. Myocardial reperfusion injury. N Engl J Med, 357, 1121-35.

YUTZEY, K. E. & ROBBINS, J. 2007. Principles of genetic murine models for cardiac disease. Circulation, 115, 792-9.

ZENG, C., MCNEIL, S., POCKWINSE, S., NICKERSON, J., SHOPLAND, L., LAWRENCE, J. B., PENMAN, S., HIEBERT, S., LIAN, J. B., VAN WIJNEN, A. J., STEIN, J. L. & STEIN, G. S. 1998. Intranuclear targeting of AML/CBFalpha regulatory factors to nuclear matrix-associated transcriptional domains. Proc Natl Acad Sci U S A, 95, 1585-9.

ZHANG, D. E., FUJIOKA, K., HETHERINGTON, C. J., SHAPIRO, L. H., CHEN, H. M., LOOK, A. T. & TENEN, D. G. 1994. Identification of a region which directs the monocytic activity of the colony-stimulating factor 1 (macrophage colony-stimulating factor) receptor promoter and binds PEBP2/CBF (AML1). Mol Cell Biol, 14, 8085-95.

ZHANG, D. E., HETHERINGTON, C. J., MEYERS, S., RHOADES, K. L., LARSON, C. J., CHEN, H. M., HIEBERT, S. W. & TENEN, D. G. 1996. CCAAT enhancer-binding protein (C/EBP) and AML1 (CBF alpha2) synergistically activate the macrophage colony-stimulating factor receptor promoter. Mol Cell Biol, 16, 1231-40.

ZHANG, J., WANG, P., HUANG, Y. B., LI, J., ZHU, J., LUO, X., SHI, H. M. & LI, Y. 2010a. Plasma Cathepsin L and Its Related Pro/Antiangiogenic Factors Play Useful Roles in Predicting Rich Coronary Collaterals in Patients with Coronary Heart Disease. Journal of International Medical Research, 38, 1389-1403.

ZHANG, J., WANG, P., HUANG, Y. B., LI, J., ZHU, J., LUO, X., SHI, H. M. & LI, Y. 2010b. Plasma cathepsin L and its related pro/antiangiogenic factors play useful roles in predicting rich coronary collaterals in patients with coronary heart disease. J Int Med Res, 38, 1389-403.

ZHANG, J. H. & XU, M. 2000. DNA fragmentation in apoptosis. Cell Res, 10, 205-11.

ZHANG, L., FRIED, F. B., GUO, H. & FRIEDMAN, A. D. 2008. Cyclin-dependent kinase phosphorylation of RUNX1/AML1 on 3 sites increases transactivation potency and stimulates cell proliferation. Blood, 111, 1193-200.

ZHANG, M., PROSSER, B. L., BAMBOYE, M. A., GONDIM, A. N., SANTOS, C. X., MARTIN, D., GHIGO, A., PERINO, A., BREWER, A. C., WARD, C. W., HIRSCH, E., LEDERER, W. J. & SHAH, A. M. 2015. Contractile Function During Angiotensin-II Activation: Increased Nox2 Activity Modulates Cardiac Calcium Handling via Phospholamban Phosphorylation. J Am Coll Cardiol, 66, 261-72.

ZHANG, T., MAEKAWA, Y., SAKAI, T., NAKANO, Y., ISHII, K., HISAEDA, H., DAINICHI, T., ASAO, T., KATUNUMA, N. & HIMENO, K. 2001. Treatment with cathepsin L inhibitor potentiates Th2-type immune response in Leishmania major-infected BALB/c mice. Int Immunol, 13, 975-82.

ZHANG, X., SZETO, C., GAO, E., TANG, M., JIN, J., FU, Q., MAKAREWICH, C., AI, X., LI, Y., TANG, A., WANG, J., GAO, H., WANG, F., GE, X. J., KUNAPULI, S. P., ZHOU, L., ZENG, C., XIANG, K. Y. & CHEN, X. 2013. Cardiotoxic and cardioprotective features of chronic beta-adrenergic signaling. Circ Res, 112, 498-509.

ZHANG, Y., BIGGS, J. R. & KRAFT, A. S. 2004. Phorbol ester treatment of K562 cells regulates the transcriptional activity of AML1c through phosphorylation. J Biol Chem, 279, 53116-25.

ZHANG, Y. & DERYNCK, R. 2000. Transcriptional regulation of the transforming growth factor-beta -inducible mouse germ line Ig alpha constant region gene by functional cooperation of Smad, CREB, and AML family members. J Biol Chem, 275, 16979-85.

ZHAO, X., JANKOVIC, V., GURAL, A., HUANG, G., PARDANANI, A., MENENDEZ, S., ZHANG, J., DUNNE, R., XIAO, A., ERDJUMENT-BROMAGE, H., ALLIS, C. D., TEMPST, P. & NIMER, S. D. 2008. Methylation of RUNX1 by PRMT1 abrogates SIN3A binding and potentiates its transcriptional activity. Genes Dev, 22, 640-53.

ZHAO, Z. Q., CORVERA, J. S., HALKOS, M. E., KERENDI, F., WANG, N. P., GUYTON, R. A. & VINTEN-JOHANSEN, J. 2003. Inhibition of myocardial injury by ischemic postconditioning during reperfusion: comparison with ischemic preconditioning. Am J Physiol Heart Circ Physiol, 285, H579-88.

ZHENG, X., CHU, F., CHOU, P. M., GALLATI, C., DIER, U., MIRKIN, B. L., MOUSA, S. A. & REBBAA, A. 2009. Cathepsin L inhibition suppresses drug resistance in vitro and in vivo: a putative mechanism. Am J Physiol Cell Physiol, 296, C65-74.

ZHOU, W. & YUAN, J. 2014. SnapShot: Necroptosis. Cell, 158, 464-464 e1.

ZIMARINO, M., SACCHETTA, D., RENDA, G. & DE CATERINA, R. 2008. Facilitated PCI: rationale, current evidence, open questions, and future directions. J Cardiovasc Pharmacol, 51, 3-10.

ZIMMER, H. G., GERDES, A. M., LORTET, S. & MALL, G. 1990. Changes in heart function and cardiac cell size in rats with chronic myocardial infarction. J Mol Cell Cardiol, 22, 1231-43.

ZOLOTAREVA, A. G. & KOGAN, M. E. 1978. Production of experimental occlusive myocardial infarction in mice. Cor Vasa, 20, 308-14.

ZWEIER, J. L., FLAHERTY, J. T. & WEISFELDT, M. L. 1987. Direct measurement of free radical generation following reperfusion of ischemic myocardium. Proc Natl Acad Sci U S A, 84, 1404-7.